



**University College London**

**Department of Chemistry**

**Faculty of Mathematical and Physical Sciences (MAPS)**

**Hydrophobic Polymers and Nanocomposites from Cassava**

**Nasirudeen Mohammed Baba**

A thesis submitted in fulfilment of the requirements for the degree of

**Doctor of Philosophy**

**Supervisors:**

Prof. Julian R. G. Evans

Prof. Helen C. Hailes

**July, 2014**

## **Declaration**

I, Nasirudeen Mohammed Baba, confirm that the work presented in this thesis is my own. Where information has been derived from other sources, I confirm that this has been indicated in the thesis.

## Abstract

This project aims to benefit the sub-Saharan African economies by exploiting cassava for chemical feedstock for materials production. It anticipates the industrial changes that will follow from increased petroleum price and regulatory control of embedded fossil carbon. It offers a way to integrate industrial and agricultural sectors.

Initially, glucose and fructose were dehydrated by reactive distillation over a sulfated zirconia catalyst and 1-butyl-3-methylimidazolium chloride (BMIM Cl) ionic liquid as solvent under a nitrogen atmosphere at 180 °C to produce 5-(hydroxymethyl) furan (5-HMF) as a precursor for polymeric materials. Solvent, catalyst and reaction conditions were varied to improve the yield of 5-HMF. Yields of 82% and 65% were obtained using fructose and glucose substrates with this catalyst.

Secondly, 2,5-furandicarboxylic acid (FDCA) and 2,5-bis-(hydroxymethyl)furan (BHMF) were synthesised as monomers from 5-HMF. The aldehyde group of 5-HMF was oxidized using potassium permanganate to FDCA with 80% yield achieved. BHMF was synthesised from 5-HMF using sodium borohydride with 88% yield achieved.

The third part focuses on the polymerization of FDCA with the following diols: 1,4-butanediol, 1,6-hexanediol, 1,8-octanediol and BHMF via esterification reactions at 160-200 °C using titanium (IV) *n*-butoxide catalyst. All diols produced polymers under the same conditions. The difference within this family of polymers was the number of carbon atoms in the linking diols and that BHMF had a different diol structure with a furan ring attached.

Furthermore, a study of the interaction of all the monomers and the 5-HMF with Na-montmorillonite clay was made. It was observed that all were intercalated into the clay paving the way for the manufacture of nanocomposites.

Finally, all the polymers were shown to be hydrophobic with PBH-2,5-F more hydrophobic with a contact angle of 91° compared to others. Water absorption, dielectric constant and mechanical properties of the polymers were recorded.

## Table of contents

Declaration.....	2
Abstract.....	3
Table of contents.....	4
Acknowledgements.....	11
Abbreviations.....	12
List of Tables.....	15
List of Figures.....	17
<b>CHAPTER 1: INTRODUCTION.....</b>	<b>24</b>
1.1 General Introduction.....	24
1.2 Motivation for this research.....	25
1.2.1 Nigeria: the background.....	26
1.2.2 Crude oil production in Nigeria.....	27
1.2.3 Crude oil Export from Nigeria.....	28
1.2.4 The Nigerian Economy.....	29
1.2.5 Nigeria’s agricultural potential.....	30
1.2.6 Land availability.....	31
1.2.7 The place of Cassava in the Nigerian economy.....	32
1.3 Aims of this research.....	34
<b>CHAPTER 2: LITERATURE REVIEW.....</b>	<b>37</b>
2.1 Biomass.....	37

2.2	Biomass resources and their composition .....	37
2.3	Chemicals from biomass .....	39
2.3.1	Carbohydrates.....	39
2.3.2	Chemicals produced from saccharides .....	39
2.3.3	Bio-based polymers.....	40
2.3.4	Classification of bio-based polymers .....	41
2.3.5	Bio-based polymers derived directly from biomass.....	42
2.3.6	Bio-based polymers from chemical synthesis of bio-derived monomers .....	50
2.3.7	Bio-based polymers derived from microorganisms .....	53
2.3.8	Other sources of bio-based polymers .....	55
2.4	Production of furan-based aldehyde.....	59
2.4.1	Furfural production .....	59
2.4.2	Catalytic conversion of carbohydrate to 5-HMF.....	62
2.4.3	Solvents used in production of 5-HMF .....	67
2.5	Furan derivatives for polymer applications.....	69
2.5.1	2,5-Furandicarboxylic acid (FDCA) .....	72
2.5.2	2,5-Diformylfuran (DFF) .....	73
2.5.3	2,5-Dimethylfuran (DMF).....	74
2.5.4	2,5-Bis-(hydroxymethyl) furan .....	74
2.6	Polymer - Clay nanocomposites .....	75
2.6.1	Types of polymer-clay nanocomposites.....	75
2.7	Preparation of nanocomposites .....	77
2.7.1	<i>In situ</i> Template synthesis .....	77
2.7.2	Intercalation of Polymer or Pre-polymer from Solution .....	78
2.7.3	<i>In situ</i> intercalative polymerization.....	80
2.7.4	Melt intercalation .....	81

2.7.5	Layered Silicates .....	82
2.8	Characterization of the structures of nanocomposites .....	83
2.8.1	X-ray diffraction.....	83
2.8.2	Transmission electron microscopy (TEM).....	85
2.9	Bio-based polymer composites .....	86
2.9.1	Thermoplastic Starch Based Composites.....	86
2.9.2	Poly Lactic Acid Based Composites .....	87
2.9.3	Cellulose Based Composites .....	88
<b>CHAPTER 3: MATERIALS AND METHODS .....</b>		<b>90</b>
3.1	Materials.....	90
3.2	Analytical Instruments .....	92
3.2.1	Nuclear Magnetic Resonance spectrophotometer (NMR) .....	92
3.2.2	Fourier Transform Infrared spectrophotometer (FTIR) .....	92
3.2.3	X-Ray diffractometer (XRD) .....	92
3.2.4	Transmission Electron Microscope (TEM).....	92
3.2.5	Thermogravimetric analysis (TGA).....	93
3.2.6	Tensile properties .....	93
3.2.7	Elemental analysis.....	94
3.2.8	Water contact angle.....	94
3.2.9	Surface tension of water .....	94
3.2.10	Capacitance and dielectric constant .....	95
3.2.11	Ultrasonic probe .....	95
3.3	Methods.....	95
3.3.1	Synthesis of sulfated zirconia catalyst .....	95
3.3.2	Dehydration of glucose to 5-HMF [43].....	96
3.3.3	Dehydration of glucose to 5-HMF by vacuum distillation .....	96

3.3.4	Yield calculation of 5-HMF produced .....	97
3.4	Synthesis of some derivatives of 5-HMF.....	97
3.4.1	Synthesis of 2,5-furandicarboxylic acid (FDCA)[323].....	97
3.4.2	Synthesis of 2, 5-bis-(hydroxymethyl) furan (BHMF) .....	97
3.4.3	Synthesis of dimethyl-2, 5-furandicarboxylate (DFD) [158].....	98
3.4.4	Sample preparation for XRD.....	98
3.4.5	Treatment of montmorillonite clay with 5-HMF and FDCA.....	98
3.4.6	Synthesis of modified MMT clay.....	99
3.5	Polymerization reactions .....	100
3.5.1	Synthesis of polyester from FDCA [323] .....	100
3.5.2	Water absorption test.....	100
3.6	Preparation of polymer/clay nanocomposites .....	101
3.6.1	Polymer/Clay Nanocomposites by Intercalation method.....	101
3.6.2	<i>In situ</i> intercalative polymerization.....	101
3.6.3	Melt intercalation .....	101
<b>CHAPTER 4: RESULTS AND DISCUSSION .....</b>		<b>102</b>
4.1	Characterisation of sulfated zirconia catalyst .....	102
4.2	X-ray diffraction of sulfated zirconia.....	102
4.3	Dehydration of glucose/fructose by solvent extraction.....	104
4.4	Dehydration of glucose/fructose by vacuum distillation .....	105
4.4.1	Testing the vacuum distillation equipment .....	109
4.5	Synthesis of 5-(hydroxymethyl) furan (5-HMF) .....	109
4.5.1	5-HMF yields from dehydration of glucose and fructose .....	109
4.5.2	Catalytic activity of the solid catalysts.....	111
4.5.3	5-HMF formation in other ionic liquids.....	111
4.5.4	Effect of reaction temperature with time on 5-HMF yield.....	112

4.5.5	Effect of catalyst dosage on 5-HMF synthesis.....	113
4.5.6	Sulfated zirconia and [BMIM]Cl recycling .....	114
4.6	Characterization of 5-HMF .....	115
4.7	Synthesis of some derivatives of 5-HMF.....	115
4.7.1	Synthesis of FDCA.....	115
4.7.2	Synthesis of 2,5-bis (hydroxymethyl) furan (BHMF).....	116
4.7.3	Synthesis of dimethyl-2, 5-furandicarboxalate (DFD).....	117
4.8	Assessment of intercalation of monomers into clay .....	117
4.8.1	5-HMF and Na-MMT clay .....	117
4.8.2	FDCA and MMT clay .....	119
4.8.3	BHMF and MMT clay.....	120
4.9	Organically modified MMT.....	120
4.10	FT-IR absorption spectra of modified MMT .....	121
4.11	Polymers derived from FDCA .....	122
4.11.1	NMR structure characterization .....	122
4.11.2	FT-IR structure characterization .....	124
4.12	Polymers from FDCA and other diols .....	126
4.12.1	NMR structure characterisation of PH-2,5-F, PO-2,5-F and PBH-2,5-F polymers .....	126
4.12.2	FT-IR characterisation of PH-2,5-F, PO-2,5-F and PBH-2,5-F polymers.....	131
4.12.3	Elemental analysis.....	134
4.12.4	Tensile properties .....	134
4.12.5	Water contact angle.....	136
4.12.6	Variation of contact angle with time .....	139
4.12.7	Capacitance and dielectric constant .....	140
4.12.8	Water absorption .....	142
4.12.9	Thermogravimetric Analysis (TGA).....	143

4.12.10	Differential Scanning Calorimetry (DSC) .....	145
4.12.11	XRD pattern of the polymer .....	145
4.12.12	Effect of grinding on XRD pattern of the polymer.....	146
4.13	Polymer/Clay nanocomposites .....	146
4.13.1	XRD pattern of the polymer/clay nanocomposites .....	146
4.13.2	XRD pattern of polymer/clay nanocomposites prepared by different methods .....	147
4.13.3	TEM images of polymer/clay nanocomposite .....	148
<b>CHAPTER 5: CONCLUSIONS AND FUTURE WORK .....</b>		<b>151</b>
5.1	Conclusions .....	151
5.2	Future work .....	153
5.2.1	Other sources of carbohydrate.....	153
5.2.2	Other derivatives of 5-HMF .....	153
5.2.3	Molar mass determination of the polymers.....	154
5.2.4	Mechanical properties of the polymers .....	154
5.2.5	Regulatory measures .....	155
Appendix 1. Vacuum distillation apparatus .....		156
Appendix 2. NMR and FT-IR spectrum of 5-HMF.....		157
Appendix 3. NMR and FT-IR spectra of FDCA.....		160
Appendix 4. NMR and FT-IR spectra of BHMF .....		162
Appendix 5. <sup>1</sup> H and <sup>13</sup> C NMR spectra of DFD .....		164
Appendix 6. Analytical instruments.....		165
1.	X-Ray Diffraction (XRD) .....	165

---

2. Nuclear Magnetic Resonance (NMR) Spectroscopy .....	167
3. Fourier Transform Infrared (FT-IR) Spectroscopy .....	169
4. Thermogravimetric analysis (TGA).....	171
5. Differential Scanning Calorimetry (DSC) .....	172
Appendix 7. Photographs of some of the equipment used.....	175
1. Bruker alpha FTIR .....	175
2. Siemens D500 X-Ray Diffractometer .....	175
3. Thermal analyser.....	176
4. Centrifuge.....	176
<b>REFERENCES.....</b>	<b>177</b>

## Acknowledgements

I would like to thank my supervisors; Prof. Julian R.G. Evans for giving me the opportunity to work with him, for his suggestions, guidance and support despite his tight schedule for the successful completion of this work and to Prof. Helen C. Hailes for her advice and support during this project.

I also appreciate the assistance from Mr. Phil Hayes and Mr. David Webb, the technical staff in the Turner Lab, for their time and guidance in the use of some of the analytical equipment. And to Dr. Jeremy Cockcroft and Mr. Martin Vickers who helped and taught me how to use the XRD equipment. Also, my appreciation goes to Dr. Steve Firth for his time and guidance on the use of TGA and TEM.

I want to acknowledge the financial support of the Tertiary Education Trust Fund (TETFund) and the Kaduna State University, Kaduna Nigeria for the Fellowship, Prof. E. M. Abdurrahman for the encouragement in accomplishing this intellectual work which gave me to opportunity to come to England and accomplish these task. Also, not forgetting the role played by Alh. Rilwanu Abdussalami to see this dream comes true.

My heartfelt appreciation to the following people who made my stay in UCL a memorable one: Brother Sa'eed Sa'eed, Mohammed Haque, Abdul-Lateef Adedigba, Tom Daley, Ahmed Akbar, Alex Bour and Sandra Aline Sanchez.

To my parents, brothers and sisters to whom I owe this success and which words are not enough to express my gratitude towards them for all their prayers, patience and encouragement during these period of my absence. I would also like to thank Ahmad Adamu Ambi (*Majidadin Bauchi*), Hamisu Kawu, Husseyn Umar Gende, Col. Muhammad S'Barak, Usman A. Shuaibu (Marshall) Sirajo Adamu, Aminu Adamu Ambi, ZMS, and their families for their prayers, care and support.

Finally, to my wife Halima for her prayers, understanding and patience throughout this period and not forgetting my kids; Aisha and AbdurRahman.

## Abbreviations

[BDMIM]PF <sub>6</sub>	1-butyl-2,3-dimethylimidazolium hexafluorophosphate
[BMIM]Cl	1-butyl-3-methylimidazolium chloride
[HMIM]Cl	1-hexyl-3-methylimidazolium chloride
5-HMF	5-(hydroxymethyl) furan
BD	1,4-butanediol
BDM	1,3-benzenedimethanol
BHMF	2,5-Bis-(Hydroxymethyl)furan
CDCl <sub>3</sub>	Chloroform
CTAB	Cetyltrimethylammonium bromide
DFD	Dimethyl-2,5-furandicarboxylate
DFF	Diformyl furan
DMAc	N,N-Dimethylacetamide
DMF	Dimethyl furan
DMSO- <i>d</i> <sub>6</sub>	Deuterated dimethyl sulfoxide
DSC	Differential Scanning calorimetry
EtOAc	Ethyl acetate
FCA	5-Formyl-2-furandicarboxylic acid

---

FDCA	2,5-Furandicarboxylic acid
FTIR	Fourier Transform infrared spectroscopy
HFCA	5-Hydroxymethyl-2-furandicarboxylic acid
Ils	Ionic Liquids
LA	Lactic Acid
Na-MMT	Sodium Montmorillonite
NMR	Nuclear Magnetic Resonance
OMLS	Organo-modified layered silicate
PB-2,5-F	Poly(butylene-2,5-furandicarboxylate)
PBH-2,5-F	Poly(2,5-furandimethylene-2,5-furandicarboxylate)
PCL	Polymer-Clay nanocomposite
PEO	Poly(ethylene oxide)
PET	Poly(ethylene terephthalate)
PH-2,5-F	Poly(hexylene-2,5-furandicarboxylate)
PLA	Poly(lactic acid)
PO-2,5-F	Poly(octylene-2,5-furandicarboxylate)
PVA	Poly(vinyl acetate)
PVOH	Poly(vinyl alcohol)

SZ	Sulfated zirconia
TEM	Transmission Electron Microscopy
TGA	Thermo Gravimetric Analysis
TPO	Thermoplastic olefin
XRD	X-ray diffraction
Z	Zirconia

## List of Tables

Table 2-1. Glass transition and melting temperature of PLA with various L-monomer copolymer ratio .....	52
Table 2-2. Trade names and suppliers of various brands of PLA [76] .....	52
Table 2-3. PHAs biosynthesis in plants [137].....	54
Table 2-4. Nanocomposites prepared by intercalation from solution [260]. .....	80
Table 2-5. Commonly used layered phyllosilicates with their general formula [263]. .....	82
Table 3-1. Materials used in this work.....	90
Table 4-1. Phase mixtures transformation of sulfated zirconia.....	104
Table 4-2. Vacuum reactive distillation of 5-HMF from the dehydration of carbohydrates with different entrainers [333]. .....	107
Table 4-3. Characteristic peaks of FDCA .....	116
Table 4-4. Maximum peak and d-spacing of Na-MMT and 5-HMF .....	118
Table 4-5. FT-IR absorption bands of polyester from FDCA.....	125
Table 4-6. Assignments of the functional groups of the polymers .....	133
Table 4-8. Elemental analysis results of the polymers* .....	134
Table 4-9. Some mechanical properties of polymers derived from FDCA .....	136
Table 4-10. Water contact angles of polymers derived from FDCA and various diols .....	139

Table 4-11. Decomposition and maximum degradation temperature of polymers.. 144

## List of Figures

Figure 1-1. Yearly oil price 2001-2013 [2].....	24
Figure 1-2. Map of Nigeria showing the 36 states and the Federal Capital Territory [14]. .....	27
Figure 1-3. Crude oil production in Nigeria 1980 – 2012 [15].....	28
Figure 1-4. Nigeria crude oils and condensate export in 2012 [15].....	28
Figure 1-5. Real Growth Rate (%), 2009: first half – 2010 first half [17]. .....	29
Figure 1-6. U.S crude oil imports (East coast) from Nigeria 1993-2013 [15]. .....	30
Figure 1-7. Map of Nigeria showing land use .....	31
Figure 1-8. World’s leading producers of cassava [22]. .....	32
Figure 1-9. Cassava production zones in Nigeria [26].....	33
Figure 1-10. Nigerian Cassava yields 2001-2013 [22] .....	33
Figure 1-11. Experimental sequence.....	35
Figure 2-1. Conversion of biomass into bio-products and energy.....	38
Figure 2-2. Cellulosic Biomass Composition. ....	38
Figure 2-3. Number of publications of bio-based polymers (source: ISI Web of Science) .....	41
Figure 2-4. Schematic classification of bio-based polymers .....	42
Figure 2-5. Cellulose structure .....	43

Figure 2-6. Hydrolysis of cellulose to glucose [78].....	44
Figure 2-7. Structure of chitin, chitosan and cellulose [83].....	46
Figure 2-8. Molecular structure of starch [110].....	48
Figure 2-9. Primary lignin monomer structure [118].....	49
Figure 2-10. Lignin degradation by oxidative pathways [78].....	49
Figure 2-11. Triglyceride generic structure [151].....	56
Figure 2-12. Typical composition of cassava root.....	56
Figure 2-13. Simple process for cassava starch production.....	58
Figure 2-14. Structures of some ionic liquids used in the synthesis of 5-HMF.....	68
Figure 2-15. Monomers derived from furfural [65].....	70
Figure 2-16. Difuran monomers derived from 2-substituted furans [65].....	70
Figure 2-17. A selection of monomers derived from HMF [65].....	71
Figure 2-18. Products of HMF oxidation [239]. .....	72
Figure 2-19. Structural similarity between terephthalic acid and FDCA.....	72
Figure 2-20. Schematic illustration of three different types of polymer clay nanocomposites, reproduced with permission [257]. .....	77
Figure 2-21. Schematic representation of polymer adsorption from solution, reproduced with permission [260]. .....	78
Figure 2-22. Structure of layered silicate reproduced with permission [260].....	83

Figure 2-23. XRD pattern of three types of silicate layers (a) Conventional (b) Intercalated (c) exfoliated nanocomposites reproduced with permission [263].	84
Figure 2-24. TEM micrographs of (a) treated hectorite, (b) thermoplastic-treated hectorite and (c) thermoplastic starch-untreated hectorite nanocomposites reproduced with permission [295].	85
Figure 4-1. XRD patterns of (a) $ZrO_2$ (b) $SO_4^{2-}/ZrO_2$ (M and T designate monoclinic and tetragonal phases)	103
Figure 4-2. 5-HMF yields by solvent extraction method	105
Figure 4-3. Plot of vapour pressure against temperature for 5-HMF [339].	108
Figure 4-4. Plot of $\ln P$ against reciprocal of temperature for 5-HMF [339].	109
Figure 4-5. Dehydration of glucose and fructose in different solid catalysts	111
Figure 4-6. 5-HMF yields in ionic liquids	112
Figure 4-7. Effect of reaction temperature and time on 5-HMF yield	113
Figure 4-8. Effect of catalyst dosage on 5-HMF yield	114
Figure 4-9. Recycling of sulfated zirconia and [BMIM]Cl	114
Figure 4-10. XRD pattern of (a) 5-HMF, MMT and solvent (b) MMT and solvent (c) MMT only	118
Figure 4-11. XRD pattern of (a) FDCA/ MMT/ DMSO (b) MMT and (c) MMT/DMSO	119
Figure 4-12. XRD pattern of: (a) BHMF/Na-MMT and (b) Na-MMT	120

Figure 4-13. XRD pattern of: (a) Organo-MMT and (b) Na-MMT.....	121
Figure 4-14. FT-IR spectra of: (a) Organo-MMT and (b) Na-MMT.....	122
Figure 4-15. <sup>1</sup> H NMR spectra of polyester from FDCA and 1, 4-butanediol in CDCl <sub>3</sub> .....	123
Figure 4-16. <sup>13</sup> C NMR spectra polyester from FDCA and 1, 4-butanediol.....	123
Figure 4-17. FTIR spectrum of PB-2,5-F polymer from FDCA and BD .....	124
Figure 4-18. FTIR spectrum of PB-2,5-F polymer, 1,4-butanediol and FDCA.....	125
Figure 4-19. <sup>1</sup> H and <sup>13</sup> C NMR spectra of PH-2,5-F polymer .....	127
Figure 4-20. <sup>1</sup> H and <sup>13</sup> C NMR spectra of PO-2,5-F polymer .....	129
Figure 4-21. <sup>1</sup> H and <sup>13</sup> C NMR spectra of PBH-2,5-F polymer.....	130
Figure 4-22. FTIR spectra of PH-2,5-F, PO-2,5-F and PBH-2,5-F polymers .....	131
Figure 4-23(a-c). FT-IR spectra of the polymers with their corresponding diols....	133
Figure 4-24. Tensile properties of the four polymers synthesized in this work: (a) Force-extension curve (b) Tensile strength-strain curve.....	135
Figure 4-25. Water contact angle of: (a) PB-2,5-F (b) PH-2,5-F (c) PO-2,5-F and (d) PBH-2,5-F .....	138
Figure 4-26. Hydrophilic and hydrophobic surfaces based on contact angle [372].	138
Figure 4-27. Water contact angle as a function of time of the various polymers ....	140
Figure 4-28. Capacitance of the four polymers derived from FDCA and diols.....	141

Figure 4-29. Dielectric constants of the four polymers derived from FDCA and diols .....	142
Figure 4-30. Water absorption of the polymers derived from FDCA and various diols .....	143
Figure 4-31. TGA traces of polyester from FDCA and various diols at 10°C/min. ....	144
Figure 4-32. DSC traces of: (a) PH-2,5-F / PO-2,5-F and (b) PB-2,5-F / PBH-2,5-F .....	145
Figure 4-33. XRD pattern of: (a) ground (b) unground PB-2,5-F polymer .....	146
Figure 4-34. XRD pattern of polymer-clay nanocomposites (a), clay (b) and polymer (c). .....	147
Figure 4-35. XRD pattern of polymer/clay nanocomposites: (a) melt (b) <i>in situ</i> and (c) solution methods .....	148
Figure 4-36: TEM image of Polymer/clay nanocomposite by the melt processing method .....	149
Figure 4-37. TEM image of PB-2,5-F/Na-MMT nanocomposites by <i>in situ</i> interaction .....	150
Figure 5-1. Vacuum distillation set-up for glucose/fructose dehydration.....	156
Figure 5-2. <sup>1</sup> H NMR spectra of 5-HMF synthesised.....	157
Figure 5-3. <sup>1</sup> H NMR spectra of 5-HMF: (a) commercially sourced and (b) Synthesised .....	158
Figure 5-4. <sup>13</sup> C NMR of synthesised 5-HMF.....	159

Figure 5-5. FT-IR spectra of (a) commercially sourced and (b) synthesized 5-HMF .....	159
Figure 5-6. $^1\text{H}$ NMR of FDCA in DMSO- $d_6$ (500 MHz) .....	160
Figure 5-7. $^{13}\text{C}$ NMR of FDCA in DMSO- $d_6$ (500 MHz) .....	160
Figure 5-8. FT-IR Spectra of prepared FDCA. ....	161
Figure 5-9. $^1\text{H}$ NMR spectra of BHMF in $\text{CDCl}_3$ (300 MHz).....	162
Figure 5-10. $^{13}\text{C}$ NMR spectra of BHMF in $\text{CDCl}_3$ (300 MHz).....	162
Figure 5-11. FT-IR spectra of (a) 5-HMF and (b) BHMF .....	163
Figure 5-12. $^1\text{H}$ NMR spectra of DFD in DMSO- $d_6$ (500 MHz).....	164
Figure 5-13. $^{13}\text{C}$ NMR of DFD in DMSO- $d_6$ (500 MHz).....	164
Figure 5-14. Bragg's Law reflection. The diffracted X-rays exhibit constructive interference when the distance between paths ABC and A'B'C' differs by an integer number of wavelengths ( $\lambda$ ). ....	165
Figure 5-15. Schematic diagram of NMR Spectrometer [383].....	168
Figure 5-16. Schematic diagram of the probe of an NMR spectrometer [383] .....	169
Figure 5-17. Schematic diagram of an FT-IR instrument [384] .....	171
Figure 5-18. A standard output for a polymer from a DSC machine.....	172
Figure 5-19. Alpha Bruker FTIR spectrophotometer.....	175
Figure 5-20. Siemens D500 X-Ray Diffractometer .....	175
Figure 5-21. Netzsch STA 449 F1 Jupiter thermal analyser .....	176

Figure 5-22. Heraeus Biofuge Primo Centrifuge machine ..... 176

# CHAPTER 1: INTRODUCTION

## 1.1 General Introduction

Research on biomass as a source of chemical feedstock has received considerable attention from the academic and industrial communities in recent years in contrast to the obscurity that has prevailed since the 1960s. This is partly because of the changes in mineral oil price. The increase in oil price is mainly a result of new extraction techniques for mineral oil and other global political situations such as trade and exchange rates. These changes could have transformative effects on the chemical and materials industries. For instance, between 2008 and 2009, although the price of oil fell rapidly by around \$33.39 per barrel from a peak of \$94.45, there is an underlying upward trend as revealed in Figure 1-1.

Furthermore, impending developments in control measures to address climate change may also encourage industries to seek independence from fossil fuels and to use biomass resources as alternatives for fossil-derived materials and energy in order to reduce the embodied carbon content. Isotopic assay can be used to distinguish mineral and biomass oil sources [1]. Again, the use of agricultural biomass as raw material realigns industrial and agricultural sectors for the establishment of an integrated-sector-economy. This would provide new opportunities for countries that depend on fossil fuel resources to diversify their economic-drivers.

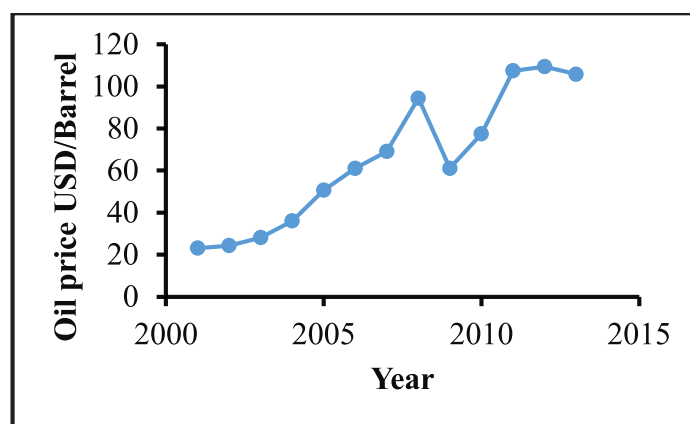


Figure 1-1. Yearly oil price 2001-2013 [2].

The use of fossil fuels for energy and chemicals is a global issue in terms of climate change and economic perspective. It is beyond the scope of this work to address these questions globally and so this thesis focuses on the agricultural opportunities offered by sub-Saharan Africa and more specifically by Nigeria as a nation because of its emerging economy which presently depends largely on its petroleum and natural gas resources despite the huge amount of agricultural resource that is presently under-utilized. Also, Nigeria, as a developing country with a population of over 160 million [3] will be significantly affected by the impacts of climate change even though it is a low carbon emitter. Indeed, the severity will be more pronounced in developing countries especially those in Africa, due to their lower level of coping capabilities and their geographical positions which make them vulnerable to desertification [4] .

Therefore, this research focuses on the production of engineering polymers that begin with cassava. Cassava is a robust plant capable of providing food, fuel and chemical feedstock [5-8]. This work builds upon the substantial emerging interest in the potential business opportunities and government initiatives centred around the exploitation of cassava products in Nigeria and indeed sub-Saharan Africa in general. These potentially open the way for export markets and for the industrial transformation of Nigeria and sub-Saharan Africa.

As part of the introduction to this thesis, the motivation for the work is explained in the context of an assessment of Nigeria and her economic potential. A comprehensive review on the available literature on bio-based polymers and nanocomposites is presented in **Chapter 2**. Details of materials and the methods used are highlighted in **Chapter 3**, while the results and discussion thereof are given in **Chapter 4**. Conclusions are provided in **Chapter 5** along with directions for further work.

## 1.2 Motivation for this research

The motivation of this work was nurtured because of the prevailing economic situation in Nigeria in trying to diversify its economy from dependence on its petroleum products as the main economic driver. Before the discovery of oil in 1970, agriculture was the main economic driver as it played a vital role by engaging both subsistence and full time farmers. However, the role of agriculture is not prioritized at present

because of oil discovery. Agricultural export has tended to be neglected in the Nigerian market [9-11].

Nigeria is one of the leading producers of petroleum in the world. It is one of the members of the Organization of Petroleum Exporting Countries (OPEC) and presently is facing a serious security challenge in the Niger Delta. This is where the country's mineral oil production is located. This could force the oil-producing companies to relocate and this will have a serious effect on the socioeconomic activities of the country. To further add to the motivational factor that encouraged this research, the Governor of the Central Bank of Nigeria, Mr. Sanusi Lamido Sanusi [12] made the following remarks recently about Nigeria at the TEDxYouth platform in Maitama, Abuja:

*“A country that specializes in exporting what it does not produce and importing that which it produces”.*

*“One of the world's largest producer of crude oil that does not refine its own petroleum products and has to import petroleum products”.*

*“The world's largest producer of cassava but does not produce starch or ethanol”.*

*“A large tomato belt, yet the world's largest importer of tomato paste”.*

It is against this background that the thesis envisages an integrated-sector-economy for Nigeria in which its economic future is re-established around agricultural potential paving the way for farmers to produce more agricultural products and investors to have the opportunity of establishing polymer/materials industries that can utilize the agricultural products particularly cassava, a unique plant providing food, fuel and materials. The thesis explains its use for the synthesis of bio-based polymers for materials application.

### **1.2.1 Nigeria: the background**

Nigeria is located in western Africa on the Gulf of Guinea and lies between latitude 4° and 14°N and longitude 2° 45 and 14° 3E. It has a total area of 923,768 km<sup>2</sup>, making it the world's 32nd-largest country [13]. The country shares about 4047 km border with

Benin (773 km), Niger (1497 km), Chad (87 km), and Cameroon (1690 km), and has a coastline of at least 853 km.



Figure 1-2. Map of Nigeria showing the 36 states and the Federal Capital Territory [14].

### 1.2.2 Crude oil production in Nigeria

Nigeria, as a member of OPEC produces mostly light, sweet (low sulfur) crude oil and exports to the global markets. Production of crude oil in Nigeria between 1980 and 2012 as represented in Figure 1-3 revealed a maximum production of crude oil in 2005 with a production capacity of  $4.84 \text{ m}^3/\text{s}$  ( $2.63 \times 10^6$  barrels per day) [15]. However, this began to decline significantly as violence from militant groups surged, forcing many companies to withdraw staff and shut down production. By 2009 crude oil production had reached about  $4.07 \text{ m}^3/\text{s}$  ( $2.21 \times 10^6$  barrels per day). Furthermore, lack of transparency in oil revenue, tension over revenue distribution and environmental degradation due to oil spillage have created a fragile situation in the oil producing states.

In order to provide a conducive atmosphere for increased production, an amnesty was granted to militants in the Niger Delta region in late 2009 and an agreement was reached whereby the militants handed in their weapons in exchange for cash payments and training opportunities. This has provided a relatively calm situation in the region:

reduction in attacks on oil facilities was witnessed and production was partially increased as can be seen in Figure 1-3.

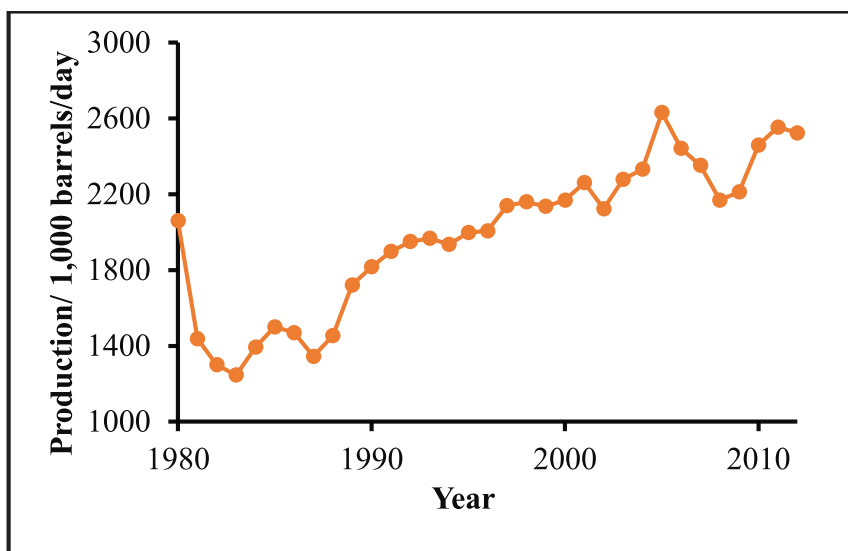


Figure 1-3. Crude oil production in Nigeria 1980 – 2012 [15].

### 1.2.3 Crude oil Export from Nigeria

As a member of OPEC, Nigeria exports her crude oil to the global markets at between 4.07 m<sup>3</sup>/s to 4.23 m<sup>3</sup>/s (2.21 x 10<sup>6</sup> barrels per day to 2.3 x 10<sup>6</sup> barrels per day) of crude oil and condensate products in 2012 [15]. In the same year, the United States imported about 406,000 billion barrels per day from Nigeria which accounted for 18% of the total exports. India, Brazil, Spain and the Netherlands made up the remaining countries that import crude oil from Nigeria. This is represented in Figure 1-4.

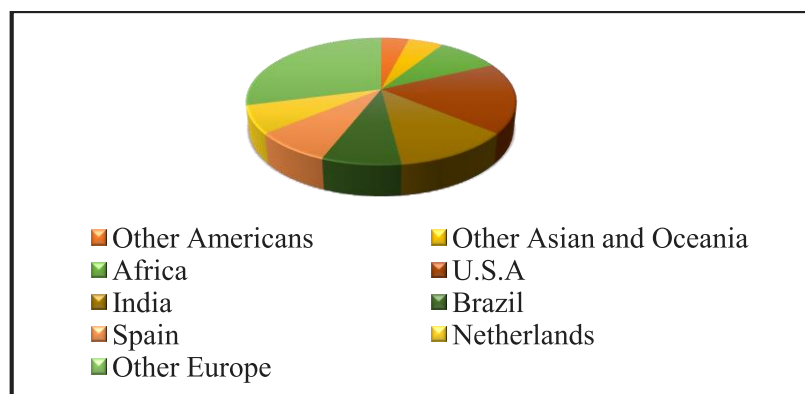


Figure 1-4. Nigeria crude oils and condensate export in 2012 [15].

### 1.2.4 The Nigerian Economy

Nigeria is a middle-income nation with developed financial, communication and transport sectors. The country's economy is one of the most developed economies in Africa because it has the second largest stock exchange in the continent [16].

During the first half of 2010, the economy recorded a slight improvement against the previous year. For instance, Real Gross Domestic Product (GDP) was N334.74 billion (\$2.069 billion) representing a rise of 7.53%, and 1.26% increase over the same period in 2009 as shown in Figure 1-5. The Gross Domestic Product (GDP) of the country as at 31st December, 2010 was \$369.8 billion.

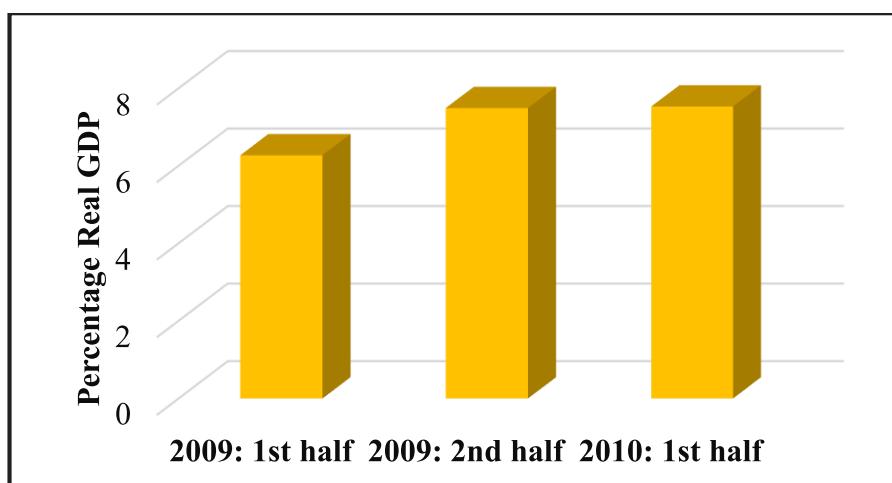


Figure 1-5. Real Growth Rate (%), 2009: first half – 2010 first half [17].

Although much has been made of its status as a major exporter of oil, Nigeria's proven oil reserve was  $37.14 \times 10^9$  barrels ( $5.9 \times 10^9 \text{ m}^3$ ) and a natural gas reserves of  $5.295 \times 10^{12} \text{ m}^3$ , making the country's gas reserves the seventh largest in the world [18], yet it produces only about 2.75% of the world's supply [15]. Although it is ranked as 15th in production at  $4.07 \text{ m}^3/\text{s}$  ( $2.21 \times 10^6$  barrels per day) putting the life index of the oil at 46 years, this implies its main export capability has a limited future.

Furthermore, the United States imported crude oil from Nigeria as one of its major supplier. U.S imported between 9% and 11% of crude oil from 1993 to 2013. However, from Figure 1-6, it was observed that in 2012, there was a drastic decline in crude oil

importation from Nigeria by U.S which fell to an average of 5% and by 2013, it dropped to about 4%. As a result, Nigeria has fallen from being the fifth largest foreign oil supplier to the United States in 2011 to eighth in 2013 [15]. This will definitely affect the country's socioeconomic activities if this trend continues.

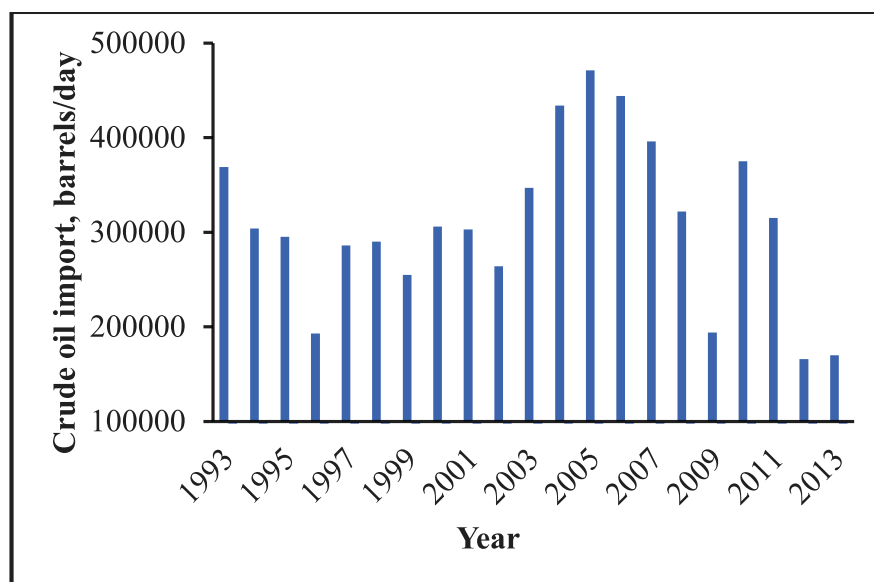


Figure 1-6. U.S crude oil imports (East coast) from Nigeria 1993-2013 [15].

### 1.2.5 Nigeria's agricultural potential

Nigerian agriculture is characterized by considerable regional and crop diversity. The sector remained stagnant during the oil boom decade of the 1970s, and this accounted largely for the declining share of its contributions. The trend in the share of agriculture in the GDP shows a substantial variation and long-term decline from 60% in the early 1960s through 48.8% in the 1970s and 22.2% in the 1980s. Unstable and often inappropriate economic policies (of pricing, trade and exchange rate), the relative neglect of the sector and the negative impact of the oil boom were also important factors responsible for the decline in its contributions [19].

On its diversity, Nigerian agriculture features tree and food crops, forestry, livestock and fisheries. In 1993 at 1984 constant factor cost, crops (the major source of food) accounted for about 30% of the Gross Domestic Product (GDP), livestock about 5%, forestry and wildlife about 1.3% and fisheries accounted for 1.2% [20].

## 1.2.6 Land availability

Nigeria has abundant land resources for agricultural purposes. It has a land area of 923,768 km<sup>2</sup> and it is used for several agricultural practices such as grazing, farming and forestry with a land use estimates as shown in Figure 1-7. Rainfall is heaviest in the southern part where the forest and savannah benefit from abundant precipitation and relatively short dry seasons. The crops grown include cassava, yam, cocoyam, and sweet potato. The main commercial product includes cocoa, oil palm, rubber and timber. Cocoa grows mostly in the southwest; oil palm is predominantly in southeast and is numerous in the southern area. Rubber stands are common in south and south-eastern Nigeria, while timber is in the south and southwest.

The northern part of the country experiences dry season of between three to four months. During this season less than 400 mm of rain fall is reported [21]. The region lies in the Sudan savannah and Sahel savannah mostly, where crops such as millet, cowpeas and drought resistant crops like cassava, sorghum, corn rice, cotton and groundnuts are cultivated [19]. Between the arid north and the moist south lies the guinea savannah region. This area produces staples such as sorghum, millet and cowpea in low quantities together with fruits such as orange and mango.

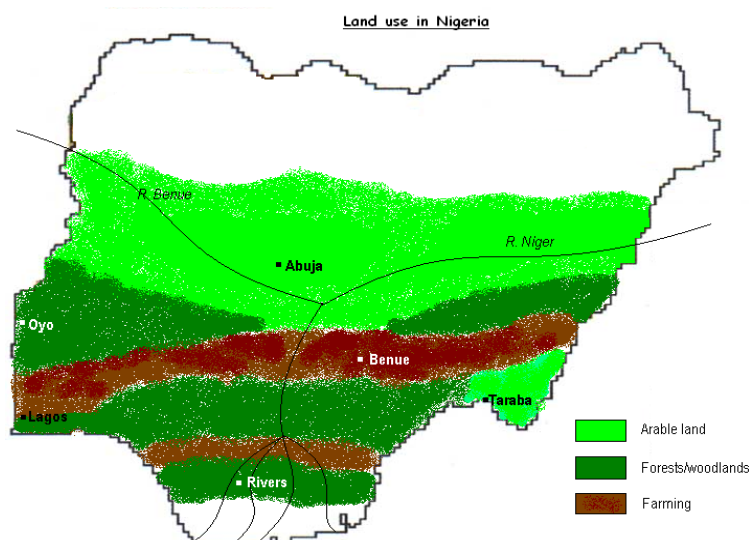


Figure 1-7. Map of Nigeria showing land use

Of all these uses, the highest percentage of land use goes to land used for pastures, forests and woodlands, making up some 56% of general land use. This region stretches

across the South including some eastern and middle belt states and 33% goes to arable land in which crops are planted throughout the year.

### 1.2.7 The place of Cassava in the Nigerian economy

Nigeria is the largest producer of cassava in the world [22] with an estimated area of 3.8 million hectare that is under cultivation and in 2011, the country produced over 50 million tonnes according to Food and Agricultural Organization (FAO) as shown in Figure 1- 8 [22].

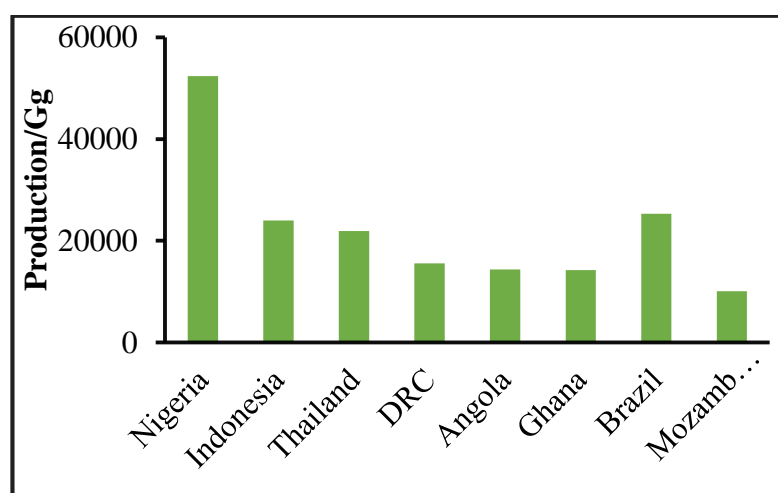


Figure 1-8. World's leading producers of cassava [22].

Cassava is cultivated widely in almost every part of the country as this biomass plays a vital role as food security and can be cultivated under marginal soil conditions as it can withstand prolonged drought and it provides a livelihood for over 30 million farmers all over the country with the southern states providing over 60% as illustrated in Figure 1- 9 [23, 24].

In terms of yield, cassava production in Nigeria has shown a significant yield (Figure 1-10) [22]. For instance, between 2010 and 2012, the yields tends to increase within the years mentioned with the exception of 2005 and 2007 where an outbreak of cassava mosaic disease was experienced. This outbreak was partially eradicated in 2006 which boasts an increased in yield. After this period, a steady increase in the yield was

achieved after some researches on how to overcome the future outbreak of the disease [25].

Therefore, Nigeria has considerable potential to diversify the use of cassava both as a primary industrial raw material and livestock feed. The two main factors that give the country this potential have been the rapid adoption of improved cassava varieties and the development of small-scale processing technologies [25].

In addition, among the many crops widely cultivated in Nigeria, research has probably made the greatest impact on cassava by increase in production over the years and also the area cultivated with production efficiency through the introduction of high yielding, disease- and pest-resistant species.

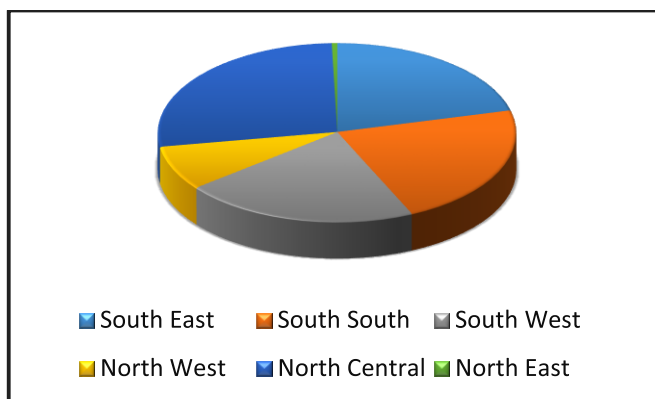


Figure 1-9. Cassava production zones in Nigeria [26].

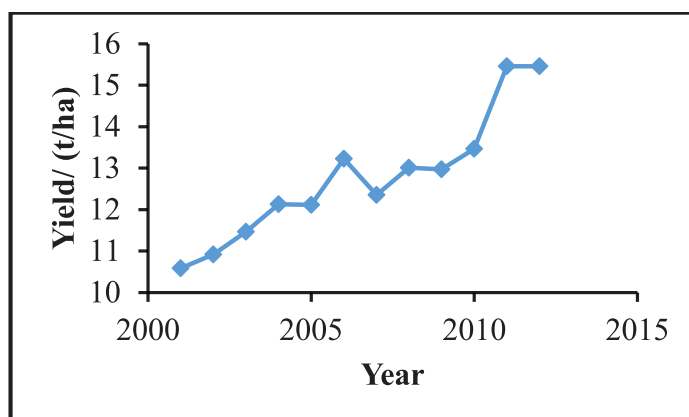


Figure 1-10. Nigerian Cassava yields 2001-2013 [22]

### 1.3 Aims of this research

The aim of this research is to synthesis hydrophobic polymers and nanocomposites for materials applications from biomass obtained from cassava. The stage from cassava to glucose and fructose is well established (Figure 1-11). Therefore, the first investigative step is to synthesise 5-(hydroxymethyl) furan (5-HMF) from glucose using ionic liquid as solvent in a solid catalyst. Next, derivatives of 5-HMF are synthesised to serve as monomers for the polymerisation reaction with commercially available diols. Then a diol is synthesised from 5-HMF and used in place of the mineral oil based diol to form the polyester. The next stage was to study the interaction of the monomers so obtained with potential reinforcement agents, such as montmorillonite clays with a view to making composites by in-situ polymerisation. Such composites should have improved elastic modulus and barrier properties. Subsequently, the interaction of clays with the polymers is studied with the aim of preparing composites based on these biomass polymers by melt or solvent intercalation. The ultimate objective, not fully realised in the timescale of this research, is to find appropriate conditions for polymerisation and reinforcement to prepare nanocomposites with mechanical properties in the range suitable for composite applications in the automotive industry.

This research will pave the way for polymer-clay nanocomposites from cassava as a biomass source in which there is no embedded carbon (depending on the source of energy used in the manufacturing process) and which are therefore largely independent of mineral oil stock and also are environmentally benign. Montmorillonite clay is selected as the reinforcement agent because it has the ability to exfoliate to about 1 nm leading to high aspect ratio reinforcement. Furthermore, this reinforcement is also of low embedded carbon and is cheap

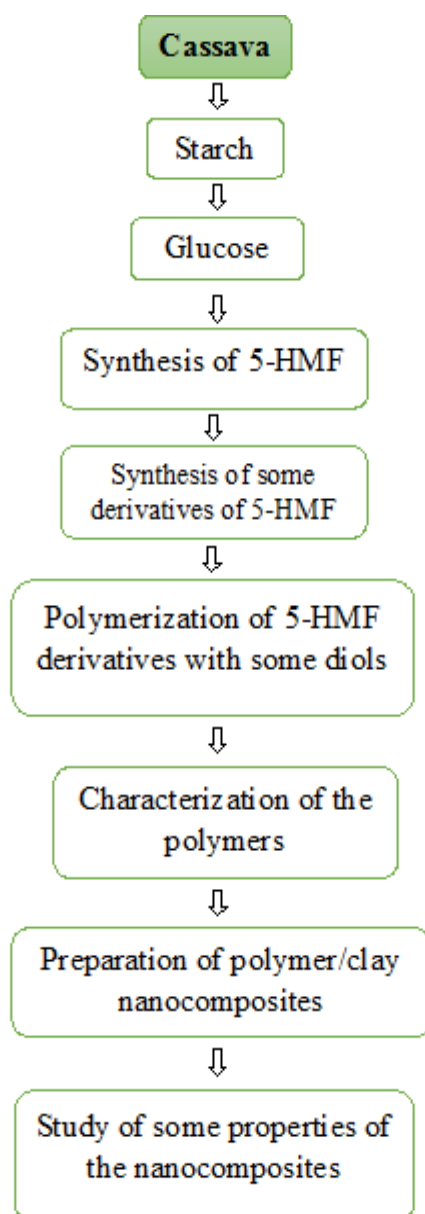


Figure 1-11. Experimental sequence.

The work will use 5-(hydroxymethyl) furan (5-HMF) derived from glucose as the biomass source which has been described as a “sleeping giant” in the field of intermediate chemicals from re-growing resources for the synthesis of various chemicals derived from petroleum source [27]. This will serve as the precursor for the synthesis of 5-HMF derivatives as monomers for the polymer synthesis such as polyesters, polyamides and polyurethanes [28-30]. Another part of the work is the synthesis of 2,5-furandicarboxylic acid (FDCA) from 5-HMF as the bio-based diacid for the synthesis of bio-based polyester as an analogue poly (ethylene terephthalate)

PET derived from petroleum source. In addition, 2,5-bis-(hydroxymethyl) furan (BHMF) as bio-based diols would be synthesised for polymerisation with FDCA.

## CHAPTER 2: LITERATURE REVIEW

### 2.1 Biomass

Biomass can be defined as any plant material that consists mainly of carbon, hydrogen, oxygen and nitrogen [31]. It can also be defined as an organic material that has stored sunlight in the form of chemical energy [32] or a plant material derived from the reaction between CO<sub>2</sub> in the air, water and sunlight, via photosynthesis to produce carbohydrates that form the building blocks of biomass [33]. Biomass has been defined also to be ‘any material, excluding fossil fuel, which was a living organism that can be used as a fuel either directly or after a conversion process.

Conversion of biomass into bio-products and energy involves a series of feed streams that are interconnected as illustrated in Figure 2-1. These operations can make use of various technologies such as chemical, biological and mechanical processes to produce chemical intermediates that are environmentally benign and renewable. By preparing for these technologies now, a company or country can anticipate a world market increasingly regulated by environmental standards and can hedge against increases in oil price that make the petrochemical market uncompetitive.

Therefore, production of high-value chemicals from biomass can become an economic driver for countries that currently depend solely on fossil fuels for revenue. This is likely to lead to profitable ventures to meet energy and chemical demands for these countries.

### 2.2 Biomass resources and their composition

Biomass resources include wood, crops (energy and agricultural), wastes (animal and plants) and seed oils [34]. The most abundant extracted feeds of biomass are cellulose, hemicelluloses and lignin [34-36]. They are of low cost and adequately available for large scale sustainable production of liquid fuels [36], with various compositions typically as 33%, 28%, and 24% of cellulose, hemicelluloses and lignin respectively. Others such as oil, fibre and starch account for 15% as shown in Figure 2-2. This lingo-

cellulosic biomass can also be converted to bio-oil through fast pyrolysis in the absence of air at atmospheric pressure and temperatures of 450-550 °C [37].

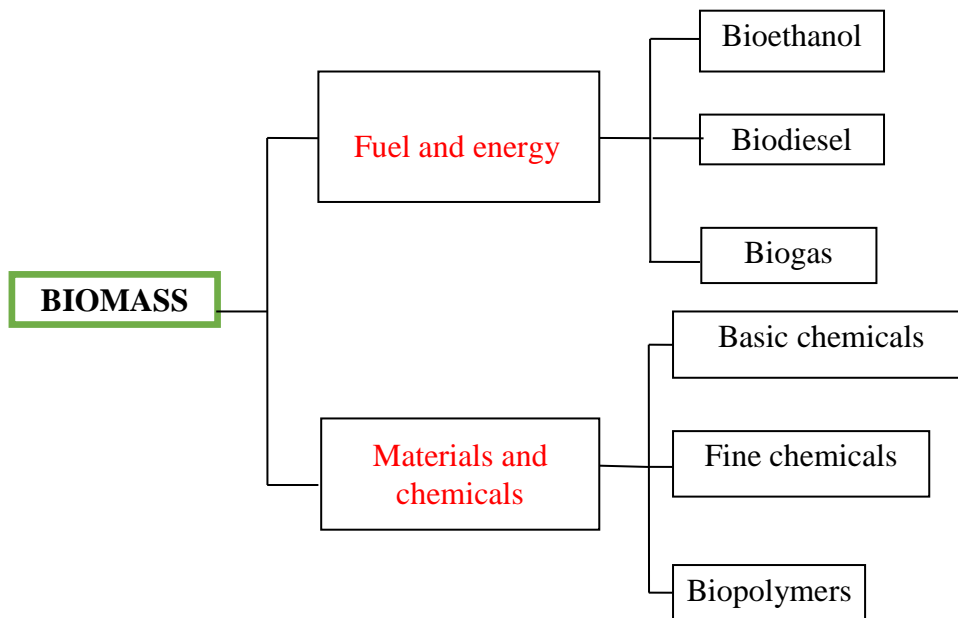


Figure 2-1. Conversion of biomass into bio-products and energy.

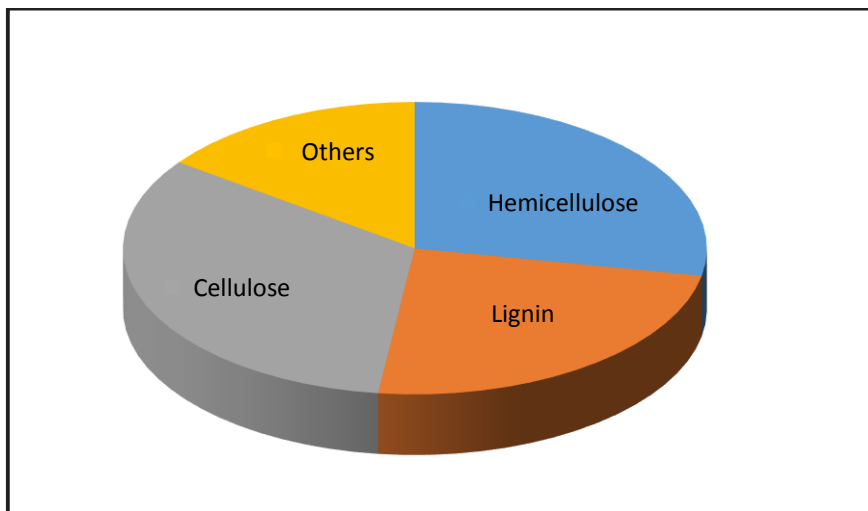


Figure 2-2. Cellulosic Biomass Composition.

## 2.3 Chemicals from biomass

Petroleum and natural gas are currently the main raw materials for the production of about 95% of the world's chemicals. Predominantly, various chemicals such as ethylene, propylene, butadiene, butanes, benzenes etc. are derived from crude oil. These chemicals could be used as end-products, monomers for the polymer industries or as precursors for the production of chemicals for other applications. However, price fluctuations of these materials in the global markets and the effect of the emission of greenhouse gases to global climate coupled with increased public awareness of these effects, has renewed interest the search for an alternative to chemicals derived from fossil resources [38-41]. In this respect, biomass, which is widespread, inexpensive and abundant is considered as an ideal replacement for fossil resources [42-44].

### 2.3.1 Carbohydrates

Carbohydrates are the predominant raw materials for the present day biorefineries [45] which account for 75% of the  $1.7 \times 10^{14}$  kg of plant biomass harvested yearly [46, 47]. These carbohydrates can be broken-down into various monomers through enzymatic hydrolysis, thermochemical degradation or a combination of these two. The major components of carbohydrates, cellulose and hemicellulose play major roles as the structural components of plant tissues and plant cell walls and these constitute the major biomass-based precursors for chemicals that can be suitable for conversion into more valuable chemicals and polymers [48-50].

### 2.3.2 Chemicals produced from saccharides

Glucose is the most abundant monosaccharide in nature that can be derived from cellulose, starch and hemicellulose and used in production of various chemicals via bioconversion and chemical modification. It can be used to produce bio-based acids and ketoacids via oxidation to synthesis D-gluconic acid which are widely used in pharmaceutical and food industries as a complexing or acidifying agents [51].

On an industrial scale, glucose is produced by the enzymatic hydrolysis of starch derived from cassava, corn, wheat and potato [52] with an annual production of over

15 million tonnes globally. It can also be obtained from lignocellulose materials via hydrolysis of the cellulose components for the synthesis of bio-based chemicals such as bioethanol, citric acid, lactic acids and 1,3-propanediol [53].

Several known processes for the conversion of carbohydrates into energy and liquid fuels have been in existence for decades. For instance, liquefaction or pyrolysis of biomass leads to formation of bio-oils [54], Fischer-Tropsch synthesis has been employed for the production of alkanes or methanol from biomass-derived CO: H<sub>2</sub> gas and the production of aromatic hydrocarbons via the conversion of sugars or methanol was reported using zeolites as catalysts [55, 56]. However, the most widely used process for producing liquid fuels from biomass is the conversion of glucose to ethanol [57].

### 2.3.3 Bio-based polymers

Bio-based polymers are defined as materials that are produced from renewable resources [58] [59, 60]. Also, the term *biopolymers* generally refers to naturally occurring long-chain materials such as proteins and carbohydrates or materials that can be prepared synthetically such as poly (lactic acid) or from bio-based monomers [61, 62]. Hence, they are referred to as *natural polymers* because their synthesis generally involves enzyme-catalyzed, chain growth polymerization reactions of activated monomers, which are typically formed within cells by complex metabolic processes [63].

These polymers have continued to draw increased interest from the scientific community in recent years. For instance, according to a recent survey of publications from the ISI Web of Science (Figure 2-3), this renewed interest is evidenced by the number of publications per year. These polymers reduce dependence on fossil fuels for materials applications and ameliorate environmental impacts by reducing carbon dioxide emissions and price fluctuations that are associated with fossil fuels [64-67].

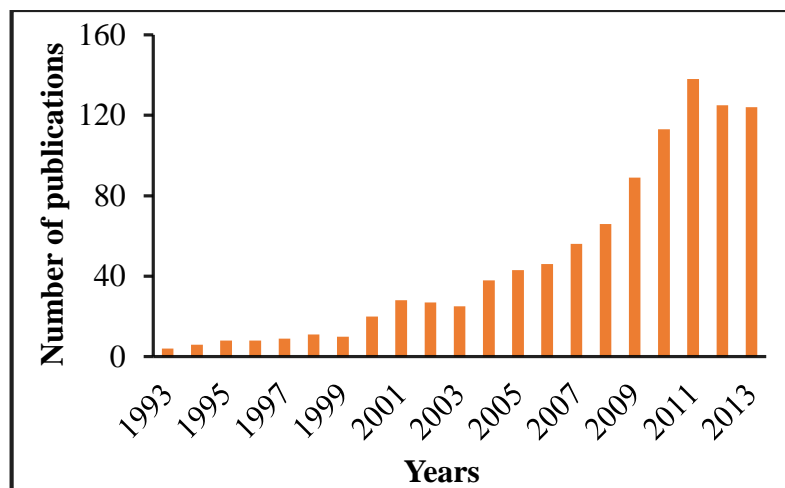


Figure 2-3. Number of publications of bio-based polymers (source: ISI Web of Science)

For these reasons, there is a motive to replace the petroleum-derived raw materials with renewable-based materials for polymer production and based on a recent study, it was predicted that the worldwide production capacity of bio-based plastics will increased from  $3.6 \times 10^8$  kg in 2007 to  $23.2 \times 10^8$  kg in 2013 and  $34.6 \times 10^8$  kg by 2020 [68].

### 2.3.4 Classification of bio-based polymers

Bio-based materials have been generally classified into three groups [59]. These are: (a) those derived directly from biomass, examples are polysaccharides such as cellulose, chitin, starch, lignin and proteins, (b) those produced by chemical synthesis of bio-derived monomers such as poly (lactic acid) and (c) those from microorganisms such as polyhydroxyalkanoates (PHAs) and polyhydroxybutyrates (PHBs). The schematic classification is presented in Figure 2-4.

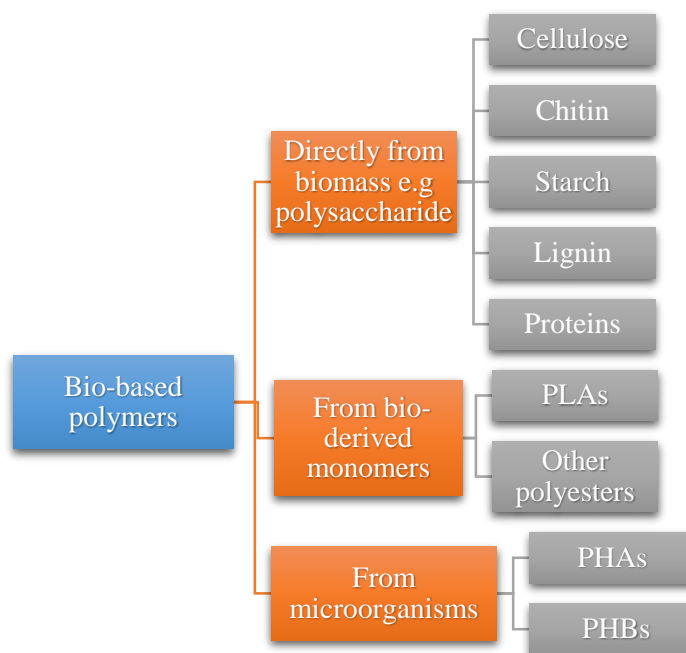


Figure 2-4. Schematic classification of bio-based polymers

### 2.3.5 Bio-based polymers derived directly from biomass

Bio-based polymers derived directly from biomass are generally polysaccharides which are carbohydrates formed through the condensation of monosaccharide residues by hemi-acetal or hemi-ketal linkages. They can also be found as a short oligosaccharide sequence or polymeric repeat units linked to other biopolymers and serve as energy storage, structural and protective components, and for gel formation depending on their specific chemical structure, composition, molecular weight and ionic character [69]. The major classes of polysaccharides are starches, celluloses and chitin which constitutes the bulk of polymers directly derived from biomass and are used in food and non-food industries due to their functional diversities [69].

Although they are naturally obtained directly from biomass, they generally need to have a bulk or surface modification chemically on the hydroxyl groups in their structure to pave the way for their application as biopolymers. In terms of bulk modification, some derivatives of these polymers are also desirable: an example of such a process is the formation of chitosan and the chemical modification involves the compatibility and minimization of the hydrophilicity of natural fibres between the fibres and the matrix [64]. Therefore, polysaccharides are generally modified for used

as biopolymers by reducing their hydrophilicity; achieved by lowering their surface energy or creating enough surface morphology in order to obtain a water contact angle higher than 90° [64, 66, 70].

### 2.3.5.1 Cellulose

Cellulose is the most abundant and widespread biopolymer on earth and its macroscopic morphology occurs in the form of fibres [71]. It is produced by plants, bacteria, algae and fungi by biosynthesis. Bacterial cellulose, with a degree of polymerization of 2000-8000 is an example of an extracellular polysaccharide that is produced by several microorganisms. This class of biopolymer is produced as a three-dimensional network of highly crystalline nano- and microfibrils having 10 – 100 nm diameter as revealed in Figure 2-5 below and unique physical and mechanical properties that makes it a very promising material for a wide range of applications. Cellulose is also characterised by its poor solubility as a result of the strong intra- and inter- molecular bonds of the hydrogens within its structure. It exhibits a chemical reactivity that is affected by its morphology and degree of crystallinity which varies according to its origin and pre-treatment [72].

Because of its abundance, biodegradability and specific properties, cellulose is used in paper making, cotton textile, coatings, biodegradable plastics and biomaterials [73-75]. It is also used in the form of a fibre for reinforcements as revealed by its macroscopic morphology, replacing glass fibre used in composite materials with thermoplastics or thermosetting polymer materials. Their use in this regard have helped dramatically in cost reduction and density in handling and transportation, recycling, combustion energy recovery and lower fibre abrasion on the processing machines, when compared with glass fibre [64].

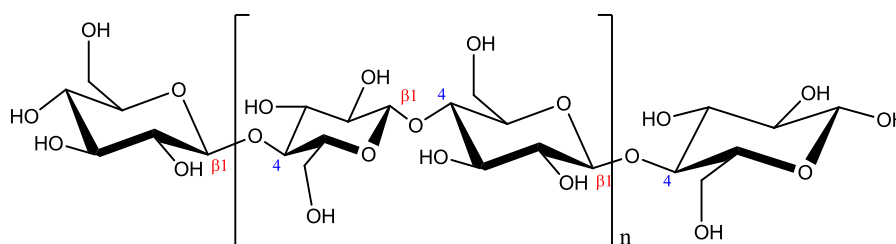


Figure 2-5. Cellulose structure

As a natural bio-based polymer, cellulose can undergo chemical modification to improve the adhesion between the polar OH groups of the cellulose fibre and that of the non-polar polymer matrix to create some sort of covalent bonds between the fibre surface and the polymer matrix which tends to reduce the hydrophilicity and also the moisture absorption of the cellulose fibre [64]. The modification of cellulose leads to formation of various derivatives by altering one or more OH groups of the structure. Some of these derivatives are ethers, esters and acetals which are found commercially [76].

Cellulose, in the form of a cotton fabric was reported to have been chemically modified via two-stage process in order to have an antibacterial properties [77]. The first stage of the modification was the treatment of the cotton fabric with chloroacetyl chloride using a THF/pyridine as a solvent/catalyst system to introduce the chloroacetate groups. The chloroacetylated cotton was treated with potassium salts of a bioactive 1-naphthylacetic acid in the second stage of the process to give a cellulose-1-naphthylacetic acid adduct. The results from these modifications was reported to have some bactericidal activity on *Escherichia coli* and also showed a high degree of hydrophobicity, with a contact angle of more 120° [77].

Cellulose can be converted into glucose through hydrolysis by enzymes such as endo-1,4- $\beta$ -glucanase and exo-1,4- $\beta$ -glucanase which are secreted from fungi, bacteria and protozoans and can catalyse the oxidation reactions of glucose, or lower molecular weight oligomers produced from the hydrolysis reactions [78]. During the hydrolysis, endo-1,4- $\beta$ -glucanase attacks the internal bonds and the exo-1,4- $\beta$ -glucanase attacks the end of the cellulose structure thereby separating the cellulose polymer into two glucose units as represented in Figure 2-6.

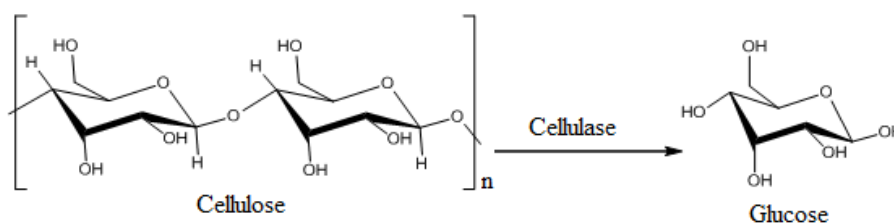


Figure 2-6. Hydrolysis of cellulose to glucose [78].

### 2.3.5.2 Chitin and Chitosan

Chitin is the second most abundant polysaccharide after cellulose that is produced annually by biosynthesis. This biopolymer is a long-chain homopolymer of *N*-acetyl-D-glucosamine (GlcNAc), (1–4)-linked 2-acetamido-2-deoxy- $\beta$ -D-glucan, a derivative of glucose as shown in Figure 2-7. It occurs in nature as ordered crystalline microfibrils forming structural components in exoskeletons of arthropods or in the cell walls of fungi and yeast [79, 80]. It can also be produced by other microorganisms such as insects and worms and is considered as one of the most abundant renewable biopolymers that can be obtained as a cheap renewable biopolymer from marine sources [81].

Chitin may be described as cellulose biomass because of its similarity in structure in that the one hydroxyl group on the monomer structure of cellulose is replaced by an acetylamine group as seen in Figure 2-7. Because of this substitution of the hydroxyl group in cellulose, chitin possesses increased strength resulting from increased hydrogen bonding between the adjacent polymer chains. This makes it a favourable bio-based material for use in surgical thread application where it is biodegradable with time as the wound heals. Furthermore, it is used industrially for the manufacture of separation membranes and ion exchange resins for water purification and as an additive in the pharmaceutical and food industries as a stabilizer [82].

Chitosan on the other hand, is the most important derivative of chitin and is also derived from natural products including the exoskeletons of insects, arthropods such as crustacean shells, prawns, crabs as well as cell walls of fungi [83]. It is made up of linear  $\beta$ -(1→4) glycosidic linkages that are similar to that of cellulose as can be seen in Figure 2-7 that the 2-acetamido-D-glucose and 2-amino-D-glucose units are combined by glycosidic bond. This biopolymer is produced by partial deacetylation (removal of an acetate moiety) of chitin under acidic conditions (concentrated NaOH) or by enzymatic hydrolysis in the presence of chitin deacetylase [84].

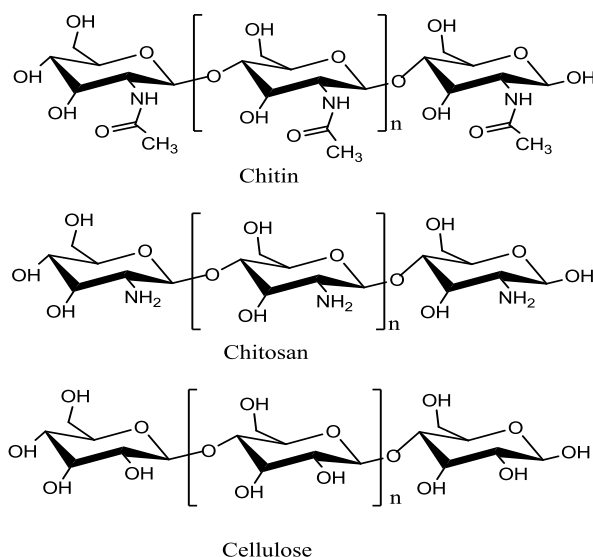


Figure 2-7. Structure of chitin, chitosan and cellulose [83].

Chitin and chitosan can undergo some form of chemical modification for further applications. For instance, based on the structure of chitin, it can be modified at the only two hydroxyl groups present while chitosan at either the hydroxyl group, amino groups or both. These chemical modifications of chitin and chitosan have been reviewed by several authors in recent times [85-87]. For example, chemical modification of some polymers was reported via graft copolymerization reactions and the following polymers were obtained: polyurethanes, poly(2-alkyl-oxazolines), poly(ethylene-glycol), block polyether, poly(ethylene-imine), poly(2-hydroxyalkanoate), poly(dimethylsiloxane) and dendrimer-like hyper branched polymers [88]. Similarly, these chemical modifications can occur as phosphorylated, acylated or alkylated with the formation of Schiff's bases [89], or carboxylates, phthaloylation, silylated, tosylated, sulfated and thiolated [87]. During the chemical modification of chitin and chitosan, the physicochemical and biochemical properties of these bio-based polymers are not altered.

On their degradation, chitin and chitosan can undergo total degradation by chemical, enzymes and by physical methods. The chemical methods involve acid hydrolysis with HCl or oxidation reactions with nitrous acid and hydrogen peroxide. In the enzymatic method, chitin and chitosan are degraded by enzymes such as chitinase, chitosanase, gluconase, proteases, lysozyme, cellulase, lipase and pectinase. In the case of physical degradation, this can be achieved by microwaves, thermal treatments, ultrasound and

ionizing radiation [90]. Furthermore, chitin and chitosan can undergo an *in-vivo* biodegradation that leads to the production of non-toxic oligosaccharides with different chain lengths that are incorporated into the metabolic pathways to give glycosaminoglycan and glycoproteins [78]. Also, the rate of biodegradation depends on the degree of acetylation, distribution of the acetyl group and the chain lengths of the bio-based polymers [78]. It is suggested that fast rates of biodegradation should be avoided if chitin or chitosan are to be considered for medical application. This is to prevent the accumulation of amino sugars which can lead to an inflammatory response [91].

Chitin and chitosan as bio-based polymers are used as food additives, in textile materials, in drug delivery, as antibacterial agents, tissue engineering, treatment of waste water and in metal nanocomposites [90-94]. Chitosan on the other hand has been reported to be moulded as fibres and films [95, 96].

### 2.3.5.3 Starch

Starch is one of the natural polymers that is generated from carbon dioxide and water during photosynthesis in plants [97]. Starch is composed of amylose (poly- $\alpha$ -1,4-D-glucan) and amylopectin (poly- $\alpha$ -1,4-D-glucan and  $\alpha$ -1,6-D-glucan) which is a biodegradable and biocompatible polymer from many renewable sources [98-100].  $\alpha$ -Amylose is a straight chain of glucose molecules joined by  $\alpha$ -1, 4-glycosidic linkages. Amylopectin is similar to amylose except that short chains of glucose molecules branch off from the main chain as shown in Figure 2-8. Starches found in nature are 10-30%  $\alpha$ -amylose and 70-90% amylopectin [101]. Based on these properties, starch has been given attention since the 1970s for the production of starch-based polymers and for other applications [102-104]. It is considered as a prime candidate for the production of bio-based materials that are sustainable because of its complete biodegradation, and low cost [105, 106] and it is found in plant roots, stalks, crop seeds and staple crops such as rice, corn, wheat, tapioca and potato [107].

The main sources of starch worldwide are maize 82%, wheat 8%, potatoes 5% and cassava 5% [108]. From Figure 2-8, it can be seen that starch structure contains many hydroxyl groups at C-2, C-3 and C-5. This suggest that starch can be oxidized or

reduced and also participate in the formation of hydrogen bonds, esters and ether which are mostly the characteristics of alcohols [109].

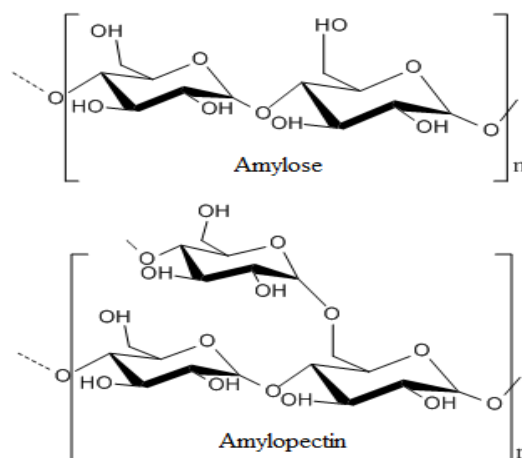


Figure 2-8. Molecular structure of starch [110].

#### 2.3.5.4 Lignin

Lignin is the only renewable source of aromatics, which consists of three basic structural units, *p*-coumaryl alcohol, coniferyl alcohol, and sinapyl alcohol in which the structural unit are connected by ether and C-C bond, as presented in Figure 2-9 [111]. These compounds offer the possibility for the synthesis of value-added renewable products for materials applications because of the presence of the phenolic functional group. For instance, lignin constitutes about 30% by weight and 40% of its biomass value which can be used to increase fuel production [111].

In lignocellulose material, lignin appeared as a matrix that surrounds the cellulosic fibre mostly in herbaceous and soft wood plants [112], with their structures as lamellar macromolecular complexes that link through non-covalent interactions [113]. As with other bio-based polymers, lignin can undergo some chemical modifications in order to be used in polymer synthesis. The modification can be done at the phenolic side or the aliphatic hydroxyl groups for the synthesis of polyesters and polyurethane by the liquefaction process [78]. Polymers synthesized from these monomeric units of lignin are said to have some advantages in terms of their thermal and mechanical properties because of their aromatic character [64].

Lignin, like other bio-based polymers can undergo some forms of biodegradation facilitated by enzymes and by extracellular lignolytic enzymes such as lignin peroxidises, the first lignolytic enzymes isolated from *Phanerochaete chrysosporium* [114] and lactases [115]. In addition to these two enzymes, fungi have also been reported to use the secretion of some metallenzymes such as manganese peroxidases in breaking down lignin [116, 117]. These enzymes oxidize the phenolic compounds and the aryl-ether position of the molecule as illustrated in Figure 2-10 [78].

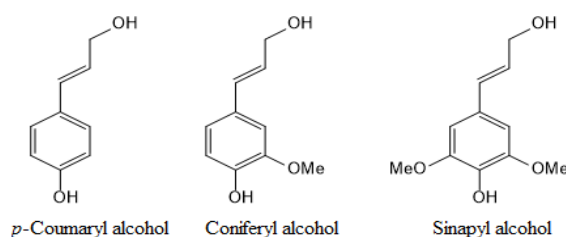


Figure 2-9. Primary lignin monomer structure [118]

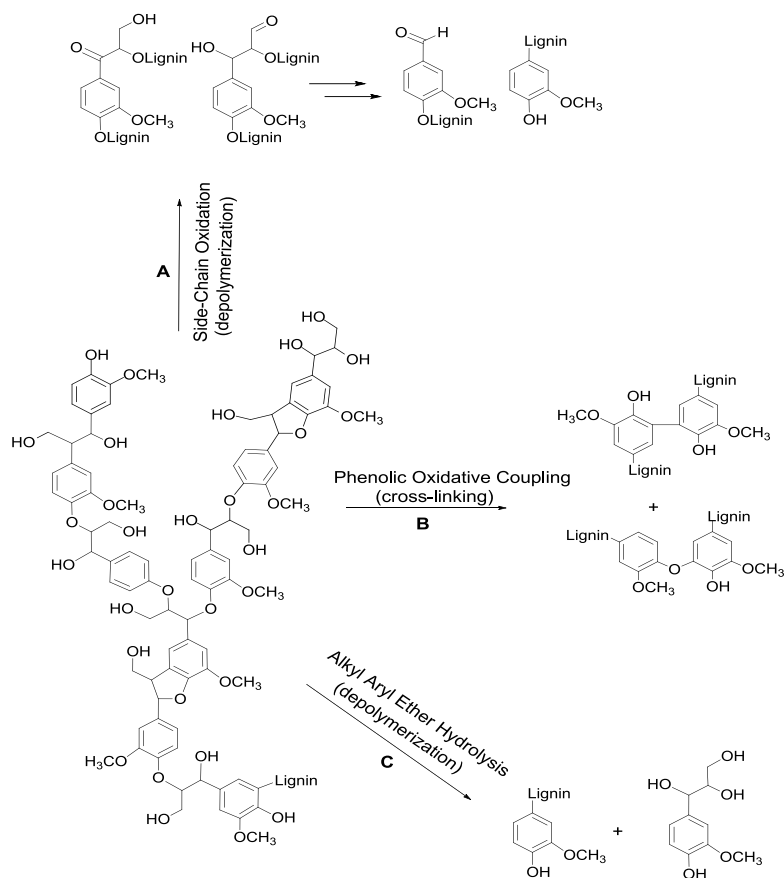


Figure 2-10. Lignin degradation by oxidative pathways [78].

### 2.3.5.5 Proteins

Proteins are copolymers of amino acids that are randomly arranged and classified based on their origins: plant proteins (e.g. soy, pea, canola etc.) and animal proteins (e.g. gelatin, whey casein and keratin). Therefore, bio-based polymers derived from proteins can be defined as a stable 3D polymeric network which is strengthened by hydrophobic interaction and hydrogen bonding [119].

Protein obtained from plants particularly from grains obtained by starch extraction from the grains are often blended with other materials for possible applications in food packaging, preservation and also in automobiles as car dashboards because of their improved water resistance [78]. For the proteins to be applied in materials application, they undergo compression moulding, injection moulding and extrusion [120].

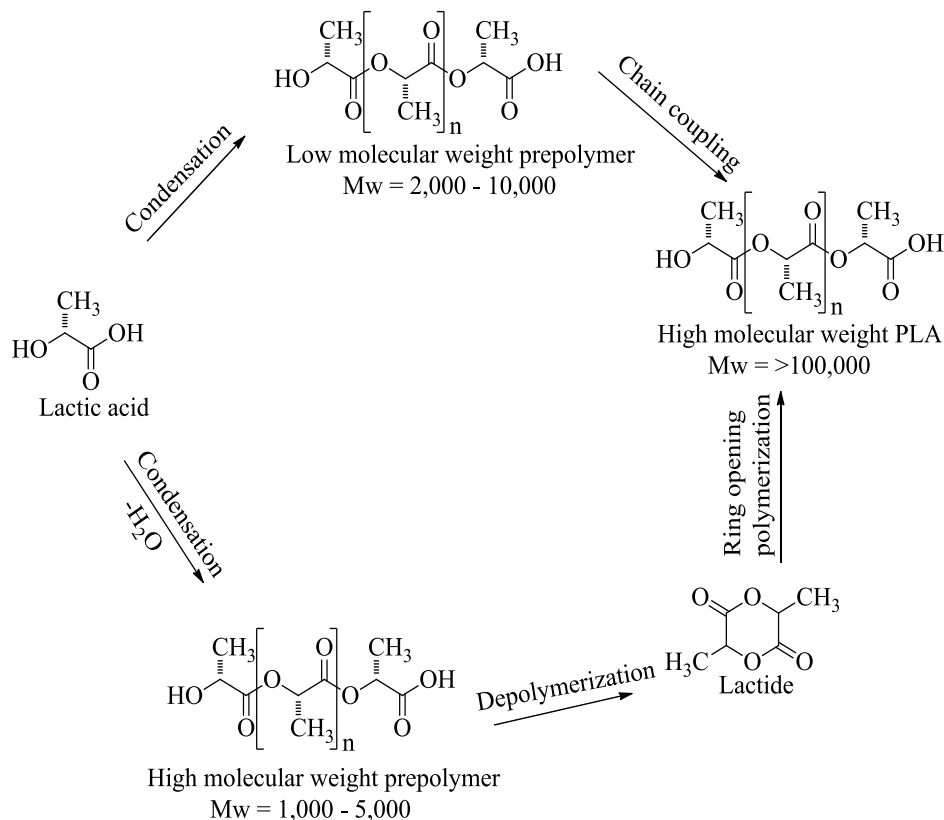
### 2.3.6 Bio-based polymers from chemical synthesis of bio-derived monomers

#### 2.3.6.1 Poly (lactic) acid

PLA, as a bio-based polymer is produced commercially because of its similarities with conventional polymers produced from fossil fuels such as polyethylene terephthalate (PET). Therefore, PLA is considered as a thermoplastic polymer that has the potential to replace polymers such as PET, PS and PCs for packaging, electronics and automobile applications [121]. However, their low thermal properties ( $T_g = 60\text{ }^\circ\text{C}$ ) make PLAs less attractive. Therefore, PLAs are often blended with other polymers changing the stereochemistry of these polymers. This influences the crystallinity of the final polymer and hence, improves the mechanical and thermal properties [122].

PLAs are produced by the polymerisation of lactic acid. The monomer, lactic acid (LA) is a hydroxyl carboxylic acid that is obtained through bacterial fermentation of starch or sugars derived from agricultural biomass and also by chemical processes. Two optical isomers of LA are obtained depending on the bacterial strain used during the fermentation process.

Synthesis of PLA is achieved by either direct polycondensation reaction of lactic acid (LA) or ring opening polymerisation of lactide, a cyclic dimer of the lactic acid (LA) as presented in scheme 2-1 below [123]. However, it was reported that the synthesis of the PLA by the polycondensation reaction is difficult due to the formation of water molecules during the reaction [58].



Scheme 2-1. Synthesis of PLA

In scheme 2-1 above, the synthesis of low-cost continuous process developed by Nature Works LLC for PLA synthesis is presented [124]. The process provides two routes for production, the first producing a low molecular weight pre-polymer of lactide dimers by a condensation process. In the second route, high molecular weight PLA is produced via the catalytic ring opening polymerization of the low-molecular weight pre-polymer earlier prepared by the condensation reaction [125].

These processes provide the opportunity to produce various types of PLA and their corresponding copolymers which depends on the ratio and stereochemical nature of

the monomers. This results in the production of PLAs with final properties based on the ratio of the monomers with an example presented in Table 2-1 [126].

Table 2-1. Glass transition and melting temperature of PLA with various L-monomer copolymer ratio

Copolymer ratio	Glass transition (T <sub>g</sub> ), °C	Melting temperature °C
100:0 (L/DL)-PLA	63	178
95:5 (L/DL)-PLA	59	164
90:10 (L/DL)-PLA	56	150
85:15 (L/DL)-PLA	56	140
80:20 (L/DL)-PLA	56	125

In the global market, PLA is produced under different brand names for various applications in the industrial sectors such as automobile, electronics, medical and commodity uses. The major producers of different grades of PLAs with various ratios of D/L lactide and trade names are listed in Table 2-2 [76].

Table 2-2. Trade names and suppliers of various brands of PLA [76]

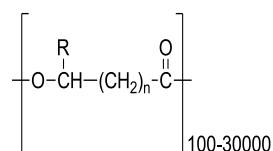
Trade Name	Suppliers	Country
Nature Works <sup>®</sup>	Cargill Dow	USA
Galacid <sup>®</sup>	Galactic	Belgium
Lacty <sup>®</sup>	Shimadzu	Japan
Heplon <sup>®</sup>	Chronopol	USA
CPLA <sup>®</sup>	Dainippon Ink Chem	Japan
Eco plastic <sup>®</sup>	Toyota	Japan
Treofan <sup>®</sup>	Treofan	Netherlands
Ecolaju <sup>®</sup>	Mitsubishi	Japan
Biomer <sup>®</sup> L	Biomer	Germany

## 2.3.7 Bio-based polymers derived from microorganisms

### 2.3.7.1 Polyhydroxyalkanoates (PHAs)

PHAs were first discovered in 1926 as an accumulated polymer within a bacterium named *Bacillus megaterium* [127] and this accumulation occurs in the presence of a carbon source together with a deprivation of some nutrients such as nitrogen [128, 129]. Therefore, these bio-based polyesters have been found in most microorganisms as intracellular granules [130-132] or secreted as extracellular by the microorganisms [127, 133]. Also, these bio-based polymers can be produced in high yields from certain genetically modified plant species [134-136]. Therefore, PHAs have the potential to replace some plastics that are derived from petroleum because they are biodegradable and biocompatible [137].

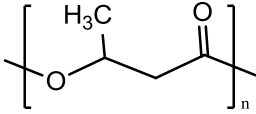
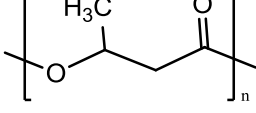
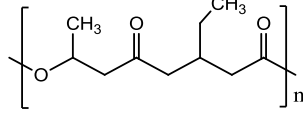
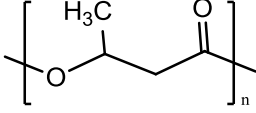
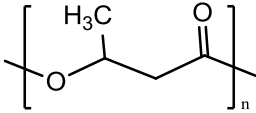
Polyhydroxyalkanoates (PHAs) are bio-based aliphatic polyesters with a general formula as shown in scheme 2-2 below [138] that are produced by numerous microorganisms through bacterial fermentation using several renewable wastes feedstock [60, 139]. Examples of microorganisms used in PHAs synthesis are: microbes such as *Bacillus megaterium*, *Azotobacter*, *Agrobacterium*, *Rhodobacter* and *Sphaerotilium* that are accumulated in the form of granules as energy storage compounds [78]. However, production of PHAs from microorganisms is very expensive as the cost of the carbon source is the main contributing factor to this [122]. Therefore, a cheaper route for their production is the use of genetically modified plants that use atmospheric carbon dioxide and sunlight for the production of PHAs [134, 140]. Table 2.3 illustrates some of the plants that have been used in the synthesis of PHAs via biosynthesis.



n = 1	R = Hydrogen	Poly (-3-hydroxypropionate)
	R = Methyl	Poly (-3-hydroxybutyrate)
	R = Ethyl	Poly (-3-hydroxyvalerate)
	R = Propyl	Poly (-3-hydroxyhexanoate)
	R = Pentyl	Poly (-3-hydroxyoctanoate)
	R = Nonyl	Poly (-3-hydroxydodecanoate)
n = 2	R = Hydrogen	Poly (-4-hydroxybutyrate)
n = 3	R = Hydrogen	Poly (-5-hydroxyvalerate)

Scheme 2-2. The general structure of Polyhydroxyalkanoates [138].

Table 2-3. PHAs biosynthesis in plants [137]

Plant	PHA genes	Product	Yield
<i>Nicotiana tabacum</i>	<i>Acinetobacter sp.</i> Thiolase ( <i>phaA</i> ), synthase ( <i>phaC</i> )	 Poly(3-hydroxybutyrate)	7.3-18.8 % DW in leaf tissue
<i>Nicotiana tabacum</i>	<i>Bacillus megaterium</i> reductase ( <i>phaB</i> )	 Poly(3-hydroxybutyrate)	8.8 % DW in total plant biomass
<i>Elaeis guineensis</i>	<i>bktB</i> , <i>phaB</i> , <i>phaC</i> and <i>tdcB</i>	 Poly(3-hydroxybutyrate-co-3-hydroxyvalerate)	~91.2 %
<i>Panicum virgatum L</i>	<i>PhaA</i> , <i>phaB</i> of <i>R. eutropha</i> hybrid <i>phaC</i>	 Poly(3-hydroxybutyrate)	3.72 % DW in leaf, 1.23 % DW in stalk
<i>A. thalia</i> , <i>Saccarum spp</i>	<i>R. eutropha phaA</i> , <i>phaB phaC</i>	 Poly(3-hydroxybutyrate)	1.6-1.8 % in the leaves.

DW = dry weight

The structure of PHAs have a great influence on their properties with the simplest PHA consisting of a hard and brittle material [141], which makes it very difficult to be manipulated using melt processing machines used for conventional plastics [142].

PHAs are classified into two groups according to the number of carbons on their monomer structure. These are: short chain length (scl-PHA) and medium chain length (mcl-PHA). The scl-PHA contains 3-5 carbon atoms and are synthesised by some bacteria such as *Cuprivadus necator* and *Alcaligenes latus*. The other group, mcl-PHA consists of 6-14 carbon atoms and are synthesised by bacteria such as *Pseudomonas putida* and *Pseudomonas mendocina* [143, 144]. Short chain length PHAs are stiff and brittle in addition to having a high degree of crystallinity while medium chain length PHAs are flexible with low degree of crystallinity, tensile strength and melting points [144]

PHAs can undergo biodegradation into water-soluble oligomers and monomers by lipases and also by microbial depolymerases excreted from various microbes found in the environment [145] and can also undergo thermal degradation as well as nonenzymatic degradation. This makes the PHAs suitable in medical applications, disposable materials and in the production of bottles, films and fibres [144].

## 2.3.8 Other sources of bio-based polymers

### 2.3.8.1 Plant oils

Plant oils such as fatty acids and terpenes have great potential as alternative renewable resources for synthesis of polymers derived from biomass because of their abundance and relatively low price [146, 147]. Furthermore, diverse chemical techniques can lead to their modification for synthesis of various monomers and polymers for material applications [148-150].

Plant oils are made up of triglycerides which are triesters of glycerol with long-chain fatty acids as shown in Figure 2-11. The structure of the fatty acids varies and is dependent on the plant, crop, season and the growing conditions. The glycerides are obtained from the esterification reaction involving glycerol with three fatty acids that

accounts for 95% of the total weight of the triglycerides and their content in each plant oil [151]. The physical and chemical properties of glycerides are generally affected by factors which include: the stereochemistry of the double bonds within the fatty acids structure, the degree of unsaturation of the double bonds and the length of the carbon chains [146].

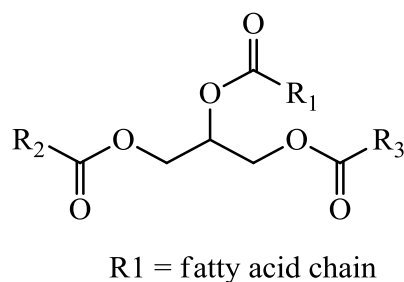


Figure 2-11. Triglyceride generic structure [151].

### 2.3.8.2 Cassava as a biomass source of starch

Cassava (*Manihot esculenta*) is one of the most important sources of biomass starch for the production of wide range of materials as well as being a food crop. Because of its ability to survive drought and conditions of low nutrients, this plant is usually planted in humid tropics [152] by stem cutting and grows to a height of 1 to 3 m with several roots with various compositions as shown in Figure 2-12.

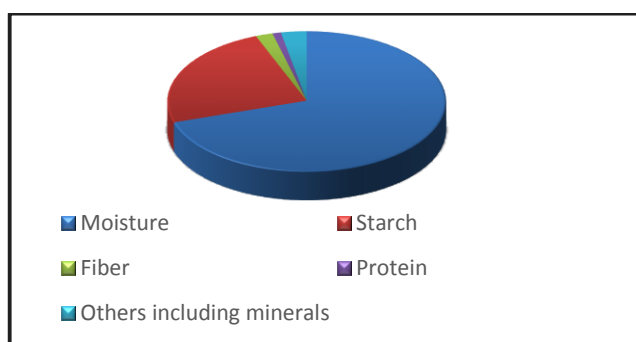


Figure 2-12. Typical composition of cassava root

Among plants that can convert large amounts of solar energy into soluble carbohydrates per unit area cassava ranks highly and can yield 40% starch higher than rice and 25% more than maize. Therefore, it is the cheapest source of energy for human

consumption and animal feed with its production requiring only marginal land for increased agricultural production [153].

### **2.3.8.3 Starch production from cassava**

Cassava is a woody shrub that was introduced by the Portuguese navigators to the African continent around the 17<sup>th</sup> century and flourished as a reliable source of food to the poor [154]. It is cultivated as an annual crop in tropical and sub-tropical regions as a major source of carbohydrate from its starchy roots. The crop is regarded as a major source of staple food in developing countries because it is the third-largest source of food carbohydrate. Because of its drought-tolerance, this crop is capable of growing on marginal soils [153].

Starch is one of the most abundant substances in nature, a renewable resource for use as a raw material for bio-based polymers. As stated earlier, starch is produced from grain or root crops. It is mainly used as food, but is also readily converted chemically, physically, and biologically into many useful products such as food, paper, textiles, adhesives, beverages, confectionery, pharmaceuticals, and building materials. Cassava starch has many remarkable characteristics, including high paste viscosity, high paste clarity, and high freeze-thaw stability, which are advantageous to many industries [155, 156].

The greatest potential of cassava as an agro-industrial crop lies in the production of starch which can generally be produced by the wet milling of fresh cassava roots but in some countries such as Thailand it is produced from dry cassava chips. The wet milling method of starch extraction from fresh cassava roots can be divided into five main stages: preparation (peeling and washing), rasping/pulping/grating, purification (starch washing), dewatering and drying, and finishing (milling and packaging) as shown in Figure 2-13.

In sub-Saharan Africa, these processes of making starch from cassava are subjected to quality control measures to prevent deterioration in the quality of the starch which might otherwise reduce its acceptability for food or pharmaceutical use. This is achieved by adding water to the mash in order to make a thin slurry. The slurry is

sieved, dewatered, and then dried, which may be by sun drying: that is, spreading thin layers of the lumps on concrete floors or raised wooden platforms for 24-120 hours. The possibility of contamination by dirt is high and poor weather extends the chances of spoilage by microbial attack. Therefore, mechanized drying at 50 °C for 6 h is employed to improve the quality of the starch. Sometimes starch is dewatered in a centrifuge or vacuum filter before drying in fluid-bed driers, tray driers, and flash driers. It is then pulverized, sifted, and packaged [157].

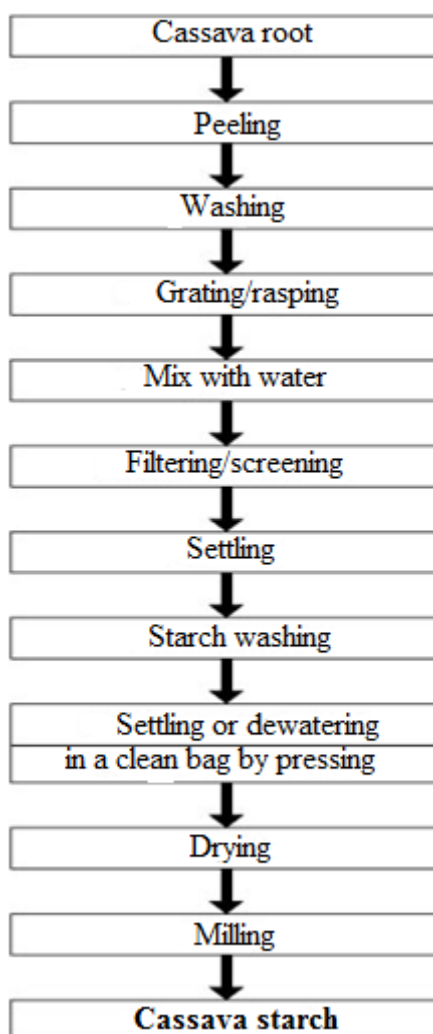


Figure 2-13. Simple process for cassava starch production

Among the chemical precursors that are derived from carbohydrates (fructose and glucose) besides their use in food chemistry are furan derivatives such as furfural and 5-hydroxymethylfuran which are produced as the major products by acid catalysed hydrolysis and dehydration of several abundant biomass carbohydrates [158]. These

can be considered as starting materials for the preparation of polymers to replace those of fossil raw materials [49, 159]. With the recently developed preparation methods, 5-hydroxymethylfurfural is expected to play a vital role in renewable energy and chemical areas, and together with related oxidation product derivatives, 2,5-dicarboxylic acid (FDCA) and 2,5-diformylfuran (DFF) can serve as excellent candidates as monomers for the development of new polymeric materials [160], that can have direct applications in the pharmaceuticals and polymer industries [161, 162].

## **2.4 Production of furan-based aldehyde**

Furan-based aldehydes derived from biomass-based carbohydrates have been produced in recent years and have found a lot of industrial applications. This is because of the availability of cheaper materials, environmentally benign catalysts and solvents used in their preparation in comparison with conventional catalytic conversion systems. The detailed advancements in their production are highlighted below.

### **2.4.1 Furfural production**

#### **2.4.1.1 Furfural from Xylose and xylan as feedstock**

Furfural is generally produced from xylose that is mainly present as xylan in the hemicellulose. Traditionally, furfurals are produced using homogeneous acid catalysts such as HCOOH, CH<sub>3</sub>COOH, HCl, H<sub>2</sub>SO<sub>4</sub>, HNO<sub>3</sub> and H<sub>3</sub>PO<sub>4</sub> in aqueous solution [163-168]. However, these homogeneous acid catalysts have some drawbacks such as being very corrosive and possessing higher environmental risks [169-171]. This prompted the scientific community to proffer some solutions by the use of solid acids, Lewis acids and various solvents that were considered to be cleaner and more environmentally benign. Based on these, dehydration of xylose in water by the use of H-ZSM-5 catalyst was investigated and 46% furfural yield was obtained at 200 °C over 18 min [167]. Similarly, a one-pot conversion of hemicellulose into furfural using K10 and HUSY in aqueous media was conducted [172] and 12% yield at 170 °C for 3 h was obtained. In addition, Sn-beta, MSHS-SO<sub>3</sub>H, graphene, graphene oxide (GO), sulfonated graphene (SG) [173] and sulfonated graphene oxide (SGO) were also

synthesized and used for furfural formation, and yields of 14.3, 43.5, 51, 53, 55 and 62% respectively were achieved [170, 174, 175].

As stated earlier, water was used as a solvent for the synthesis of furfural with a reasonable yield and is considered as the most economical solvent for the synthesis of furfural. However, it can lead to formation of some undesired side reactions that decrease the yields of furfural [176]. Therefore, polar aprotic solvents were subsequently introduced to the production of furfural. Takagaki *et al* [177] showed that a furfural yield of 37% was obtained from xylose in N,N-dimethylformamide (DMF) using Amberlyst-15 with addition of hydrotalcite (HT). When the dehydration of xylose was performed in dimethyl sulfoxide (DMSO) by the use of Nafion 117, 60% furfural yield was achieved [178]. Although polar aprotic solvents have been used in furfural production, they have also been found to inhibit the formation of side-products to some extent, and suffer from the drawback of poor solubility of carbohydrates and the problem of high boiling points, which are unfavourable in the production and separation of furfural [176].

In recently times, mixed solvents consisting of water and toluene or methyl isobutyl ketone (MIBK) in the presence of H-form mordenite were found to be effective for the conversion of xylose into furfural [179]. In these systems, the dehydration reaction takes place in the aqueous phase and furfural is extracted to the organic phase as soon as it is formed [179] and this contributes to reduction of several unwanted secondary reactions and improves furfural yields. Hence, the biphasic systems were further studied by a number of research groups that used various solid acids including ion-exchange resins, zeolites, sulphated metal oxides and supported heteropoly acids, furfural yields ranging from 20.2 to 98% were obtained [180, 181].

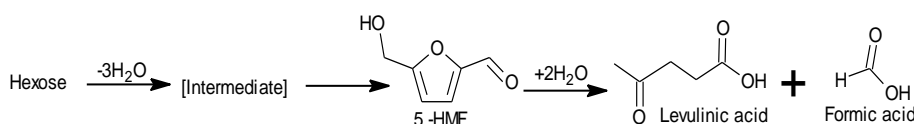
Another acid option for the production of furfural is solid acids. These solid acids are considered an attractive option for the synthesis of furfural because they are less corrosive and can be easily separated and reused [176]. However, solid acids may be gradually deactivated due to the deposition of humins and the loss of active sites after a few reaction cycles, and consequently, require frequent regeneration by calcination and impregnation.

### 2.4.1.2 Production of 5-(hydroxymethyl) furfural (5-HMF)

5-hydroxymethylfurfural (HMF) is a yellow organic compound with a low melting point (30 - 34 °C) that is produced by dehydration of carbohydrates, such as fructose, glucose, sucrose, cellulose and inulin. HMF is regarded as a key building block in biomass-based bio refinery because it can produce a variety of useful derivatives, including 2,5-dimethylfuran, which is a promising biofuel, 2,5-diformylfuran, 2,5-furandicarbaldehyde and 2,5-furandicarboxylic acid [41]

Generally, production of 5-(hydroxymethyl) furfural (5-HMF) is based on the triple dehydration of C<sub>6</sub> sugar (hexose) as shown in scheme 2-3. 5-hydroxymethylfurfural (HMF) is being considered as a key intermediate for chemicals derived from biomass. Its potential has been identified by several authors as biofuel intermediates [59, 182, 183], polymeric materials and fine chemicals [184, 185], pharmaceuticals [162] and solvents [49, 186].

It can also be produced from oligo- and polysaccharides by more complex catalytic systems and reaction media [187, 188]. The dehydration reaction of hexose is usually carried out in the presence of acid catalysts. Efficient yield of HMF is achieved when the dehydration reaction is carried out in a non-aqueous medium rather than in aqueous media. This efficient yield was reported to be attributed to the degradation of HMF to the side reactions such as the formation of levulinic acids [38]. The experimentally observed mechanism for the dehydration of hexose is proposed to consist of a cyclic intermediate [176, 189] and an open-chain mechanism [190] in aqueous and non-aqueous media.



Scheme 2-3. Production of HMF and the corresponding side reaction [162].

## 2.4.2 Catalytic conversion of carbohydrate to 5-HMF

Dehydration of carbohydrate, particularly fructose is known to be catalysed by Bronsted acids and Lewis acids. Catalysts used in the dehydration are classified as mineral acids, solid acids and metal-containing catalysts [162].

### 2.4.2.1 Mineral acids

Mineral acids have been employed widely in studies relating to catalytic conversion of carbohydrates [164] producing yields of 40 - 60% of HMF at 70 - 90% fructose conversion [173]. The most commonly used mineral acids are  $H_2SO_4$ ,  $H_3PO_4$  and  $HCl$  because they are not expensive [191]. However, these homogenous acids have some disadvantages being particular difficult in terms of separation from the reaction mixtures and subsequent recycling. Furthermore they have the possibility of corroding the reaction vessel materials when they are in contact.

Dehydration of D-fructose was reported using  $H_2SO_4$  as catalyst in sub-critical water at 250 °C [27, 189]. The results indicate that 53% yield of HMF was obtained. Similarly, 78% yield was obtained at 180 °C when a sub-critical or supercritical acetone-water mixture was used as the reaction medium [27]. Another mineral acid used in fructose dehydration is  $HCl$  as the catalyst. The acid was used in a two-phase reactor system. In this process, DMSO and poly (1-vinyl-2-pyrrolidinone) (PVP) were employed to suppress the undesired side reactions [162]. Similarly, glucose was reported to be hydrated using mineral acid such as  $H_3PO_4$  at a temperature of 190 °C. The results indicate a low yield of 15.5% and were attributed to the stable ring structure of the glucose [162].

Dehydration of carbohydrate can also be achieved using mineral acids as catalyst in a biphasic reactor system. It was reported that a high yield of 5-HMF (63.3%) was obtained from glucose hydrolysis in a water-butanol biphasic reactor system using  $HCl$  as catalyst [49]. This approach can also be employed to polysaccharides such as sucrose, starch, cellobiose and xylan using mineral acids catalysts [164].

Therefore, it has been established that mineral acids have been employed broadly in dehydration of carbohydrate and found to be effective: 5-HMF was obtained at reasonable yields. However, mineral acids have some drawbacks in terms of separation and recycling as well as material corrosion.

#### 2.4.2.2 Solid acid catalysts

Solid acid catalysts are used because they have some advantages over liquid acid catalysts. Some of these advantages include: their ability to facilitate the separation of products, they can be recycled easily and can work at elevated temperatures, thereby lowering the rate of reactions and favouring the formation of 5-HMF [162].

Recently, dehydration of fructose was carried out using niobic acid as a solid acid catalyst and a stable 5-HMF product was obtained without the formation of side products [192]. The reaction was carried out using water as the solvent because the acid is known to be water-tolerant [193, 194]. Also, hydrated niobium pent oxide ( $\text{Nb}_2\text{O}_5 \cdot n\text{H}_2\text{O}$ ) was reported to have shown high catalytic activity in the dehydration of carbohydrates to 5-HMF [195] and from the results, 74% yield of 5-HMF was obtained. Furthermore, this hydrated niobium oxide is relatively cheap, low toxicity and provides easy handling. Other solid acids used in dehydration of carbohydrates are H-form mordenite [196], vanadyl phosphate [197], ion-exchange resins [162] and sulphated zirconia [198].

Dehydration of carbohydrate was studied using dealuminated H-form mordenite in a solvent mixture of water-methylisobutylketone (MIBK) at 165 °C [196] and the results obtained indicate a 5-HMF yield of 69.2% at 76.0% conversion was accomplished in one hour. The authors further stated that the conversion and selectivity of the 5-HMF depends on both the acidic and structural properties of the catalyst.

Catalytic properties of vanadyl phosphate as a solid catalyst were also reported in the dehydration of D-fructose in aqueous solution and 40.2% yield of 5-HMF was obtained within 30 minutes [197]. Other phosphate-based catalysts like niobium phosphate ( $\text{NbOPO}_4$ ) and phosphoric acid-treated niobium oxide were also used and

delivered 70 - 80% selectivity of 5-HMF at a D-fructose conversion of 30 - 50% in pure water, achieved at 100 °C without any extracting solvent [199].

Fructose dehydration was investigated using acidic ion-exchange resins and 80% yield of 5-HMF was obtained [200]. Similarly, 80 - 90% yield of 5-HMF was obtained using Levitit® SPC-108 and Diaion® PK-216 resins as catalysts [201, 202]. Furthermore, high selectivity of 5-HMF was obtained in the presence of ion-exchange resin catalyst and DMSO as the solvent medium. From the results obtained in DMSO, 90% yield of 5-HMF was reported while 80% yield was obtained in water as the reaction medium. This suggests that both DMSO and water as solvents can effectively give 5-HMF in high yield. In addition, DMSO is a dipolar aprotic solvent and can prevent the formation of side products; however, separation of the solvent (DMSO) and 5-HMF remained a major challenge [162]. Amberlyst-15 is also used as catalyst in the dehydration reaction of fructose. This catalyst was in various ionic liquids and 5% yield of 5-HMF was obtained at 80 °C in 1-butyl-3-methylimidazolium tetrafluorophosphate and closed to 80% in the same ionic liquid (1-butyl-3-methylimidazolium hexafluorophosphates) in a micro batched reactor [203]. Also, Ilgen *et al.* [186] reported a 40% yield of 5-HMF using Amberlyst-15 catalyst in a cholin chloride (ChCl)/D-fructose system.

### 2.4.2.3 Sulfated zirconia as a solid catalyst

The use of liquid acid catalysts is very important in commercial and industrial applications. However, the uses of these liquid catalysts have some safety and environmental drawbacks such as toxicity, corrosion, pollution, separation of products, and problems associated with storage, disposal, transportation and handling. Therefore, replacing those acids with more environmentally benign solid catalysts is desirable to overcome these environmental and safety drawbacks. Among these solid catalysts, sulfated zirconia has attracted much attention since it exhibited a promising catalytic activity in many reactions such as isomerization, hydrocracking, alkylation, condensations, and oligomerizations [204]. The use of sulfated zirconia as a solid catalyst was first reported by Arata *et al.* [205] used in *n*-butane isomerization at moderate temperatures. The results showed that the reaction mechanism involved the formation of carbenium ions via protonation of the alkane, and this demonstrated the

super acidity of sulfated zirconia. However, catalytic activity of sulfated zirconia is not only affected by acid strength alone, but also the type of the acid sites, Brønsted and Lewis acid sites, plays an important role in determining the catalytic properties.

It is generally accepted that the essential properties of sulfated zirconia, such as the acid strength, the nature of the Lewis and Brønsted acid sites, and catalytic properties, are strongly influenced by the method of preparation, nature of the starting materials, types of sulfating agent, and thermal treatment [206]. Conventional sulfated zirconia is generally synthesized by two step methods [207, 208]. In the first step, zirconium hydroxide is prepared by hydrolysis of an aqueous solution of a zirconium salt. The second step involves treatment of the zirconium hydroxide with a suitable sulfating agent to form strong acid zirconia upon pyrolysis. An alternative one step preparation procedure has also been developed for the synthesis of sulfated zirconia. In the one step method, alcogel is formed by mixing the zirconium alkoxide, usually zirconium propoxide, in alcohol with nitric acid in the presence of sulfuric acid. The alcohol is then dried to form aerogel which in turn forms sulfated zirconia when calcined at high temperature [209]. These methods are affected by the type of hydrolysing and precipitation agents, pH of the solution, type of the zirconium precursor, sulfating agents, and finally the drying and calcination procedures. Typical sulfating agents reported in the literature are  $\text{H}_2\text{SO}_4$ ,  $(\text{NH}_4)_2\text{SO}_4$ ,  $\text{SO}_2$ ,  $\text{H}_2\text{S}$ , and  $\text{SO}_2\text{Cl}_2$ , and typical zirconium precursors are zirconium chloride, zirconium nitrate, zirconium isopropoxide, and zirconium oxychloride [210].

Recently, production of 5-HMF catalyzed by  $\text{TiO}_2$  and  $\text{ZrO}_2$  was examined under microwave irradiation [211, 212]. In these approaches, 38.5% yield was obtained using  $\text{TiO}_2$  with D-fructose conversion of 83.6% and 30.5% yield at 65% conversion using  $\text{ZrO}_2$  all at 5 minutes reaction time. Sulfated zirconia was impregnated with  $\text{H}_2\text{SO}_4$  used in dehydration of fructose as catalyst [199, 213]. From the results obtained, 72.8% yield of 5-HMF was reported at 180 °C at 93.6% fructose conversion in acetone-DMSO solvent mixtures. This suggests that sulfated zirconia is an effective solid catalyst that can catalyse fructose in non-aqueous solvents.

#### 2.4.2.4 Metal-Containing catalysts

Transition metal elements have found applications in dehydration of D-fructose as far back as the 1960s [162]. 5-HMF was prepared using thorium and zirconium metals as catalysts [162]. Similarly, lanthanide (III) ions were reported to catalyse the dehydration of six carbon sugars in aqueous media at 140 °C without the formation of side reactions [214] and also dehydration of D-glucose to 5-HMF was catalyzed by lanthanide (III) ions, but the 5-HMF was observed to be decomposed further in the reaction [215].

Several authors have recently reported some remarkable achievements in metal catalyzed reactions in carbohydrate dehydration to 5-HMF. Zhao et al. [216] reported that metal halides particularly, chromium chloride can effectively catalyse D-fructose and D-glucose in ionic liquids. From their findings, 70% yield of 5-HMF was obtained from D-fructose and glucose using  $\text{CrCl}_2$  as catalyst in 1-ethyl-3-methylimidazolium chloride (BMIMCl) [217]. In a similar report, Igen et al. [186] obtained 60% yield of 5-HMF from fructose using  $\text{CrCl}_3$  catalyst in a medium consisting of  $\text{ChCl}$  and 50wt. % of the fructose substrate. Furthermore, 55% yield of 5-HMF was obtained in a single-step conversion of cellulose components catalyzed by metal chlorides basically  $\text{CuCl}_2$  and  $\text{CrCl}_2$  in 1-ethyl-3-methylimidazolium chloride (EMIMCl) [217] [218] and 89% conversion of cellulose was achieved in EMIMCl-water mixture [217] [219].

From these studies, it can be seen that metal-containing catalysts can be applied effectively in the dehydration reaction of hexose sugars for the synthesis of 5-HMF.

#### 2.4.2.5 Other catalysts

Presently, ionic liquids are applied in the synthesis of bio-based materials because they are stable, have low vapour pressure and can be recycled [220, 221]. These ionic liquids can serve as catalysts as well as solvents in green chemistry [222]. For instance, a 74.8% yield of 5-HMF was obtained from fructose dehydration at 90 °C using N-methyl-morpholinium methyl sulphonate as catalyst under a nitrogen atmosphere [223]. Also, 88% yield of 5-HMF was reported using 1-ethyl-3-methylimidazolium hydrogen sulphate as catalyst at 30 min in MIKB as co-solvent [223]. Therefore, their

use has been explored extensively in the dehydration of sugars mostly in the presence of metal chlorides and acidic resins [216, 224].

### 2.4.3 Solvents used in production of 5-HMF

Solvents that are commonly used in the dehydration of hexose are dimethylsulphoxide (DMSO), n-butanol, acetone, dioxane, polyglycol ether and dimethylformamide (DMF) [190]. Water is also considered as a possible solvent based on economic and environmental perspectives and recently was applied as a reaction medium in the dehydration reaction of fructose over a niobic acid catalyst without the formation of any side-reactions [192]. Among these solvents, dimethylsulphoxide (DMSO) has been reported many times as the most widely used in carbohydrate dehydration reactions. It was reported that dehydration of fructose to HMF with DMSO as solvent was found to be possible without a catalyst [225]. However, product separation and reactant solubility using this solvent has been identified as its major disadvantage. In addition, economic feasibility and environmental impact of using these non-aqueous solvents in HMF production on a large scale is also a challenge [189]. In order to overcome these challenges facing solubility of the products, mixed solvents such as water - organic systems are used because non-aqueous solvents are often partially miscible with water and therefore, they can serve as phase modifiers of the aqueous medium [226].

In summary, the solvents mentioned above have been reported to be used as reaction media in hexose dehydration by several authors. HMF can be decomposed to levulinic and formic acids by taking up two molecules of water under acidic, hence this may affect the HMF yield and separation of HMF from levulinic acid tends to be difficult [227]. Therefore, the presence of water should be avoided if one is to obtain HMF in high yield in acid catalysed dehydration of hexose.

#### 2.4.3.1 Ionic liquids as solvents

Ionic liquids are used as solvents in dehydration of hexose. They are regarded as novel environmentally benign solvents mainly because of their very low vapour pressures. Ionic liquids are defined as salts that melt at or below 100 °C, affording liquids

exclusively composed of ions [159]. They are generally organic salts with low melting point which usually appear crystalline under ambient conditions, however at relatively low temperature (less than 100 °C) they can be molten and dissociate [217]. One of their most important features is that they present a very low vapour pressure.

Dehydration of glucose to HMF was reported by several authors using ionic liquids as solvents [47, 216, 228-231] some of them are shown in Figure 2-14.

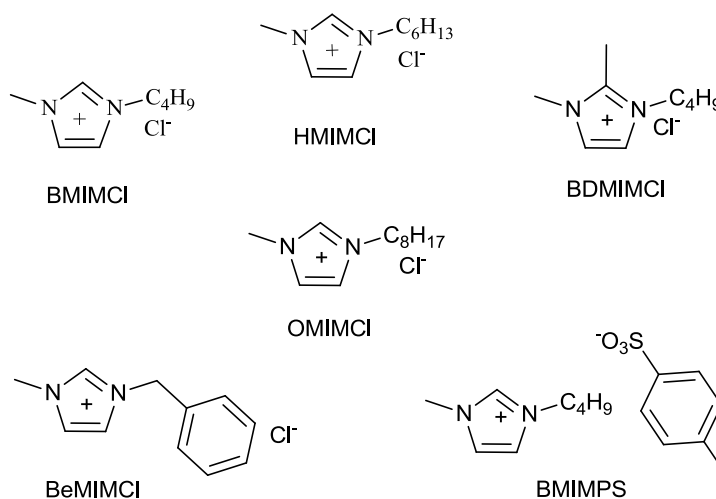


Figure 2-14. Structures of some ionic liquids used in the synthesis of 5-HMF

HMF yield of about 70% was reported using 1-ethyl-3-methylimidazolium chloride (EMIMCl) as ionic liquid in the presence of chromium (II) chloride catalyst at 100 °C for 3 hours [216]. These authors were the first to report such a significant yield of HMF in ionic liquid. Furthermore, 1-butyl-3-methylimidazolium chloride (BMIMCl) was used in the production of HMF and 88.4% yield was obtained with a fructose conversion of 95.8% at 100 °C for 30 minutes reaction time catalyzed by sulphated zirconia [230]. From their results, it appears that the ionic liquid can be recycled up to 6 times with the catalyst without loss of activity for both the ionic liquid and catalyst. This suggests that ionic liquids used as solvent can be recycled in the course of carbohydrate dehydration without loss of activity.

Cao *et al* [232] have studied the effects of ionic liquid structure and the amount of catalyst used in 5-HMF synthesis. From their findings, it was observed that 5-HMF yield of 63% was achieved using 1-butyl-3-methylimidazolium chloride (BMIMCl)

while 1-butyl-2, 3-dimethylimidazolium chloride yielded no 5-HMF. They observed that the structural difference between these ionic liquids is the position of hydrogen and methyl group on the C-2 position in which the reaction was affected the acidic nature of the C-2 hydrogen.

A recent study on the conversion of glucose to HMF was conducted using an inexpensive tetraethyl ammonium chloride (TEAC) ionic liquid and the results show an HMF yield of 71.3% was achieved in 30 minutes reaction time at 130 °C [229]. Based on these results, the authors have argued that though higher yield was obtained by others, the ionic liquids were expensive and the reaction proceeds in relatively long reaction times of 3-6 h. Furthermore, the ionic liquids used were reported to be highly problematic for actual industrial application, hence the need to develop relatively inexpensive ionic liquids for the production of HMF from glucose [229].

## 2.5 Furan derivatives for polymer applications

Recently, interest of the scientific community is focusing on furan derivatives for polymer production and applications because of their distinct characteristics that are associated with the peculiar behaviour of the furan ring. Furans being heterocyclic compounds possess an aromatic-dienic character that opens vast perspectives for the production of polymeric materials [64, 233]. Compared with benzene and its homologues such as pyrrole and thiophene, furan has the lowest aromatic character as well as highest dienic character. The supremacy of the dienic character is positioning some monosubstituted furan derivatives as precursors for new methods in polymer synthesis and modification, such as by Diels-Alder (DA) reactions. In this case, the furan ring plays the role of dienic reagent with a variety of dienophiles such as maleiamides [65, 234, 235]. This may represent a starting point for the preparation of polymeric materials with novel properties and applications.

Furthermore, furan derivatives such as 2,5-disubstituted furans can be suitable precursors of condensation polymers such as polyesters and most commercial polymers with furan version like poly(butylene terephthalate) (PBT) and poly(propylene terephthalate) (PPT) [236-238]. These polymers are dependent on

furans and 5-HMF that can be converted into two distinct large families of monomers that may replace those available from petrochemicals [65, 233].

Monomers derived from furfural are illustrated in Figure 2-15. They are prepared by connecting the various vinyl moieties and acrylic or epoxide groups of the furan ring which can be polymerized or copolymerised by either free radical, anionic or cationic polymerisations via these moieties.

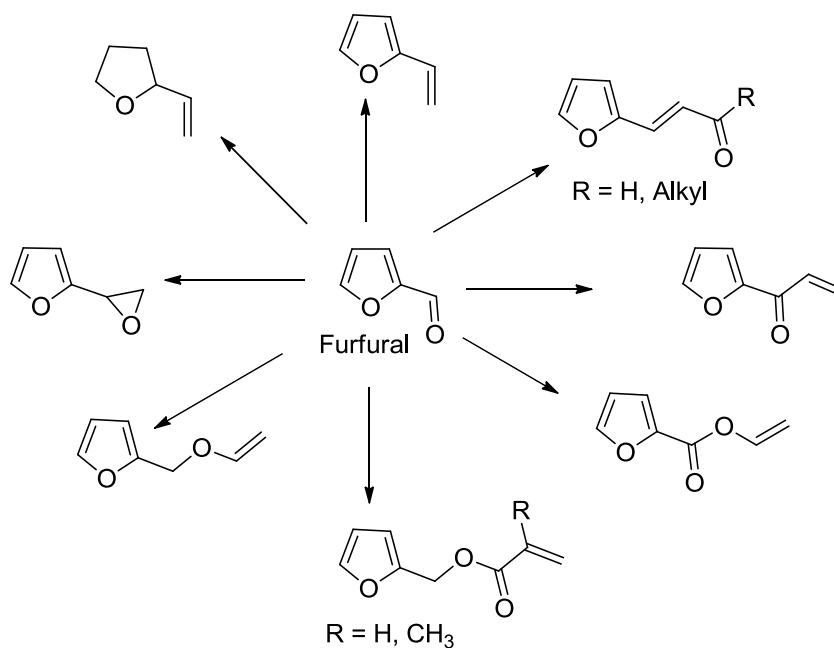


Figure 2-15. Monomers derived from furfural [65].

Additionally, furfural derivatives are reported as serving as precursors of difunctional difuran monomers appropriate for step-growth polymerizations and their production is based on the acid-catalysed condensation of the corresponding 2-substituted furan derivatives in the presence of an aldehyde or ketone as illustrated in Figure 2-16 [64, 65].

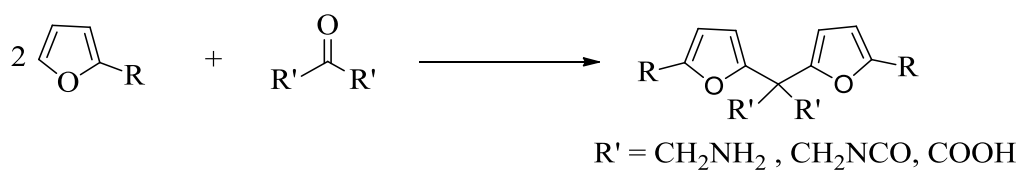


Figure 2-16. Difuran monomers derived from 2-substituted furans [65].

Other monomers are derived from 5-HMF as illustrated in Figure 2-17. They are prepared like those of furfural but in this case, the carbonyl, hydroxyl, amino or isocyanate functional groups are connected to the heterocyclic ring of the 5-HMF which are suitable for step-growth reactions. These types of monomers when polymerised can give rise to polycondensation products with the furan ring being part of the polymer's backbone unlike those from furfural which are pendant on the backbone of the polymers [64].

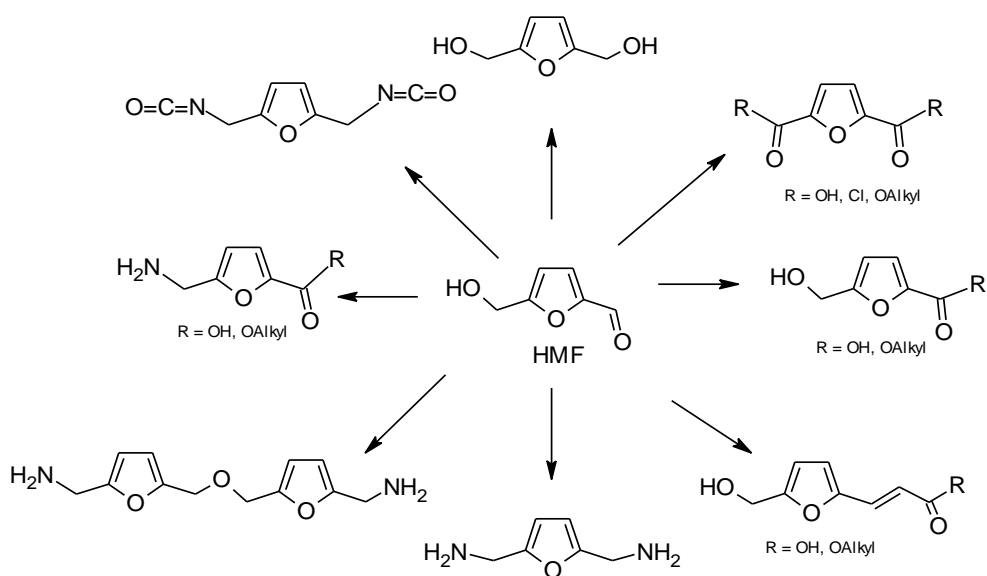


Figure 2-17. A selection of monomers derived from HMF [65].

Therefore, from all these monomers derived from furfural and 5-HMF as illustrated in Figures 2-16 and 2-17, FDCA and its derivatives such as the corresponding esters ( $R=OAlkyl$ ) and dichloride ( $R=Cl$ ) are potential precursors for the synthesis of 2, 5-disubstituted furan polyesters.

Other derivatives of 5-HMF that can serve as monomers for the production of polymers to replace those derived from fossil are 2,5-furandicarboxylic acids (FCDA), 2,5-bis(hydroxymethyl)furan (BHMF), 2,5-bis(aminomethyl)furan 2,5-diformylfuran (DFF), and 2,5-dimethylfuran (DMF) [64, 238] (Figure 2-18). These compounds are oxidation products of 5-HMF and can be used in the production of polyesters, polyamides and polyurethane [34].

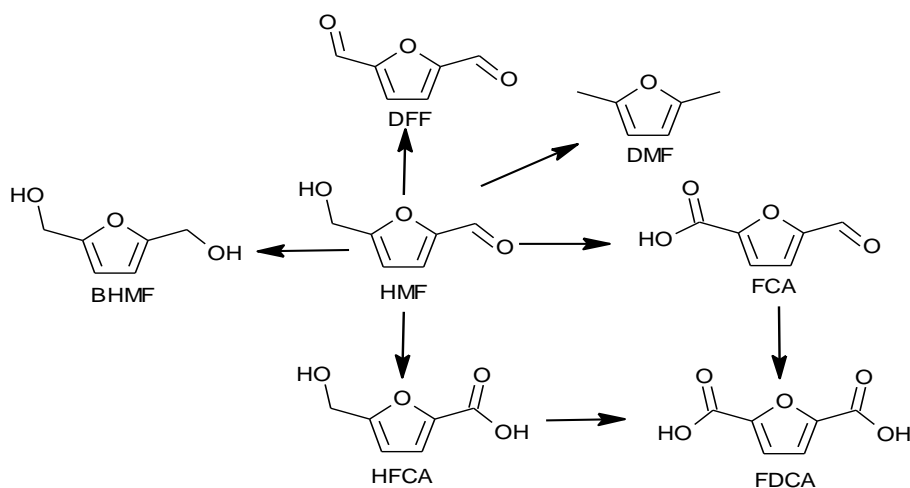


Figure 2-18. Products of HMF oxidation [239].

### 2.5.1 2,5-Furandicarboxylic acid (FDCA)

2,5-furandicarboxylic acid is synthesised from the oxidation of 5-HMF. This has properties and applications that are similar to terephthalic and isophthalic acids which are used in the production of polymers and chemicals [158, 233]. For instance, FDCA has a similar structure to terephthalic acid (Figure 2-19) that is used in the production of polyethylene terephthalate (PET). Therefore, FDCA has been found to be an alternative for the petroleum-based terephthalic acid counterparts used in the chemical industry [240]. Furthermore, the US department of Energy has also identified FDCA as one of the 12 top potential chemicals that can be derived from biomass [241].

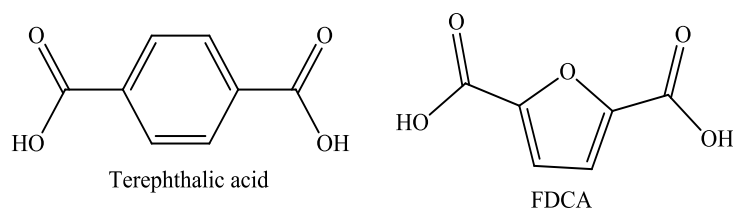


Figure 2-19. Structural similarity between terephthalic acid and FDCA

The oxidation of 5-HMF has been studied using variety of catalysts. For instance, 5-HMF oxidation over Pt/Pb catalysts was studied [242]. It was found that the reaction proceeds via two stages; the aldehydes side chain was first oxidized to a carboxylic acid, producing 5-hydroxymethyl-2-furancarboxylic acid (HFCA), and the oxidation

of the hydroxymethyl side chain follows to yield FDCA. The same authors also found that hydroxide base was more effective in producing FDCA than carbonate base, which favoured the production of HFCA. Furthermore, metallic catalysts such as carbon or alumina-supported platinum are found to be efficient for the oxidation of 5-HMF to FDCA [243]. Similarly, high yield of 2,5-FDCA was obtained using Pt/Pb bimetallic catalysts [242] and 60% yield based on air oxidation of 5-HMF using Co/Mn/Br catalysts was reported [242]. The reaction was performed at 125 °C under 7.0 MPa air pressure for 3 hours. Also, 99 mol.% yield of 2,5-FDCA from 5-HMF was obtained when the reaction was performed under mild conditions (65-130 °C, 1.0 MPa air) in water and gold nanoparticles supported on Au-CeO<sub>2</sub> catalyst [244].

Recently, supported Pt, Pd and Au catalysts were evaluated in the aqueous-phase oxidation of 5-HMF to FDCA at 295K and high pH in a semi batch reactor [239]. The results showed that Pt and Pd were able to oxidise the HFCA effectively to FDCA under identical conditions.

### 2.5.2 2,5-Diformylfuran (DFF)

2,5-diformylfuran has been considered as an important derivative of 5-HMF because it can serve as a potential intermediate for a vast array of chemicals [162]. This bio-based material had been reported to have potential applications in pharmaceuticals [245], fungicides [246], and a cross-linking agent for poly (vinyl alcohol). Also, DFF can be applied as a monomer for polymeric materials due to its symmetrical and unsaturated structure [247, 248].

In terms of manufacture, DFF is produced mostly by selective oxidation of 5-HMF, using metallic catalysts such as Pt/C [242], Co/Mn/Zr/Br [249], V<sub>2</sub>O<sub>5</sub> [250], and VOPO<sub>4</sub> · 2H<sub>2</sub>O [251]. These catalysts have been found to show excellent catalytic activity with significant yield of DFF produced. For instance, DFF yield of 90% was obtained from 5-HMF using V<sub>2</sub>O<sub>5</sub>/TiO<sub>2</sub> using toluene at 90 °C and 1.6 MPa air pressure within 4 h [250]. Also, 77% yield was obtained over vanadylacetylacetonate/PVP catalyst in trifluorotoluene via aerobic oxidation of HMF to DFF [252]. However, isolation and purification of 5-HMF requires a large amount of energy, and so pure 5-HMF might be costly; hence DFF production may be limited and incur very high cost.

Since glucose is cheap and readily available, it can be regarded as a prime candidate for the synthesis of 5-HMF as stated earlier and subsequently to DFF.

### 2.5.3 2,5-Dimethylfuran (DMF)

Among the furan derivatives, 2,5-dimethylfuran (DMF) is the most attractive as a biofuel because it has an energy content of  $31.5 \text{ MJ L}^{-1}$ , which is similar to that obtained from gasoline ( $35 \text{ MJ L}^{-1}$ ) and greater than that of ethanol ( $23 \text{ MJ L}^{-1}$ ) by 40% [42]. Other advantages of DMF over ethanol include higher boiling point ( $92 - 94 \text{ }^\circ\text{C}$ ) than ethanol ( $78 \text{ }^\circ\text{C}$ ), which makes it less volatile and more suitable as a transportation fuel [42]. Furthermore, DMF can be more stable during storage than ethanol because it is insoluble in water and also consumes only one-third of the energy used in its production compared with that required during fermentation of ethanol [253]. Therefore, this physicochemical property makes DMF a very promising gasoline alternative from biomass resources.

DMF is produced from hexoses by selective removal of five oxygen atoms. Recently, catalytic routes for its manufacture have been developed using D-fructose by two-step processes: acid catalysed dehydration of fructose which produced 5-HMF using a biphasic reactor and then conversion to 2,5-DMF by hydrogenolysis of the C-O bond over copper-ruthenium catalyst [253].

### 2.5.4 2,5-Bis-(hydroxymethyl) furan

2,5-Bis-(hydroxymethyl)furan (BHMF) was reported to be synthesised by the reduction of the formyl group of HMF in the presence of nickel, copper chromites, platinum oxide and sodium amalgam as catalysts [254]. Similarly, catalytic hydrogenation of HMF in an aqueous medium was conducted in the presence of nickel, copper, palladium and platinum catalysts [162] and BHMF was obtained as the major product.

## 2.6 Polymer - Clay nanocomposites

The manufacture of new materials with enhanced properties and performance is presently an expanding area at the interface of chemistry and materials science. A significant advanced in these fields has been the synthesis of polymer-clay nanocomposites.

Toyota Motor Corporation were the pioneers in polymer-clay nanocomposites which reported the exfoliation of montmorillonite clay by incorporating polyamide-6 via *in situ* polymerization [255, 256]. Also, reports by other research groups [257-259] on blending of layered silicates with polymers in molten state provided an environmental benign and versatile approach in the production of polymer-clay nanocomposites. Therefore, these breakthrough have attracted much attention from the academic and industrial communities and since then, extensive research has been carried out to investigate the reinforcing effects of clay in other polymer matrices, such as polyolefin, epoxies, polyesters, and polyurethanes (PU) [259].

Polymer-clay nanocomposites are materials in which nanoscopic inorganic particles, typically 1-10 nm in at least one dimension, are dispersed in an organic polymer matrix in order to improve the performance of the polymer. These concepts have attracted a great deal of attention recently in materials science because of their superior engineering properties and represent a new alternative to conventionally filled polymers. Because of their nanometre sizes, filler dispersion nanocomposites exhibit markedly improved properties when compared to the pure polymers or their traditional composites. These properties include increased modulus and strength, outstanding barrier properties, improved solvent and heat resistance and decreased flammability and, because the reinforcement is at such a fine scale, the same processing operations that are used for the unfilled polymer, such as extrusion and injection moulding can be applied to the composite.

### 2.6.1 Types of polymer-clay nanocomposites

Three types of polymer-clay nanocomposites are thermodynamically achievable depending on the strength of interfacial interactions between the polymer matrix and

the layered clay silicates [257]. These are: intercalated, intercalated-and-flocculated and exfoliated nanocomposites as illustrated in Figure 2-20.

### 2.6.1.1 Intercalated nanocomposites

In intercalated nanocomposites, the guest species is reversibly inserted into a host solid while maintaining the structural features of the host. Intercalated nanocomposites are formed when the insertion of an organic molecule such as a polymer into the layered silicate structure occurs in a crystallographically regular fashion, regardless of the clay to polymer ratio. This results in a well ordered multilayer structure of alternating polymeric and inorganic layers with a repeat distance between them [260]. Furthermore, this type of nanocomposites can also be described based on the distance between a plane in the unit layer and the corresponding plane in the next unit layer defined as the basal plane spacing,  $d_{001}$  [261]. If there is an increase in  $d_{001}$  as an organic species enters the galleries and the clay layers remain stacked, the composite formed is 'intercalated' [261].

### 2.6.1.2 Intercalated-and-flocculated nanocomposites

Intercalated-and-flocculated nanocomposites represent another type of nanocomposites that is conceptually the same as intercalated nanocomposites as defined by Ray *et al*; containing flocculated intercalated silicate layers due to hydroxylated edge-edge interaction of the silicate layers [259].

### 2.6.1.3 Exfoliated nanocomposites

In exfoliated nanocomposites, the individual clay layers are separated in a continuous polymer matrix by extended distances that depends on clay loading. Usually, the clay content of an exfoliated nanocomposites is much lower than that of intercalated nanocomposites [259]. If the clay layers are pushed apart completely leading to a disordered array, an exfoliated nanocomposite results [261], and some authors classified composites as exfoliated if the basal plane spacing such as  $d_{001} > 10$  nm that cannot be determined by conventional X-ray diffractometer [261, 262].

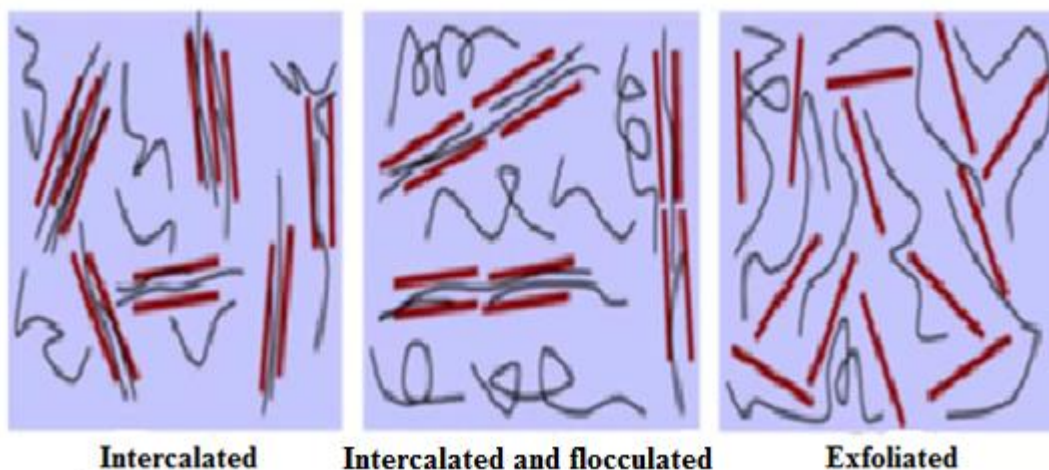


Figure 2-20. Schematic illustration of three different types of polymer clay nanocomposites, reproduced with permission [257].

## 2.7 Preparation of nanocomposites

Four main routes for the preparation of nanocomposites have been reported [260, 263]. These are: *In situ* template synthesis, intercalation of polymer or prepolymer from solution, *in situ* intercalative polymerization and melt intercalation.

### 2.7.1 *In situ* Template synthesis

In *in situ* template synthesis, the inorganic material is prepared within the polymer matrix using an aqueous solution containing the polymer and the silicate building blocks. This method has been reported for the synthesis of double-layer hydroxide-based nanocomposites in an aqueous solution of the polymer and silicate building block [264]. The polymer is said to aid nucleation and growth of the inorganic host crystal and gets trapped within the layers as they grow [260]. However, this method is not commonly used in nanocomposite preparation because it requires high temperature in the synthesis of the clay minerals which tends to decompose the polymers. Also, the aggregation tendency of the growing silicate layers is another challenge for this method [260].

## 2.7.2 Intercalation of Polymer or Pre-polymer from Solution

This method involves the dispersion of organically modified silicate in a solvent in which the polymer is also soluble. The dispersion is achievable because the weak forces that stack the layers together can easily be overcome in an appropriate solvent to produce dispersion. In this case, the polymer then adsorbs onto the delaminated sheets and when the solvent is evaporated (or the mixture precipitated), the sheets reassemble, sandwiching the polymer to form, in the best case, an ordered multilayer structure [263]. This method may lead to the formation of intercalated nanocomposites. It is not necessarily environmentally benign because of the use of large amounts of solvent. The schematic of the process is shown in Figure 2-21 [260].

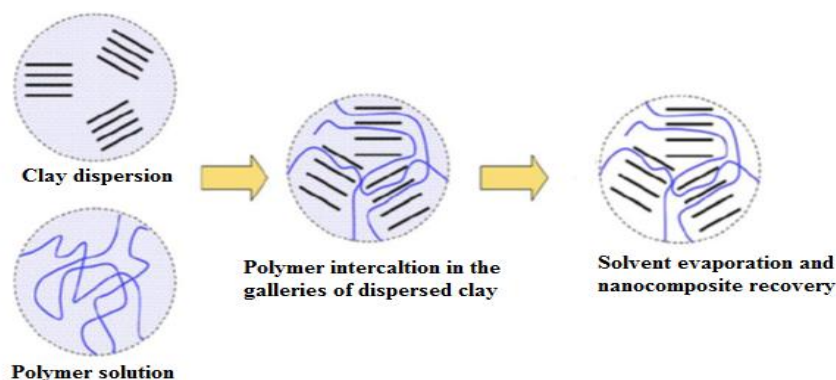


Figure 2-21. Schematic representation of polymer adsorption from solution, reproduced with permission [260].

This technique is well suited for the intercalation of water soluble polymers such as poly (vinyl alcohol), poly (ethylene oxide), poly (acrylic acid) and poly (vinylpyrrolidone) [265, 266]. It has been used in organic solvents for polymers that are insoluble in water. For instance, high density polyethylene was used as polymer matrix which was dissolved in a mixture of xylene and benzonitrile [267]. Similarly, biodegradable nanocomposites using poly(lactic acid) as polymer matrix were also reported using dichloromethane as solvent and some exfoliated and intercalated nanocomposites were obtained based on the type of organically modified montmorillonite [268]. However, some polymers like poly (imides) do not dissolve in

organic solvents, therefore, in such cases, a pre-polymer or polymer precursor is intercalated in the silicate interlayers and subsequently converted in the polymer matrix [263]. Toyota researchers [269] reported the preparation of poly(imide) montmorillonite nanocomposites by mixing poly(amic acid) in dimethylacetamide in the presence of modified montmorillonite. From their findings, the montmorillonite was exchanged with dodecylammonium hydrochloride resulting in the generation of exfoliated nanocomposites. This was confirmed by the absence of diffraction peaks from the XRD diffractograms. Conjugated polymers can also be intercalated in the filler interlayers by a similar precursor intercalation approach [270] and poly(p-phenylenevinylene)/montmorillonite intercalated nanocomposites were produced with layered silicates using poly(xylenylenedimethylsulfonium bromide) as precursor [270, 271]. The precursor was then transformed into polymer by base-mediated elimination of dimethylsulfide and HBr. Furthermore, emulsion polymerization of monomers in the presence of the layered silicates has also been reported to generate intercalated and exfoliated nanocomposites using methyl methacrylate and styrene as monomers [272]. The monomer is suspended in water along with varying amounts of silicates in the presence of emulsifier and then polymerized which results in the generation of nanocomposites with a part of silicate embedded inside the polymer particles and a part adsorbed on the surface of the particles [272].

Table 2-4 shows representative examples of polymer-clay nanocomposites produced by intercalation from solution. This method is only possible for certain polymer, clay and solvent systems. This implies that for a given polymer one has to find the right clay, organic modifier and solvents [257, 263]. Moreover, the use of these organic solvents is not economically viable from an industrial point of view and as such they are not environmentally benign [257].

Table 2-4. Nanocomposites prepared by intercalation from solution [260].

Nanocomposite	Solvent(s)
PVOH/Na <sup>+</sup> -MMT	Water
PVA/Na <sup>+</sup> -MMT	Water
TPO/OMLS	Toluene/DMAc
PEO/ Na <sup>+</sup> -MMT or Na <sup>+</sup> -hectorite	Acetonitrile
PEO/MMT	Chloroform
PLA/OMLS	Dichloromethane
PLA/OMLS	DMAc

### 2.7.3 *In situ* intercalative polymerization

This method involves the dispersion of particles first in a monomer and then the mixture is polymerized. It is applied in the polymerization of thermoplastic and thermosetting polymers. Nanocomposites were prepared with polyamide-6 matrix and silica inclusions by first drying the particles to remove water adsorbed on the surface. Then, the particles were mixed with caproamide and concurrently a suitable polymerization initiator was added. The mixture was then polymerized at a high temperature under nitrogen [273]. This technique produced well-dispersed samples when the inclusions were around 50 nm in size, but aggregation occurred for smaller particles around 12 nm in size.

## 2.7.4 Melt intercalation

This method involves the mixing of the layered silicates by either annealing or under shear with the polymer while heating the mixture above the softening temperature of the polymer. The polymer chains are diffused from the bulk polymer melt during the annealing process into the clay galleries [263, 274-277].

This technique is attractive because of its versatility and compatibility with existing processing infrastructure and it is now applied in commercial applications [278]. The structure of nanocomposites formed by this method depends on the thermodynamic interaction between the polymer and the clay as well as the movement of polymer chains from the bulk melt into the clay galleries [279].

Polypropylene (PP)/calcium carbonate nanocomposites were made by melt intercalation method [280]. The authors mixed the polypropylene first with antioxidant and calcium carbonate (44 nm in diameter) which was added slowly and mixing continued for a fixed time after all particles were added. The results indicate a well dispersed sample at lower filler volume fractions of 4.8% and 9.2% respectively. However, aggregation was found to be at a higher volume fraction of 13.2%.

Although this method has been applied for the synthesis of nanocomposites, it has some limitations for two reasons:

First, production of nanocomposites involving high-temperature processes leads to low thermal stability of the clay modifier and hence, decrease in the distance between the clay sheets as a result of the thermal degradation of the clay modifier. Furthermore, loss in hydrophobicity of the clay surface occurs which leads to a hydrophilic surface [281, 282]. These limitations were confirmed by Park *et al* [283] who discovered that the d-spacing of the clay galleries decreased when the reaction temperature was increased from 200 °C to 280 °C because of the degradation of the clay particles and this affected the intercalation of the polymer and the clay.

Second, it was reported that this method seems to be unsuitable for the synthesis of some polymer nanocomposites such as those from amorphous PS even though PS can

be intercalated into clay through weak interaction between the phenyl group of PS and the clay surface. The interplanar spacing was observed to be decreased upon heating PS and clay [284].

### 2.7.5 Layered Silicates

Layered silicates are clay minerals, built of two structural units. The simplest are the 1:1 structures (e.g. in kaolinite) where a silica tetrahedral sheet is joined to an aluminium octahedron, sharing the oxygen atoms [285]. Most of the layered silicates commonly used in nanocomposite preparation are of 2:1 phyllosilicate types which includes: smectite clays (e.g montmorillonite, saponite, and hectorite) [286]. Their detailed general formulae are presented in Table 2-5. Among these silicates, montmorillonite (MMT) with the general formula  $M_x(Al_{4-x}Mg_x)Si_8O_{20}(OH)_4$  (where, M is sodium, calcium) is the filler chosen for most studies of polymer nanocomposites because it is of low-cost and is environmentally benign [287]. Furthermore, its unique layered structure, cation exchangeability and expandability makes it a better candidate than others [288].

Table 2-5. Commonly used layered phyllosilicates with their general formula [263].

2:1 Phyllosilicate	General formula
Montmorillonite	$M_x(Al_{4-x}Mg_x)Si_8O_{20}(OH)_4$
Hectorite	$M_x(Mg_{6-x}Li_x)Si_8O_{20}(OH)_4$
Saponite	$M_x(Mg_x)(Si_{8-x}Al_x)O_{20}(OH)_4$

The montmorillonite crystal structure consists of layers formed by sandwiching an aluminium octahedral sheet between two silicon tetrahedral sheets. Stacking of the layers leads to a van der Waals gap between the layers. Substitution of aluminium ( $Al^{3+}$ ) for magnesium ( $Mg^{2+}$ ) in the octahedron sheet gives each three-sheet layer an overall negative charge in the range 0.2–0.6 per formula unit, which is normally counterbalanced by exchangeable metal cations residing in the interlayer space. The

interlayer cations hold the individual negatively charged silicate layers together through electrostatic forces. Due to the weak interaction between layers, organic monomers can be intercalated into these interlayer spaces and react with the interlayer cations as shown in Figure 2-23 [260].

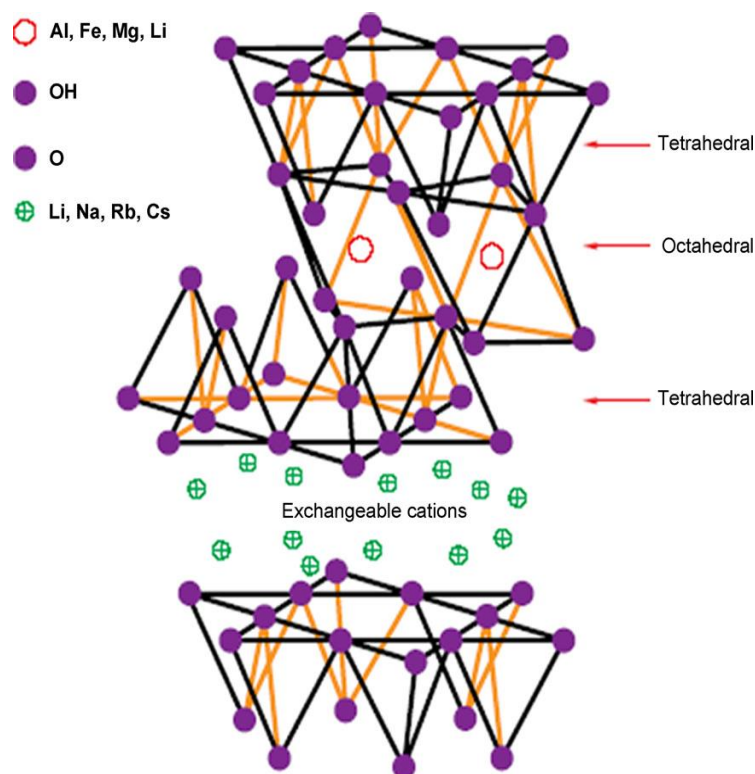


Figure 2-22. Structure of layered silicate reproduced with permission [260].

## 2.8 Characterization of the structures of nanocomposites

Structures of nanocomposites are characterized by two main techniques. These are X-ray diffraction and transmission electron microscopy [289]. These structures can be distinguished based on the ordering and the clay dispersion into the polymer matrix as conventional (immiscible), intercalated and exfoliated (delaminated) [290].

### 2.8.1 X-ray diffraction

This technique is used to determine the distance  $d$  between the basal layers of the clay or layered material by the use of Bragg's law:  $n\lambda = 2d \sin\theta$  where,  $\lambda$  corresponds to the wavelength of the X-ray radiation used in the diffraction experiment,  $d$  is the

spacing between diffraction lattice planes and  $\theta$  is the measured diffraction angle [277].

Among the three distinguished nanocomposite structures, intercalation and exfoliation are associated with the change in the distance between the clay layers and the polymer. An increase in the value of  $d$  indicates that an intercalated nanocomposite has been formed implying that the polymer chains have entered clay galleries which expand. The absence of diffraction peaks suggests an exfoliated (delaminated) nanocomposites indicating that a great amount of polymer has entered the clay galleries and disordered the platelets [291]. Furthermore, conventional (immiscible) polymer nanocomposites exhibit no change in  $d$ -spacing with respect to pristine clay, meaning that no polymer has entered the gallery and that the spacing between clay layers is unchanged [292-294]. Therefore, the value of  $d$ -spacing observed in XRD describes the nanoscale dispersion of the clay in the polymer matrix [292]. The three types of structures that are obtained by XRD measurements are illustrated in Figure 2-24.

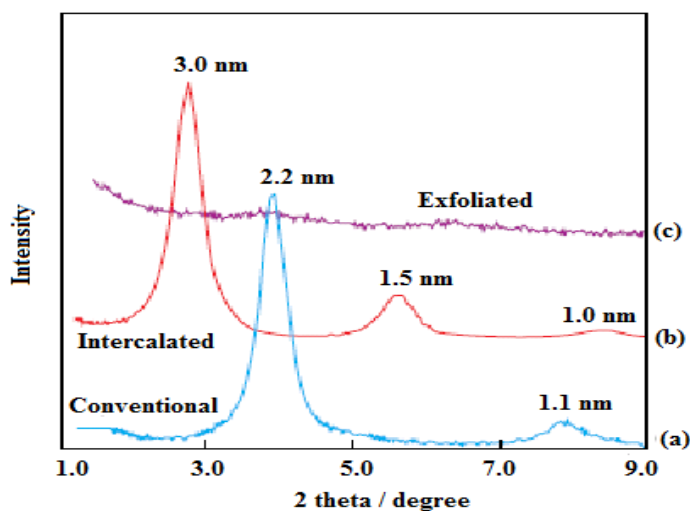


Figure 2-23. XRD pattern of three types of silicate layers (a) Conventional (b) Intercalated (c) exfoliated nanocomposites reproduced with permission [263].

As stated earlier, XRD is a useful technique for measuring the  $d_{(001)}$ -spacing of ordered miscible and intercalated nanocomposites [259]. However, it has some limitations or drawbacks in that it is not sufficient in measuring disordered and exfoliated nanocomposites that do not give XRD peaks. In other words, the absence of peaks may be misinterpreted [289, 294]. Some factors can influence the XRD pattern which may

results in the absence of peaks and some of these factors are concentration and ordering of the clay [294]. Therefore, absence of peak from the XRD pattern of a polymer-clay nanocomposites cannot prove or disprove the presence of exfoliated clay platelets in the nanocomposites. XRD relates only to the degree of dispersion of clay sheets with respect to each other in the polymer matrix, and does not give information with respect to interaction between the organic and inorganic phase in the composite materials [294].

## 2.8.2 Transmission electron microscopy (TEM)

As XRD patterns of polymer-clay nanocomposites have some limitations, TEM is the next available instrument to determine quantitatively how the layered silicate filler (clay) is dispersed into the polymer. Usually a thin cross-section of approximately 40-50 nm of the nanocomposite is microtomed and observed via the TEM. When nanocomposites are formed, a dark lines are observed signifying the formation of a polymer-clay nanocomposite as illustrated in Figure 2-25 [259, 263, 295].

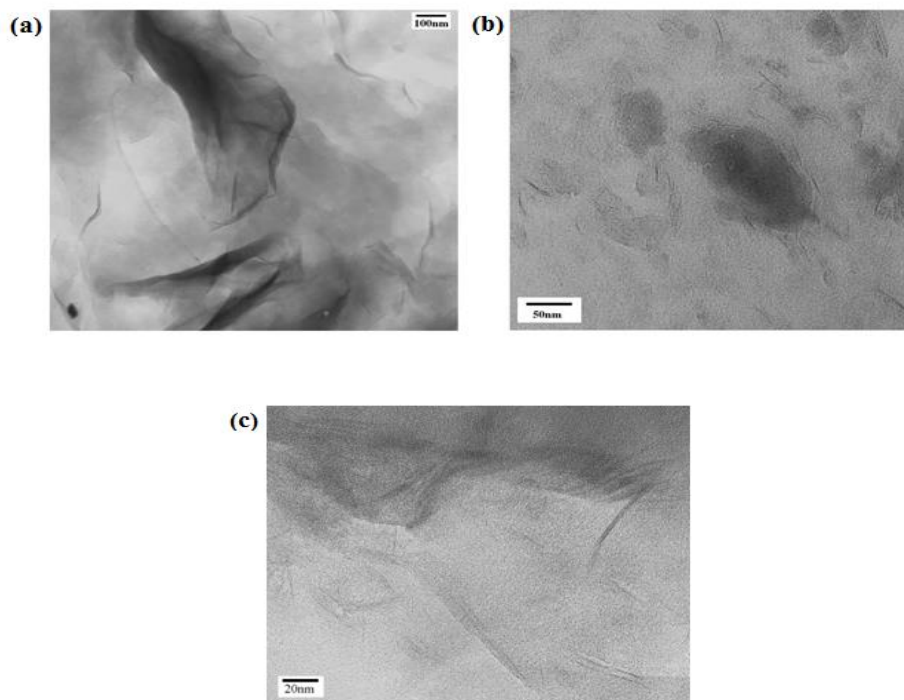


Figure 2-24. TEM micrographs of (a) treated hectorite, (b) thermoplastic-treated hectorite and (c) thermoplastic starch-untreated hectorite nanocomposites reproduced with permission [295].

## 2.9 Bio-based polymer composites

### 2.9.1 Thermoplastic Starch Based Composites

Thermoplastic starch based composites have been synthesized by melt-processing of starch and glycerol for the manufacture of bio-based nanocomposites for materials application [295]. Thermoplastic starch was first reported as a bio-based material for the production of polymer nanocomposites by melt intercalation methods in a twin screw extruder [296]. The composites were prepared with regular corn starch plasticized with glycerine and reinforced with hydrated kaolin and the results afforded an increased in tensile strength of the nanocomposites from 5 to 7.5 MPa with 50% clay composition. Similarly, the modulus of elasticity increased from 120 to 290 MPa while the tensile strain at break was observed to decrease from 30 to 14%. The results further revealed the occurrence of strong bonding between kaolin and the matrix as obtained by the scanning electron microscopy of the nanocomposite.

The effect of varying the amount of plasticizer on the mechanical and structural properties of starch nanocomposite was investigated by the solution method [297]. From these results, it was observed that the sequence of addition of components (starch/plasticizer/clay) had a significant effect on the nature and properties of nanocomposites formed. The results further revealed that the dispersion of the filler was more heterogeneous and brittle when the starch was plasticized prior to the addition of the clay and as a result of that the modulus of elasticity was increased significantly in all the nanocomposites produced irrespective of the preparation method. These authors concluded that all the properties of the nanocomposites derived from starch could be achieved by proper dispersion of the clay filler and not necessarily on varying the sequence in which the addition of plasticizers occurred.

Modified starch with acetate was used in the synthesis of bio-based nanocomposites with cellulose fibres [298]. In this approach, 70% corn starch was extruded with 10, 20 and 30% (w/w) cellulose and 20% (w/w) ethanol for the synthesis of bio-based nanocomposites at 150, 160 and 170 °C barrel temperatures and 170, 200 and 230 rpm screw speeds in a twin screw extruder. The results further revealed from the XRD pattern that the crystallinity of the starch and cellulose reduced drastically. Also, the

melting temperatures of the composites were observed to change significantly when higher DS starch acetates were used. Experimental variables such as cellulose content, barrel temperature and screw speed have profound effects on thermal, physical and mechanical properties of extruded foams. For the extruded starch foams, thermal properties were strongly related to blend composition, barrel temperature and screw speed.  $T_g$  and  $T_m$  of the extruded foams decreased as cellulose content increased. The author noted that as barrel temperature and screw speed increased,  $T_g$  and  $T_m$  increased initially and then decreased when barrel temperature and screw speed were higher than 160 °C and 200 rpm respectively.

Further studies by Kumar and Singh [299] were done through starch modification by photo-induced cross linking. Composite films were made from the aqueous dispersions of starch with microcrystalline cellulose using glycerol as plasticizer and irradiated under ultraviolet (UV) light using sodium benzoate as photo-sensitizer via casting. Young's modulus of composites reinforced with 5, 10 and 15 wt. % which were irradiated for 30 minutes improved by 72.41%, 42.5% and 32% respectively, when compared to control samples.

The elongation (%) values were found to decrease with increasing cellulose fibre content and time of photo-irradiation. Other researches on the use of thermoplastic starch without further modification (*i.e.*, changes in experimental conditions) also reported significant increase in tensile and thermal properties of thermoplastic research when reinforced with nanofibres [300-305].

## 2.9.2 Poly Lactic Acid Based Composites

Bio-based nanocomposites were prepared using poly (lactic) acid (PLA) with organically modified clay by dissolving the PLA in hot chloroform in the presence di methyl ammonium modified MMT [306]. The results of this study as revealed by the XRD pattern indicated that the silicate layered clay could not be intercalated by PLA to form nanocomposites by the solvent casting method. In a recent study, PLA/organically modified clay nanocomposites were prepared by dissolving the polymer in hot chloroform in the presence of dimethyl distearyl ammonium modified MMT and the results revealed that the clay layers were unable to be intercalated based

on the XRD pattern [306]. It was reported that the clay existed in the form of tactoids with several stacked silicate layers which could lead to an increase in the Young's modulus of the nanocomposites. Similarly, other research groups have reported the synthesis of nanocomposites derived from PLAs [307-313], and the results indicate improved mechanical, thermal and impact properties of the nanocomposites. For instance, a nanocomposite of PLA/Wood flour (WF) was prepared by melt compounding and injection moulding and it was found that the tensile modulus of this composite increased from 62.5 to 169.5% and the tensile strength increased 13.7%, 16.7% and 13.9% at the loading levels of 10, 20, and 30 wt.% WF, respectively [314]. Furthermore, nanocomposites of PLA with a compatibilizer and cellulose fibrils have been developed by Qu, *et al* [315]. It was observed that the tensile test results and the elongation rate increased by 56.7% and 60% by adding PEG to the PLA and the cellulose nanofibrils matrix, compared with the PLA/cellulose nanofibrils composites. The authors explained that PEG covers the surface of the cellulose nanofibrils and acts not only as a plasticizer for PLA to improve its elongation, but also as a compatibilizer between the hydrophobic PLA and the hydrophilic cellulose nanofibrils. It was also stated that PEG prevents the aggregation of the nanofibrils, so that the cellulose nanofibrils disperse in the PLA matrix homogeneously to form a network structure.

### 2.9.3 Cellulose Based Composites

As stated in section 2.5.1.1, cellulose from biomass has been identified as a source of biopolymer that can replace petroleum polymers. Bio-based nanocomposites have been successfully produced from cellulose acetate (CA), triethyl citrate (TEC) plasticizer and organically modified clay via melt compounding [316]. The cellulosic plastic with 80 wt. % pure cellulose acetate and 20 wt. % triethyl citrate plasticizer was used as the polymer matrix for nanocomposite production. Mechanical properties of the composites were determined and correlated with observations from X-ray diffraction and transmission electron microscopy. The results obtained indicate that cellulosic plastic-based nanocomposites containing 5 and 10 wt. % organoclay have better exfoliated and intercalated structure than those of 15 wt. % organoclay. Tensile strength and modulus of cellulosic plastic reinforced with 10 wt. % organoclay improved by 75 and 180% respectively.

Furthermore, a cellulose-based nanocomposite material has been investigated and the results revealed that this nanocomposites can serve as humidity and temperature sensors [317]. The cellulose employed in this study was obtained from cotton pulp via acid hydrolysis using a solution of lithium chloride and N,N-dimethylacetamide. During the experiment, nanoscaled polypyrrole was used as the second component of the nanocomposite and the composites were prepared by a polymerization-induced adsorption process. The polypyrrole was coated onto the surface of the cellulose and its influence on the cellulose membrane was determined by atomic force microscopy technique. These authors primary aim in this experiment was basically on the sensing ability and not the structural integrity of the nanocomposite material. Therefore, the study shows that successful deposition of the polypyrrole nanolayer onto the cellulose surface was achieved because the material was not analyzed on a structural basis it could not determine if cellulose served as the reinforcement or the polypyrrole.

In summary, many agricultural products can serve as a source of bio-based polymers and these include: terpenes, sugars, celluloses, starches, lignin, proteins, polyphenols and fibres. Others have utilized wastes produced from these agro materials and food wastes for the production of bio-based polymers. Both materials can undergo three basic strategic pathways for the production of bio-based polymers. These pathways are: (i) those that are derived directly from biomass (ii) biochemical modification of the bio-based components and (iii) those produced from genetically modified transgenic plants. All these pathways produce polymers with added importance to the bio-based industries and in which their characteristics can be improved by using some reinforcements sourced from natural resources such as plant fibres and smectite clays.

## CHAPTER 3: MATERIALS AND METHODS

### 3.1 Materials

The details of materials used in this work are given in Table 3-1. All chemicals and reagents were used as received without further purification.

Table 3-1. Materials used in this work

Reagent	Supplier	Purity/% Grade	Location
1,2-dichlorobenzene	Sigma-Aldrich	99	Gillingham, Dorset ,UK
1,4-butanediol	Sigma-Aldrich	99	Gillingham, Dorset ,UK
1,4-dioxane	Alfer Aeser	99.8	Heysham, Lancashire, UK
1,6-hexanediol	Sigma-Aldrich	99	Gillingham, Dorset ,UK
1,8-octanediol	Alfer Aeser	98+	Heysham, Lancashire, UK
12-tungstophosphoric acid	Strem Chemicals Ltd	99	Massachusetts, U.S.A
1-butyl-3-methylimidazolium chloride	Io.li.tec	99	Germany
2,5-Furandicarboxylic acid	Sequoia Research Products Ltd	97	Pangbourne, UK
5-(Hydroxymethyl) furfural	Sigma-Aldrich	99	Gillingham, Dorset ,UK
Anhydrous sodium carbonate	VWR International Ltd	AnalaR	West Sussex, UK
Benzylamine	Sigma-Aldrich	99	Gillingham, Dorset ,UK
Chromium (III) chloride	Sigma-Aldrich	99	Gillingham, Dorset ,UK

---

Ethylene glycol	VWR International Ltd	Technical	West Sussex, UK
Formic acid	Sigma-Aldrich	95	Gillingham, Dorset, UK
Fructose	Sigma-Aldrich	99.5	Gillingham, Dorset, UK
Glucose	Sigma-Aldrich	99.5	Gillingham, Dorset, UK
Levulinic acid	Sigma-Aldrich	98	Gillingham, Dorset, UK
Nanofil 116 clay	Rockwood Additives Ltd	-	Widnes, Cheshire, UK
Nitric acid	VWR International Ltd	68	West Sussex, UK
Palladium on activated carbon	Sigma-Aldrich	5 wt	Gillingham, Dorset, UK
Potassium per manganate	Sigma-Aldrich	99, ACS grade	Gillingham, Dorset, UK
Sodium borohydride	Sigma-Aldrich	98	Gillingham, Dorset, UK
Sodium cyanoborohydride	Alfer Aeser	95	Heysham, Lancashire, UK
Sodium hydroxide	Fisher Chemicals	Analytical grade	Loughborough, UK
Sulphuric acid	VWR International Ltd	95	West Sussex, UK
Titanium (IV) n-butoxide	Across Organics	99	Loughborough, UK
Trifluoroacetic acid	VWR International Ltd	99	West Sussex, UK
Zirconium (IV) hydroxide	Sigma-Aldrich	99.5	Gillingham, Dorset, UK

---

## 3.2 Analytical Instruments

### 3.2.1 Nuclear Magnetic Resonance spectrophotometer (NMR)

All  $^1\text{H}$  and  $^{13}\text{C}$  NMR were recorded using a Bruker AMX 300 MHz and 500 MHz spectrometers. Data were processed by ACD/NMR Processor Academic Edition and sample dilutions were made in  $\text{CDCl}_3$  and  $\text{DMSO-d}_6$  respectively. All chemical shifts ( $\delta$ ) are reported in parts per million (ppm).

### 3.2.2 Fourier Transform Infrared spectrophotometer (FTIR)

FTIR spectra obtained in this work were conducted with an ALPHA Bruker Optics FTIR spectrophotometer equipped with ZnSe ATR crystal. The samples were scanned from  $400 - 4000 \text{ cm}^{-1}$  wavenumber with a 32 scan per sample circle and a resolution of 4 [318].

### 3.2.3 X-Ray diffractometer (XRD)

All XRD data were collected using a Siemens D500 X-Ray diffractometer using  $\text{Cu K}\alpha 1$  radiation with wavelength of 0.154056 nm. The diffractometer was operated at 40 kV and 30 mA. Scans began at a low angle of  $2^\circ$  and scanned to  $25^\circ$  of  $2\theta$  in  $0.05^\circ$  steps at 6 seconds per step.

### 3.2.4 Transmission Electron Microscope (TEM)

TEM was conducted on a JEOL JEM-2100 electron microscope with digital image capture operating at 200 kV. TEM specimens were embedded into a resin and were sectioned with a Leica EM UC6 microtome (Leica microsystems, Wetzlar, Germany), equipped with diamond knife (Diatome, Hatfield, PA, USA) into thin sections at the Anatomy Department, UCL. Sections were transferred to 300 mesh copper grids coated with carbon [319].

### 3.2.5 Thermogravimetric analysis (TGA)

Thermal analysis of the polymers and nanocomposites were conducted on Netzsch STA 449 F1 Jupiter thermal analyser. Samples (~ 10-15 mg) were heated using an aluminium pan at a constant rate of 10 °C min<sup>-1</sup> under helium at a flow rate of 20 mL min<sup>-1</sup> between 20 °C and 600 °C. The onset of thermal degradation was determined according to the method developed by Marsh [320].

### 3.2.6 Tensile properties

Tensile testing of the polymer and its nanocomposites was performed using a Tinius Olsen H10KM/0348 testing machine (Salford Redhill, Surrey, UK) with 1 kN load cell and a crosshead speed of 10 mm per minute. Tensile stress and elongation at break were calculated from the average of five duplicate readings for each polymer and nanocomposites at ambient temperature. The calibration of the machine was done using dead weight and the deviation between recorded and actual force was 0.4% upon which a calibration factor was based. Gauge lengths were measured using a vernier calliper and was set at 70 mm. Samples were prepared by solvent (ethyl acetate) casting on a Petri dish and left overnight under ambient temperature and cut with a hot knife to give sections of 10 mm x 0.13 mm.

The tensile stress and strain were calculated based on the following equations:

$$\text{Tensile stress, } \sigma = \frac{\text{Force}}{\text{Area}} = \frac{F}{A} \text{----- (3.1)}$$

$$\text{Tensile strain, } \varepsilon = \frac{\text{Change in length}}{\text{Original length}} = \frac{\Delta L}{L_0} \text{----- (3.2)}$$

The Young's modulus,  $E$ , was estimated from the slope of stress-strain curve derived as a tangent modulus of the various polymers and this was accomplished using equation (3.3).

$$\text{Young's modulus } E = \frac{\text{Tensile stress}}{\text{Tensile strain}} = \frac{\sigma}{\varepsilon} \text{----- (3.3)}$$

### 3.2.7 Elemental analysis

Elemental analysis of the polymers were conducted using Exeter analytical CE440 analyser (Warwick, UK) for the determination of carbons and hydrogens by placing 1-3 mg of the samples in an aluminium pan for combustion in an excess of oxygen under static conditions at about 600 °C. Helium was used to carry the combustion products through the analytical system to atmosphere, as well as for purging the instrument and the concentrations of carbon and hydrogen are measured by displacing the sample gas through the detectors and were recorded as a percentage. The oxygen concentrations were obtained as the difference from the percentage of carbons and hydrogens.

### 3.2.8 Water contact angle

Water contact angles on the polymer surfaces were determined using a camera STC-TC-83USB-AT and a cold light source (Schott 150 w) attached to a fibre optic cable. Distilled water droplets of ~0.8 mm diameter as determined from the volume of the sessile hemispherical drop, were placed using a stainless steel needle on a horizontal surface of the polymer inside a glass cell with a ground glass rim and covered with a glass lid. Distilled water was placed inside the cell to provide a buffered atmosphere of 100% RH. The needle was cleaned with a blue flame prior to placing the water droplets. Images of the sessile drops were captured after 10-120 seconds and at later times to assess stability and the contact angles were measured from enlarged prints using a protractor. A graticule was photographed at the same magnification to provide scaling.

### 3.2.9 Surface tension of water

Distilled water for contact angle measurements was obtained directly from the glass condenser without contact with polymeric tubing. Surface tension was measured using Du Nouüy balance (White electrical company, Worcestershire, UK) at a room temperature of 18.9 °C using a platinum ring which was previously cleaned by heating in a blue flame to just close to orange colour. The result was compared to the literature

[321, 322] values interpolated for exact temperature and the distilled water was then used for the contact angle measurements explained in section 3.2.8 above.

### 3.2.10 Capacitance and dielectric constant

Samples for the capacitance measurements were electroded with a conductive silver ink (Johnson Matthey, London U.K) to provide rectangular electrodes approximately 12 x 12 mm<sup>2</sup> and the capacitance was obtained using an Agilent 4294A 40Hz-110 MHz precision impedance analyser in the frequency range 1-10 MHz.

The dielectric constants of the polymers were calculated from equation (3.4).

$$\epsilon_r = \frac{Cd}{\epsilon_0 A} \text{-----} (3.4)$$

where  $C$  is the capacitance,  $\epsilon_r$  is the relative permittivity of the dielectric,  $\epsilon_0$  the permittivity constant =  $8.85 \times 10^{-12} \text{ Fm}^{-1}$ ,  $A$  is the area of the electrode and the thickness of the polymers is  $d$ .

### 3.2.11 Ultrasonic probe

This instrument was used during the study of the interaction of the monomers with the montmorillonite clay. Ultrasonic vibrations were used to assist in the dispersion of the monomer and polymer into the clay galleries. Ultrasonic homogenizer sonicator model U200S-Control from IKA Labortechnik Staufen, Germany was used at duty cycle 0.5 with constant amplitude of 60%.

## 3.3 Methods

### 3.3.1 Synthesis of sulfated zirconia catalyst

Sulfated zirconia ( $\text{SO}_4^{2-}/\text{ZrO}_2$ ) was prepared according to the method described by Qi *et al* [43, 213]. Briefly, 1 g of zirconium hydroxide was dissolved in 10 mL of 1M  $\text{H}_2\text{SO}_4$  and stirred vigorously at room temperature for 3 h. The suspension was centrifuged using a Heraeus Biofuge Primo Centrifuge machine set at 3000 rpm for 15 minutes and

the supernatant was discarded. The deposition at the bottom of the centrifuge tube was dried in a vacuum at 60 °C overnight. It was ground into a fine powder using pestle and mortar, and further calcined at 500 °C in a muffle furnace for 3 h. The catalyst was characterised by XRD and FT-IR.

### 3.3.2 Dehydration of glucose to 5-HMF [43]

To glucose (5.0 g, 0.028 mol) was added BMIMCl (20.0 g, 0.11 mol) and the following catalysts at 10 mol. %: H<sub>2</sub>SO<sub>4</sub>, HCl, HNO<sub>3</sub>, CrCl<sub>3</sub>.6H<sub>2</sub>O, ZrO<sub>2</sub>, and SO<sub>4</sub><sup>2-</sup>/ZrO<sub>2</sub>. The mixture was heated to 120 °C for 2 h and samples were withdrawn at 30 minute intervals and immersed in an ice bath to quench the reaction in order to assess the progress of conversion.

After completion of the reaction, ethyl acetate (50 mL) was added and the mixture separated by decanting the upper layer. The same procedure was repeated three times and the combined ethyl acetate extracts were dried (sodium sulfate) and evaporated *in vacuo* at (50 °C) to isolate 5-HMF as a thick pale yellow liquid. An identical procedure was used for fructose.

<sup>1</sup>H NMR (300 MHz; CDCl<sub>3</sub>) δ 9.57 (1H, s, CHO), 7.22 - 7.21 (1H, d, *J* = 3.0 Hz, 3-H), 6.50 (1H, d, *J* = 6.0 Hz, 4-H), 4.70 (2H, s, OCH<sub>2</sub>); <sup>13</sup>C NMR (75 MHz; CDCl<sub>3</sub>) δ 177.8 (C=O), 160.9 (C-5), 152.2 (C-2), 122.9 (C-3) 109.8 (C-4), 57.7 (OCH<sub>2</sub>); FT-IR (cm<sup>-1</sup>) 3345br, 1660s, 1250s, 1188s, 1160s.

### 3.3.3 Dehydration of glucose to 5-HMF by vacuum distillation

Glucose (5.0 g, 0.028 mol) and BMIMCl (20.0 g, 0.11 mol) were heated in an oil bath at a temperature of 120 °C and stirred for 300 s to allow the dissolution of the glucose in the ionic liquid. The reaction was started by adding 10 mol. % of the following catalysts: CrCl<sub>3</sub>.6H<sub>2</sub>O, ZrO<sub>2</sub>, and SO<sub>4</sub><sup>2-</sup>/ZrO<sub>2</sub>. After completion of the reaction, 5-HMF was collected by vacuum distillation at 180 °C, 2.7 kPa. The same procedure was used for fructose.

### 3.3.4 Yield calculation of 5-HMF produced

The yield of 5-HMF produced was calculated from the following equation:

$$\text{5-HMF yield (mol. \%)} = \frac{\text{Moles of 5-HMF produced}}{\text{Moles of carbohydrate used}} \times 100\% \text{ ----- (3.5)}$$

## 3.4 Synthesis of some derivatives of 5-HMF

### 3.4.1 Synthesis of 2,5-furandicarboxylic acid (FDCA)[323]

To 5-HMF (1.26 g, 0.01 mol) was added a solution of NaOH (0.92 g, 0.023 mol). Potassium permanganate (3.6 g, 0.023 mol) was added and the reaction stirred at ambient temperature for 0.5 h. The mixture was filtered and to the filtrate 1 mL of concentrated HCl was added to adjust the pH to 1 or less. The precipitate was collected by suction filtration, washed with distilled water (50 mL) and FDCA isolated as a yellow solid (1.25 g, 80%).

$^1\text{H}$  NMR (500 MHz, DMSO- $d_6$ )  $\delta$  13.56 (2H, s, COOH), 7.29 (2H, s, 2 x =CH);  $^{13}\text{C}$  NMR (126 MHz, DMSO- $d_6$ )  $\delta$  158.5(COOH), 149.5 (C-2 and C-5), 118.3 (C-3 and C-4); FT-IR ( $\text{cm}^{-1}$ ) 3117s, 1665s, 1570s, 1418s, 960s, 851s.

### 3.4.2 Synthesis of 2, 5-bis-(hydroxymethyl) furan (BHMF)

To 5-HMF (2.0 g, 0.016 mol) in methanol (40 mL, 0 °C), sodium borohydride (2.4 g, 0.063 mol) was slowly added. The reaction was stirred for 3 h at room temperature, quenched with saturated aqueous sodium chloride solution (40 mL) and stirred for a further 30 minutes. The methanol was removed *in vacuo* at 40 °C. The product was extracted with ethyl acetate (3 x 40 mL), the organic layers combined and washed with brine (60 mL) and dried (sodium sulfate). The solvents were removed *in vacuo* to give BHMF as a pale yellow powder (1.8 g, 88%).

$^1\text{H}$  NMR (300 MHz,  $\text{CDCl}_3$ )  $\delta$  6.22 (2H, s, 3-H and 4-H), 4.56 (4H, s,  $\text{OCH}_2$ );  $^{13}\text{C}$  NMR (75 MHz,  $\text{CDCl}_3$ )  $\delta$  154.1 (C-2 and C-5), 108.7 (C-3 and C-4), 57.5 ( $\text{OCH}_2$ ); FT-IR ( $\text{cm}^{-1}$ ) 3310br, 1730s, 1240s, 971s, 810s, and 756s.

### 3.4.3 Synthesis of dimethyl-2, 5-furandicarboxylate (DFD) [158]

To FDCA (10.0 g, 0.064 mol) in 130 mL of methanol, *p*-toluenesulfonic acid monohydrate (30.5 g, 0.16 mol) was added. The mixture was heated at reflux for 3 h and distilled water (130 mL) added. The precipitate formed was collected and recrystallized from methanol to give DFD as colourless crystals (10.6 g, 91%).

$^1\text{H}$  NMR (500 MHz; DMSO- $d_6$ )  $\delta$  7.27 (2H, s, 2 x =CH), 3.84 (6H, s, 2 x OMe);  $^{13}\text{C}$  NMR (126 MHz; DMSO- $d_6$ ) 157.8 (C=O), 146.0 (C-2 and C-5), 118.9 (C-3 and C-4).

### 3.4.4 Sample preparation for XRD

The samples prepared from 5-HMF and FDCA by the solution and melt intercalation methods were carefully ground into fine powders using a pestle and mortar and pressed with a microscope slide into a copper sample holder and analysed using an X-ray diffractometer (Siemens D500) in the Chemistry Department of UCL using Cu K $\alpha$ 1 radiation with wavelength of 0.154056 nm. The diffractometer, running at 40 kV, and 30 mA was set at a low initial angle of 2° and scanned to 25° 2 $\theta$  in 0.05° steps. Counts were collected for 6 s at each step and the XRD pattern of the samples was obtained.

### 3.4.5 Treatment of montmorillonite clay with 5-HMF and FDCA

#### 3.4.5.1 Dispersion of clay and 5-HMF

A suspension of 1 g of montmorillonite clay (Nanofill 116) was made in 25 mL of ethyl acetate in a glass bottle with lid and 2 g of 5-HMF was added. The contents were stirred with the aid of an ultrasonic probe (U200s control, IKA Labortechnik Germany) at 0.5 duty cycle to limit the heating effect, 60% amplitude and poured into a Petri dish and left to stand for 86 ks (24 h) for drying. Control samples were prepared with solvent but without 5-HMF.

#### 3.4.5.2 Melt intercalation method of clay and 5-HMF

1 g of 5-HMF was carefully weighed into a 10 mL beaker and 0.05 g of montmorillonite clay was added. The contents were covered with an aluminium foil and heated on a hot

plate at a temperature of 75 °C for 20 minutes. The contents were cooled at 2 °C and analysed by XRD.

### 3.4.5.3 Dispersion of clay and FDCA

1 g of montmorillonite clay was dissolved in 25 mL of DMSO in a 50 mL glass bottle and dispersed with an ultrasonic probe at 0.5 duty cycle, 60% amplitude for 20 minutes. To the contents in the 50 mL glass bottle, 2 g of FDCA were added and the dispersion continued for further 20 minutes. The contents were poured into an evaporating basin and placed on a hot plate pre-set at 150 °C to evaporate the DMSO. After 30 minutes, the evaporating basin was cooled to room temperature and dried in a vacuum oven at 60 °C for 72 h.

### 3.4.5.4 Melt intercalation of clay and FDCA

Montmorillonite clay and FDCA were weighed in a ratio of 1:2 and placed into a 400 mL cylindrical glass vessel. Nitrogen gas was introduced into the glass vessel with the aid of a balloon as inlet and an empty balloon was placed at the outlet. The contents were heated in a furnace to 330 – 344 °C and allowed to cool to room temperature.

### 3.4.6 Synthesis of modified MMT clay

Organically modified MMT clay was synthesis according to the protocol described by Yuan *et al.* [324]. Briefly, 15 g of Na-MMT was suspended in 400 mL of distilled water and stirred for 6 hrs at ambient temperature. A mixture of hydrochloric acid (HCl) and cetyltrimethylammonium bromide (CTAB) as an organic treatment agent in a mole ratio of 1:1 was added slowly to the clay suspension and stirring continued for another 3 h at 80 °C. A precipitate was formed and filtered, washed with distilled water several times and the filtrate was tested with 0.1 mol/L AgNO<sub>3</sub> until no further bromide ions were detected. The result product was dried in a vacuum at 60 °C overnight and ground with a pestle and mortar to a fine powder.

## 3.5 Polymerization reactions

### 3.5.1 Synthesis of polyester from FDCA [323]

FCDA (5.0 g, 0.03 mol), 1,4-butanediol (13.523 g, 0.15 mol) and titanium (IV) *n*-butoxide (0.102 g, 0.0003 mol) were heated at 160 °C for 6 h under a N<sub>2</sub> atmosphere. Excess diol was then removed under vacuum and the reaction heated at 200 °C for further 2 h under vacuum. Upon cooling to room temperature, 6 mL of 1,2-dichlorobenzene was added and heating continued at 200 °C under vacuum to remove traces of diol. The resulting polyester was dissolved in 30 mL of trifluoroacetic acid (TFA) and precipitated using methanol (300 mL). The precipitates were centrifuged at 3000 rpm for 10 minutes, washed with methanol (3 x 5 mL) and dried at 50 °C under vacuum for 18 h.

### 3.5.2 Water absorption test

Water absorption tests were conducted by following ASTM D570-98: standard test method for water absorption of plastics [325]. Briefly, the samples were conditioned by drying in an oven for 24 h at 50 ± 3 °C, cooled in a desiccator and immediately weighed to the nearest 0.001g. The conditioned samples were immersed entirely in a 50 mL glass beaker containing 25 mL of distilled water maintained at ambient temperature. The immersed samples were removed after specific time intervals and all surface water was gently wiped with dried lint-free filter paper and weighed to the nearest 0.001g. Percentage increased in weight during immersion was calculated using the following equation:

$$\text{Increase in weight, \%} = \frac{W_f - W_o}{W_o} \times 100 \text{ ----- (3.6)}$$

$W_f$  is the weight of the water absorbed sample and  $W_o$  is the weight of the conditioned sample.

## 3.6 Preparation of polymer/clay nanocomposites

Polymer/clay nanocomposites were prepared by intercalation from solution, in situ intercalative polymerization and melt intercalation as follows:

### 3.6.1 Polymer/Clay Nanocomposites by Intercalation method

Montmorillonite clay (10 mg) was weighed and dispersed in chloroform (25 mL) by ultrasonication. Polyester (200 mg) was added to the clay solution and dispersed for a further 30 minutes. The contents were transferred into a Petri dish and dried in a fume cupboard overnight to evaporate the chloroform. After drying, the mixture was ground with a pestle and mortar to a fine powder and the XRD pattern of the polyester/clay was obtained.

### 3.6.2 *In situ* intercalative polymerization

FDCA (4.5 g), montmorillonite clay (0.225 g), 1,4-butandiol (13.53 g, 30 mmol) and titanium (IV) n-butoxide were charged into a 50 mL round bottom flask and heated in an oil bath set at 160 °C under reflux and in a N<sub>2</sub> atmosphere for 6 h. The excess diol was removed under vacuum and the reaction continued for further 2 h at 200 °C under vacuum. The reaction mixture was cooled at room temperature and the resulting polyester was dissolved in trifluoroacetic acid (30 mL). Methanol (100 mL) was added to precipitate the polyester/clay and the precipitate was centrifuged at 3000 rpm for 10 minutes, washed with methanol (10 mL 3 times) and dried under vacuum at 50 °C overnight.

### 3.6.3 Melt intercalation

Montmorillonite clay (10 mg) and polyester (200 mg) were charged into a 50 mL round bottom flask and heated at 40 °C with constant stirring at 300 rpm for 1h. The melt sample was cooled to 4 °C and ground with a pestle and mortar to a fine powder and analysed by XRD.

## CHAPTER 4: RESULTS AND DISCUSSION

### 4.1 Characterisation of sulfated zirconia catalyst

Sulfated zirconia ( $\text{SO}_4^{2-}/\text{ZrO}_2$ ), has been reported as a solid acid catalyst used in various reactions such as acylation, alkylation, nitration, etherification and esterification [43]. In this work, it was used in the dehydration of glucose to 5-HMF with other solid catalysts such as  $\text{CrCl}_3 \cdot 6\text{H}_2\text{O}$  and zirconium dioxide ( $\text{ZrO}_2$ ). The sulphated zirconia prepared was characterized by XRD.

### 4.2 X-ray diffraction of sulfated zirconia

XRD was used to elucidate the changes in the crystalline phase of zirconia before and after treatment with sulphuric acid. It was observed that the XRD patterns exhibited tetragonal–monoclinic phase transformation as revealed in Figure 4-1. From literature, it was revealed that sulfate treatment of zirconia retards its crystallization which leads to its transition from the tetragonal phase to the monoclinic phase occurs [326]. Furthermore, it was reported that during monoclinic–tetragonal phase transformation of zirconia, the tetragonal phase should be formed above 1170 °C [43, 213], but in this experiment the zirconia prepared occurred as a tetragonal phase at lower temperature. This might be that the transformation was hindered in fine  $\text{SO}_4^{2-}/\text{ZrO}_2$  powders because of the sulfate treatment of pure zirconia [327]. Moreover, this transformation of the tetragonal phase into the monoclinic phase was probably due to the lower surface energy of the tetragonal phase compared to monoclinic phase [328].

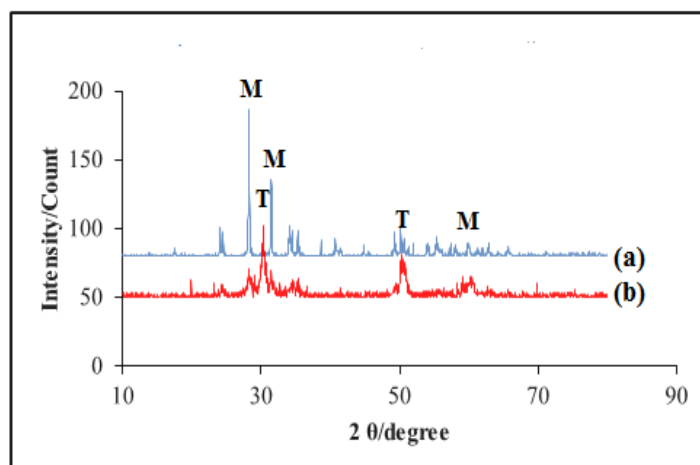


Figure 4-1. XRD patterns of (a) ZrO<sub>2</sub> (b) SO<sub>4</sub><sup>2-</sup>/ZrO<sub>2</sub> (M and T designate monoclinic and tetragonal phases)

Therefore, sulfate treatment of zirconia can lead to retention of the tetragonal phase and this indicates a strong effect of the sulfate ions on phase modification of zirconia and allowed the catalyst to retained its stability in the tetragonal phase as reported elsewhere [213].

The phase composition in Figure 4-1 was established using JCPDS card index nos. 14-0534, 17-0923, 79-1770 and 85-1081 for tetragonal phase and 13-0307, 37-1484 and 07-0343 for monoclinic phase as reported by Evans, *et al* [329] and the phase mixtures are presented in Table 4-1. Furthermore, the amount of tetragonal ZrO<sub>2</sub> was calculated using intensity measurements as suggested by Evans, *et al* [329] and Schmid [330] using the following equation:

$$f_{(i)} = \frac{I_i(111)}{I_i(111) + I_m(111)} \text{-----} (4.1)$$

Where,  $f_{(i)}$  fraction of tetragonal phase,  $I_i(111)$  and  $I_m(111)$  are X-ray intensity peaks of tetragonal and monoclinic phases in 111 ( $hkl$ ) planes.

From the results obtained, it was observed that 27% represents the tetragonal ZrO<sub>2</sub> is present in pure zirconia and 73% in sulfated zirconia using JCPDS card index numbers 17.0923 and 13-0307.

Table 4-1. Phase mixtures transformation of sulfated zirconia

Phase	JCPDS card index	<i>hkl</i>	$2\theta$	$\theta$	d/nm
Tetragonal ZrO <sub>2</sub>	14-0534	111	30.28	15.14	0.294900
Tetragonal ZrO <sub>2</sub>	17-0923	111	30.17	15.08	0.296000
Monoclinic ZrO <sub>2</sub>	13-0307	111	31.54	15.77	0.283400
Monoclinic ZrO <sub>2</sub>	37-1484	111	31.47	15.73	0.284069

### 4.3 Dehydration of glucose/fructose by solvent extraction

Synthesis of 5-HMF via the dehydration of glucose and fructose were investigated using a solvent extraction method. This is to provide a preliminary investigation on the yields obtained using these liquid catalysts and the sulfated zirconia catalyst. The results obtained are presented in Figure 4-2 from which it was observed that higher yield (36%) was obtained from SZ catalyst using fructose as a substrate. This is only a slightly higher yield compared to H<sub>2</sub>SO<sub>4</sub> using the same substrate. However, glucose substrate revealed a lower yield in SZ (18%) compared to H<sub>2</sub>SO<sub>4</sub> (26%). This can be attributed to the isomerization of glucose to fructose which has been reported to undergo a different reaction mechanism to form 5-HMF [331]. Therefore, SZ was subsequently used with other solid catalysts for 5-HMF synthesis via vacuum distillation and the results are discussed in section 4.4.

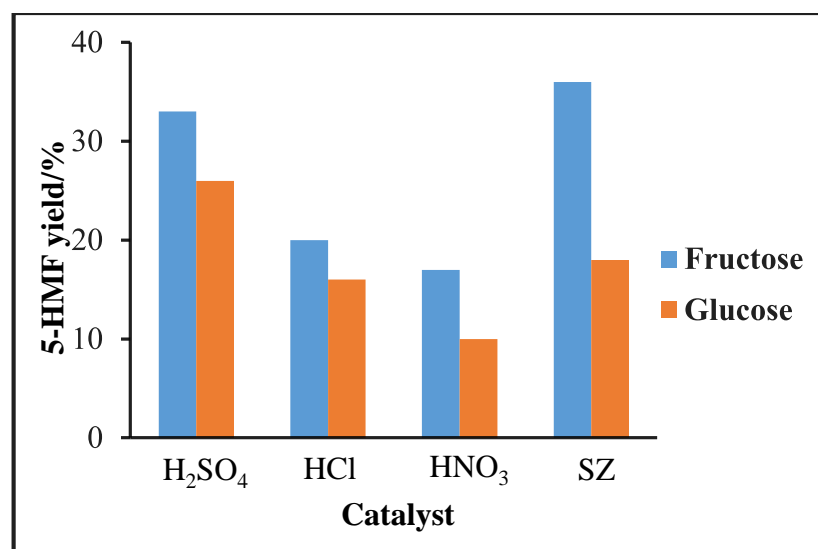


Figure 4-2. 5-HMF yields by solvent extraction method

#### 4.4 Dehydration of glucose/fructose by vacuum distillation

The dehydration of glucose and fructose were investigated using a reactive vacuum distillation approach. This is to provide an avenue whereby the production of 5-HMF is conducted and separated with minimal use of volatile solvents: almost all reported literature on the synthesis of 5-HMF is based on solvent extraction [43, 164, 212, 213, 231, 332]. To date, only one paper reported the separation of 5-HMF under vacuum distillation [333]. These authors reported the dehydration of glucose and fructose using a vacuum distillation set-up with so-called ‘entrainers’ and reported a yield of 94.4% at 180 °C and 93.2% at 150 °C using fructose as reactant for 10 and 30 minutes reaction times respectively. Furthermore, they reported yields of 68.5% and 65.2% of 5-HMF also using glucose at the same temperatures and reaction times. From their stated operating conditions, 2 g of fructose/glucose and 0.065 g of IrCl<sub>3</sub>·(1-2)H<sub>2</sub>O/0.049 g of CrCl<sub>3</sub>·6H<sub>2</sub>O were dissolved in 20 g of ionic liquids. It could be argued that based on these stated reaction conditions, the level of precision claimed in their results is not justified by the likely associated weighing errors. Whether the results support the conclusions is therefore somewhat controversial.

Wei *et al* [333] used nitrogen, hexane and methyl isobutyl ketone (MIBK) as entrainers. These entrainers were used to increase the evaporation efficiency of the distillation process and effectiveness of the recovery of 5-HMF. Their suggestion was

that the solvents hexane and MIBK enhanced the process. Inspection of rows 1, 3 and 5 in their results (reproduced here as Table 4-2) shows that there may be no significant difference in yield compared to the use of nitrogen alone (Entry 1) and that improvements in recovery are marginal. Since the use of the solvents introduces a downstream separation stage and nitrogen does not, there is a case for using nitrogen only to enhance the distillation.

Therefore, considering the boiling point of 5-HMF which is 114 -116 °C at 1 mbar, a reactive vacuum distillation procedure involving both the chemical reaction and product separation steps within a single unit was applied for the production of 5-HMF from glucose dehydration. This reactive distillation method can have a wide range of industrial applications [334-336]. The process results in the evaporation of the most volatile component because when the pressure is reduced, the molecules are few and hence, it is possible for vaporization and distillation to take place. A continuous operation procedure could be envisaged.

As stated earlier, the reaction involves the dehydration of glucose and fructose in BMIMCl ionic liquid with separation by vacuum distillation [337]. It was aimed to provide a commercially viable pathway that avoids a discrete separation stage and efficiency savings in any heating costs. It also helps to keep the product from decomposing at the high temperatures that would be required for atmospheric pressure distillation. In general, thermally sensitive substances can be processed easily and separated from component mixtures by this technique. In previous work on the dehydration of glucose as reported by some authors, a reaction step was followed by a liquid-liquid separation stage with attendant redistillation and capture of solvents [43, 338]. This makes the process considerably less attractive from a manufacturing viewpoint.

Table 4-2. Vacuum reactive distillation of 5-HMF from the dehydration of carbohydrates with different entrainers [333].

Entry	Carbohydrate	Entrainer	Temp. (°C)	Time (min)	Recovery (%)	Yield (%)
1	Fructose	N <sub>2</sub>	180	10	90.6	94.4
2			150	30	89.4	93.2
3		Hexane	180	10	94.6	93.8
4			150	30	93.6	93.7
5		MIBK	180	10	95.0	95.1
6			150	30	93.6	94.6
7 <sup>a</sup>	Glucose	-	180	10	-	92.5
8 <sup>a</sup>		-	150	30	-	90.8
9 <sup>a</sup>		-	120	20	-	89.0
10		N <sub>2</sub>	180	10	88.3	68.5
11			150	30	85.3	65.2
12		Hexane	180	10	87.5	70.4
13	150		30	88.6	64.8	
14	MIBK	180	10	88.2	71.8	
15		150	30	88.4	66.2	
16 <sup>a</sup>	-	180	10	-	51.3	
17 <sup>a</sup>	-	150	30	-	42.1	
18 <sup>a</sup>	-	100	180	-	35.1	

<sup>a</sup> Reaction carried out without vacuum distillation

The relationship between vapour pressure and temperature of 5-HMF from thermodynamic data reported [339] was used to determine the actual boiling point of the 5-HMF at the pressure used (Figures 4-3 and 4-4).

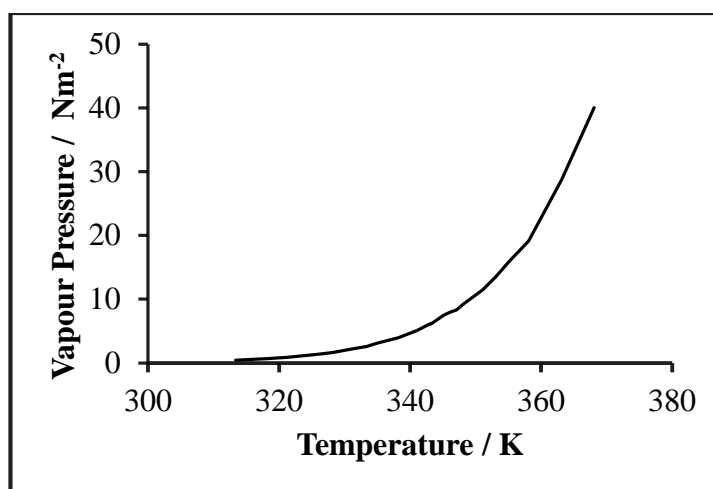


Figure 4-3. Plot of vapour pressure against temperature for 5-HMF [339].

The relationship between the temperature of a liquid and its vapour pressure is logarithmic and can be explained by the Clausius-Clapeyron equation as:

$$\frac{d \ln P}{dT} = \frac{\Delta H_{\text{vap}}}{RT^2} \text{-----} (4.2)$$

From the above equation, the rate at which the natural logarithm of the vapour pressure changes with temperature is determined by the molar enthalpy of vaporization  $\Delta H_{\text{vap}}$ , the ideal gas constant  $R$ , and the temperature  $T$  (K) of the system.

Assuming that  $\Delta H_{\text{vap}}$  does not change very much with temperature, equation (4.2) can be expressed in the following integrated form where  $C$  is a constant.

$$\ln P = -\frac{\Delta H_{\text{vap}}}{RT} + C \text{-----} (4.3)$$

This form of the Clausius-Clapeyron equation (4.3), is been used to measure the enthalpy of vaporization of the 5-HMF from plots of the natural logarithm of its vapour pressure versus temperature.

The logarithm of the vapour pressure increases as the temperature of the system increases. Thus the  $\ln P$  vs  $1/T$  plot shown in Figure 4-4 is linear as expected.

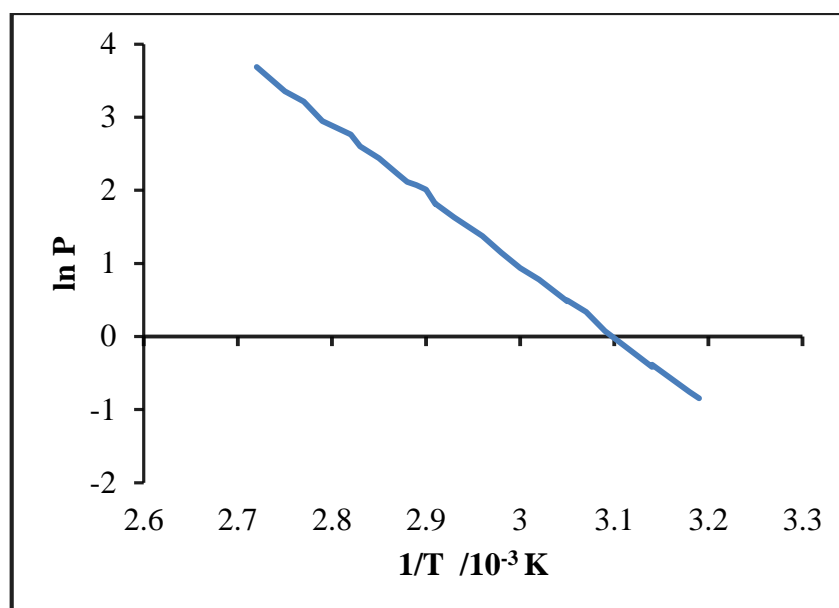


Figure 4-4. Plot of  $\ln P$  against reciprocal of temperature for 5-HMF [339].

#### 4.4.1 Testing the vacuum distillation equipment

To test the efficacy of the arrangement for vacuum distillation, water was initially used and operating at a pressure of 27 kPa to 53 kPa, 94% of the water was collected at 45 °C. The same process was repeated with the addition of 5-HMF dissolved distilled water (ratio of 0.2: 25). After 30 min, 94% of water was collected as the distillate while a pale yellow liquid remained as undistilled material. This was dried under vacuum for 1 h to remove traces of water and the amount of 5-HMF remaining was 60% of what was initially added. This indicated that the experimental arrangement was able to separate 5-HMF from the solvent (water) used in 60% yield and the equipment was therefore employed in the dehydration of glucose and fructose.

### 4.5 Synthesis of 5-(hydroxymethyl) furan (5-HMF)

#### 4.5.1 5-HMF yields from dehydration of glucose and fructose

The dehydration of glucose was conducted as reported by Wei *et al* [333] with some modifications of their experimental conditions. These modifications included a change in catalyst, entrainer and the use of the vacuum distillation equipment as highlighted

above. The catalysts used in this work have been used previously in dehydration of carbohydrate. However, they have not been employed with reactive vacuum distillation equipment.

The results of the dehydration of glucose and fructose conducted under vacuum at 180 °C in 1-butyl-3-methylimidazolium chloride (BMIMCl) solvent with 10 mol.% of the catalysts,  $\text{CrCl}_3 \cdot 6\text{H}_2\text{O}$ ,  $\text{ZrO}_2$  and  $\text{SO}_4^{2-}/\text{ZrO}_2$  designated as Cr (III), Z and SZ respectively, are presented in Figure 4-5. From these results, it was observed that higher yields (82%, 75% and 55%) of 5-HMF were obtained using fructose as a substrate with catalysts SZ, Cr (III) and Z, respectively. When using glucose as a substrate, the yields were lower compared with those for fructose as substrate. This lower yield may be as a result of the glucose straight chain and pyranose ratio (63%  $\beta$ -glucopyranose and 37%  $\alpha$ -glucopyranose) in water and hence, the enolisation rates might be slow [48]. Since fructose forms less stable ring structures, more open chains structures are likely to be present in BMIMCl and therefore the enolisation rates might be higher. Fructose and glucose have been reported to exhibit different reaction mechanisms to form 5-HMF as glucose isomerizes to fructose on dehydration [340], and this might account for the lower yield of 5-HMF from glucose as compared to that of fructose. This observation was also explained elsewhere [341]. The results of the 5-HMF yields from glucose (65%, 63% and 34%) using SZ, Z and Cr (III) catalysts in BMIMCl solvent was higher in this work as compared to 22%, 24% and 27% using the same solvent and catalysed by zeolite (H-ZMS-5) as reported from literature [342]. Therefore, this study revealed that SZ can effectively catalysed the dehydration of glucose to 5-HMF in higher yield as compared to zeolite even though both catalysts are environmentally benign.

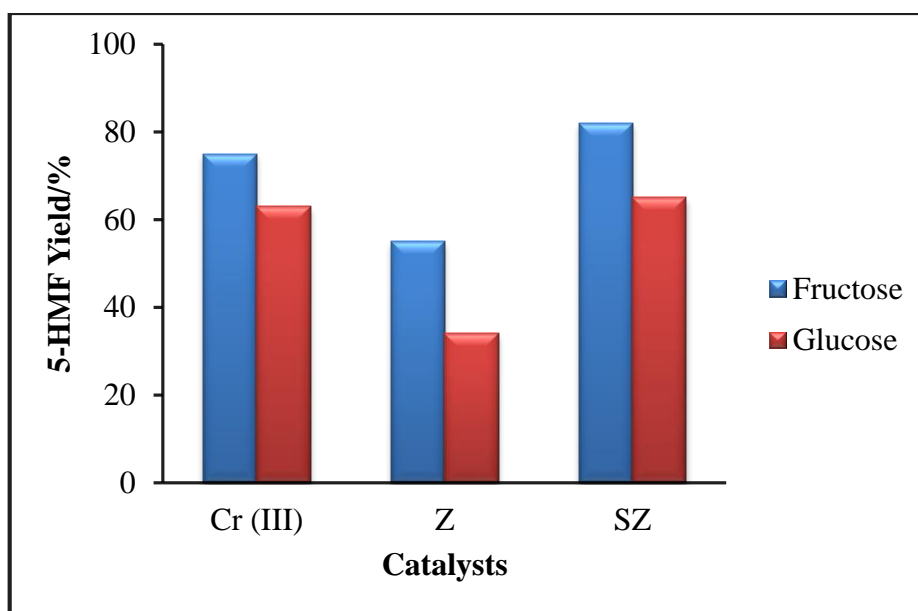


Figure 4-5. Dehydration of glucose and fructose in different solid catalysts

#### 4.5.2 Catalytic activity of the solid catalysts

Based on catalytic activity, it was observed that SZ exhibited a strong catalytic activity as can be seen (Figure 4-5) which gave almost 80% and 65% yields from fructose and glucose substrates. Also, the catalytic activity of SZ was compared with an untreated Z catalyst and lower yields were obtained from the latter. This increased catalytic activity of SZ may be attributed to the increased acid sites of SZ in comparison to Z.

#### 4.5.3 5-HMF formation in other ionic liquids

In order to optimise 5-HMF yield, the use of other ionic liquids; 1-hexyl-3-methylimidazolium chloride ([HMIM]Cl) and 1-butyl-2,3-dimethylimidazolium hexafluorophosphate ([BDMIM]PF<sub>6</sub>) were used. The results compared to those when using [BMIM]Cl ionic liquid are presented in Figure 4-6. Among the ionic liquids used in the synthesis of 5-HMF, [BMIM]Cl clearly gave 5-HMF in higher yields.

Ionic liquids [BMIM]Cl and [HMIM]Cl media provided significant yields of 5-HMF in the dehydration reaction of fructose and glucose substrates. This may be due to the fact that the chloride ions form only weak ion pairs [343], which leads more readily to the isomerization of carbohydrates [216] and the subsequent dehydration process.

Furthermore, as a result of the weak coordination of the ionic liquid structures, they do not compete with sugar for the binding of metal chlorides; therefore it is more likely that a sugar-metal coordination complex will be formed [344].

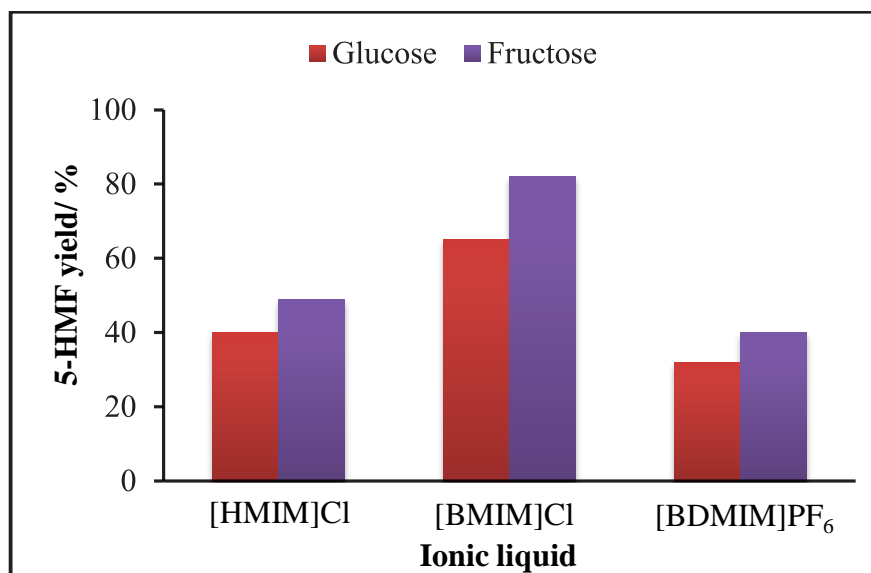


Figure 4-6. 5-HMF yields in ionic liquids

#### 4.5.4 Effect of reaction temperature with time on 5-HMF yield

The effect of reaction temperature with time on 5-HMF yield in the dehydration of fructose catalysed by sulfated zirconia (SZ) using [BMIM]Cl solvent was investigated and the results are presented in Figure 4-7. The reactions were conducted at 100 °C, 120 °C, 150 °C and 180 °C. As shown in Figure 4-7, it was observed that the reaction temperatures have a significant effect on the 5-HMF yield. When the reactions were conducted at 100 °C, a lower yield (18%) was obtained after 2 h and a maximum yield of 82% was obtained at 180 °C after the same time of 2 h. It was also observed that the yield tended to increase gradually with increasing reaction time up to 120 minutes. Beyond 120 minutes, a decrease in yield of 5-HMF was observed in these temperature regimes. These results indicate that the degradation of 5-HMF was significant at higher reaction time even though increase in temperature speeds up the reaction initially and this behaviour was also reported elsewhere [41, 189, 254]. Furthermore, it was reported that [BMIM]Cl is known for its reaction with aldehyde functional group [345] and this decreased in yield might also be a side product formed from the reaction between 5-HMF and [BMIM]Cl as reported in literature [331].

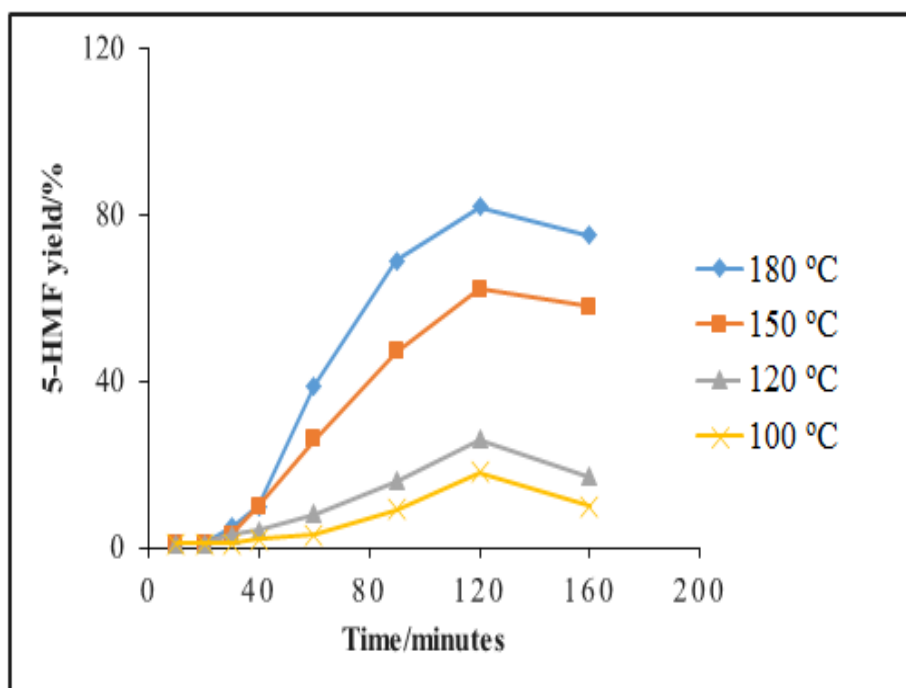


Figure 4-7. Effect of reaction temperature and time on 5-HMF yield

#### 4.5.5 Effect of catalyst dosage on 5-HMF synthesis

The effect of catalyst dosage on 5-HMF synthesis was investigated using fructose and glucose as substrates and the results are presented in Figure 4-8. This result is based on the dehydration of the substrates in BMIMCl ionic liquid solvent and sulfated zirconia catalyst at 180 °C, where the highest yield of 5-HMF was obtained (Figure 4-7). When the catalyst dosage was increased from 2.5 mol. % to 10 mol. %, the yield of 5-HMF increased, at 180 °C for a reaction time of 120 minutes, from 22% to 82% with fructose as substrate and 16% to 65% when using glucose as substrate. However, when the amount of the sulfated zirconia was increase from 10 mol. % to 30 mol. %, there was a decrease in the 5-HMF yield with both fructose and glucose as substrates. Therefore, 10 mol. % of catalyst dosage was chosen as the most suitable condition.

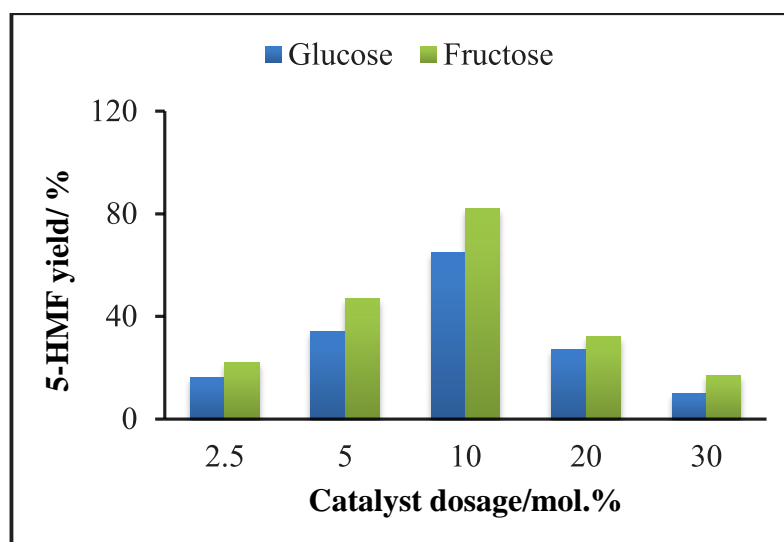


Figure 4-8. Effect of catalyst dosage on 5-HMF yield

#### 4.5.6 Sulfated zirconia and [BMIM]Cl recycling

Recycling of catalysts and solvents is very important based on the principles of green engineering [346] and therefore, recycling of sulfated zirconia catalyst and [BMIM]Cl ionic liquid was examined. The result of this study is presented in Figure 4-9 which shows that the recycled catalyst and ionic liquid gave comparable results on 5-HMF yields. For instance, the catalyst and the solvent retained a very high activity up to the third cycle and tended to lose their activity slightly from fourth to fifth cycle. This might be due to the retention of some 5-HMF or unreacted substrates in these cycles.

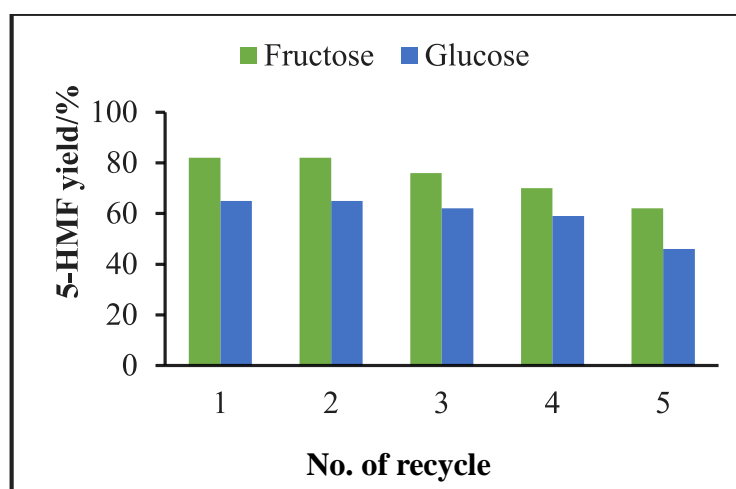


Figure 4-9. Recycling of sulfated zirconia and [BMIM]Cl

## 4.6 Characterization of 5-HMF

The synthesised 5-HMF was characterised by  $^1\text{H}$  NMR,  $^{13}\text{C}$  NMR and FT-IR and were similar to previous data reported [333]. From the analysis of the  $^1\text{H}$  and  $^{13}\text{C}$  NMR data, only 5-HMF was present indicating a purity >95%. In addition, the FT-IR data indicated that the absorption bands were in agreement with NMR data as assigned in section 3.3.2. All spectral data are compared with commercially sourced 5-HMF and are presented in appendix 2.

## 4.7 Synthesis of some derivatives of 5-HMF

Some derivatives of 5-HMF were synthesised in order to select the optimal monomer for treatment with montmorillonite clays for subsequent production of polymer-clay nanocomposites. These derivatives were 2,5-FDCA and 2,5-BHMF which were characterised by FT-IR and NMR spectroscopy and their spectra are shown in appendix 3.

### 4.7.1 Synthesis of FDCA

Stated in the experimental section, FDCA was synthesised by oxidation of 5-HMF by potassium permanganate in a solution of sodium hydroxide and a pale yellow solid was isolated by filtration as the product. The product was characterized by NMR and FT-IR spectroscopy.

#### 4.7.1.1 Characterization of FDCA

The  $^1\text{H}$  and  $^{13}\text{C}$  NMR results as assigned in section 3.4.1 were similar as to reported values found in literature [65, 237, 347].

In addition, the expected FT-IR absorption bands were observed (section 3.4.1). The C = O stretching vibration characteristic of the carbonyl group occurs at  $1670\text{ cm}^{-1}$  in agreement with others [348]. Using the C = O stretching absorption resulting from that of carboxylic acids occurs near  $1760\text{ cm}^{-1}$  [347]. This decrease may be attributed to the conjugation effects of the carbonyl group with the unsaturation of the furan ring

which decreases the bond order of the C=O slightly and this leads to shifting of the absorption band to a lower frequency [348].

The FT-IR peaks observed are summarised in Table 4-3 which are in agreement with the values reported elsewhere [65, 237, 347, 349].

Table 4-3. Characteristic peaks of FDCA

Assignment	Wavenumber / cm
C = O stretching	1670
C – H	3150, 3120
OH (Acid)	2700 - 3400
C = C (Furan ring)	1569
C – O – H bending (Acid)	1418
C – H bending and Furan ring	960, 851, 762

#### 4.7.2 Synthesis of 2,5-bis (hydroxymethyl) furan (BHMF)

2,5-bis (hydroxymethyl) furan was synthesised by oxidation of 5HMF using NaBH<sub>4</sub> and KMnO<sub>4</sub>. The product was recrystallized in a refrigerator and a light yellow powder and was characterized by NMR and FT-IR spectroscopy.

##### 4.7.2.1 Characterization of BHMF

From the analysis of the <sup>1</sup>H NMR data, the BHMF was present indicating a purity >90%. Furthermore, the FT-IR data confirmed the various functional groups associated with BHMF as assigned by NMR. Both data assigned were presented in section 3.4.2 and the spectra are in appendix 3.

Therefore, this product will either serve as a monomer or diol for esterification reactions and also will be treated with Na-MMT clay for an attempt to carry out an *in situ* polymerization for the synthesis of polymer-clay nanocomposite.

### 4.7.3 Synthesis of dimethyl-2, 5-furandicarboxalate (DFD)

In order to establish if the intercalation of 2,5-FDCA with Na-MMT clay was due to the acid functional group, the corresponding dimethyl dicarboxylate was synthesised in excess methanol. An analysis of the  $^1\text{H}$  NMR results revealed that DFD was obtained as the only product as confirmed by the assignment of the protons shown in section 3.4.3 and the spectra in appendix 4.

## 4.8 Assessment of intercalation of monomers into clay

### 4.8.1 5-HMF and Na-MMT clay

An assessment of the intercalation of 5-HMF into a natural montmorillonite clay (MMT) was conducted and the results obtained by XRD (Figure 4-10) are presented in Table 4-4. The XRD pattern of the clay shows a strong basal reflection at  $6.95^\circ$  of  $2\theta$  which from the Bragg equation ( $\sin \theta = \lambda/2d$ ) corresponds to  $d_{(001)}$  of 1.271 nm which is close to values usually reported for natural montmorillonite [257, 259, 261, 295, 308, 350-353]. After introducing 5-HMF into the solvent (ethyl acetate) and Na-MMT clay, the contents were dispersed by the aid of an ultrasonic probe for 15 minutes. The corresponding  $d_{(001)}$  reflection of 5-HMF-Na-MMT appears at a lower angle ( $4.30^\circ$  of  $2\theta$ ), indicating an increased basal spacing to 2.053 nm. This can be attributed to the intercalation of 5-HMF into the Na-MMT galleries. The other reflections such as that observed at  $19.60^\circ$  of  $2\theta$  were not shifted by the introduction of 5-HMF. Thus the inner sheet structure of the Na-MMT was not affected by the intercalation and geometrical irregularities in the sample which are amplified at low angles were not responsible for the displacement. It is often assumed that the intercalating species, in this case 5-HMF is lying flat on the silicate surface, which could maximise the electrostatic interaction [354].

In order to be sure that ethyl acetate, the solvent used for intercalation of 5-HMF did not play a part in the basal plane expansion, a control was used consisting of clay that had been soaked in ethyl acetate without 5-HMF and subsequently dried in the same procedure and then tested. XRD patterns of 5-HMF and Na-MMT/ethyl acetate were obtained separately as shown in Figure 4-10. It was observed that the solvent in the Na-MMT has been completely evaporated and gave exactly the  $d_{(001)}$  of as-received Na-MMT.

Table 4-4. Maximum peak and d-spacing of Na-MMT and 5-HMF

Samples	Maximum peak, $2\theta$ /degree	Basal spacings, $d_{001}$ / nm
Na-MMT	6.95	1.27
Na-MMT/EtOAc	6.95	1.27
Na-MMT, 5-HMF and EtOAc	4.30	2.05

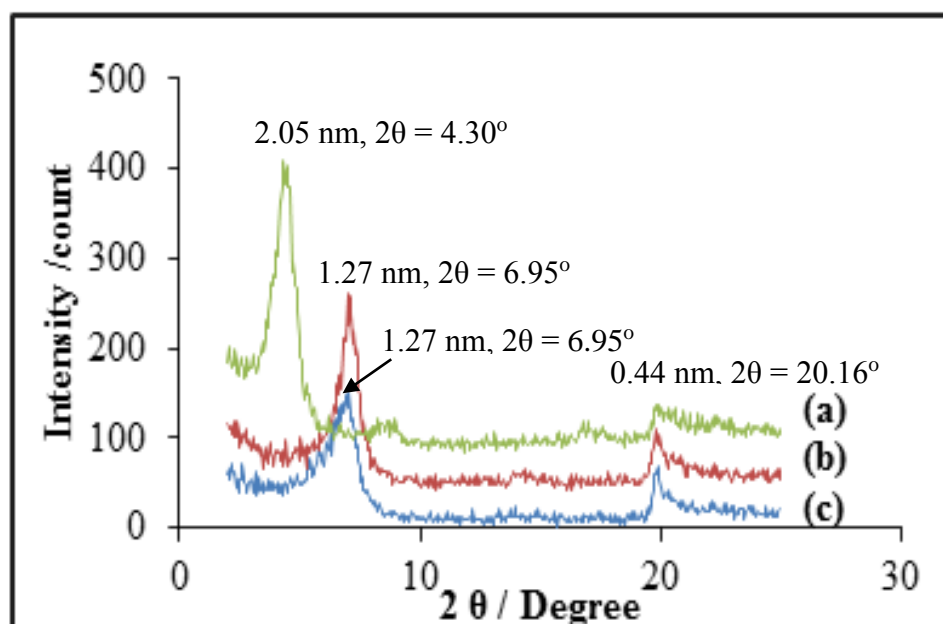


Figure 4-10. XRD pattern of (a) 5-HMF, MMT and solvent (b) MMT and solvent (c) MMT only

## 4.8.2 FDCA and MMT clay

XRD was used to assess whether the monomer (FDCA) synthesized in this work intercalated into MMT clay and the results are presented in Figure 4-11. From these results, there was a slight increase of the basal reflection from  $6.95^\circ$  to  $5.2^\circ$  of  $2\theta$  for the clay after treatment with FDCA dissolved in DMSO, evaporated to dryness at  $190^\circ\text{C}$  and then dried in a vacuum. The evaporation technique was applied considering the boiling point of the DMSO in relation to that of the FDCA. As shown in Figure 4-15b, the XRD pattern revealed an increase from 1.27 nm to 1.70 nm, an increase of 0.43 nm relative to that obtained from as-received Na-MMT. Also, the XRD pattern of MMT/DMSO revealed that the DMSO was not present within the MMT galleries as there is not much difference with that of the MMT alone. Therefore, this result indicates an intercalation of the diacid into the clay galleries by this technique.

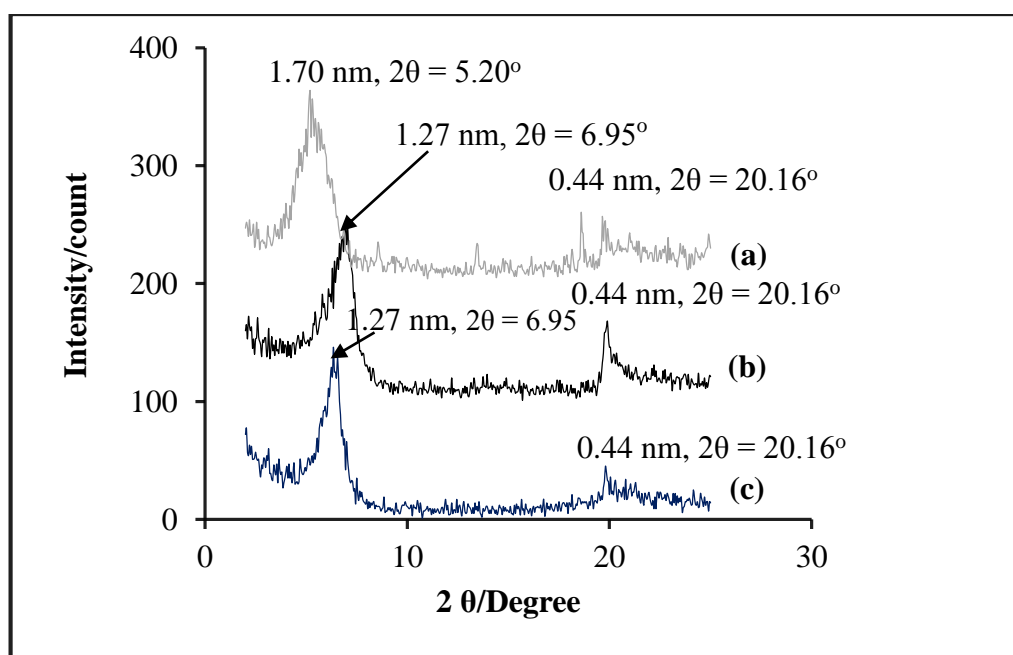


Figure 4-11. XRD pattern of (a) FDCA/ MMT/ DMSO (b) MMT and (c) MMT/DMSO

### 4.8.3 BHMF and MMT clay

The synthesized BHMF was tested with Na-MMT clay to investigate if the monomer would be incorporated into this clay. The XRD pattern in Figure 4-12 revealed an increase in the basal spacing  $d_{(001)}$  from 1.25 nm to 1.67 nm when this monomer was added to clay. Also observed on the XRD patterns are peaks at  $2\theta = 10.85^\circ$ ,  $15.75^\circ$  and  $21.7^\circ$ . These are diffraction patterns associated with this monomer as they are present on the XRD pattern of the monomer without clay (Figure 4-12). Based on this result, intercalation of this monomer into the clay galleries is said to occur and this might possibly lead to the production of polymer-clay nanocomposites by *in situ* polymerization of the diacid (FDCA) synthesized earlier with this monomer. Therefore, it is worth noting that this is the first investigation on the intercalation of Na-MMT clay with BHMF: there is no reported literature on this.

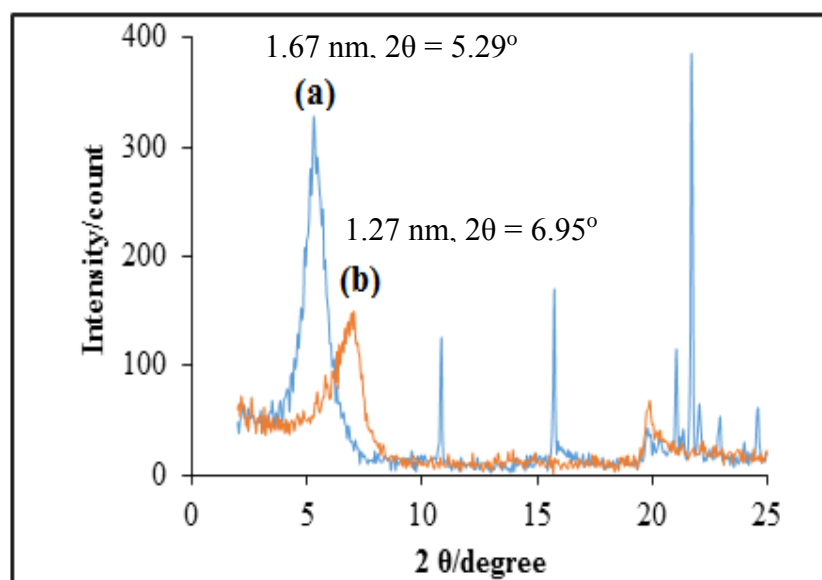


Figure 4-12. XRD pattern of: (a) BHMF/Na-MMT and (b) Na-MMT

## 4.9 Organically modified MMT

Organically modified MMT was synthesised (section 3.3.10) and characterised by XRD and compared with that of the Na-MMT are presented in Figure 4-13. From Figure 4-13 the  $d_{(001)}$  of the organo-MMT calculated from Bragg's equation is about 1.94 nm for  $2\theta = 4.55^\circ$  compared with  $d_{(001)}$  of the Na-MMT 1.27 nm for  $2\theta = 6.95^\circ$ .

Therefore, this basal spacing increase indicates intercalation of the CTAB into Na-MMT. This is due to ion-exchange of the organic ammonium cations of the CTAB with Na ions of the MMT resulting in the expansion of the galleries [355].

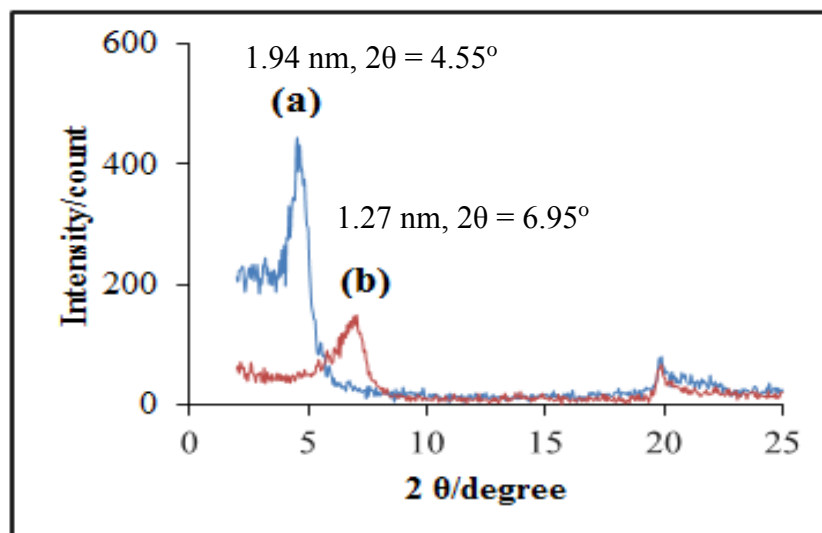


Figure 4-13. XRD pattern of: (a) Organo-MMT and (b) Na-MMT

#### 4.10 FT-IR absorption spectra of modified MMT

The FT-IR absorption spectra of Na-MMT and organo-MMT clays were recorded and are presented in Figure 4-14. It can be observed that an absorption band around  $3620\text{ cm}^{-1}$  was noted on both the Na-MMT and organo-MMT spectra. This is as a result of the stretching vibrations of OH groups that are coordinated to Al-Al pairs [356]. Also observed on the spectra are absorptions at  $2919\text{ cm}^{-1}$  and  $2849\text{ cm}^{-1}$  (Figure 4-14(a)) which are the characteristic bands of the CTAB which indicates that intermolecular attractions occurred between the adjacent alkyl chains of CTAB in Na-MMT. This is also confirmed elsewhere [357, 358]. Therefore, these observed absorption bands are attributed to the organophilic modification of Na-MMT clay [359-361].

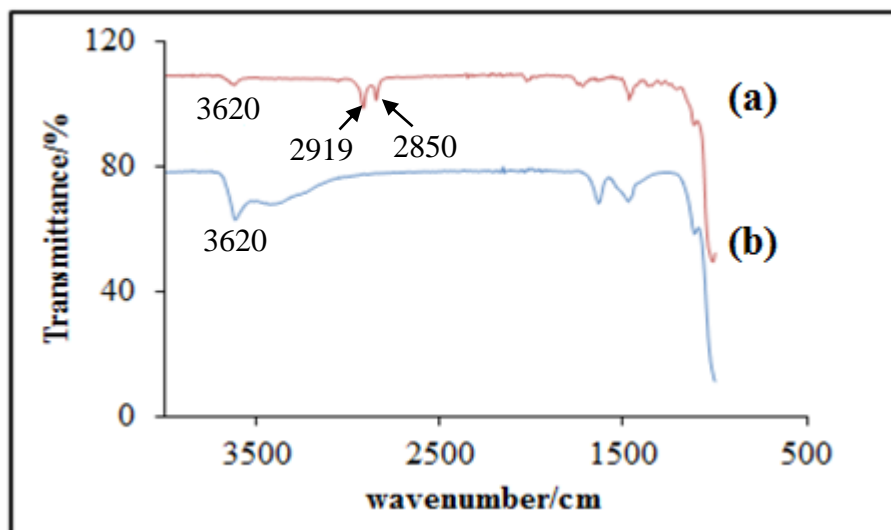
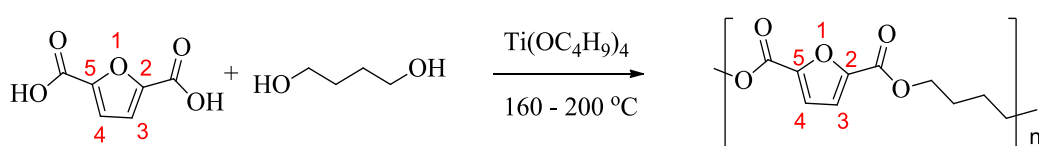


Figure 4-14. FT-IR spectra of: (a) Organo-MMT and (b) Na-MMT

## 4.11 Polymers derived from FDCA

Initial polymerisation reactions were conducted at 200 °C using esterification and polycondensation method (section 3.4.1). At the end of the polymerization reaction, methanol was added to precipitate the polymer formed which was collected via centrifugation. A fibrous polymer was obtained and after drying was characterized by NMR, FTIR and TGA instruments. The reaction scheme is presented in scheme 4-1.



Scheme 4-1. Synthesis of poly (butylene-2, 5-furandicarboxylate) (PB-2,5-F)

### 4.11.1 NMR structure characterization

The  $^1\text{H}$  NMR and  $^{13}\text{C}$  NMR spectra for the polymer product are presented in Figures 4-15 and 4-16. From Figure 4-15, it was observed that the resonance peaks of 3-H and 4-H of the furan protons appeared at 7.21 ppm and that at 4.38 is attributed to ester  $\text{OCH}_2$  group. Also observed were two peaks due to  $\text{OCH}_2\text{CH}_2$  at 1.89 ppm as expected.

In the  $^{13}\text{C}$  NMR spectrum (Figure 4-16), the C = O, C-2/C-5 and C-3/C-4 associated with the furan ring were observed at 160.0, 147.8 and 118.5 ppm respectively. Also observed are the carbon atoms associated with the ester at 65.0 ppm and 25.2 ppm corresponding to  $\text{OCH}_2$  and  $\text{OCH}_2\text{CH}_2$  respectively. These resonances were comparable to those for the same polymer reported elsewhere [362].

From these results, it was concluded that the furan ring remained thermally stable in the final product despite the extensive heating at 200 °C during the polymerization reaction.

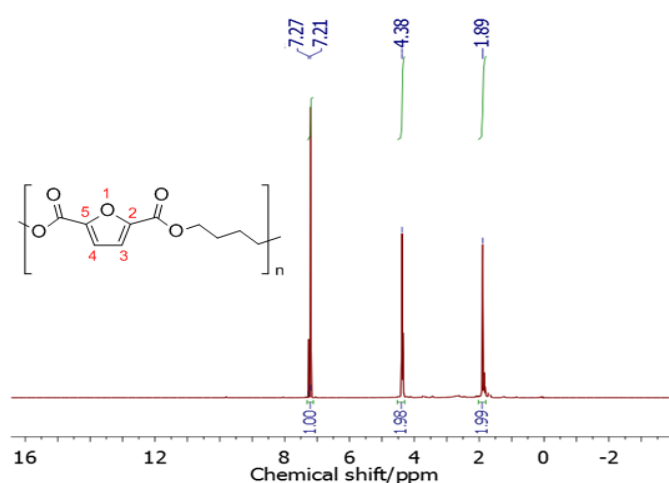


Figure 4-15.  $^1\text{H}$  NMR spectra of polyester from FDCA and 1,4-butanediol in  $\text{CDCl}_3$

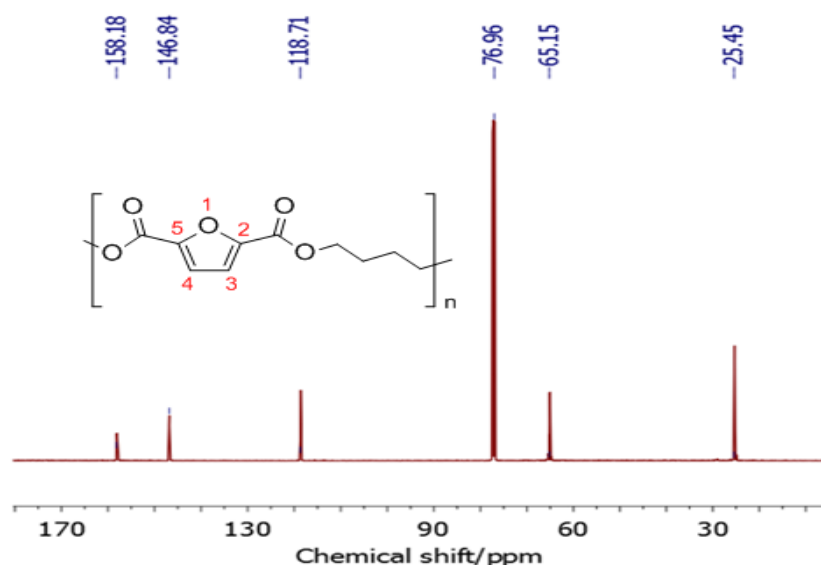


Figure 4-16.  $^{13}\text{C}$  NMR spectra polyester from FDCA and 1,4-butanediol

### 4.11.2 FT-IR structure characterization

The resulting polymer synthesized from FDCA and 1,4-butanediol (BD) was characterized by FT-IR. The FT-IR spectra shown in Figure 4-17 provided evidence for characteristic absorptions of the furan ring at 3117, 1570, 1040, 975, 824 and 771  $\text{cm}^{-1}$ , and those of the ester carbonyl at 1722  $\text{cm}^{-1}$  which were all observed. This also confirmed the results obtained from the NMR spectrum. The detailed functional group assignments are presented in Table 4-5.

To ascertain the total elimination of the 1,4-butanediol from the polymer, the FT-IR spectrum of 1,4-butanediol and FDCA was compared with that of the polyester product as shown in Figure 4-18 and it can be seen that the absorption band of the OH group present on the 1,4-butanediol (BD) spectra was absent on the polyester. This indicates that the polymerization reaction proceeds and the expected product was obtained.

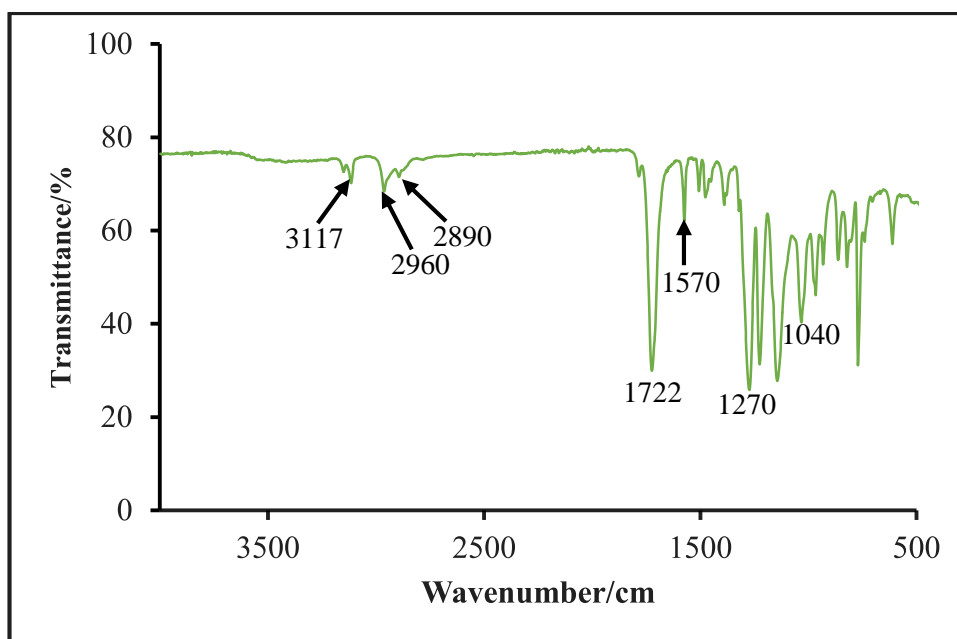


Figure 4-17. FTIR spectrum of PB-2,5-F polymer from FDCA and BD

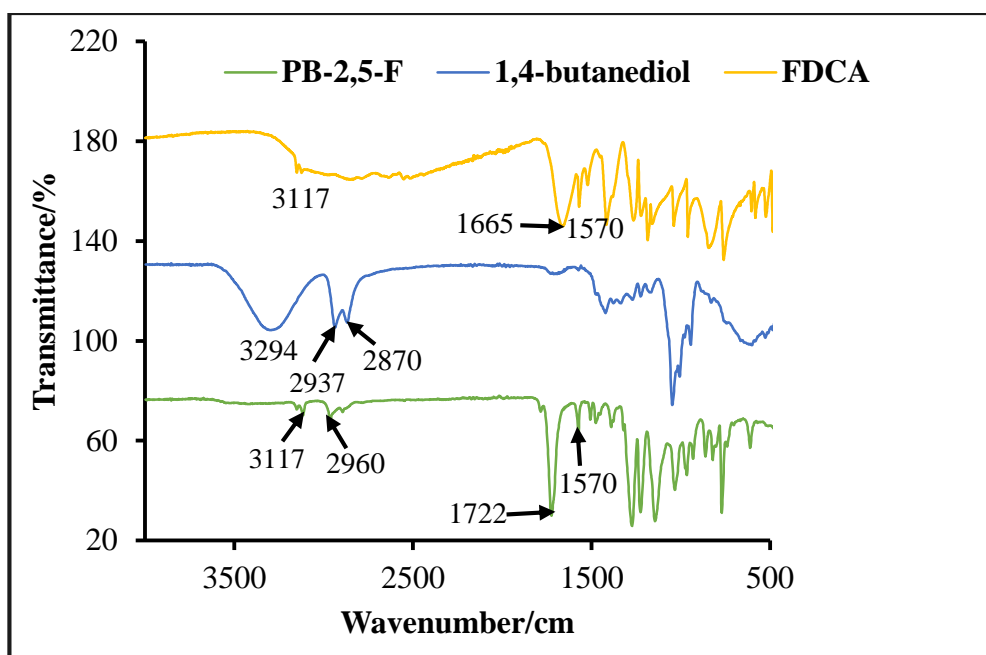


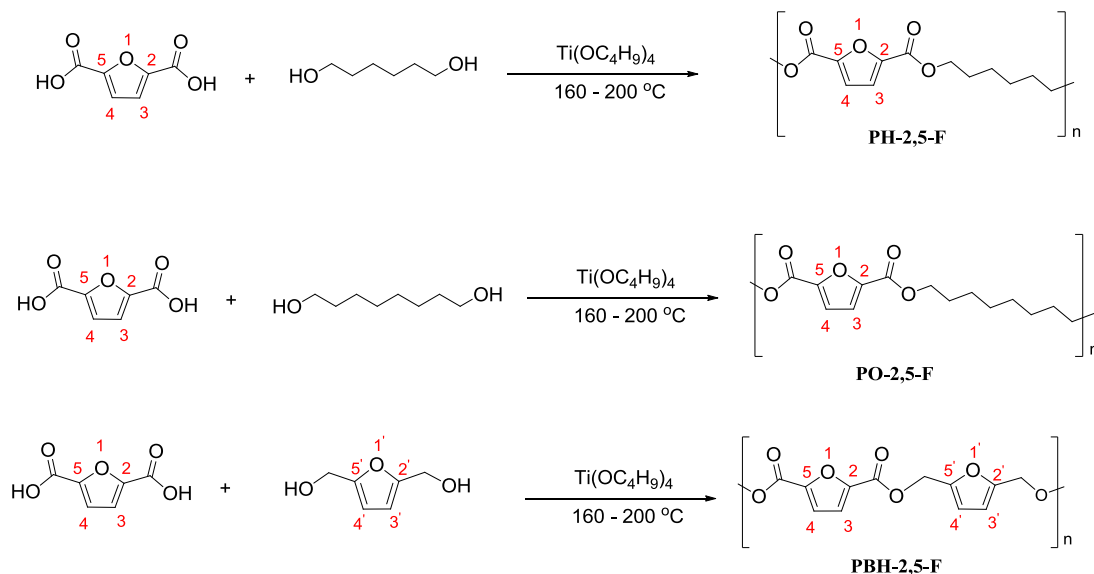
Figure 4-18. FTIR spectrum of PB-2,5-F polymer, 1,4-butanediol and FDCA

Table 4-5. FT-IR absorption bands of polyester from FDCA

Assignment	Wavenumber/cm
=CH	3117
C-H	2960, 2890
C=O	1722, 1785
C=C	1570
C-O	1270
Furan breathing	1040
Furan bending motion	975, 824, 771

## 4.12 Polymers from FDCA and other diols

Further polymers were synthesised using different diols, 1,6-hexanediol, 1,8-octanediol and the synthesised furan-based diol, BHMF (scheme 4-2). The products were characterised by NMR and FT-IR spectroscopy as described for PB-2,5-F polymer.



Scheme 4-2. Synthesis of PH-2,5-F, PO-2,5-F and PBH-2,5-F polymers

### 4.12.1 NMR structure characterisation of PH-2,5-F, PO-2,5-F and PBH-2,5-F polymers

NMR spectroscopy was employed to elucidate the structures of PH-2,5-F, PO-2,5-F and PBH-2,5-F polymers and the results are presented below.

#### 4.12.1.1 NMR spectra of PH-2,5-F polymer

The  $^1\text{H}$  and  $^{13}\text{C}$  NMR spectra of PH-2,5-F polymer are presented in Figure 4-19. The peak at 7.12 ppm was attributed to 2H of the furan ring at H-3 and H-4 and that at 4.33 ppm was assigned to the 4H at  $\text{OCH}_2$ . The peak at 1.77 ppm was due to 4H of  $\text{OCH}_2\text{CH}_2$ . Furthermore, a peak at 1.45 ppm was the methylene groups at  $\text{O}(\text{CH}_2)_2\text{CH}_2$ . The  $^{13}\text{C}$  NMR of this polymer revealed some peaks at 158.2 and 146.9

ppm and these were attributed to C=O and C-2/C-5 of the furan ring. The C-3 and C-4 of the furan ring was observed at 118.4 ppm and the peaks at 65.4 ppm, 28.4 ppm and 25.5 ppm corresponds to OCH<sub>2</sub>H<sub>2</sub>, OCH<sub>2</sub>CH<sub>2</sub> and OCH<sub>2</sub>CH<sub>2</sub>CH<sub>2</sub> respectively.

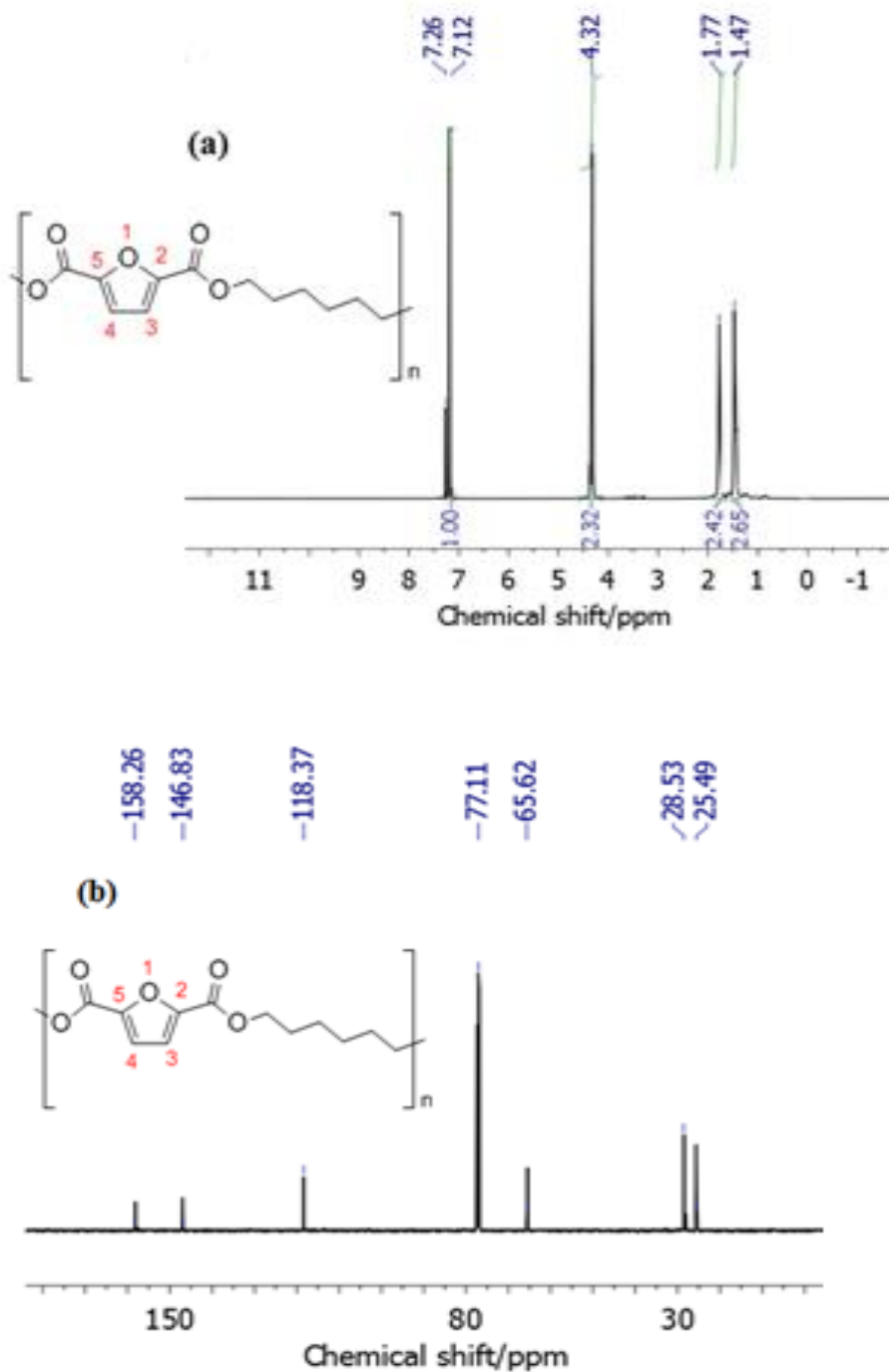
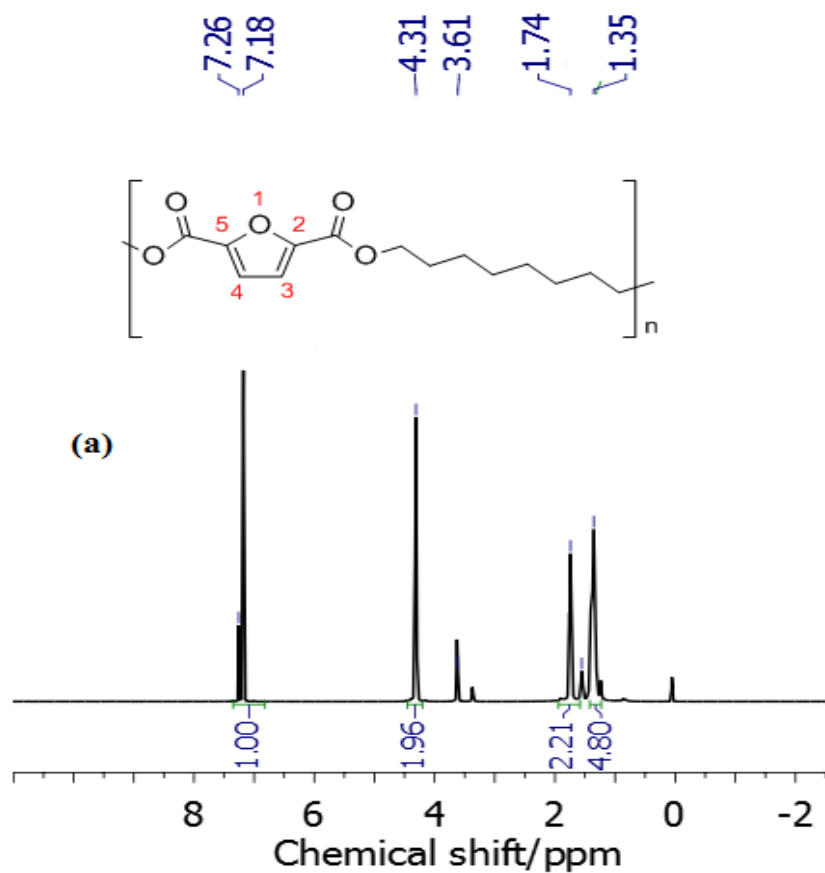


Figure 4-19. <sup>1</sup>H and <sup>13</sup>C NMR spectra of PH-2,5-F polymer

#### 4.12.1.2 $^1\text{H}$ and $^{13}\text{C}$ NMR spectra of PO-2,5-F polymer

The  $^1\text{H}$  and  $^{13}\text{C}$  NMR spectra of PO-2,5-F polymer are presented in Figure 4-20. This polymer resembled that explained in section 4.10.2.2 in terms of its structural characterisation by NMR. For instance peaks at 7.18 ppm and 4.31 ppm are associated with the 2H of the furan ring and 4H of the methylene protons of  $\text{OCH}_2\text{CH}_2$ . The same observation was made in terms of the  $^{13}\text{C}$  NMR in relation to other polymers, PB-2,5-F and PH-2,5-F respectively.



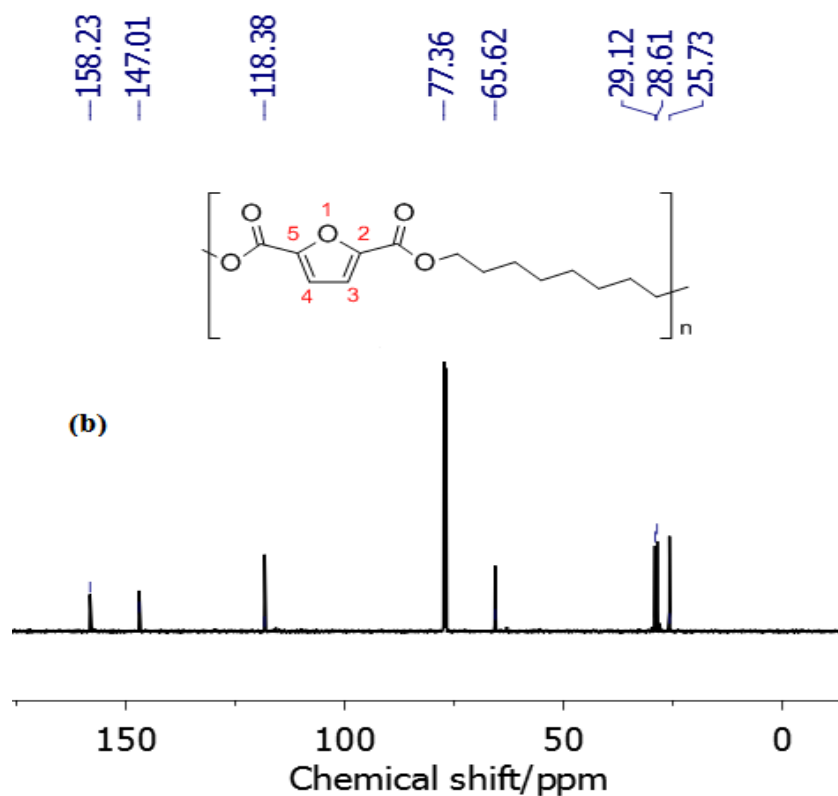


Figure 4-20.  $^1\text{H}$  and  $^{13}\text{C}$  NMR spectra of PO-2,5-F polymer

#### 4.12.1.3 $^1\text{H}$ and $^{13}\text{C}$ NMR spectra of PBH-2,5-F polymer

PBH-2,5-F polymer was characterized by  $^1\text{H}$  and  $^{13}\text{C}$  NMR. From the results in Figure 4-21, it was observed that the  $^1\text{H}$  NMR spectrum (Figure 4-21(a)) is characterized by the presence of three singlet peaks at 7.26 ppm, 6.12 ppm and 4.33 ppm. The peak at 7.26 ppm is attributed to the 2H resonances at 3-H and 4-H of the furan ring and at 4.33 ppm is due to 2H of  $\text{OCH}_2$ . Also observed on the spectrum is a chemical shift at 6.12 ppm and is attributed to the 3'-H and 4'-H due to the deshielding effect of the 2,5-dicarbonyl groups on these protons..

For the  $^{13}\text{C}$  NMR spectrum (Figure 4-21(b)), it was observed that this polymer consists of six resonance peaks. The resonance peaks associated with the furan carbons were observed at 154.6 ppm, 118.4 ppm, 147.0 and 107.4 ppm. These are attributed to C-2/C-5, C-3/C-4, C-2'/C-5' and C-3'/C-4' respectively. Also observed are peaks present at 158.9 ppm and 55.8 ppm. These corresponds to the resonances of  $\text{C}=\text{O}$  and  $\text{OCH}_2$ . The higher chemical shifts for the resonances of C-2/C-5 and C-3/C-4 when compared

with those for C-2'/C-5' and C-3'/C-4' carbons correlates with the  $^1\text{H}$  NMR results of this polymer which are due to deshielding effects of the 2,5-dicarbonyl groups on these carbons as earlier reported.

All the assignments were similar with those established for similar 2,5-disubstituted furan polyesters [237, 363].

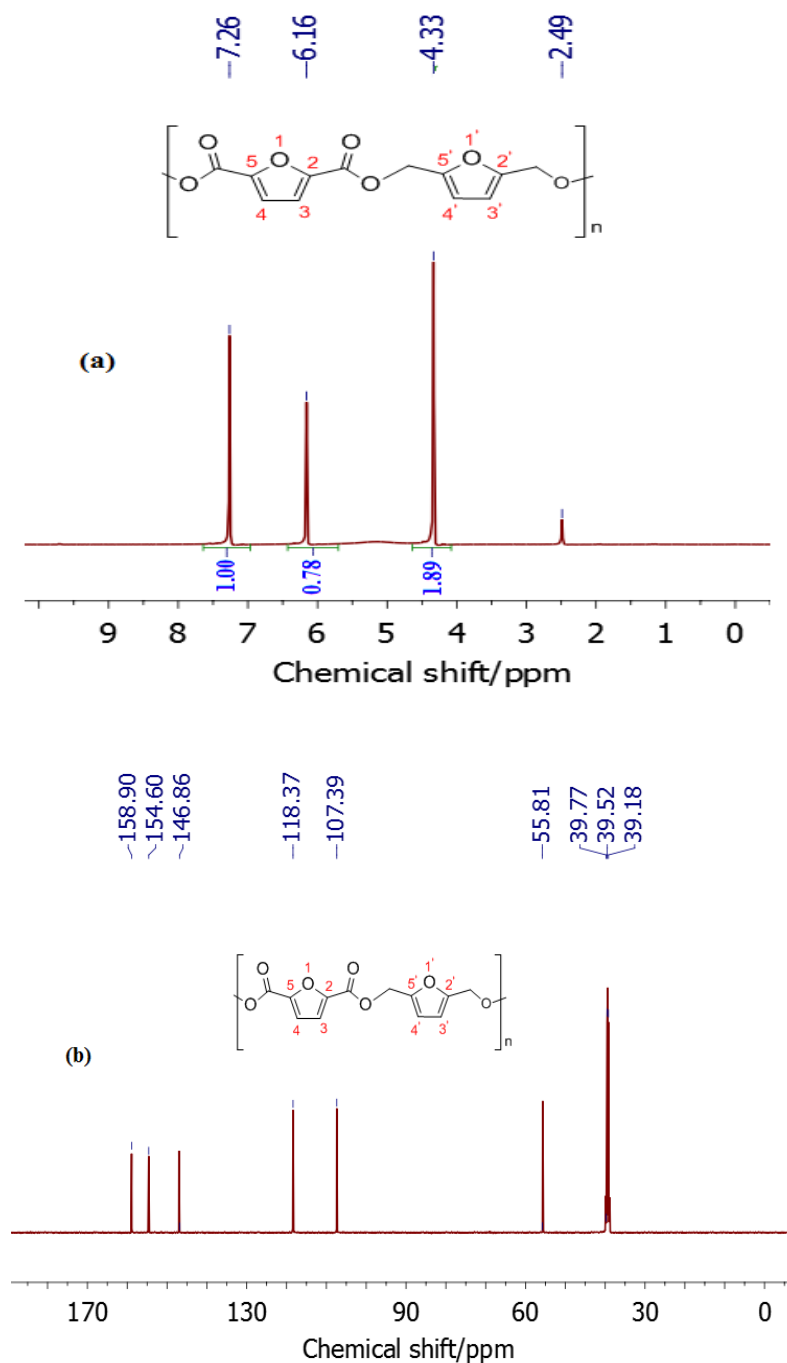


Figure 4-21.  $^1\text{H}$  and  $^{13}\text{C}$  NMR spectra of PBH-2,5-F polymer

### 4.12.2 FT-IR characterisation of PH-2,5-F, PO-2,5-F and PBH-2,5-F polymers

The polymers PH-2,5-F, PO-2,5-F and PBH-2,5-F (scheme 4-2) were characterised by FT-IR and the results are presented in Figure 4-22. It was evident that they possessed similar functional groups. For instance, all absorption peaks indicated the presence of furan rings. For example, absorption bands were observed at approximately  $3117\text{ cm}^{-1}$  and attributed to the =C-H groups of the furan rings of PH-2,5-F, PO-2,5-F and PBH-2,5-F polymers respectively. The carbonyl, C = O, functional groups of these polymers were observed at approximately  $1722\text{ cm}^{-1}$ .

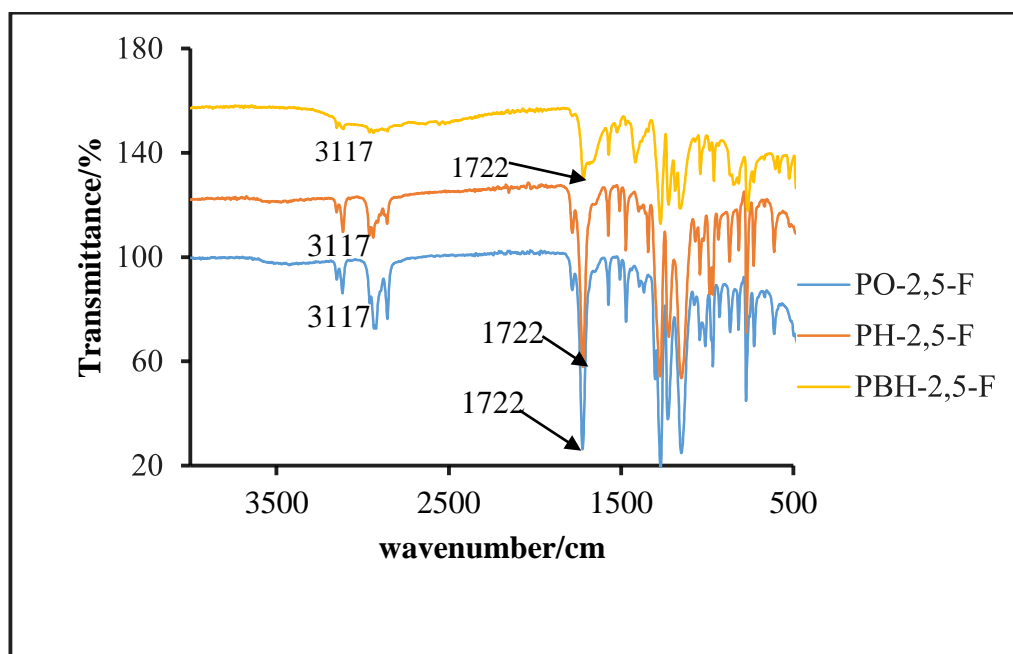
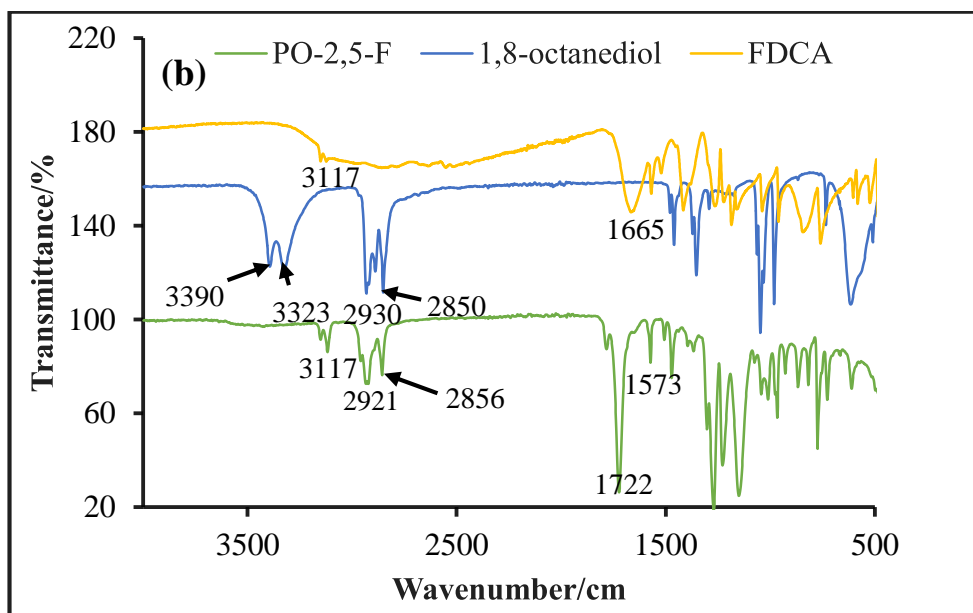
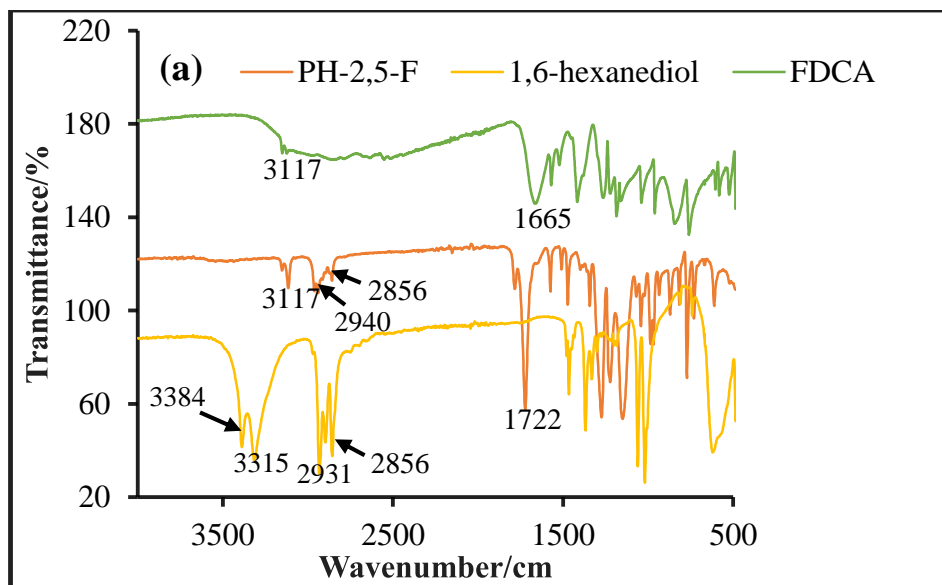


Figure 4-22. FTIR spectra of PH-2,5-F, PO-2,5-F and PBH-2,5-F polymers

In order to ascertain that the polymerisation reactions proceed without any traces of the OH functional group in the final products, FT-IR spectra of the polymers were compared with the various diols and FDCA used in their synthesis and are presented in Figure 4-23(a-c). It can be observed that in all the polymers produced, there was no absorption band around the OH regions of the polymers spectra.



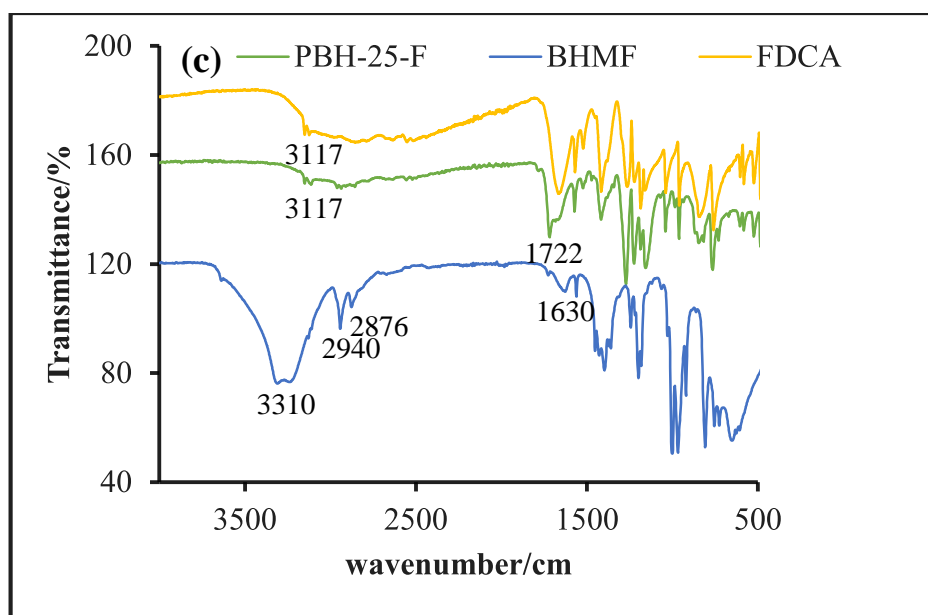


Figure 4-23(a-c). FT-IR spectra of the polymers with their corresponding diols

Table 4-6. Assignments of the functional groups of the polymers

Assignment	Wavenumber/cm		
	PH-2,5-F	PO-2,5-F	PBH-2,5-F
=CH (furan )	3117	3117	3117
C – H (CH <sub>2</sub> )	2939, 2858	2922, 2857	2937, 2859
C = C	1574, 1509	1573, 1506	1572, 1500
C = O	1722	1722	1722
C - O	1274	1271	1271
Furan breathing	1043	1011	1040
Furan bending motion	967, 871, 772	967, 867, 774	962, 846, 764

In summary, the details of the functional groups found in these polymers are presented in Table 4-6 which suggests that all the assigned groups are in agreement with the proposed structures. Also, these assignments are similar to those reported by Jiang *et al* [364].

### 4.12.3 Elemental analysis

The values for elemental analyses of the polymers produced are given in Table 4-8 and they indicate that the percentage hydrogens in all the polymers were slightly higher than the theoretical values. This may be attributed to the residual moisture. It has been reported elsewhere that residual moisture can cause these values to be slightly higher than the calculated values [365]. Using the excess, the equivalent percentage of residual water was calculated and found to be within ~ 0.1 wt. % - 0.2 wt. % for all the polymers. These results are compared with water uptake experiments as reported in section 4.12.9 which establish that the polymers are capable of absorbing up to 0.8 wt.% water.

Table 4-7. Elemental analysis results of the polymers\*

Polymer	% C		% H		% O**	
	<u>Calculated</u>	<u>Found</u>	<u>Calculated</u>	<u>Found</u>	<u>Calculated</u>	<u>Found</u>
PB-2,5-F	57.14	53.53	4.80	4.90	38.06	41.57
PH-2,5-F	60.50	58.13	5.92	7.19	33.58	34.68
PO-2,5-F	63.66	64.21	4.41	4.56	31.93	31.23
PBH-2,5-F	65.12	64.92	3.90	4.13	30.98	30.95

\* The manufacturer, Exeter Analytical Inc., authenticate the quotation of results to 0.01% and claim a typical deviation theoretical values of 0.03%

\*\* Values calculated by difference

### 4.12.4 Tensile properties

The tensile stress, tensile modulus and elongation at break of polymers prepared from 2,5-furandicarboxylic acid and various diols (1,4-butanediol, 1,6-hexanediol, 1,8-octanediol and 2,5-Bis-(hydroxymethyl)furan) designated as PB-2,5-F, PH-2,5-F,

PO-2,5-F and PBH-2,5-F were determined using the Tinius Oslen H10KM/0348 testing machine. Examples of results obtained from these studies are presented in Figure 4-24.

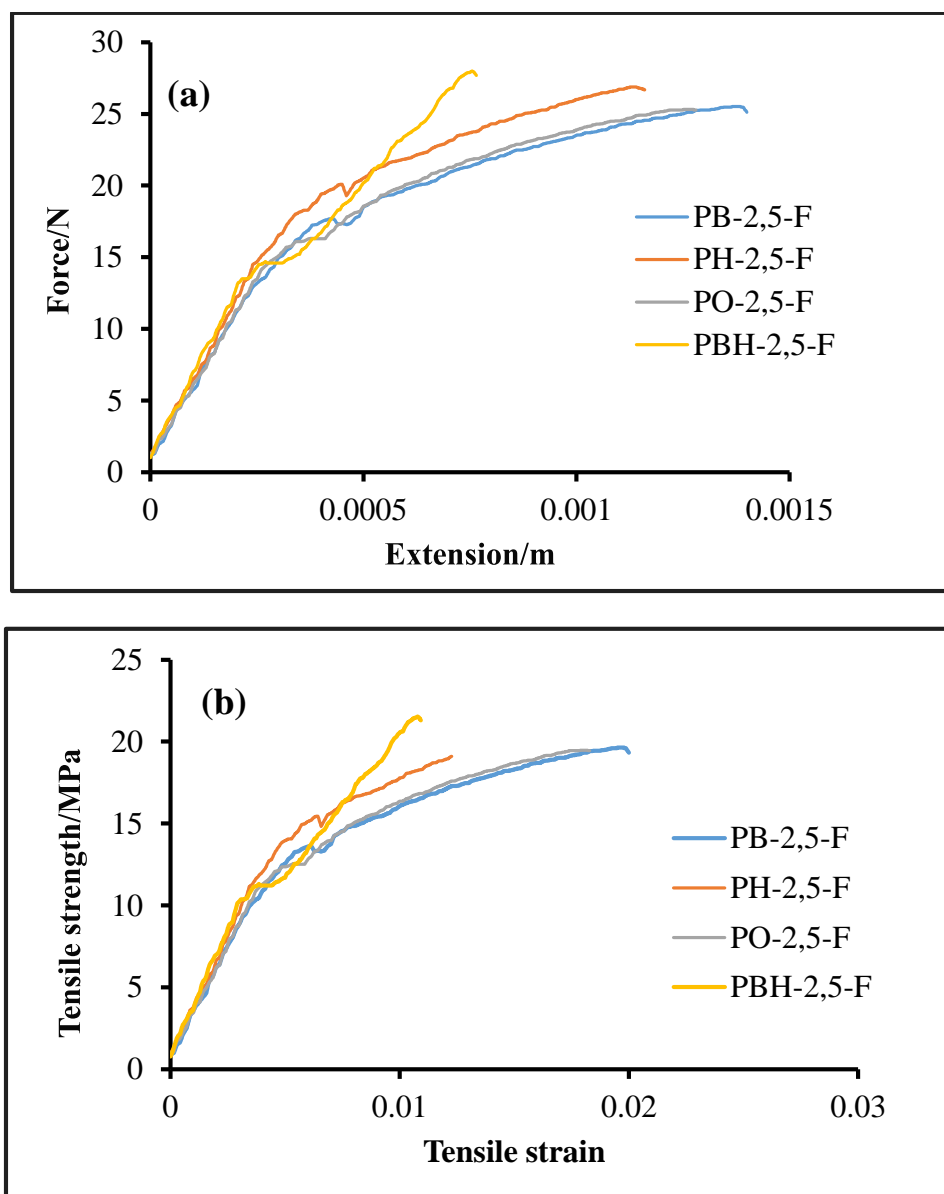


Figure 4-24. Tensile properties of the four polymers synthesized in this work: (a) Force-extension curve (b) Tensile strength-strain curve

Of the four polymers prepared, the elastic properties are similar but the PBH-2, 5-F has a higher tensile failure stress compared to others and PO-2, 5-F possesses the least. When compared with the strength of PET as reported elsewhere [366] the tensile failure stress of these polymers was lower than that of PET and this can be attributed

in part to the fact that a great deal of refinement to the synthesis is needed to obtain a high and narrow molecular weight distribution. Such refinement is beyond the scope of the present work.

It is normal practice for Young's modulus of polymers to be obtained using an extensometer which measures the elongation of the sample directly and eliminates machine compliance. Unfortunately, an extensometer was not available for use during the course of this investigation. Since the loads recorded in figure 4-24(a) are low, it can be argued that machine compliance has minimal effect and a 'nominal Young's modulus' is recorded for the purpose of comparison.

These estimated Young's modulus results are within the range reported for phenolic resins (2.8 - 4.8 GPa) and polyester resins (2.1 - 4.4 GPa) [367]. The detailed results obtained are summarized in Table 4-7.

Table 4-8. Some mechanical properties of polymers derived from FDCA

Polymers	Tensile strength/MPa		Young's modulus/GPa		Elongation at break (%)		
	Mean	95%*	Mean	95%*	Mean	95%*	n**
PB-2,5-F	19	1	2.9	0.1	2.0	0.1	5
PH-2,5-F	21	2	2.8	0.1	1.7	0.1	5
PO-2,5-F	19	2	2.6	0.1	1.8	0.1	5
PBH-2,5-F	21	2	3.0	0.1	1.1	0.2	5

\*Confidence limit, \*\*Number of population

#### 4.12.5 Water contact angle

The water contact angle gives an indication of hydrophobicity which in turn is related to the number of permanent dipoles in the structure and hence to dielectric constant.

This reveals how a water drop on a solid or liquid surface spreads. Water contact angle is defined as the included angle that water makes with a solid surface or capillary walls of a porous material when both materials come into contact [368].

As one of the aims of this research is the synthesis of hydrophobic polymers, contact angle of the polymer surface was determined to study wettability and the results are presented in Figure 4-25. The contact angle as measured with a protractor on printed images of droplets such as those displayed in Figure 4.26 was  $91^\circ$  for PBH-2, 5-F polymer (Figure 4-25). During the measurements of the contact angle, the advancing angles were measured and not the receding angle. This is because the measurements were conducted within 10-120 seconds and the formation of receding angles was prevented by buffering the atmosphere to stop evaporation from the water droplets. Therefore, the results suggest that the PBH-2,5-F polymer is slightly more hydrophobic than the others based on their water contact angle measurements [368, 369]. In general, a material or surface is designated hydrophobic if the water contact angle is greater than  $90^\circ$  but this is an arbitrary criterion. An angle less than  $90^\circ$  corresponds to high wettability or hydrophilicity of the surface as illustrated in Figure 4-26. However, others have argued that  $65^\circ$  should be the criterion for hydrophobic surfaces [370, 371]. As shown in Table 4-10, the other polymers: PB-2,5-F, PH-2,5-F and PO-2,5-F also have contact angles close to  $90^\circ$  and therefore also fall into the category of hydrophobic. The actual angles can be seen in Table 4-10.

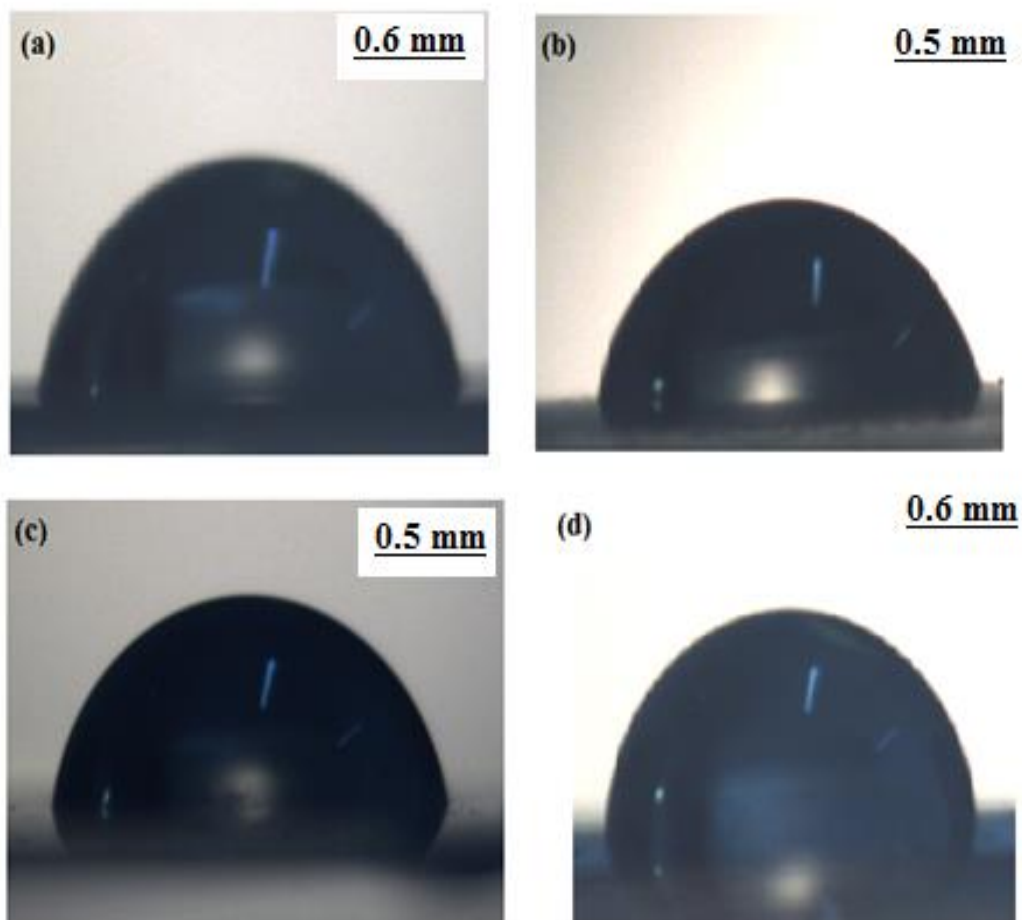


Figure 4-25. Water contact angle of: (a) PB-2,5-F (b) PH-2,5-F (c) PO-2,5-F and (d) PBH-2,5-F

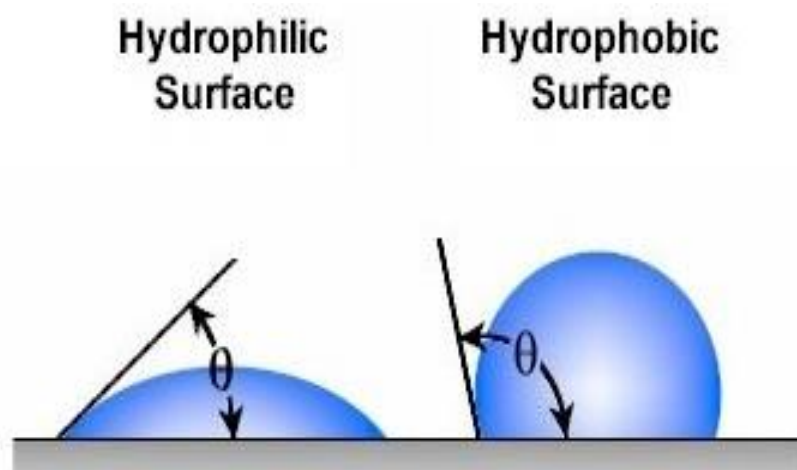


Figure 4-26. Hydrophilic and hydrophobic surfaces based on contact angle [372].

Table 4-9. Water contact angles of polymers derived from FDCA and various diols

Polymers	Water contact angle/ °		
	Mean	95% *	n **
PB-2,5-F	83	1	6
PH-2,5-F	85	1	6
PO-2,5-F	87	2	6
PBH-2,5-F	91	1	6

\*Confidence limit

\*\*Number of population

#### 4.12.6 Variation of contact angle with time

The relationship between contact angle and time was investigated and the results are presented in Figure 4-27. The contact angles of the sessile drops were also measured between 10-120 seconds and it was found out that PB-2,5-F, PH-2,5-F and PO-2,5-F polymers have the same contact angles of 83° at 10s while PBH-2,5-F has an angle of 89°. This study revealed that the contact angles on these polymers increase slightly with time as observed on different polymers [373]. The reason is that the approach to equilibrium is slow: some authors have advised vibrating the sessile drop to obtain an equilibrium angle [374].

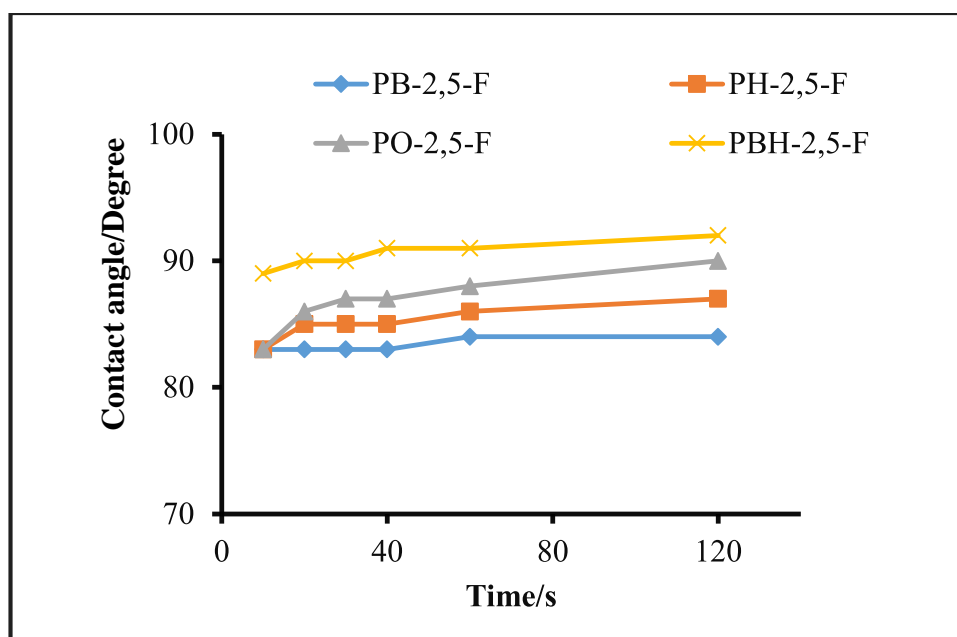


Figure 4-27. Water contact angle as a function of time of the various polymers

In conclusion, water droplets on these polymers rest on their surfaces with a high contact angle which is stable in a 100% RH buffered atmosphere.

#### 4.12.7 Capacitance and dielectric constant

Studies on the electrical properties of polymers are important for industrial applications involving, for example, insulation of cables, encapsulates for electric components, interlayer dielectrics, and printed wiring board materials [375].

In this work, the capacitance and dielectric constants were determined and Figure 4-28 shows the frequency dependences of the capacitance of simple capacitors made from the four polymers produced from FDCA and various diols. It can be observed that PBH-2,5-F and PB-2,5-F polymers have almost the same capacitance values at 24-25 pF when compared to the remaining two polymers. The capacitance value for PH-2, 5-F was lower than that of the others. These values of the capacitance were used to determine the dielectric constants of all the polymers synthesised in this work.

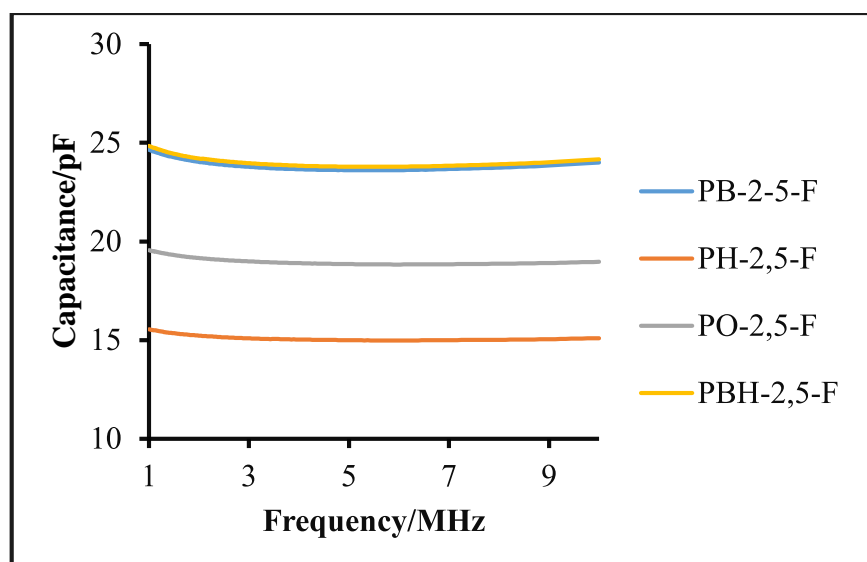


Figure 4-28. Capacitance of the four polymers derived from FDCA and diols

The dielectric constant or relative permittivity ( $\epsilon_r$ ), was obtained from the capacitance values of the various polymers using equation 3.4 in section 3.2.10. A frequency range that avoided space charge effects from electroding and high frequency effects was used. Permittivity is also useful in predicting other electrical properties of the polymers [376, 377]. The results are presented in Figure 4-29 as derived from the capacitance-frequency curves (Figure 4-28).

From Figure 4-29, it can be observed that PBH-2,5-F polymer has the highest value of the dielectric constants among the four polymers with a dielectric constant of about 3.25 which is similar to the reported value for an analogous polyester, PET which was 3.4 [378]. The dielectric constants of PH-2,5-F and PO-2,5-F polymers were found to be 2.7 and 2.6 while that of PB-2,5-F and PBH-2, 5-F polymers were 2.8 and 3.2 respectively. The dielectric constants of PH-2,5-F and PO-2,5-F in the range exhibited by common thermoplastics such as polystyrene and acrylonitrile butadiene styrene [379]. This variations in the dielectric constants can be attributed to the structure and composition of the polymer which have strong effects on the dielectric constant [378].

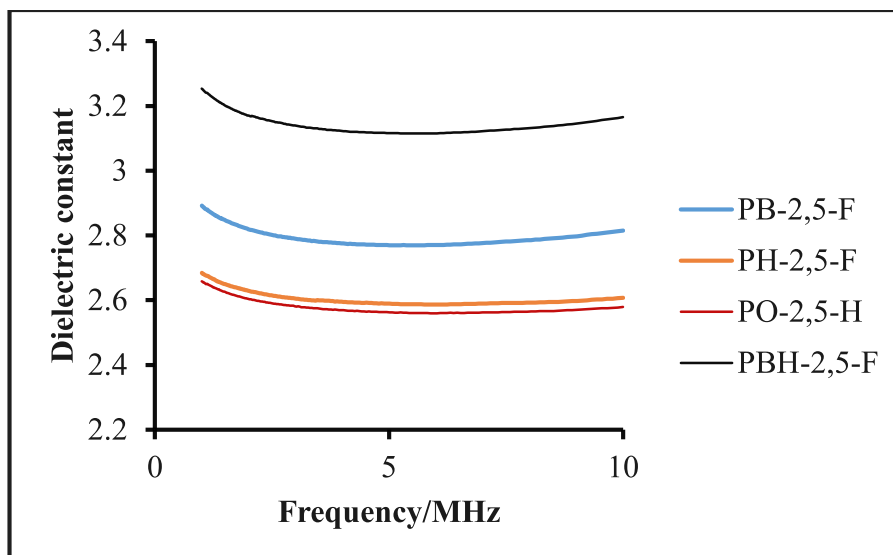


Figure 4-29. Dielectric constants of the four polymers derived from FDCA and diols

#### 4.12.8 Water absorption

Water absorption tests were conducted on the polymers produced at different times and the results are presented in Figure 4-30. It can be seen that all the polymers have absorbed a significant but low amount of water rising to about 1% at saturation. Among the four polymers produced, PHB-2, 5-F shows the least water absorbed compared to others. After 14 days of immersion in water, this polymer was able to absorb only about 0.8% water. This correlates with the contact angle value of this polymer: it gave the highest contact angle of about  $91^\circ$  compared to others. Similarly, PB-2, 5-F polymer was observed to have the highest water absorption value of 1% after 14 days of immersion which correlates with lowest water contact angle as earlier shown in Table 4-8. In general therefore, these polymers are able to absorb about 1% of water when in contact with water for extended times during their potential applications.

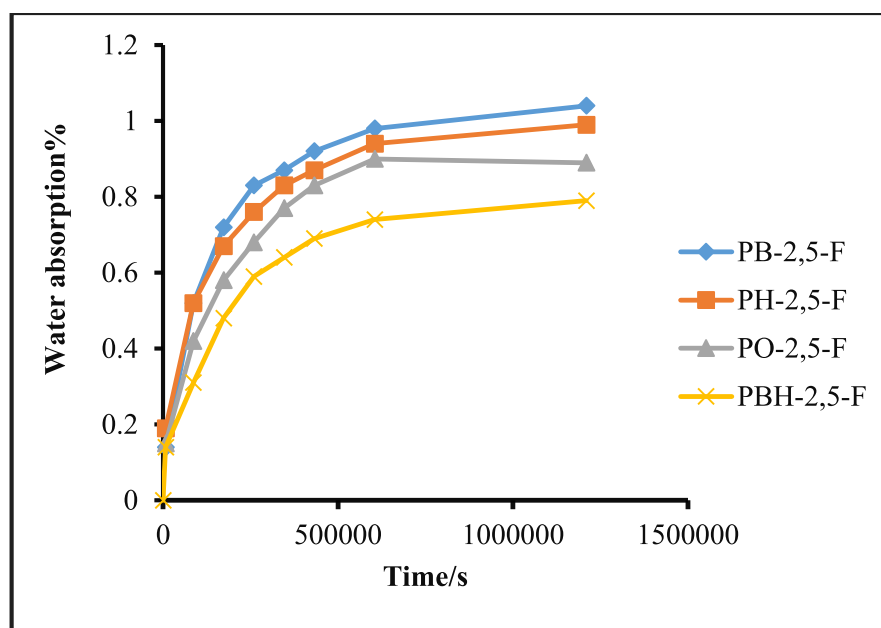


Figure 4-30. Water absorption of the polymers derived from FDCA and various diols

#### 4.12.9 Thermogravimetric Analysis (TGA)

To anticipate the potential applications of the polymers produced, thermal stability and degradation behaviour of these polymers are of great importance. Thus, thermogravimetric analyses were conducted to assess their thermal behaviour and stability. As shown in Figure 4-31, the first stage involves a mass loss of around 9 wt. %, and corresponds to the vaporization of moisture, to desorption of water and to the possible emission of volatile organic compound [380]. For PB-2,5-F polymer, the TGA curves have a main weight loss onset at above 324 °C representing about 85% of the total weight PB-2,5-F polymer, with a maximum degradation rate at 381 °C. Also noted was a minor weight loss commencing at 200 °C which may be due to low molecular weight fractions. In the region below 200°C there are fluctuations of the weighing balance due to vibrations from adjacent equipment located in the same vicinity. The other polymers (PBH-2,5-F, PH-2,5-F and PO-2,5-F) showed similar thermal behaviour and both exhibit some weight loss at 300 °C. Among the polymers synthesised, PB-2,5-F possessed the highest temperature of maximum degradation at 381 °C with a weight loss of 85% at that temperature. The decomposition and maximum degradation temperatures of these polymers are summarised in Table 4-11. These represent thermal degradation processes in helium at a rate of 10 °C/min. Also,

it is observed that the polymers prepared from the aliphatic diols, maximum degradation temperature decreased with increasing methylene number of the diols in the following order: PB-2,5-F > PH-2,5-F > PO-2,5-F polymers respectively.

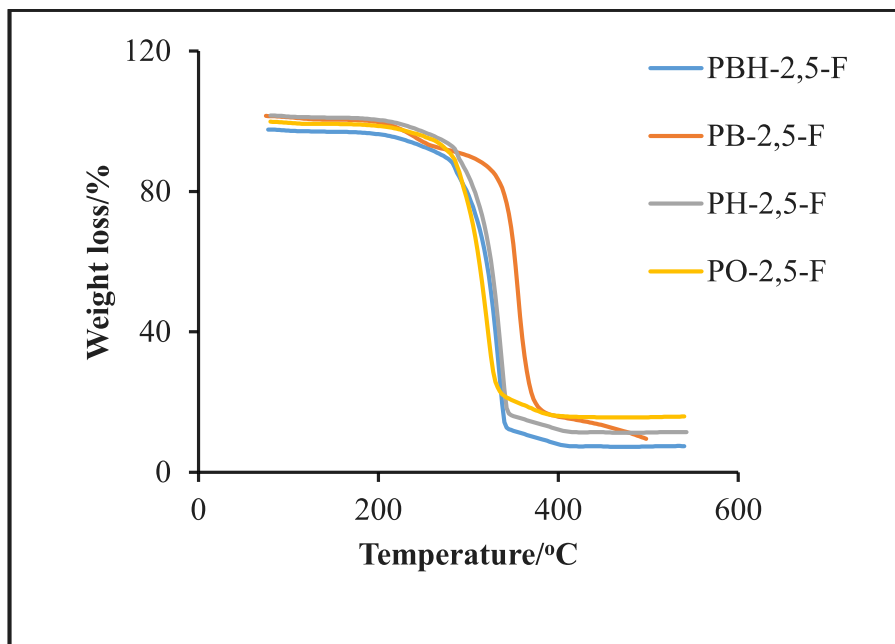


Figure 4-31. TGA traces of polyester from FDCA and various diols at 10°C/min.

Table 4-10. Decomposition and maximum degradation temperature of polymers

Polymer	Decomposition/°C	Maximum degradation /°C
PB-2,5-F	324	381
PBH-2,5-F	280	350
PH-2,5-F	287	346
PO-2,5-F	281	336

### 4.12.10 Differential Scanning Calorimetry (DSC)

Differential scanning calorimetry (DSC) of the polymers was obtained and the results are presented in Figure 4-32. The DSC results of PH-2,5-F and PO-2,5-F polymers (Figure 4-32a) exhibit an endotherm starting at 100 °C which ends at 125 °C. If the area of these endotherms are converted to energy (J) then, using the enthalpy of vaporization of water ( $2257 \text{ Jg}^{-1}$  at 373 K), it corresponds to a loss of  $\sim 1 \text{ wt. \%}$  of water which was in agreement with the water uptake results obtained in section 4.12.9. The second endothermic peak comprises a shoulder at  $\sim 290 \text{ °C}$  which is the crystalline melting endotherm and correlates with the melting point determination (Section 4.12.3). This merges with the endotherm which ends at about  $350 \text{ °C}$  and is associated with thermal degradation of these polymers and volatilisation of products. For PH-2,5-F this is preceded by an exotherm and it is not clear what this represents. Exothermic behaviour would be expected if oxygen was present but these tests are done in flowing helium. PB-2,5-F and PBH-2,5-F polymers (Figure 4-32b) exhibit similar behaviour in the region 100-125 °C corresponding to water loss but the second endotherms involve much lower enthalpies. These results confirm the TGA traces and suggest that the polymers have substantial thermal stability under these experimental conditions.

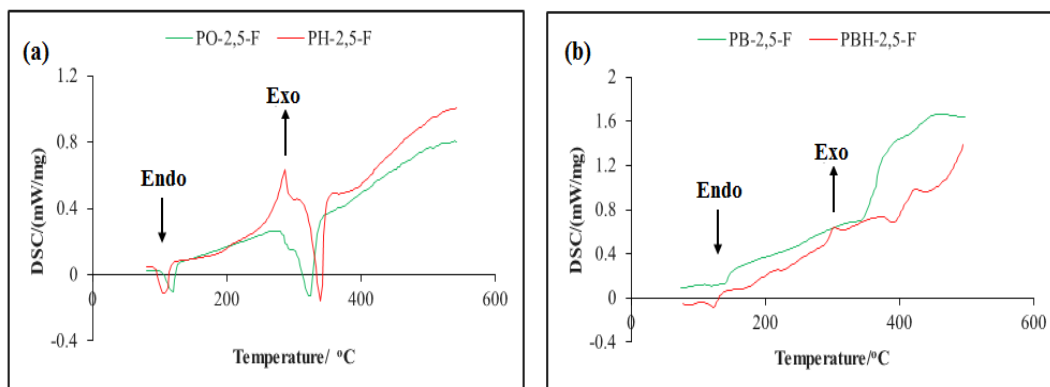


Figure 4-32. DSC traces of: (a) PH-2,5-F / PO-2,5-F and (b) PB-2,5-F / PBH-2,5-F

### 4.12.11 XRD pattern of the polymer

The crystalline structures of polymers have a significant impact both on their mechanical properties and biodegradability. Therefore, the presence of crystallinity in

PB-2,5-F polymer was assessed by XRD. The XRD pattern as presented in Figure 4-33(a) revealed some prominent reflections at  $2\theta = 17.9^\circ$  and  $22.5^\circ$ . This result suggests that there might be a crystalline melting endotherm in the DSC trace of this polymer [362].

#### 4.12.12 Effect of grinding on XRD pattern of the polymer

The polymer produced (PB-2,5-F) was obtained as fibrous lumps of material and was subjected to grinding by pestle and mortar in order to obtain a fine powder material for XRD measurements. In order to control for the effect of grinding, a sample that had not been ground was carefully placed into the XRD sample holder and tested. The XRD patterns were almost identical (Figure 4-33) confirming that grinding the polymer prior to XRD measurement had no effect on the trace.

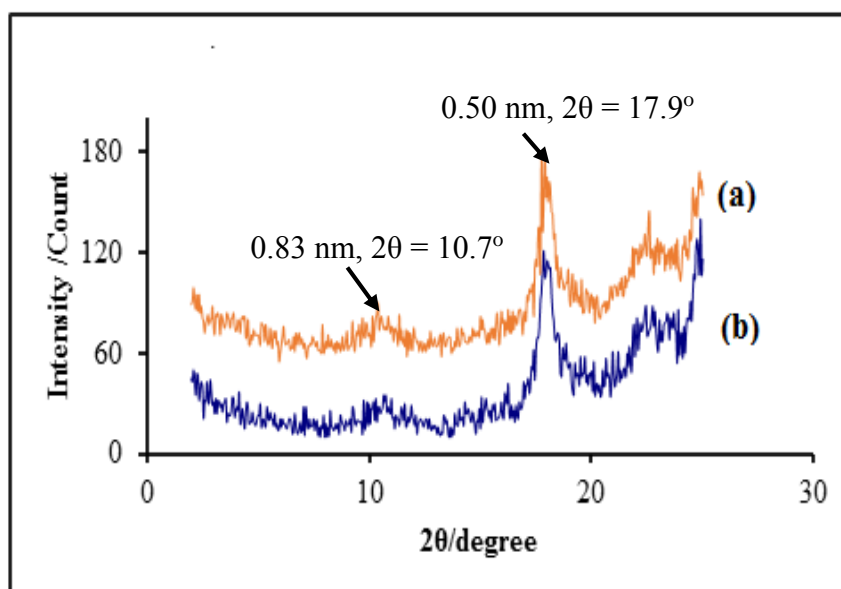


Figure 4-33. XRD pattern of: (a) ground (b) unground PB-2,5-F polymer

### 4.13 Polymer/Clay nanocomposites

#### 4.13.1 XRD pattern of the polymer/clay nanocomposites

Assessment of intercalation and/or exfoliation of the polymer clay nanocomposites produced by *in situ* polymerization of PB-2,5-F polymer was investigated by XRD

(Figure 4-34(a)) from which it can be observed that the basal spacing ( $d_{001}$ ) of the nanocomposite was 1.45 nm ( $2\theta = 6.1^\circ$ ). In comparison with the XRD pattern of the clay with basal spacing ( $d_{001}$ ) of 1.27 nm (Figure 4-34(b)), this suggest the formation of an intercalated nanocomposites. It can also be noted from Figure 4-34(c) that the polymer without clay has no  $d_{001}$  reflection in the region 2-10° of  $2\theta$ .

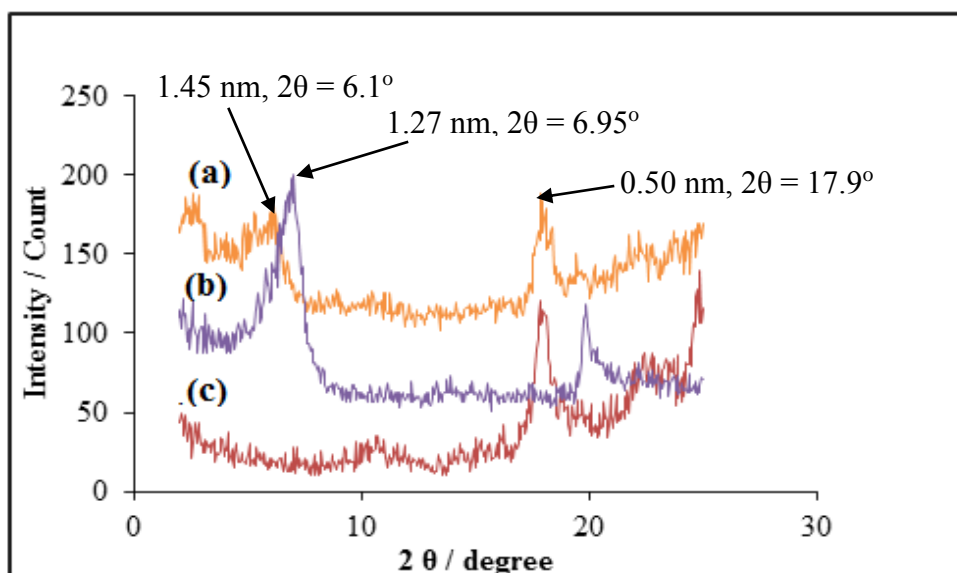


Figure 4-34. XRD pattern of polymer-clay nanocomposites (a), clay (b) and polymer (c).

#### 4.13.2 XRD pattern of polymer/clay nanocomposites prepared by different methods

PB-2,5-F/clay nanocomposites were prepared by solution in ethyl acetate, *in situ* polymerization and melt intercalation methods at 200 °C as described in section 3.6. It was observed that the contents in the flask melted and then solidified on cooling at ambient temperature. The solidified product was ground by pestle and mortar and all the products obtained by the three methods were characterized by XRD and are presented in Figure 4-35.

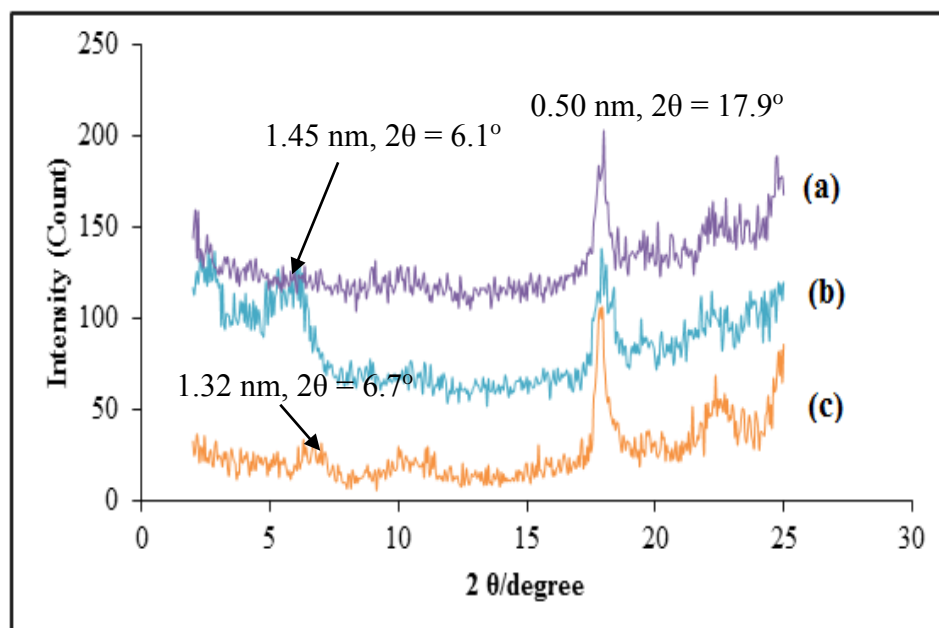


Figure 4-35. XRD pattern of polymer/clay nanocomposites: (a) melt (b) *in situ* and (c) solution methods

The XRD patterns of PB-2,5-F/clay nanocomposites made by melt processing (Figure 4-35(a)) revealed that there were no  $d_{(001)}$  reflections above  $2^\circ$  of  $2\theta$ . This suggests that an exfoliated nanocomposite was made by the melt processing method. However, nanocomposites produced by *in situ* and solution methods revealed some  $d_{001}$  reflections at  $2\theta = 6.1^\circ$  and  $2\theta = 6.7^\circ$ . The  $d$ -spacings of these nanocomposites calculated from Bragg's equation revealed a value of 1.45 nm and 1.32 nm for *in situ* polymerization and solution methods respectively, thereby affording intercalated nanocomposites based on the XRD measurements.

In summary, PB-2,5-F/clay nanocomposite prepared by *in situ* and from solution methods revealed an intercalated polymer/clay nanocomposites and by melt method an exfoliated nanocomposites was produced.

#### 4.13.3 TEM images of polymer/clay nanocomposite

TEM was used to explore whether the nanocomposites were intercalated or exfoliated as the results obtained by XRD alone cannot provide evidence of partial exfoliation. The results of polymer/clay nanocomposite prepared by the melt method are presented

in Figure 4-36. The TEM image indicates structures of light and dark stripes [261, 295] with a spacing of about 5 nm. Obviously the exact spacing can only be deduced if the clay layers are perpendicular to the beam but the XRD trace for this system (Figure 4.35(a)) gives no peaks above  $2\theta = 2^\circ$  which corresponds to 4.4 nm. The dark regions represent layers that are not completely ordered intercalative structures but might be seen as partially exfoliated with an orderly structure. Therefore, this results might suggest that an exfoliated nanocomposite was prepared by melt intercalation method as earlier proposed by the XRD results [381].

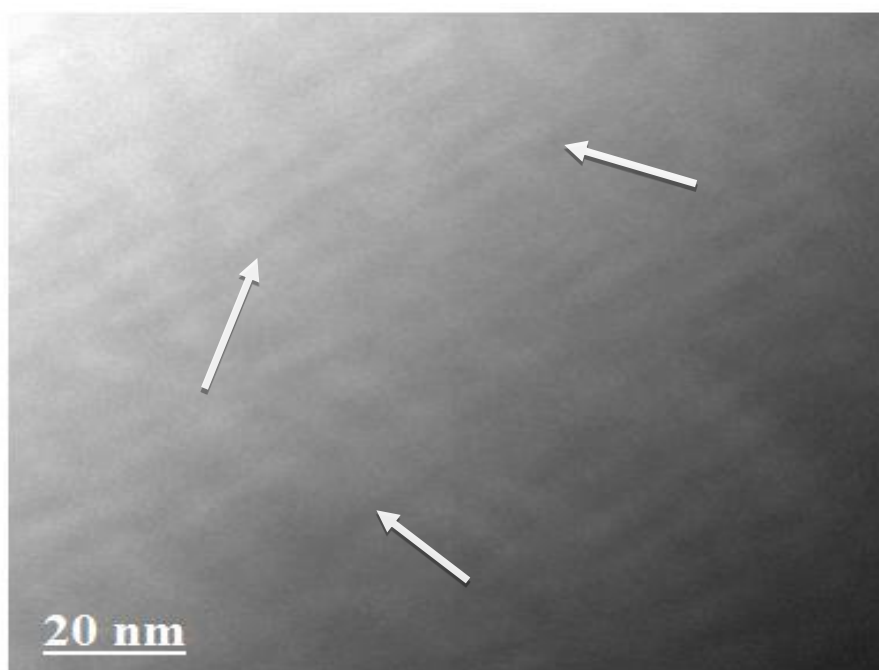


Figure 4-36: TEM image of Polymer/clay nanocomposite by the melt processing method

Similarly, the TEM image of PB-2,5-F/Na-MMT nanocomposite containing 5 wt % clay platelets produced by *in situ* intercalation method was obtained and the image is presented in Figure 4-37. The silicate layers exist mostly as an ordered structure and the arrows correspond to two spacings each about 4 nm. The XRD trace (Figure 4.35(b)) gives a broad and rather flat peak with maximum spacing 1.8 nm which would produce a spacing of 4 nm in the TEM image if the plates were aligned at  $27^\circ$  to the surface. This implies that an intercalated nanocomposite was obtained via the *in situ*

polymerization technique which confirmed the results of the XRD as explained in section 4.12.12 above.

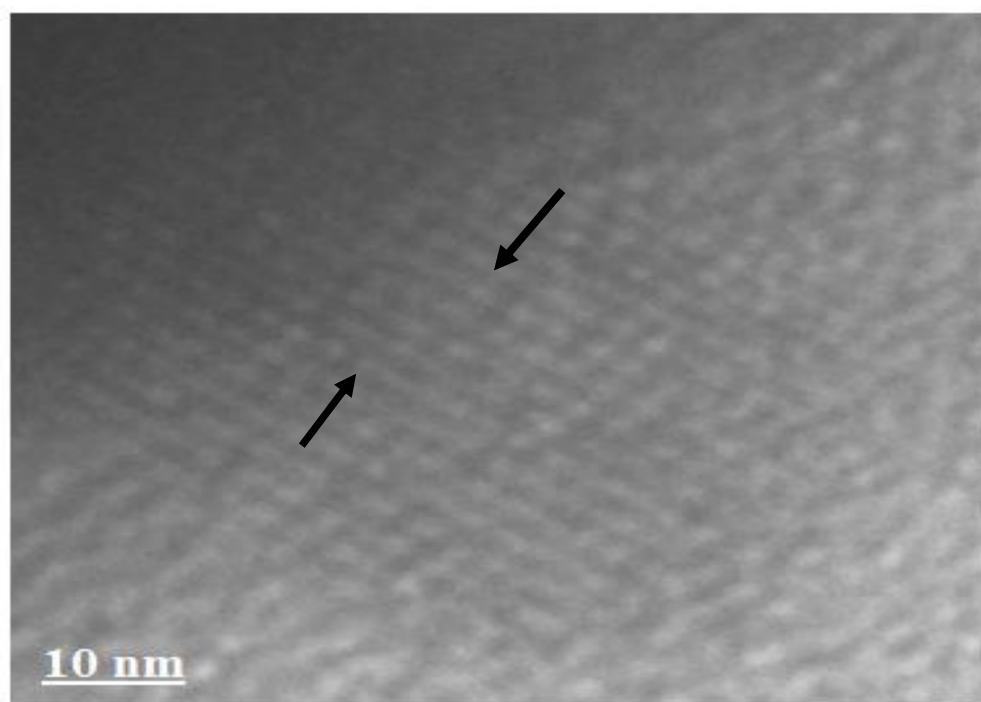


Figure 4-37. TEM image of PB-2,5-F/Na-MMT nanocomposites by *in situ* interaction .

## CHAPTER 5: CONCLUSIONS AND FUTURE WORK

### 5.1 Conclusions

The overall conclusion from this research work is that it is feasible to manufacture hydrophobic polymers and their composites from cassava as a starting material and in so doing to extend materials markets towards bio-based resources and away from mineral oil feedstock. This approach, in the context of the economies of sub-Saharan Africa potentially realigns the agricultural and industrial economic sectors helping to establish an integrated-sector-economy, providing a stronger relationship between farmers and manufacturers, extending employment and thus providing social stability in these regions of the world.

The first part of this work demonstrates that it is possible to use carbohydrates particularly glucose and fructose to obtain 5-(hydroxymethyl) furan (5-HMF) via a reactive vacuum distillation process (based on the boiling point of 5-HMF as 114 - 116 °C at 1 mbar) so that the chemical reaction and product separation take place within a single vessel. This process provides an avenue whereby the production of 5-HMF is conducted and separated with minimal use of volatile solvents and offers the possibility of a semi-continuous industrial processes to produce 5-HMF as a precursor for the production of hydrophobic polymers from biomass. The novelty in this part is the dehydration of glucose and fructose using sulfated zirconia and BMIMCl ionic liquid as solvent by the reaction distillation process which afforded 5-HMF as the main product. This the first investigative research involving this catalyst and the solvent by this method. Another novelty part was the intercalation of Na-MMT with the 5-HMF affording an increased d-spacing of the clay from 1.27 nm to 2.05 nm determined by Bragg's equation from the XRD pattern. There was no report from literatures on the intercalation of Na-MMT clay with 5-HMF prior to this report and this suggest that the precursors derived from 5-HMF as monomers could potentially produce polymer-clay nanocomposites.

The second part of this work makes use of the 5-HMF for the production of derivatives to serve as monomers for the synthesis of hydrophobic polymers by esterification. Two monomers were synthesised and these are: 2,5-furandicarboxylic acid (FDCA) and 2,5-bis-(hydroxymethyl) furan (BHMF). FDCA was obtained at 80% yield by oxidation of 5-HMF using potassium permanganate. A yield of 88% BHMF was obtained by the reduction of 5-HMF using sodium borohydride ( $\text{NaBH}_4$ ) as reducing agent. This product was synthesis so as to pave way for the synthesis of polymers that encompass the starting materials: diacid and diol both derived from biomass sourced carbohydrate via esterification reaction. Furthermore, these diols were treated with Na-MMT clay and the results obtained indicate an intercalation of the clay with the monomers. For instance, the d-spacing of the clay as determined from the XRD patterns using Bragg's equation increased from 1.27 nm to 1.70 nm for FDCA and to 1.67 nm for BHMF respectively. Again, this is the novelty part of this research as there was no reported literature on this.

The third part of this work was the polymerization of FDCA monomer with various diols including BHMF as the reduction product of 5-HMF. The other diols used were 1,4-butanediol, 1,6-hexanediol, and 1,8-octanediol. The FDCA monomer was used to produce polymers using these various diols namely: poly (butylene-2,5-furandicarboxylate) (PB-2,5-F), poly (hexylene-2,5-furandicarboxylate) (PH-2,5-F) and poly (octylene-2,5-furandicarboxylate) (PO-2,5-F). Another polymer, poly (2,5-furandimethylene 2,5-furandicarboxylate) (PBH-2,5-F) was produced from FDCA and BHMF. Their structures were confirmed by  $^1\text{H}$  NMR and FT-IR spectroscopies after precipitation in methanol.

As one of the aims is the synthesis of hydrophobic polymers, the wettability of these polymers was determined by water contact angle measurement. The contact angle on PBH-2,5-F was  $91^\circ$  and this is the more hydrophobic. For the others, the angle was just below  $90^\circ$ . Water uptakes during immersion were in the region of 0.8-1.0% for all these polymers. Dielectric constant was comparable to that of PET.

Furthermore, the mechanical properties of the four polymers are similar but the PBH-2,5-F has a higher tensile failure stress compared to the others and PO-2,5-F possesses the least. The tensile failure stress of these polymers were lower than that of PET and

this can be attributed in part to the fact that a great deal of refinement to the synthesis is needed to obtain a high and narrow molecular weight distribution. Similarly, Young's modulus of the polymers, obtained as 'nominal modulus', were similar within the range of 2.6-3.0 GPa comparable to that of PET.

Finally a study of the interaction between the monomers and Na-montmorillonite clay was made. Results shows that 5-HMF, FDCA and BHMF were able to intercalate between the clay layers which suggests that production of polymer-clay nanocomposites are possible based on the *in-situ* polymerisation of intercalated monomers. An attempt to produce polymer-clay nanocomposites from PB-2,5-F polymer and Na-montmorillonite clay via the *in situ* polymerization technique produced a polymer accompanied by increased basal spacing of the montmorillonite, confirming that a polymer-clay nanocomposite had been prepared. This is also the originality aspect of this project as there was no literature report on this type of polymer-clay nanocomposites.

The success of this sequence of laboratory experiments provides sufficient confidence for a materials production strategy based on derivatives of biomass in the form of cassava and suggests the feasibility of scale-up, highlighting the areas of refinement to the process that are needed.

## 5.2 Future work

### 5.2.1 Other sources of carbohydrate

Other sources of carbohydrates which can be obtained from biomass should be explored to find an alternatives to fossil-derived chemicals. These sources includes wastes crop residues such as sugar cane bagasse, wheat straw, rice straw and corn stover which can serve as raw materials for the synthesis of glucose.

### 5.2.2 Other derivatives of 5-HMF

In addition to FDCA and BHMF, other derivatives of 5-HMF that can be obtained from carbohydrate biomass are 2,5-diformyl furan (DFF) and 2,5-dimethylfuran

(DMF). These derivatives could potentially provide vast arrays of important chemicals and biofuels. It is suggested that effective approaches for their synthesis and potential applications as bio-based materials and starting materials for polymers should be investigated.

### **5.2.3 Molar mass determination of the polymers**

It is of great importance for these polymers to be characterised by molar mass. Various methods are available for the determination of molar mass of polymers. Some of these methods are: (i) light scattering (ii) ultracentrifugation (iii) osmotic pressure (iv) gel permeation chromatography (GPC) and (v) viscosity. Among these techniques, the absolute method for molar mass determination are light scattering, ultracentrifugation and osmotic pressure as they determine the molar mass of polymers directly. The other two methods are GPC and viscosity which do not directly give the values of molar mass and are termed as relative methods. These methods use calibration curves or evaluation of unknown constants by first finding out the molecular weight of the standard or reference polymers.

These methods with the exception of viscosity requires equipment which was not available during the course of this work. Also, molecular weight of a reference standard polymer was not published or established elsewhere. Therefore, molar mass determination of these polymers should be investigated and most importantly molecular mass distribution should be measured and the synthesis process interactively developed to avoid low molecular mass fractions and increase overall molecular mass in order to improve the mechanical and formability properties.

### **5.2.4 Mechanical properties of the polymers**

Generally, polymers and nanocomposites exhibit mechanical deterioration over time which affect their durability and long term performance. Therefore, detailed mechanical behaviour and mechanisms of failure during creep and oxidative and UV degradation should be investigated for future work. Furthermore, the mechanical properties of the composites depends on the composite constituents as well as on the interfacial strength between them. There is a need to determine their long term

performance by the use of reliable tools to determine mechanical durability with the aim of developing polymers and nanocomposites with enhanced mechanical properties for a wide range of applications. Furthermore, other reinforcements such as graphene or graphene oxide could be added to the polymers and their behaviour and properties studied. Again, the volume fraction of reinforcing agents should be studied to find the favourable amount that could provide a nanocomposites with much improved properties.

### **5.2.5 Regulatory measures**

Regulatory measures addressing climate change and environmental legislation should be revisited so as to incorporate the use of biomass as a resource for bio-based materials. This will encourage Governments to focus their attention and investments in biomaterials research in order counter-balance the effects of oil price increase and to safeguard their long term energy security.

Looking at the future, the use of biomass as a resource for bio-fuel and biomaterials will diversify the economies of sub-Saharan Africa particularly Nigeria from dependence on fossil fuel for their economic drivers and this will create more jobs for the teaming unemployed population. Therefore the use of agricultural biomass will realign the industrial and agricultural sectors. An agreement between Governments and industries has to be made in order to assure availability and therefore sustainability for this project.

## Appendix 1. Vacuum distillation apparatus

The vacuum distillation set-up in this work consisted of a rotary vacuum pump, a condenser with coolant recirculation, a silicone oil bath and a hot plate. The hot plate was fitted with a type K thermocouple inserted by drilling into the plate and its temperature was controlled by a Eurotherm 815 programmable controller (Worthing UK). Vacuum connection was via a needle valve (Ham-Let, Sussex, UK) with a ‘T’ to another needle valve for air entry (labeled I and J respectively in Figure 5-1) and a Bourdon-type pressure gauge. Valve A was opened slowly and the vacuum gauge registered its lowest pressure which was 2.7 kPa. This was done several times until a desired vacuum level was obtained. Needle valve B allows gas (air or nitrogen) to bleed into the chamber.



Figure 5-1. Vacuum distillation set-up for glucose/fructose dehydration

Key: A: 100 ml round bottom flask. B: Oil bath set at predetermined temperature, C: Hot plate with magnetic stirrer, D: Reflux condenser, E: Vacuum pump, F: 50 ml round bottom flask for product collection, G: Thermometer, H: Pressure gauge, I: Valve B and J: valve A.

## Appendix 2. NMR and FT-IR spectrum of 5-HMF

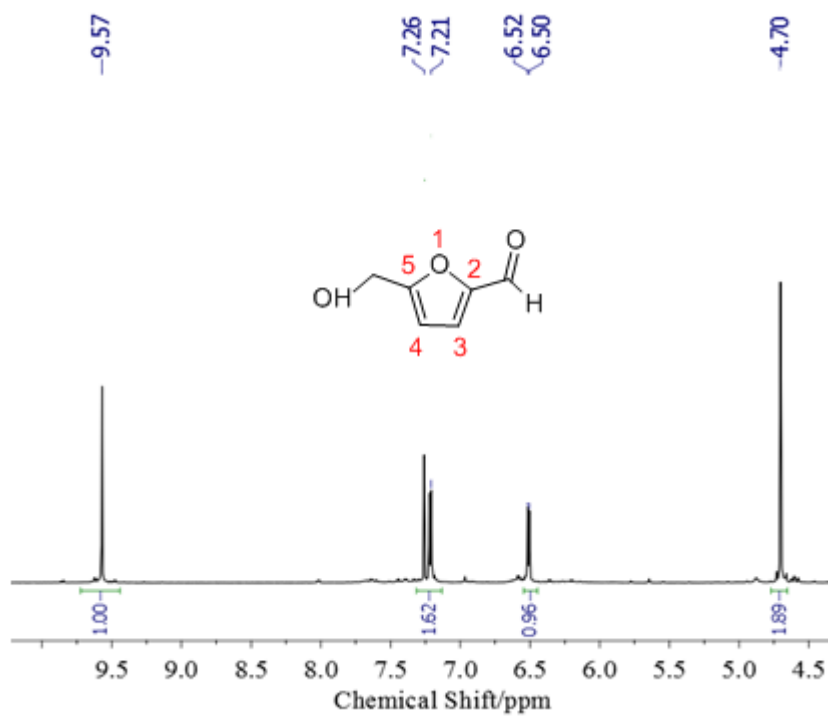


Figure 5-2. <sup>1</sup>H NMR spectra of 5-HMF synthesised

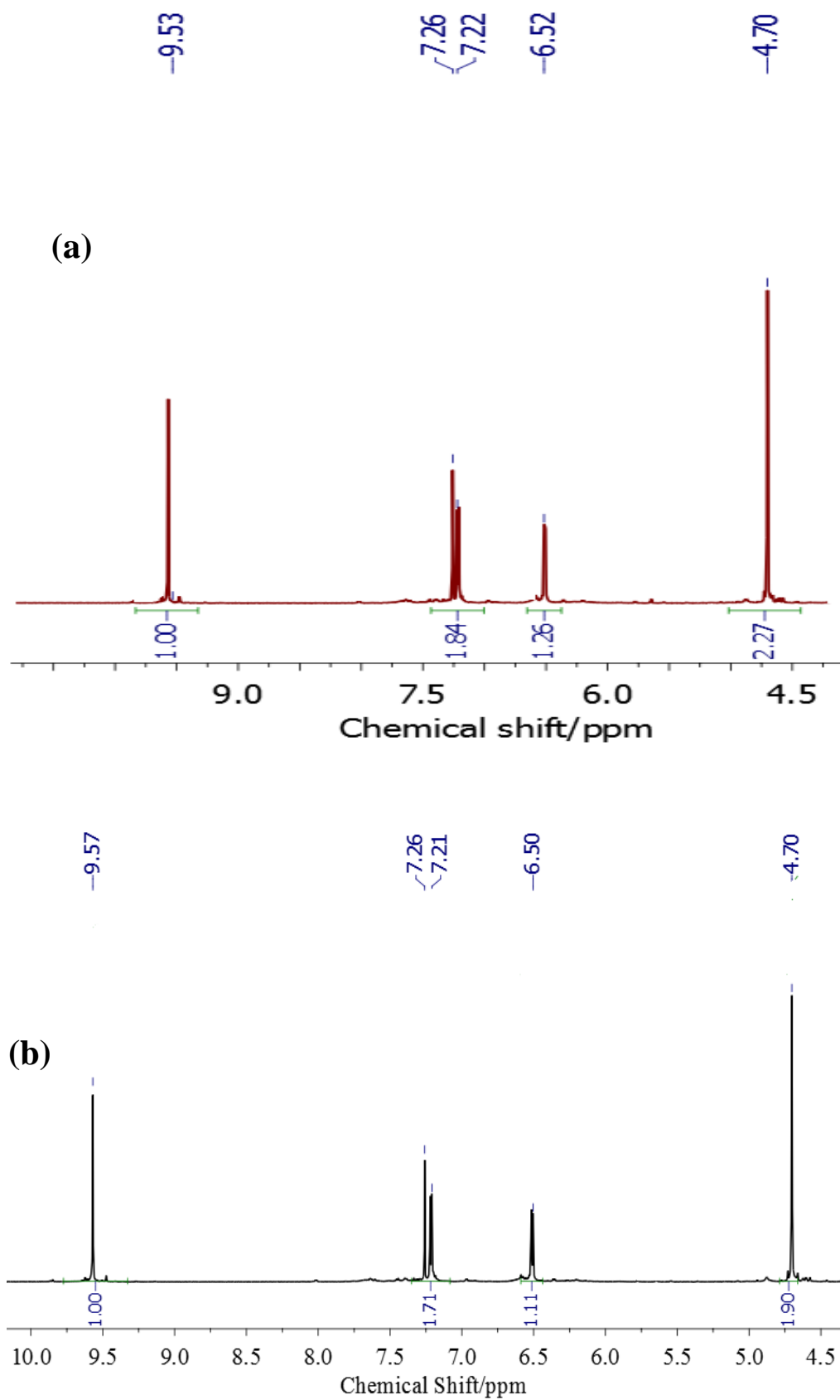


Figure 5-3.  $^1\text{H}$  NMR spectra of 5-HMF: (a) commercially sourced and (b) Synthesised

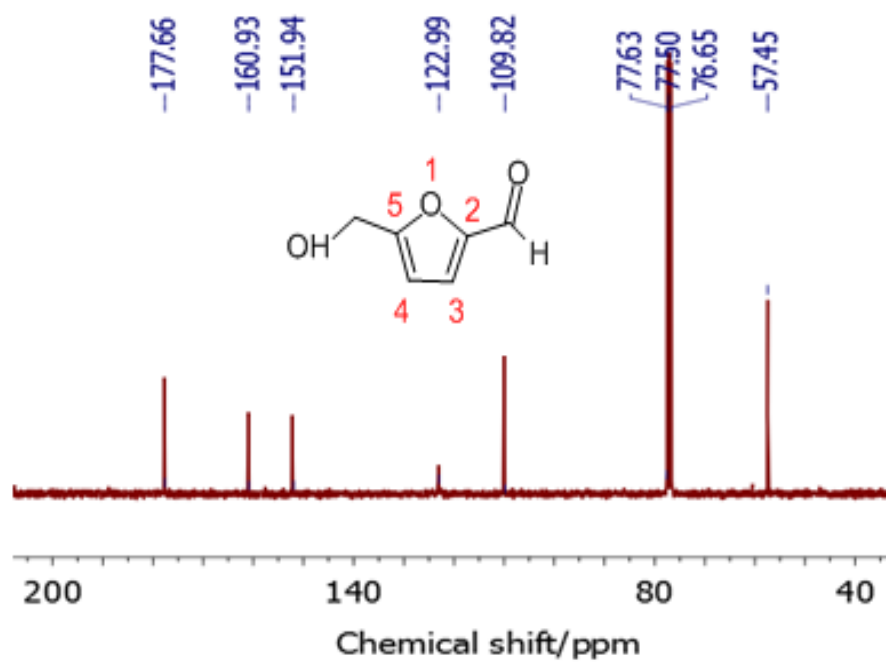
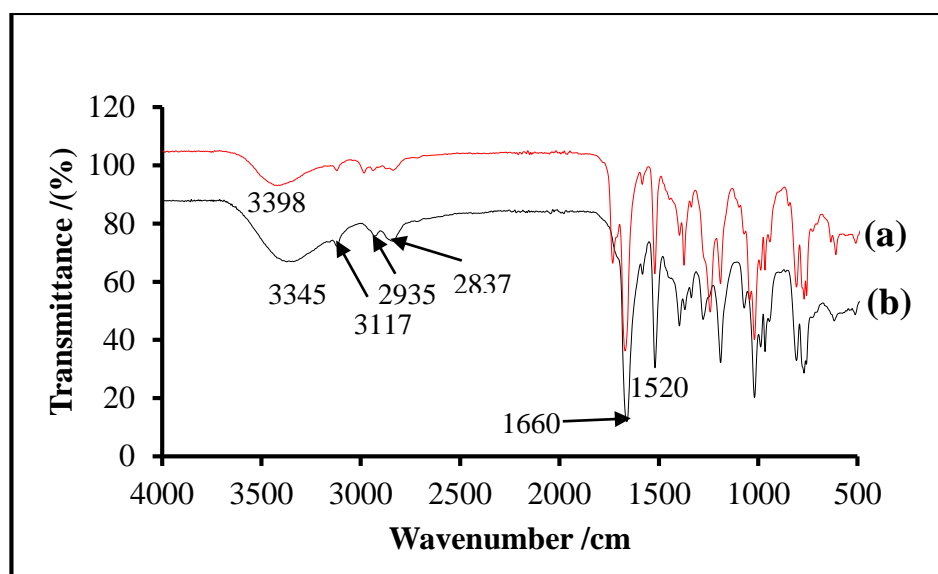
Figure 5-4. <sup>13</sup>C NMR of synthesised 5-HMF

Figure 5-5. FT-IR spectra of (a) commercially sourced and (b) synthesized 5-HMF

### Appendix 3. NMR and FT-IR spectra of FDCA

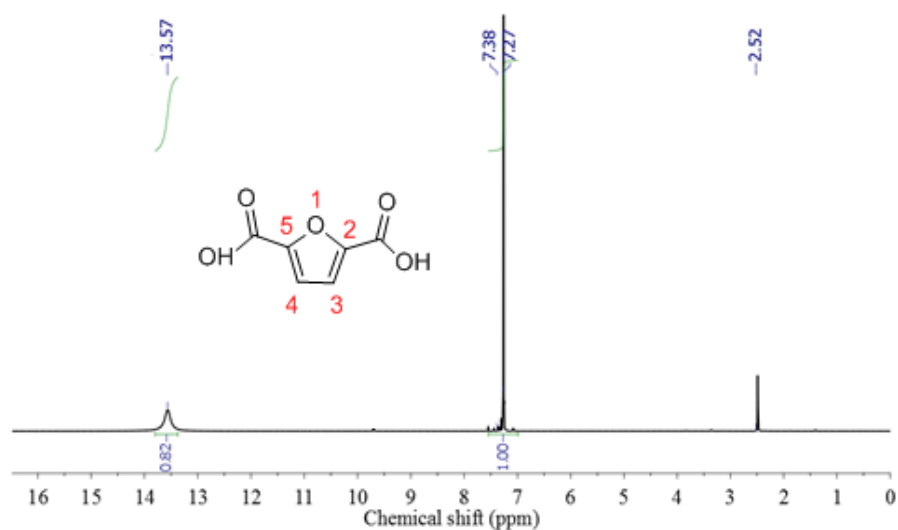


Figure 5-6.  $^1\text{H}$  NMR of FDCA in  $\text{DMSO-d}_6$  (500 MHz)

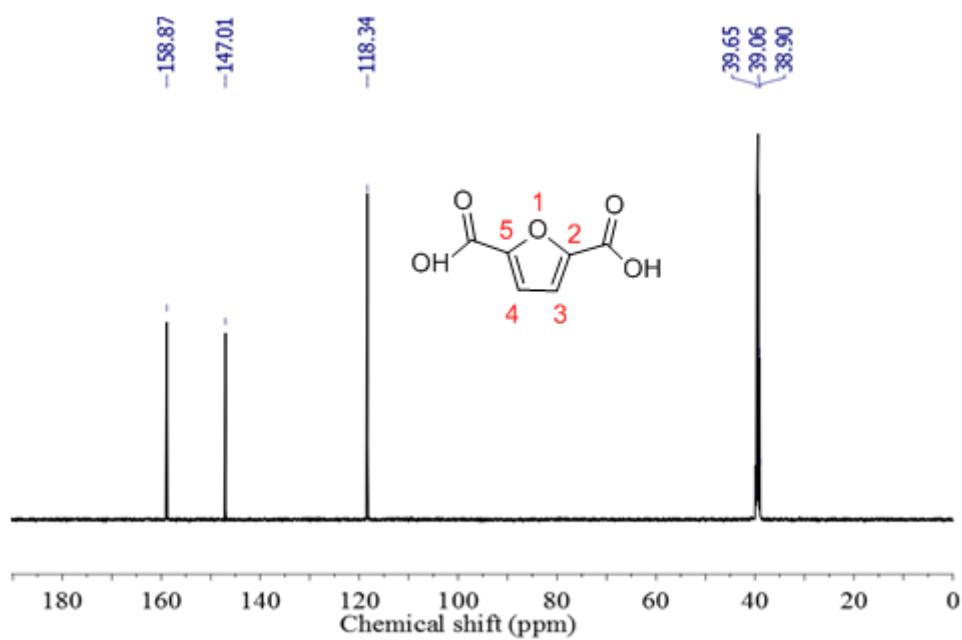


Figure 5-7.  $^{13}\text{C}$  NMR of FDCA in  $\text{DMSO-d}_6$  (500 MHz)

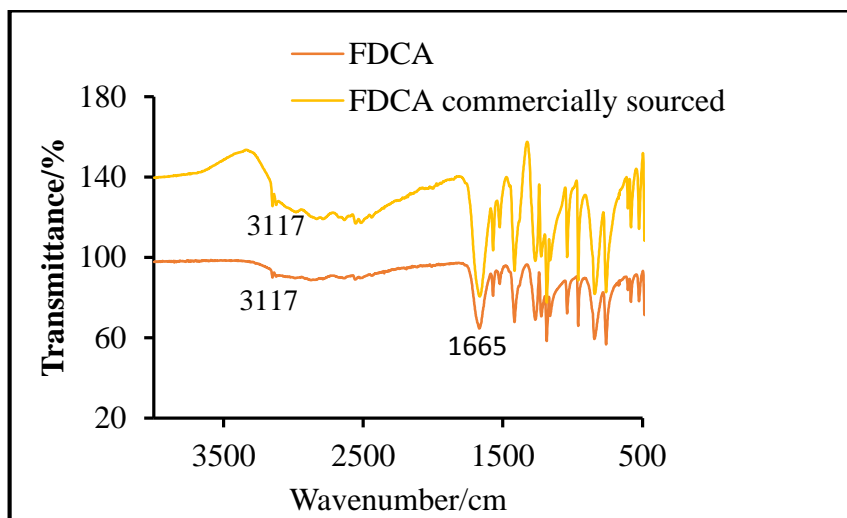


Figure 5-8. FT-IR Spectra of prepared FDCA.

## Appendix 4. NMR and FT-IR spectra of BHMf

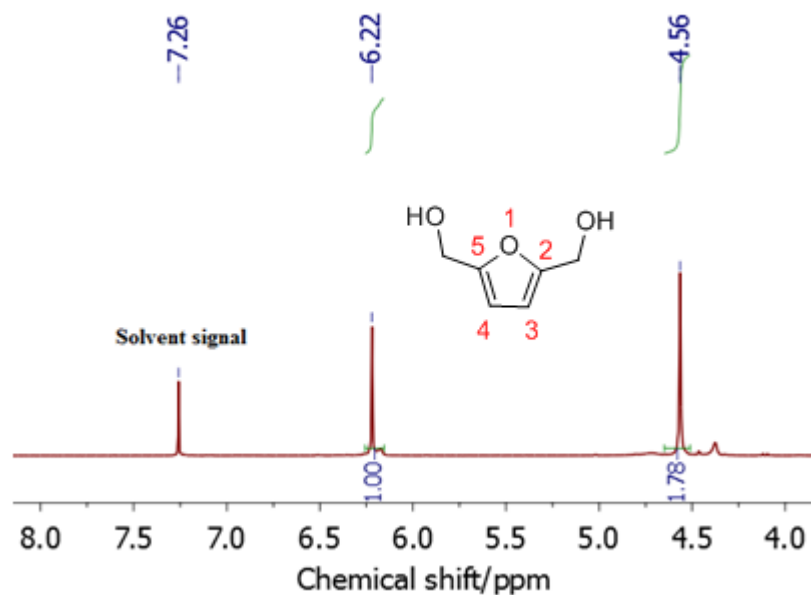


Figure 5-9. <sup>1</sup>H NMR spectra of BHMf in CDCl<sub>3</sub> (300 MHz)

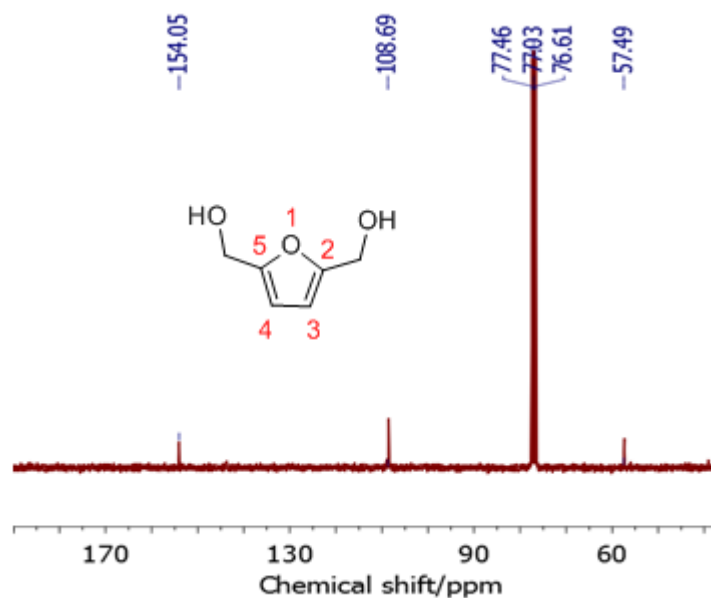


Figure 5-10. <sup>13</sup>C NMR spectra of BHMf in CDCl<sub>3</sub> (300 MHz)

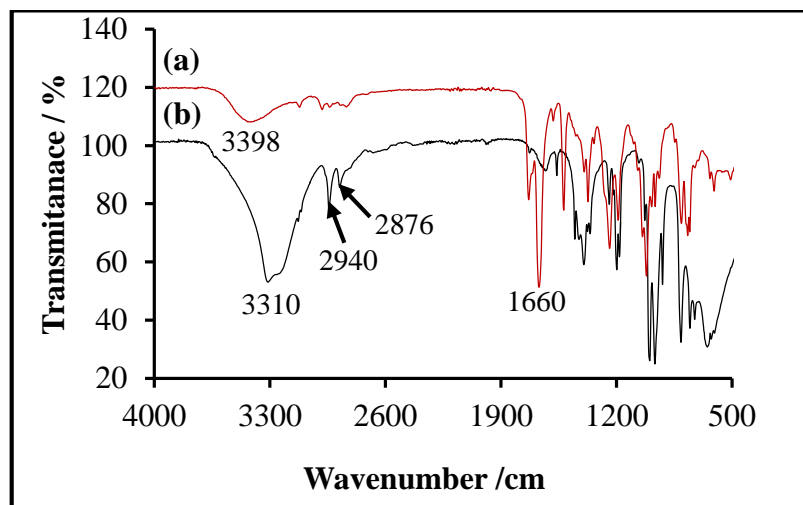


Figure 5-11. FT-IR spectra of (a) 5-HMF and (b) BHMF

## Appendix 5. $^1\text{H}$ and $^{13}\text{C}$ NMR spectra of DFD

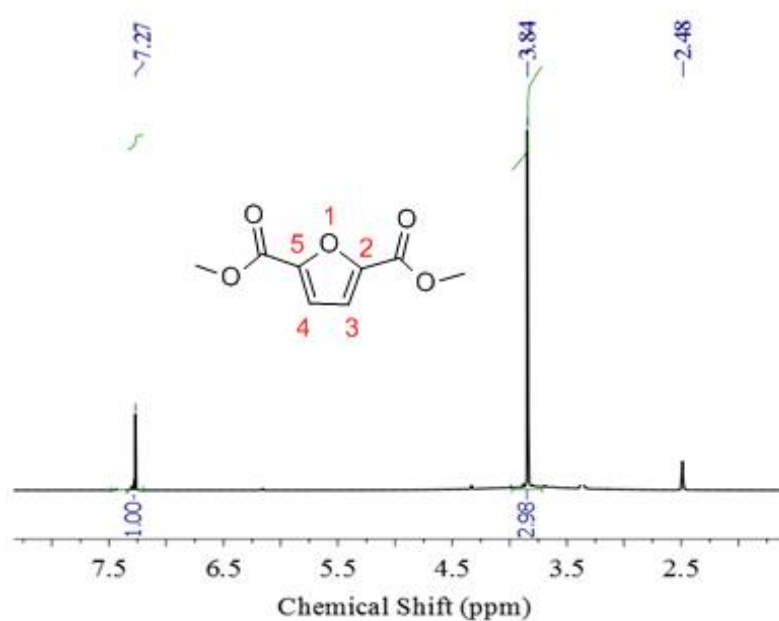


Figure 5-12.  $^1\text{H}$  NMR spectra of DFD in  $\text{DMSO-d}_6$  (500 MHz)

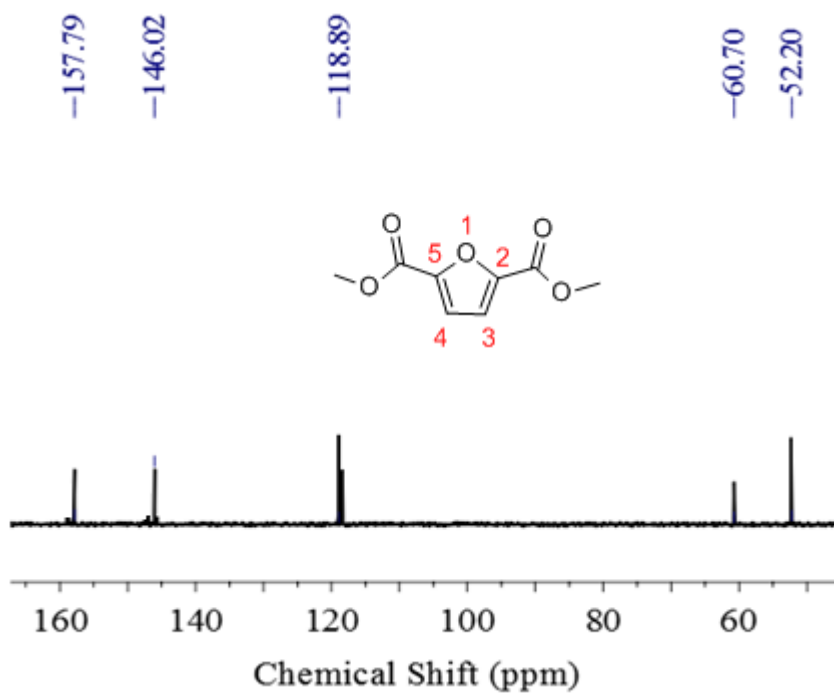


Figure 5-13.  $^{13}\text{C}$  NMR of DFD in  $\text{DMSO-d}_6$  (500 MHz)

## Appendix 6. Analytical instruments

### 1. X-Ray Diffraction (XRD)

X-ray diffraction technique is used to determine the crystal lattice structure and the spacing between atomic planes which will constructively interfere to yield peaks at discrete angles. In another words, when a crystal is irradiated with X-rays that are similar to the spacing of the atomic-scale lattice and at certain incidence angles, then intense reflected X-rays are produced when the wavelengths of the scattered X-rays interfere constructively as illustrated in Figure 5-14.

For the waves to interfere constructively, the differences in the travel path must be equal to integer multiples of the wavelength which will results into a diffracted beam of X-rays that will leave the crystal at an angle equals to that of the incident beam [382].

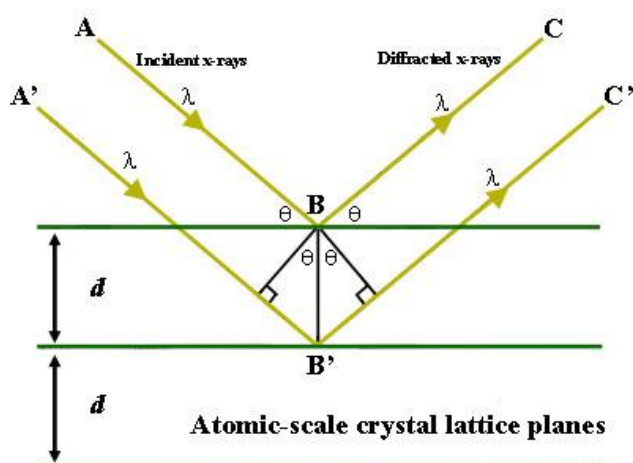


Figure 5-14. Bragg's Law reflection. The diffracted X-rays exhibit constructive interference when the distance between paths ABC and A'B'C' differs by an integer number of wavelengths ( $\lambda$ ).

To illustrate this phenomena, consider a crystal with crystal lattice planar distances  $d$  (right). Where the travel path length difference between the ray paths ABC and A'B'C' is an integer multiple of the wavelength, constructive interference will occur for a combination of that specific wavelength, crystal lattice planar spacing and angle of

incidence ( $\theta$ ). Each rational plane of atoms in a crystal will undergo refraction at a single, unique angle (for X-rays of a fixed wavelength).

The general relationship between the wavelength of the incident X-rays, angle of incidence and spacing between the crystal lattice planes of atoms is known as Bragg's Law, expressed as:

$$n\lambda = 2d \sin\theta \text{-----} (5.1)$$

Where  $n$  (an integer) is the "order" of reflection,  $\lambda$  is the wavelength of the incident X-rays,  $d$  is the interplanar spacing of the crystal and  $\theta$  is the angle of incidence.

#### Application of Bragg's equation

In X-ray diffraction (XRD) the interplanar spacing ( $d$ -spacing) of a crystal is used for identification and characterization purposes. In this case, the wavelength of the incident X-ray is known and measurement is made of the incident angle ( $\theta$ ) at which constructive interference occurs. Solving Bragg's Equation gives the  $d$ -spacing between the crystal lattice planes of atoms that produce the constructive interference. A given unknown crystal is expected to have many rational planes of atoms in its structure; therefore, the collection of "reflections" of all the planes can be used to uniquely identify an unknown crystal. In general, crystals with high symmetry (e.g. isometric system) tend to have relatively few atomic planes, whereas crystals with low symmetry (in the triclinic or monoclinic systems) tend to have a large number of possible atomic planes in their structures.

In the case of wavelength dispersive spectrometry (WDS) or X-ray fluorescence spectroscopy (XRF), crystals of known  $d$ -spacing are used as analyzing crystals in the spectrometer. Because the position of the sample and the detector is fixed in these applications, the angular position of the reflecting crystal is changed in accordance with Bragg's Law so that a particular wavelength of interest can be directed to a detector for quantitative analysis. Every element in the Periodic Table has a discrete energy difference between the orbital "shells" (e.g. K, L, M), such that every element will produce X-rays of a fixed wavelength. Therefore, by using a spectrometer crystal

(with fixed d-spacing of the crystal) and positioning the crystal at a unique and fixed angle ( $\theta$ ), it is possible to detect and quantify elements of interest based on the characteristic X-ray wavelengths produced by each element.

## 2. Nuclear Magnetic Resonance (NMR) Spectroscopy

Nuclear Magnetic Resonance popularly called NMR spectroscopy is an instrumental technique usually applied in structural elucidation and conformational analysis in organic and inorganic compounds. It gives detailed information about molecules and their environment based on the interactions of nuclear magnetic moments with electromagnetic radiation. Therefore, this technique is a quantitative technique based on the fundamental properties of magnetic resonance and according to quantum mechanics, separation between energy levels are quantized. This resonance frequency information on the chemical structure and the magnetic environment can be obtained and also the information on the spin system because of the disturbance from equilibrium. In NMR spectroscopy, magnetic resonance is exhibited by the presence of a magnetic moment provided by the NMR with a non-zero nuclear spin and are aligned with the magnetic fields applied in the form of radio frequencies

Therefore, in determining the structures of compounds by NMR, the samples are subjected to the electromagnetic waves with various frequencies and those that matched the frequencies of the nuclei or electrons are sent to the detector as an electric signals. These signals are then recorded as plots of voltage as a function of time which are converted to peaks as a function of frequencies by the mathematical method of Fourier transformations as hydrogen and carbon nuclei represented as  $^1\text{H}$  NMR and  $^{13}\text{C}$  NMR.

NMR samples are prepared as solutions in deuterated solvents and placed in 5 or 10 mm glass tubes. The tubes are inserted into a cryomagnet probe (Figure 5- 15) that are positioned between the poles of an electro- or permanent magnet or inside a solenoid of a superconducting magnet under liquid helium conditions as illustrated in Figure 5- 15 [383].

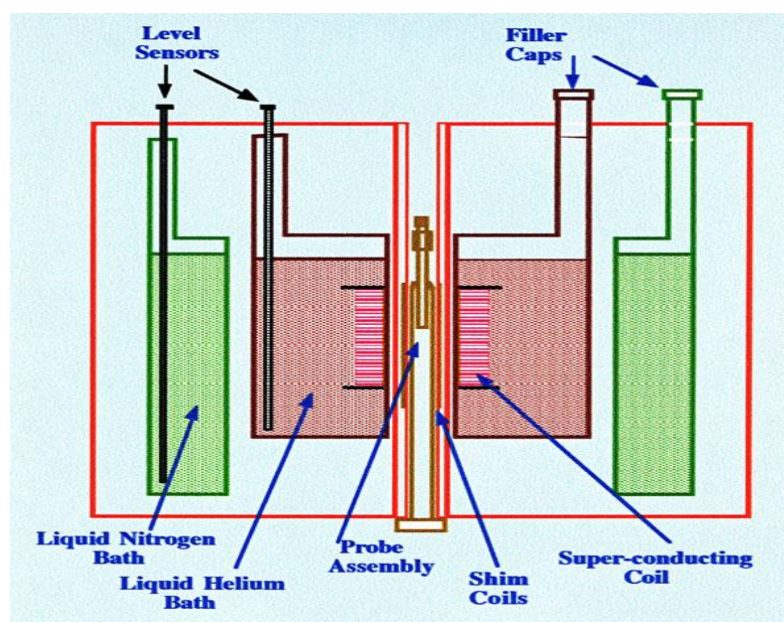


Figure 5-15. Schematic diagram of NMR Spectrometer [383].

The schematic representation of the probe is illustrated in Figure 5-16. A Dewar vessel is attached to the probe which holds the sample tube, the various sensor coils and the conduits of the entire system. Attached to the Dewar vessel is a heater which controls the probe and the samples at a prescribed temperature. Also attached to the Dewar are two coils: RF lock-coil and the RF coil. The RF lock-coil is usually tuned to deuterium as the reference nucleus and this provides the calibrating scale for the spectrum and the RF coil for the nucleus under examination [383]. The probe is integrated by radio-frequency transmitter and receiver coils and a spinner which spins the tube sample in its vertical axis in order to average out the magnetic field inhomogeneity across all the sample.

Therefore, the NMR spectroscopy is used as a quantitative method as the time domain signals are directly related to the peak intensities in the frequency spectrum. Furthermore, each frequency component corresponds to a peak at a specific frequency and amplitude and its own line-width. The resolution of a NMR spectrum depends on the atomic motions, i.e. faster molecular motions lead to sharper lines and higher resolutions. As well, impurities like solid particles or viscous solutions can cause peak broadening and degrade the quality of the spectrum [384].

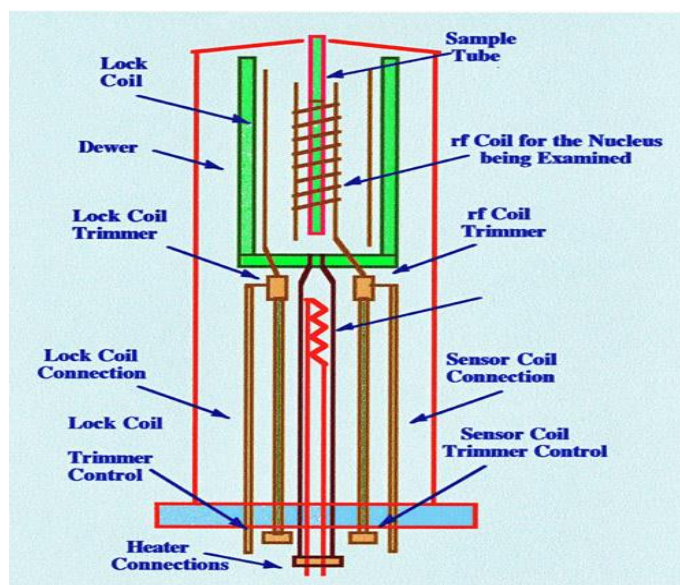


Figure 5-16. Schematic diagram of the probe of an NMR spectrometer [383]

### 3. Fourier Transform Infrared (FT-IR) Spectroscopy

FT-IR spectroscopy is an analytical technique that is used in the areas of determination of molecular structure, identification of chemical species and also quantitative/qualitative determination of chemical species based on their functional groups. This technique is applied to organic and inorganic materials present in either solid, liquids or gaseous states. It involves the interaction between an electromagnetic field with a molecule such that the dipole moment of the molecule changes due to a molecular vibration. This provides an idea of the structural characteristics of the molecules based on the molecular vibrations produced by absorptions frequencies, leading to distinctive physical properties produced by the spectrum. The different absorption frequencies can provide information about a molecule such as linear or branched chains, unsaturation, aromatics and various functional groups. Depending on the number of functional group present in a given molecule, additional absorption bands are observed which provide an avenue to possibly determine their location and orientation within the molecular structure. This is because the peaks of some functional groups tends to be displaced from their theoretical ranges as a results of the influences from other functional group in the molecular structure, their spatial orientation and entropy related effects.

FT-IR spectrum is generated when an electromagnetic radiation adsorption occurs at a frequency that correlates to the vibration associated with a particular chemical bond within a molecule. When the number of electrons that are involved in bond formation in a molecule are greater, then higher energy is required for the excitation of the electrons to a higher energy level. This implies that the energy applied is proportional to the frequency, therefore absorptions due to stretching vibrations are observed at higher frequencies (wavenumbers) than the corresponding bending deformation vibrations. Similarly, symmetric vibrations are easier to excite than asymmetric vibrations. However, in terms of masses, the frequencies are inversely proportional which suggests that light elements vibrate at higher frequencies than the heavy elements.

The FT-IR spectrometer consists of an infrared source (S), a beam splitter (BS), movable mirrors (M1 and M2) for frequency change and a detector as presented in Figure 5-17. Thermally sourced infrared radiation is generated and sent to the beam splitter, represented here as BS which takes the incoming infrared beam and divides it into two optical beams. One beam reflects off of a flat mirror, M1 which is on a mechanism which allows the mirror to move a short distance  $2L$  away from the beam splitter and the other beam is remitted to the movable mirror, M2. The movable mirror M2 makes an additional distance  $x$  resulting in the entire distance moved by the radiation  $2L + x$  and directed onto the sample and subsequently to the detector which records the intensity of the radiation as a function of the displacement  $x$ . This resulting signal is called an **interferogram** which has the unique property that every data point (a function of the moving mirror position) which makes up the signal has information about every infrared frequency which comes from the source. As the interferogram is measured, all other frequencies are also measured at the same time and Fourier transformation by the computer displays the result as a frequency spectrum. The frequency spectrum is scanned several times to reduce the noise and provide a greater sensitivity and the unknown substances measured are compared with tables of spectral data [384].

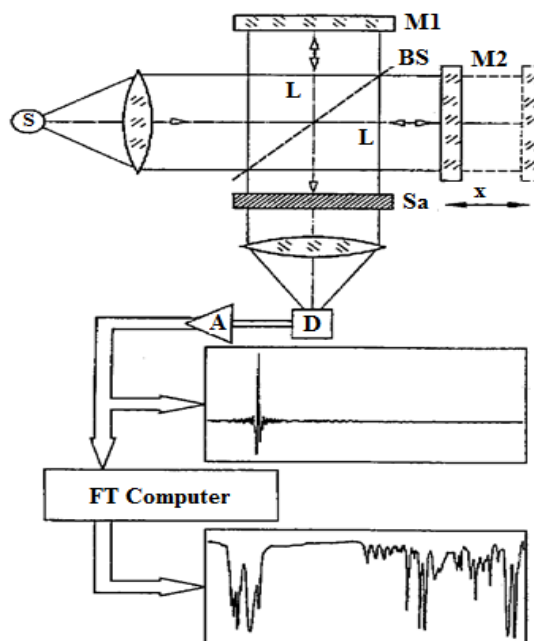


Figure 5-17. Schematic diagram of an FT-IR instrument [384]

#### 4. Thermogravimetric analysis (TGA)

Thermogravimetric analysis (TGA) is an analytical technique that is applied in polymer characterisation to determine the decomposition, thermal stability and fractions of volatile components of polymers. This is achieved by measuring the weight change of a polymer sample as a function of temperature or time. In this technique, the polymer is subjected to a controlled heating while the weight loss of the sample is recorded at the same time. The measurements are carried out in air or in an inert atmosphere, such as helium or argon.

In addition to changes in mass of a polymer, some TGA instruments are capable of measuring the temperature difference between the polymer sample and a reference pans (differential thermal analysis, DTA) or the heat flow into the sample pan compared to that of the reference pan (differential scanning Calorimetry, DSC)

## 5. Differential Scanning Calorimetry (DSC)

Differential Scanning Calorimetry is a technique used to measure thermal properties of polymers based on the rate at which they absorb heat energy compared to a reference material. The technique takes advantage of the energy changes involved in the various phase transitions of certain polymer molecules. This allows several properties of the material to be ascertained; melting points, enthalpies of melting, crystallisation temperatures, glass transition temperatures and degradation temperatures.

A heat flux differential scanning calorimeter is used in the experiment. This is one in which a sample is heated along with a reference material with a known specific heat. One of the criteria of this technique is that the sample and reference material remain at the same temperature during heating. This can be achieved by setting the machine to heat both the sample and reference material at a specific rate (In this experiment, the rate is set to 10°C per minute). This allows the heat flux or difference in energy input between the sample and reference to be measured. Maintaining a constant supply of heat to both materials would not (unless the materials have the same heat capacity at all points, which is unlikely) maintain a minimal temperature difference between them. Instead, a computer is connected to the machine, and using the software and various signals from the calorimeter, “decides” when to supply heat to either material. This information is then dealt with by the computer software and presents it as a graph of the energy changes versus the temperature. A standard DSC curve for a particular polymer is shown in Figure 5-18.

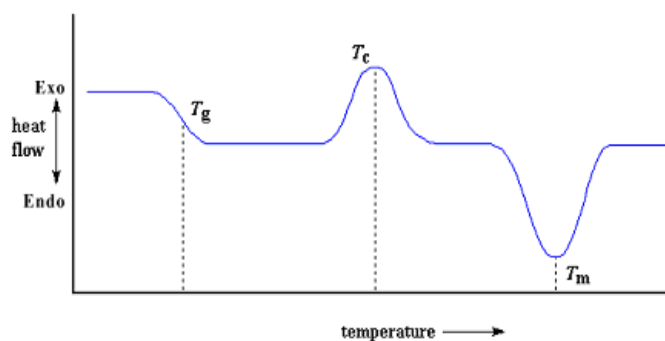


Figure 5-18. A standard output for a polymer from a DSC machine.

From the diagram, it can be seen that a sudden upward jump in the curve signifies an exothermic process. A sudden drop in heat flux indicates an endothermic process.

It is possible to approximate the heat flow into the sample holder using the following equation:

$$\frac{dQ}{dT} = K(T_b - T) \text{-----} (5.2)$$

T is the sample temperature,  $T_b$ : programmed block temperature and K: thermal conductivity of the material.

$$T_b = T_0 + qt \text{-----} (5.3)$$

$T_0$  is the initial temperature and q is the programmed heating rate.

The heat capacity is defined as the amount of heat energy required to raise the temperature of a body by 1K. For a substance with a constant heat capacity:

$$Q = C_p(T - T_0) \text{-----} (5.4)$$

It is possible to derive an equation from equations 5.3 and 5.4 that forms the basis for the DSC experiment as follows:

$$\Delta T = q \frac{C_p}{K} \text{-----} (5.5)$$

$\Delta T$  is the difference in temperature between the reference material and the sample.

The heat capacity is given as

$$C_p = mc_p \text{-----} (5.6)$$

Where  $C_p$  is the specific heat (Amount of heat required to raise the temperature of unit mass by 1K).

The enthalpy change for a given phase transition may be found by integrating over the area in which the transition is seen to occur on the DSC plot. This change may be described by the following integral:

$$\Delta H = \int_{T_i}^{T_f} C_p dt = \int_{T_i}^{T_f} \left( \frac{K\Delta T}{q} \right) dT \text{----- (5.7)}$$

Where the limits of integration  $T_i$  and  $T_f$  are the initial and final temperatures over which the graph is integrated. Therefore it is the area under the curve that gives information about the enthalpy changes involved in the various transitions.

## Appendix 7. Photographs of some of the equipment used

### 1. Bruker alpha FTIR



Figure 5-19. Alpha Bruker FTIR spectrophotometer

### 2. Siemens D500 X-Ray Diffractometer



Figure 5-20. Siemens D500 X-Ray Diffractometer

### 3. Thermal analyser



Figure 5-21. Netsch STA 449 F1 Jupiter thermal analyser

### 4. Centrifuge



Figure 5-22. Heraeus Biofuge Primo Centrifuge machine

## REFERENCES

1. Berner, R.A., Petsch, S.T., Lake, J.A., Beerling, D.J., Popp, B.N., Lane, R.S., Laws, E.A., Westley, M.B., Cassar, N., Woodward, F.I. and Quick, W.P., *Isotope fractionation and atmospheric oxygen: Implications for phanerozoic O<sub>2</sub> evolution*. Science, 2000, **287**(5458): pp. 1630-1633.
2. Organization of Petroleum Exporting Countries; (2014) *Yearly oil price*. Retrieved from: [http://www.opec.org/opec\\_web/en/data\\_graphs/40.htm](http://www.opec.org/opec_web/en/data_graphs/40.htm). [Accessed 20th January,2014].
3. National Population Commission of Nigeria; *2006 population and housing census*. Retrieved from: [www.population.gov.ng](http://www.population.gov.ng) [Accessed 20th June 2011].
4. Moomow, W., Yamba, F., Kamimoto, M., Maurice, L., Nyboer, J., Urama, K. and Weir, T., *Introduction-IPCC special report on renewable energy sources and climate change mitigation*. In: Edenhofer, O., Pichs-Madruga, R., Sokona, Y., Seyboth, K., Matschoss, P., Kadner, S., Zwickel, T., Eickemeier, P., Hansen, G., Schlömer, S., and Von Stechow, C.(eds), 2011, Cambridge University Press, United Kingdom, pp 1-45.
5. Ohimain, E.I., *The benefits and potential impacts of household cooking fuel substitution with bio-ethanol produced from cassava feedstock in Nigeria*. Energy for Sustainable Development, 2012, **16**(3): pp. 352-362.
6. Wu, C.Z., Yin, X.L., Yuan, Z.H., Zhou, Z.Q. and Zhuang, X.S., *The development of bioenergy technology in China*. Energy, 2010, **35**(11): pp. 4445-4450.
7. Nguyen, T.L.T., Gheewala, S.H. and Bonnet, S., *Life cycle cost analysis of fuel ethanol produced from cassava in Thailand*. International Journal of Life Cycle Assessment, 2008, **13**(7): pp. 564-573.
8. Zhang, H.L., Baeyens, J. and Tan, T.W., *The bubble-induced mixing in starch-to-ethanol fermenters*. Chemical Engineering Research and Design, 2012, **90**(12): pp. 2122-2128.
9. Omotor, D.G., Orubu, C.O. and Inoni, E., *Policy reforms and agricultural exports in Nigeria: An empirical analysis*. Singapore Economic Review, 2009, **54**(4): pp. 589-603.
10. Aigbedion, I. and Iyayi, S.E., *Diversifying Nigeria's petroleum industry*. International Journal of Physical Sciences, 2007, **2**(10): pp. 263-270.
11. Okonkwo, I.C., *The erosion of agricultural exports in an oil economy - The case of Nigeria*. Journal of Agricultural Economics, 1989, **40**(3): pp. 375-380.
12. Sanusi, S.L.(2013) *Overcoming the fear of vested interest*. Retrieved from: <http://www.youtube.com/watch?v=IjViGLJIU9g> [Accessed 14th January, 2014].
13. Central Intelligent Agency; (2014) *The world fact book*. Retrieved from: <https://www.cia.gov/library/publications/the-world-factbook/rankorder/2147rank.html> [Accessed 16th April, 2014].
14. United Nations; (2011) *Map of nigeria*. Retrieved from: [www.un.org/Depts/Cartographic/map/profile/nigeria.pdf](http://www.un.org/Depts/Cartographic/map/profile/nigeria.pdf).
15. United States Energy Information Administration (2014); Retrieved from: [http://www.eia.gov/beta/state/seds/data.cfm?incfile=/state/seds/sep\\_sum/html/sum\\_btu\\_1.html&sid=US](http://www.eia.gov/beta/state/seds/data.cfm?incfile=/state/seds/sep_sum/html/sum_btu_1.html&sid=US); [ Accessed 21th January, 2014].
16. World Bank (2014) *World bank list of economies*. Retrieved from: <http://www.worldbank.org> [Accessed 16th April,2014].

17. National Bureau of Statistics; (2010) *2009 and estimates for 2010 Q1 and Q2 gross domestic products (GDP) for Nigeria*. 1-15]. Retrieved from: <http://www.nigerianstat.gov.ng/> [Accessed 21st June, 2011].
18. Odumugbo, C.A., *Natural gas utilisation in Nigeria: Challenges and opportunities*. Journal of Natural Gas Science and Engineering, 2010, **2**(6): pp. 310-316.
19. Adamu, A., *Agricultural production on the Soba plains in the nineteenth century*. Zaria Archaeol. Papers (ZAP), 2000, **9**: pp. 82-88.
20. Muhammed-Lawal, A. and Atte, O.A., *An analysis of agricultural production in Nigeria*. African Journal of General Agriculture, 2006, **2**(1): pp. 1-6.
21. Ati, O.F., Stigter, C.J., Iguisi, E.O. and Afolayan, J.O., *Profile of rainfall challenges and variability in the northern Nigeria, 1953-2002*. Research Journal of Environmental and Earth Sciences, 2009, **1**(2): pp. 58-63.
22. Food and Agriculture Organization (2011) *Online statistical database*. Retrieved from: <http://faostat.fao.org/site/339/default.aspx> [Accessed 27th January, 2014].
23. Nweke, F.I., Spencer, D. and Lynam, J., *The cassava transformation: Africa's best kept secret*. 2002, Michigan State University Press., pp. 273-275.
24. Nweke, F.I., *Cassava processing in sub-Saharan Africa: Implications for expanding cassava production*. IITA Research, 1996, **12**: pp. 7-14.
25. Tarawali, G., Abdoulaye, T., Ellis-Jones, J., Asumugha, G., Dixon, A., Okechukwu, R., Ezedinma, C., Sanni, L., Isife, B., Ogisi, D. and Ekpere, J., *An impact assessment of the cassava enterprise development project*. 2013, IITA, Ibadan, Nigeria, pp 1-63.
26. International Institute of Tropical Agriculture (IITA) (2011); *Towards production of bread from cassava*. Retrieved from: [http://www.iita.org/search/-/journal\\_content/56/25357/55843](http://www.iita.org/search/-/journal_content/56/25357/55843). [Accessed, 20th January, 2012].
27. Bicker, M., Hirth, J. and Vogel, H., *Dehydration of fructose to 5-hydroxymethylfurfural in sub- and supercritical acetone*. Green Chemistry, 2003, **5**(2): pp. 280-284.
28. Gandini, A. and Belgacem, M.N., *Furans in polymer chemistry*. Progress in Polymer Science 1997, **22**(6): pp. 1203-1379.
29. Gandini, A. and Belgacem, M.N., *Furfural and furanic polymers*. Le furfural et les polymères furaniques, 2002(11-12): pp. 56-61.
30. Gandini, A. and Belgacem, M.N., *Recent contributions to the preparation of polymers derived from renewable resources*. Journal of Polymers and the Environment, 2002, **10**(3): pp. 105-114.
31. Serdar, Y., *Pyrolysis of biomass to produce fuels and chemical feedstock*. Energy Conservation and Management, 2004, **45**: pp. 651-671.
32. Demirbas, A., *'Sub- and Super-critical water depolymerization of biomass'*. Energy Sources Part A: Recovery, Utilization and Environmental Effects, 2010, **32**(12): pp. 1100-1110.
33. Mckendry, P., *Energy production from biomass (part 1): Overview of biomass*. Bioresource Technology, 2002, **83**(1): pp. 37-46.
34. Kroger, M., Prusse, U. and Vorlop, K.D., *A new approach for the production of 2,5-furandicarboxylic acid by in situ oxidation of 5-hydroxymethylfurfural starting from fructose*. Topics in Catalysis, 2000, **13**(3): pp. 237-242.

35. Paster, M., Pellegrino, J.L. and Carole, T.M., *Industrial bioproducts: Today and tomorrow*, US Department of Energy, W.D., Editor. 2003, Energetics Inc. Columbia, pp 1-89.
36. Li, N., Tompsett, G.A., Zhang, T.Y., Shi, J.A., Wyman, C.E. and Huber, G.W., *Renewable gasoline from aqueous phase hydrodeoxygenation of aqueous sugar solutions prepared by hydrolysis of maple wood*. *Green Chemistry*, 2011, **13**(1): pp. 91-101.
37. Taufiqurrahmi, N. and Bhatia, S., *Catalytic cracking of edible and non-edible oils for the production of biofuels*. *Energy & Environmental Science*, 2011, **4**(4): pp. 1087-1112.
38. Alonso, D.M., Bond, J.Q. and Dumesic, J.A., *Catalytic conversion of biomass to biofuels*. *Green Chemistry*, 2010, **12**(9): pp. 1493-1513.
39. Geboers, J.A., Van De Vyver, S., Ooms, R., Op De Beeck, B., Jacobs, P.A. and Sels, B.F., *Chemocatalytic conversion of cellulose: Opportunities, advances and pitfalls*. *Catalysis Science & Technology*, 2011, **1**(5): pp. 714-726.
40. Kobayashi, H., Ohta, H. and Fukuoka, A., *Conversion of lignocellulose into renewable chemicals by heterogeneous catalysis*. *Catalysis Science & Technology*, 2012, **2**(5): pp. 869-883.
41. Rosatella, A.A., Simeonov, S.P., Frade, R.F.M. and Afonso, C.A.M., *5-hydroxymethylfurfural (HMF) as a building block platform: Biological properties, synthesis and synthetic applications*. *Green Chemistry*, 2011, **13**(4): pp. 754-793.
42. Binder, J.B. and Raines, R.T., *Simple chemical transformation of lignocellulosic biomass into furans for fuels and chemicals*. *Journal of the American Chemical Society*, 2009, **131**(5): pp. 1979-1985.
43. Qi, X.H., Guo, H.X. and Li, L.Y., *Efficient conversion of fructose to 5-hydroxymethylfurfural catalyzed by sulfated zirconia in ionic liquids*. *Industrial & Engineering Chemistry Research*, 2011, **50**(13): pp. 7985-7989.
44. Wang, P., Yu, H., Zhan, S. and Wang, S., *Catalytic hydrolysis of lignocellulosic biomass into 5-hydroxymethylfurfural in ionic liquid*. *Bioresource Technology*, 2011, **102**(5): pp. 4179-4183.
45. Koutinas, A.A., Du, C., Wang, R.H. and Webb, C., *Production of chemicals from biomass*. In: *Introduction to chemicals from biomass*. Clark, J.H. and Fabien, E.I.D., Editors. Wiley-VCH, UK, pp. 77-101.
46. Stahlberg, T., Sorensen, M.G. and Riisager, A., *Direct conversion of glucose to 5-(hydroxymethyl)furfural in ionic liquids with lanthanide catalysts*. *Green Chemistry*, 2010, **12**(2): pp. 321-325.
47. Zakrzewska, M.E., Bogel-Lukasik, E. and Bogel-Lukasik, R., *Ionic liquid-mediated formation of 5-hydroxymethylfurfural-A promising biomass-derived building block*. *Chemical Reviews*, 2011, **111**(2): pp. 397-417.
48. Kuster, B.F.M., *5-hydroxymethylfurfural (HMF) - A review focusing on its manufacture*. *Starch-Starke*, 1990, **42**(8): pp. 314-321.
49. Huang, R.L., Qi, W., Su, R.X. and He, Z.M., *Integrating enzymatic and acid catalysis to convert glucose into 5-hydroxymethylfurfural*. *Chemical Communications*, 2010, **46**(7): pp. 1115-1117.
50. Huber, G.W., Iborra, S. and Corma, A., *Synthesis of transportation fuels from biomass: Chemistry, catalysts, and engineering*. *Chemical Reviews*, 2006, **106**(9): pp. 4044-4098.

51. Climent, M.J., Corma, A. and Iborra, S., *Converting carbohydrates to bulk chemicals and fine chemicals over heterogeneous catalysts*. Green Chemistry, 2011, **13**(3): pp. 520-540.
52. Patel, M., Crank, M., Dornburg, V., Hermann, B., Roes, L., Husing, B., Overbeek, L., Terragni, F. and Recchia, E.(2006) *The brew project report: Medium and long-term opportunities and risks of the biotechnological production of bulk chemicals from renewable resources*. Retrieved from: [http://www.chem.uu.nl/brew/BREW\\_Final\\_Report\\_September\\_2006.pdf](http://www.chem.uu.nl/brew/BREW_Final_Report_September_2006.pdf) [Accessed 25th February, 2013].
53. Hu, S., Zhang, Z., Song, J., Zhou, Y. and Han, B., *Efficient conversion of glucose into 5-hydroxymethylfurfural catalyzed by a common lewis acid  $SnCl_4$  in an ionic liquid*. Green Chemistry, 2009, **11**: pp. 1746-1749.
54. Elliott, D.C., Beckman, D., Bridgwater, A.V., Diebold, J.P., Gevert, S.B. and Solantausta, Y., *Developments in direct thermochemical liquefaction of biomass - 1983-1990*. Energy & Fuels, 1991, **5**(3): pp. 399-410.
55. Chen, N.Y., Degnan, T.F. and Koenig, L.R., *Liquid fuel from carbohydrates*. Chemtech, 1986, **16**(8): pp. 506-511.
56. Weisz, P.B., Haag, W.O. and Rodewald, P.G., *Catalytic production of high-grade fuel (gasoline) from biomass compounds by shape-selective catalysis*. Science, 1979, **206**(4414): pp. 57-58.
57. Katzen, R. and Tsao, G.T., *A view of the history of biochemical engineering*. Advances in biochemical engineering/biotechnology, 2000, **70**: pp. 77-91.
58. Kalendova, A., Merinska, D., Gerard, J.F. and Slouf, M., *Polymer/clay nanocomposites and their gas barrier properties*. Polymer Composites, 2013, **34**(9): pp. 1418-1424.
59. Abdelmagid, A.F., Carson, K.G., Harris, B.D., Maryanoff, C.A. and Shah, R.D., *Reductive amination of aldehydes and ketones with sodium triacetoxyborohydride: Studies on direct and indirect reductive amination procedures*. Journal of Organic Chemistry, 1996, **61**(11): pp. 3849-3862.
60. Babu, R., O'connor, K. and Seeram, R., *Current progress on bio-based polymers and their future trends*. Progress in Biomaterials, 2013, **2**(1): pp. 1-16.
61. Song, J.H., Murphy, R.J., Narayan, R. and Davies, G.B.H., *Biodegradable and compostable alternatives to conventional plastics*. Philosophical Transactions of the Royal Society B-Biological Sciences, 2009, **364**(1526): pp. 2127-2139.
62. Mohamed, A.M.E., *Synthesis and characterisation of novel biopolymers via click chemistry*. 2010, University of Durham, pp 1- 259.
63. Chandra, R. and Rustgi, R., *Biodegradable polymers*. Progress in Polymer Science, 1998, **23**(7): pp. 1273-1335.
64. Gandini, A., *Polymers from renewable resources: A challenge for the future of macromolecular materials*. Macromolecules, 2008, **41**(24): pp. 9491-9504.
65. Gandini, A., Coelho, D., Gomes, M., Reis, B. and Silvestre, A., *Materials from renewable resources based on furan monomers and furan chemistry: Work in progress*. Journal of Materials Chemistry, 2009, **19**(45): pp. 8656-8664.
66. Gandini, A., *The irruption of polymers from renewable resources on the scene of macromolecular science and technology*. Green Chemistry, 2011, **13**(5): pp. 1061-1083.
67. Gallezot, P., *Conversion of biomass to selected chemical products*. Chemical Society Reviews, 2012, **41**(4): pp. 1538-1558.

68. Shen, L., Worrell, E. and Patel, M., *Present and future development in plastics from biomass*. Biofuels Bioproducts & Biorefining-Biofpr, 2010, **4**(1): pp. 25-40.
69. Ramesh, H.P. and Tharanathan, R.N., *Carbohydrates - the renewable raw materials of high biotechnological value*. Critical Reviews in Biotechnology, 2003, **23**(2): pp. 149-173.
70. Cunha, A.G. and Gandini, A., *Turning polysaccharides into hydrophobic materials: A critical review. Part I. Cellulose*. Cellulose, 2010, **17**(5): pp. 875-889.
71. Gandini, A. and Belgacem, M.N., *The state of the art*. In: Belgacem, M.N. and Gandini, A.(eds) Monomers, polymers and composites from renewable resources, 1st edn. 2008, Elsevier, Amsterdam, pp 1-16.
72. Krassig, H., *Cellulose - morphology, structure, accessibility and reactivity*. Papier, 1990, **44**(12): pp. 617-623.
73. Klemm, D., Heublein, B., Fink, H.P. and Bohn, A., *Cellulose: Fascinating biopolymer and sustainable raw material*. Angewandte Chemie-International Edition, 2005, **44**(22): pp. 3358-3393.
74. Czaja, W., Krystynowicz, A., Bielecki, S. and Brown, R.M., *Microbial cellulose - the natural power to heal wounds*. Biomaterials, 2006, **27**(2): pp. 145-151.
75. Iguchi, M., Yamanaka, S. and Budhiono, A., *Bacterial cellulose - a masterpiece of nature's arts*. Journal of Materials Science, 2000, **35**(2): pp. 261-270.
76. Vroman, I. and Tighzert, L., *Biodegradable polymers*. Materials, 2009, **2**(2): pp. 307-344.
77. Jantas, R. and Gorna, K., *Antibacterial finishing of cotton fabrics*. Fibres and Textiles in Eastern Europe, 2003, **14**(1): pp. 88-91.
78. Sanchez-Vazquez, S.A., Hailes, H.C. and Evans, J.R.G., *Hydrophobic polymers from food waste: Resources and synthesis*. Polymer Reviews, 2013, **53**(4): pp. 627-694.
79. Park, B.K. and Kim, M.M., *Applications of chitin and its derivatives in biological medicine*. International Journal of Molecular Sciences, 2010, **11**(12): pp. 5153-5165.
80. Jayakumar, R., Menon, D., Manzoor, K., Nair, S.V. and Tamura, H., *Biomedical applications of chitin and chitosan based nanomaterials—A short review*. Carbohydrate Polymers, 2010, **82**(2): pp. 227-232.
81. Yeul, V.S. and Rayalu, S.S., *Unprecedented chitin and chitosan: A chemical overview*. Journal of Polymers and the Environment, 2013, **21**(2): pp. 606-614.
82. Vaca-Garcia, C., *Biomaterials*. In: Clark, J. and Deswarte, F.(eds) Introduction to chemicals from biomass, 2008, Wiley, UK, pp 103-142.
83. Shukla, S.K., Mishra, A.K., Arotiba, O.A. and Mamba, B.B., *Chitosan-based nanomaterials: A state-of-the-art review*. International Journal of Biological Macromolecules, 2013, **59**(0): pp. 46-58.
84. Suh, J.K.F. and Matthew, H.W.T., *Application of chitosan-based polysaccharide biomaterials in cartilage tissue engineering: A review*. Biomaterials, 2000, **21**(24): pp. 2589-2598.
85. Zohuriaan-Mehr, M.J., *Advances in chitin and chitosan modification through graft copolymerization: A comprehensive review*. Iranian Polymer Journal, 2005, **14**(3): pp. 235-265.

86. Jayakumar, R., Selvamurugan, N., Nair, S.V., Tokura, S. and Tamura, H., *Preparative methods of phosphorylated chitin and chitosan - An overview*. International Journal of Biological Macromolecules, 2008, **43**(3): pp. 221-225.
87. Kurita, K., *Chitin and chitosan: Functional biopolymers from marine crustaceans*. Marine Biotechnology, 2006, **8**(3): pp. 203-226.
88. Hirano, S., *Chitin and chitosan as novel biotechnological materials*. Polymer International, 1999, **48**(8): pp. 732-734.
89. Sashiwa, H. and Aiba, S.I., *Chemically modified chitin and chitosan as biomaterials*. Progress in Polymer Science, 2004, **29**(9): pp. 887-908.
90. Prashanth, K.V.H. and Tharanathan, R.N., *Chitin/chitosan: Modifications and their unlimited application potential - An overview*. Trends in Food Science & Technology, 2007, **18**(3): pp. 117-131.
91. Ren, D.W., Yi, H.F., Wang, W. and Ma, X.J., *The enzymatic degradation and swelling properties of chitosan matrices with different degrees of n-acetylation*. Carbohydrate Research, 2005, **340**(15): pp. 2403-2410.
92. Kumar, M., *A review of chitin and chitosan applications*. Reactive & Functional Polymers, 2000, **46**(1): pp. 1-27.
93. Boerjan, W., Ralph, J. and Baucher, M., *Lignin biosynthesis*. Annual Review of Plant Biology, 2003, **54**: pp. 519-546.
94. Khoushab, F. and Yamabhai, M., *Chitin research revisited*. Marine Drugs, 2010, **8**(7): pp. 1988-2012.
95. Pillai, C.K.S., Paul, W. and Sharma, C.P., *Chitin and chitosan polymers: Chemistry, solubility and fiber formation*. Progress in Polymer Science, 2009, **34**(7): pp. 641-678.
96. Souza, V.C., Monte, M.L. and Pinto, L.A.A., *Preparation of biopolymer film from chitosan modified with lipid fraction*. International Journal of Food Science and Technology, 2011, **46**(9): pp. 1856-1862.
97. Teramoto, N., Motoyama, T., Yosomiya, R. and Shibata, M., *Synthesis, thermal properties, and biodegradability of propyl-etherified starch*. European Polymer Journal, 2003, **39**(2): pp. 255-261.
98. Wang, N., Zhang, X.X., Han, N. and Liu, H.H., *A facile method for preparation of thermoplastic starch/urea modified montmorillonite nanocomposites*. Journal of Composite Materials, 2010, **44**(1): pp. 27-39.
99. Averous, L. and Halley, P.J., *Biocomposites based on plasticized starch*. Biofuels Bioproducts & Biorefining-Biofpr, 2009, **3**(3): pp. 329-343.
100. Averous, L., *Biodegradable multiphase systems based on plasticized starch: A review*. Journal of Macromolecular Science-Polymer Reviews, 2004, **44**(3): pp. 231-274.
101. Flaris, V. and Singh, G., *Recent developments in biopolymers*. Journal of Vinyl and Additive Technology, 2009, **15**(1): pp. 1-11.
102. Park, J.S., Yang, J.H., Kim, D.H. and Lee, D.H., *Degradability of expanded starch/pva blends prepared using calcium carbonate as the expanding inhibitor*. Journal of Applied Polymer Science, 2004, **93**(2): pp. 911-919.
103. Schwach, E. and Averous, L., *Starch-based biodegradable blends: Morphology and interface properties*. Polymer International, 2004, **53**(12): pp. 2115-2124.
104. Le Corre, D., Bras, J. and Dufresne, A., *Starch nanoparticles: A review*. Biomacromolecules, 2010, **11**(5): pp. 1139-1153.

105. Araujo, M.A., Cunha, A.M. and Mota, M., *Enzymatic degradation of starch-based thermoplastic compounds used in prostheses: Identification of the degradation products in solution*. *Biomaterials*, 2004, **25**(13): pp. 2687-2693.
106. Zhang, J.F. and Sun, X.Z., *Mechanical properties of poly(lactic acid)/starch composites compatibilized by maleic anhydride*. *Biomacromolecules*, 2004, **5**(4): pp. 1446-1451.
107. Buleon, A., Colonna, P., Planchot, V. and Ball, S., *Starch granules: Structure and biosynthesis*. *International Journal of Biological Macromolecules*, 1998, **23**(2): pp. 85-112.
108. Angellier, H., Choisnard, L., Molina-Boisseau, S., Ozil, P. and Dufresne, A., *Optimization of the preparation of aqueous suspensions of waxy maize starch nanocrystals using a response surface methodology*. *Biomacromolecules*, 2004, **5**(4): pp. 1545-1551.
109. Tomasik, P. and Schilling, C.H., *Chemical modification of starch*. *Advances in Carbohydrate Chemistry and Biochemistry*, Vol 59, 2004, **59**: pp. 175-403.
110. Lu, D.R., Xiao, C.M. and Xu, S.J., *Starch-based completely biodegradable polymer materials*. *Express Polymer Letters*, 2009, **3**(6): pp. 366-375.
111. Kang, S., Li, X., Fan, J. and Chang, J., *Hydrothermal conversion of lignin: A review*. *Renewable and Sustainable Energy Reviews*, 2013, **27**(0): pp. 546-558.
112. Jorgensen, H., Kristensen, J.B. and Felby, C., *Enzymatic conversion of lignocellulose into fermentable sugars: Challenges and opportunities*. *Biofuels Bioproducts & Biorefining-Biofpr*, 2007, **1**(2): pp. 119-134.
113. Rouilly, A. and Rigal, L., *Agro-materials: A bibliographic review*. *Journal of Macromolecular Science-Polymer Reviews*, 2002, **C42**(4): pp. 441-479.
114. Brown, M.E. and Chang, M.C.Y., *Exploring bacterial lignin degradation*. *Current Opinion in Chemical Biology*, 2014, **19**(0): pp. 1-7.
115. Crestini, C., Melone, F. and Saladino, R., *Novel multienzyme oxidative biocatalyst for lignin bioprocessing*. *Bioorganic & Medicinal Chemistry*, 2011, **19**(16): pp. 5071-5078.
116. Zeng, Y., Zhao, S., Yang, S. and Ding, S.-Y., *Lignin plays a negative role in the biochemical process for producing lignocellulosic biofuels*. *Current Opinion in Biotechnology*, 2014, **27**(0): pp. 38-45.
117. Hofrichter, M., *Review: Lignin conversion by manganese peroxidase (MNP)*. *Enzyme and Microbial Technology*, 2002, **30**(4): pp. 454-466.
118. Ghaffar, S.H. and Fan, M., *Lignin in straw and its applications as an adhesive*. *International Journal of Adhesion and Adhesives*, 2014, **48**(0): pp. 92-101.
119. Verbeek, C.J.R. and Van Den Berg, L.E., *Extrusion processing and properties of protein-based thermoplastics*. *Macromolecular Materials and Engineering*, 2010, **295**(1): pp. 10-21.
120. Raquez, J.M., Deleglise, M., Lacrampe, M.F. and Krawczak, P., *Thermosetting biomaterials derived from renewable resources: A critical review*. *Progress in Polymer Science*, 2010, **35**(4): pp. 487-509.
121. Majid, J., Elmira, A.T., Muhammad, I., Muriel, J. and St'ephane, D., *Poly-lactic acid: Production, applications, nanocomposites, and release studies*. *Comprehensive Review on Food Science and Safety*, 2010, **9**(5): pp. 552-571.
122. Babu, R.P., O'connor, K. and Seeram, R., *Current progress on bio-based polymers and their future trends*. *Progress in Biomaterials*, 2013, **2**(8): pp. 1-16.

123. Sun, Z.M., Park, Y., Zheng, S.L., Ayoko, G.A. and Frost, R.L., *XRD, TEM, and thermal analysis of arizona Ca-montmorillonites modified with didodecyldimethylammonium bromide*. Journal of Colloid and Interface Science, 2013, **408**: pp. 75-81.
124. Erwin, T.H., David, A.G., Jeffrey, J.K., Robert, J.W. and Ryan, P.O., *The eco-profiles for current and near-future natureworks polylactide (PLA) production*. Industrial Biotechnology, 2007, **3**: pp. 58-81.
125. Drumright, R.E., Gruber, P.R. and Henton, D.E., *Polylactic acid technology*. Advanced Materials, 2000, **12**(23): pp. 1841-1846.
126. Garlotta, D., *A literature review of poly(lactic acid)*. Journal of Polymers and the Environment, 2001, **9**(2): pp. 63-84.
127. Prieto, M.A., *From oil to bioplastics, a dream come true?* Journal of Bacteriology, 2007, **189**(2): pp. 289-290.
128. Hassan, M.A., Yee, L.-N., Yee, P.L., Ariffin, H., Raha, A.R., Shirai, Y. and Sudesh, K., *Sustainable production of polyhydroxyalkanoates from renewable oil-palm biomass*. Biomass and Bioenergy, 2013, **50**(0): pp. 1-9.
129. Lee, G.N. and Na, J., *Future of microbial polyesters*. Microbial Cell Factories, 2013, **12**: pp. 4.
130. Ko-Sin, N., Wong, Y.M., Tsuge, T. and Sudesh, K., *Biosynthesis and characterization of poly(3-hydroxybutyrate-co-3-hydroxyvalerate) and poly(3-hydroxybutyrate-co-3-hydroxyhexanoate) copolymers using jatropha oil as the main carbon source*. Process Biochemistry, 2011, **46**(8): pp. 1572-1578.
131. Ni, Y.Y., Kim, D.Y., Chung, M.G., Lee, S.H., Park, H.Y. and Rhee, Y.H., *Biosynthesis of medium-chain-length poly(3-hydroxyalkanoates) by volatile aromatic hydrocarbons-degrading pseudomonas fulva TY16*. Bioresource Technology, 2010, **101**(21): pp. 8485-8488.
132. Hofer, P., Vermette, P. and Groleau, D., *Production and characterization of polyhydroxyalkanoates by recombinant methylobacterium extorquens: Combining desirable thermal properties with functionality*. Biochemical Engineering Journal, 2011, **54**(1): pp. 26-33.
133. Abu-Elreesh, G., Zaki, S., Farag, S., Elkady, M.F. and Abd-El-Haleem, D., *Exobiopolymer from polyhydroxyalkanoate-producing transgenic yeast*. African Journal of Biotechnology, 2011, **10**(34): pp. 6558-6563.
134. Bohmert-Tatarev, K., Mcavoy, S., Daughtry, S., Peoples, O.P. and Snell, K.D., *High levels of bioplastic are produced in fertile transplastomic tobacco plants engineered with a synthetic operon for the production of polyhydroxybutyrate*. Plant Physiology, 2011, **155**(4): pp. 1690-1708.
135. Tilbrook, K., Gebbie, L., Schenk, P.M., Poirier, Y. and Brumbley, S.M., *Peroxisomal polyhydroxyalkanoate biosynthesis is a promising strategy for bioplastic production in high biomass crops*. Plant Biotechnology Journal, 2011, **9**(9): pp. 958-969.
136. Van Beilen, J.B. and Poirier, Y., *Production of renewable polymers from crop plants*. Plant Journal, 2008, **54**(4): pp. 684-701.
137. Gumel, A.M., Annuar, M.S.M. and Chisti, Y., *Recent advances in the production, recovery and applications of polyhydroxyalkanoates*. Journal of Polymers and the Environment, 2013, **21**(2): pp. 580-605.
138. Lee, S.Y., *Bacterial polyhydroxyalkanoates*. Biotechnology and Bioengineering, 1996, **49**(1): pp. 1-14.

139. Koller, M., Salerno, A., Dias, M., Reiterer, A. and Braunegg, G., *Modern biotechnological polymer synthesis: A review*. Food Technology and Biotechnology, 2010, **48**(3): pp. 255-269.
140. Ariffin, N., Abdullah, R., Muad, M.R., Lourdes, J., Emran, N.A., Ismail, M.R., Ismail, I., Fadzil, M.F.M., Ling, K.L., Siddiqui, Y., Amir, A.A., Berahim, Z. and Omar, M.H., *Constructions of expression vectors of polyhydroxybutyrate-co-hydroxyvalerate (phbv) and transient expression of transgenes in immature oil palm embryos*. Plasmid, 2011, **66**(3): pp. 136-143.
141. Barham, P.J. and Keller, A., *The relationship between microstructure and mode of fracture in polyhydroxybutyrate*. Journal of Polymer Science Part B-Polymer Physics, 1986, **24**(1): pp. 69-77.
142. Noda, I., Green, P.R., Satkowski, M.M. and Schechtman, L.A., *Preparation and properties of a novel class of polyhydroxyalkanoate copolymers*. Biomacromolecules, 2005, **6**(2): pp. 580-586.
143. Akaraonye, E., Keshavarz, T. and Roy, I., *Production of polyhydroxyalkanoates: The future green materials of choice*. Journal of Chemical Technology and Biotechnology, 2010, **85**(6): pp. 732-743.
144. Philip, S., Keshavarz, T. and Roy, I., *Polyhydroxyalkanoates: Biodegradable polymers with a range of applications*. Journal of Chemical Technology and Biotechnology, 2007, **82**(3): pp. 233-247.
145. Tokiwa, Y. and Calabia, B.P., *Degradation of microbial polyesters*. Biotechnology Letters, 2004, **26**(15): pp. 1181-1189.
146. Meier, M.a.R., Metzger, J.O. and Schubert, U.S., *Plant oil renewable resources as green alternatives in polymer science*. Chemical Society Reviews, 2007, **36**(11): pp. 1788-1802.
147. Metzger, J.O., *Fats and oils as renewable feedstock for chemistry*. European Journal of Lipid Science and Technology, 2009, **111**(9): pp. 865-876.
148. Guner, F.S., Yagci, Y. and Erciyes, A.T., *Polymers from triglyceride oils*. Progress in Polymer Science, 2006, **31**(7): pp. 633-670.
149. Sharma, V. and Kundu, P.P., *Condensation polymers from natural oils*. Progress in Polymer Science, 2008, **33**(12): pp. 1199-1215.
150. Sharma, V. and Kundu, P.P., *Addition polymers from natural oils - a review*. Progress in Polymer Science, 2006, **31**(11): pp. 983-1008.
151. Montero De Espinosa, L. and Meier, M.a.R., *Plant oils: The perfect renewable resource for polymer science?!* European Polymer Journal, 2011, **47**(5): pp. 837-852.
152. Burrell, M.M., *Starch: The need for improved quality or quantity - an overview*. Journal of Experimental Botany, 2003, **54**(382): pp. 451-456.
153. Cock, J.H., *Cassava - a basic energy-source in the tropics*. Science, 1982, **218**(4574): pp. 755-762.
154. Campbell, D.J., *An atlas of cassava in africa: Historical, agroecological and demographic aspects of crop distribution: S. E. Carter, I. O. Fresco and P. G. Jones, with J. N. Fairbairn. Centro internacional de agricultura tropical, CIAT publication no. 206, Cali, Colombia, June 1992. 86 pp* Agricultural Systems, 1994, **46**(2): pp. 239-242.
155. Defloor, I., Dehing, I. and Delcour, J.A., *Physico-chemical properties of cassava starch*. Starch-Starke, 1998, **50**(2-3): pp. 58-64.
156. Tonukari, N.J., *Cassava and the future of starch*. Electronic Journal of Biotechnology, 2004, **7**(1): pp. 5-8.

157. Taiwo, K.A., Oladepo, O.W., Ilori, M.O. and Akanbi, C.T., *A study on the nigerian food industry and the impact of technological changes on the small-scale food enterprises*. Food Reviews International, 2002, **18**(4): pp. 243-261.
158. Lewkowski, J., *Convenient synthesis of furan-2,5-dicarboxylic acid and its derivatives*. Polish Journal of Chemistry, 2001, **75**(12): pp. 1943-1946.
159. Tadesse, H. and Luque, R., *Advances on biomass pretreatment using ionic liquids: An overview*. Energy and Environmental Science, 2011, **4**(10): pp. 3913-3929.
160. Roman-Leshkov, Y., Chheda, J.N. and Dumesic, J.A., *Phase modifiers promote efficient production of hydroxymethylfurfural from fructose*. Science, 2006, **312**(5782): pp. 1933-1937.
161. Rosatella, A.A., Simeonov, S.P., Frade, R.F.M. and Afonso, C.a.M., *5-hydroxymethylfurfural (HMF) as a building block platform: Biological properties, synthesis and synthetic applications*. Green Chemistry, 2011, **13**: pp. 754-793.
162. Tong, X.L., Ma, Y. and Li, Y.D., *Biomass into chemicals: Conversion of sugars to furan derivatives by catalytic processes*. Applied Catalysis A-General, 2010, **385**(1-2): pp. 1-13.
163. Antal, M.J., Leesomboon, T., Mok, W.S. and Richards, G.N., *Mechanism of formation of 2-furaldehyde from D-xylose*. Carbohydrate Research, 1991, **217**(0): pp. 71-85.
164. Chheda, J.N., Roman-Leshkov, Y. and Dumesic, J.A., *Production of 5-hydroxymethylfurfural and furfural by dehydration of biomass-derived mono- and poly-saccharides*. Green Chemistry, 2007, **9**(4): pp. 342-350.
165. Montane', D., Salvado', J., Torras, C. and Farriol, X., *High-temperature dilute-acid hydrolysis of olive stones for furfural production*. Biomass and Bioenergy, 2002, **22**(4): pp. 295-304.
166. Yemis, O. and Mazza, G., *Acid-catalyzed conversion of xylose, xylan and straw into furfural by microwave-assisted reaction*. Bioresource Technology, 2011, **102**(15): pp. 7371-7378.
167. Yemis, O. and Mazza, G., *Optimization of furfural and 5-hydroxymethylfurfural production from wheat straw by a microwave-assisted process*. Bioresource Technology, 2012, **109**(0): pp. 215-223.
168. Taarning, E., Osmundsen, C.M., Yang, X., Voss, B., Andersen, S.I. and Christensen, C.H., *Zeolite-catalyzed biomass conversion to fuels and chemicals*. Energy & Environmental Science, 2011, **4**(3): pp. 793-804.
169. Serrano-Ruiz, J.C., Luque, R. and Sepulveda-Escribano, A., *Transformations of biomass-derived platform molecules: From high added-value chemicals to fuels via aqueous-phase processing*. Chemical Society Reviews, 2011, **40**(11): pp. 5266-5281.
170. Lam, E., Chong, J.H., Majid, E., Liu, Y., Hrapovic, S., Leung, A.C.W. and Luong, J.H.T., *Carbocatalytic dehydration of xylose to furfural in water*. Carbon, 2012, **50**(3): pp. 1033-1043.
171. Mamman, A.S., Lee, J.-M., Kim, Y.-C., Hwang, I.T., Park, N.-J., Hwang, Y.K., Chang, J.-S. and Hwang, J.-S., *Furfural: Hemicellulose/xylo-derived biochemical*. Biofuels, Bioproducts and Biorefining, 2008, **2**(5): pp. 438-454.
172. Dhepe, P.L. and Sahu, R., *A solid-acid-based process for the conversion of hemicellulose*. Green Chemistry, 2010, **12**(12): pp. 2153-2156.

173. Asghari, F.S. and Yoshida, H., *Acid-catalyzed production of 5-hydroxymethyl furfural from D-fructose in subcritical water*. Industrial & Engineering Chemistry Research, 2006, **45**(7): pp. 2163-2173.
174. Choudhary, V., Pinar, A.B., Sandler, S.I., Vlachos, D.G. and Lobo, R.F., *Xylose isomerization to xylulose and its dehydration to furfural in aqueous media*. ACS Catalysis, 2011, **1**(12): pp. 1724-1728.
175. Jeong, G.H., Kim, E.G., Kim, S.B., Park, E.D. and Kim, S.W., *Fabrication of sulfonic acid modified mesoporous silica shells and their catalytic performance with dehydration reaction of D-xylose into furfural*. Microporous and Mesoporous Materials, 2011, **144**(1-3): pp. 134-139.
176. Amarasekara, A.S., Williams, L.D. and Ebede, C.C., *Mechanism of the dehydration of D-fructose to 5-hydroxymethylfurfural in dimethyl sulfoxide at 150 °C: An NMR study*. Carbohydrate Research, 2008, **343**(18): pp. 3021-3024.
177. Takagaki, A., Ohara, M., Nishimura, S. and Ebitani, K., *One-pot formation of furfural from xylose via isomerization and successive dehydration reactions over heterogeneous acid and base catalysts*. Chemistry Letters, 2010, **39**(8): pp. 838-840.
178. Lam, E., Majid, E., Leung, A.C.W., Chong, J.H., Mahmoud, K.A. and Luong, J.H.T., *Synthesis of furfural from xylose by heterogeneous and reusable nafion catalysts*. Chemsuschem, 2011, **4**(4): pp. 535-541.
179. Moreau, C., Durand, R., Peyron, D., Duhamet, J. and Rivalier, P., *Selective preparation of furfural from xylose over microporous solid acid catalysts*. Industrial Crops and Products, 1998, **7**(2-3): pp. 95-99.
180. Agirrezabal-Telleria, I., Larreategui, A., Requies, J., Gãemez, M.B. and Arias, P.L., *Furfural production from xylose using sulfonic ion-exchange resins (amberlyst) and simultaneous stripping with nitrogen*. Bioresource Technology, 2011, **102**(16): pp. 7478-7485.
181. Antunes, M.M., Lima, S.R., Fernandes, A., Pillinger, M., Ribeiro, M.F. and Valente, A.A., *Aqueous-phase dehydration of xylose to furfural in the presence of MCM-22 and ITQ-2 solid acid catalysts*. Applied Catalysis A: General, 2012, **417-418**(0): pp. 243-252.
182. Schmidt, L.D. and Dauenhauer, P.J., *Chemical engineering - hybrid routes to biofuels*. Nature, 2007, **447**(7147): pp. 914-915.
183. Kamm, B., *Production of platform chemicals and synthesis gas from biomass*. Angewandte Chemie-International Edition, 2007, **46**(27): pp. 5056-5058.
184. Mascal, M. and Nikitin, E.B., *High-yield conversion of plant biomass into the key value-added feedstocks 5-(hydroxymethyl)furfural, levulinic acid, and levulinic esters via 5-(chloromethyl)furfural*. Green Chemistry, 2010, **12**(3): pp. 370-373.
185. Gorbanev, Y.Y., Klitgaard, S.K., Woodley, J.M., Christensen, C.H. and Riisager, A., *Gold-catalyzed aerobic oxidation of 5-hydroxymethylfurfural in water at ambient temperature*. Chemsuschem, 2009, **2**(7): pp. 672-675.
186. Ilgen, F., Ott, D., Kralisch, D., Reil, C., Palmberger, A. and König, B., *Conversion of carbohydrates into 5-hydroxymethylfurfural in highly concentrated low melting mixtures*. Green Chemistry, 2009, **11**(12): pp. 1948-1954.
187. Narayan, R., *Polymeric materials from agricultural feedstocks*. In: Fishman, M.L., Friedman, R.B., and Huang, J.S.(eds) Polymers from agricultural

- coproducts, 1994, American Chemical Society Symposium Series 579, Washington DC, pp 44-52.
188. Climent, M.J., Corma, A. and Iborra, S., *Heterogeneous catalysts for the one-pot synthesis of chemicals and fine chemicals*. Chemical Reviews, 2011, **111**(2): pp. 1072-1133.
189. Antal, M.J., Mok, W.S.L. and Richards, G.N., *Kinetic-studies of the reactions of ketoses and aldoses in water at high-temperature .1. Mechanism of formation of 5-(hydroxymethyl)-2-furaldehyde from D-fructose and sucrose*. Carbohydrate Research, 1990, **199**(1): pp. 91-109.
190. James, O.O., Maity, S., Usman, L.A., Ajanaku, K.O., Ajani, O.O., Siyanbola, T.O., Sahu, S. and Chaubey, R., *Towards the conversion of carbohydrate biomass feedstocks to biofuels via hydroxymethylfurfural*. Energy & Environmental Science, 2010, **3**(12): pp. 1833-1850.
191. Kuster, B.F.M. and Vanderbaan, H.S., *Dehydration of d-fructose (formation of 5-hydroxymethyl-2-furaldehyde and levulinic acid) .2. Influence of initial and catalyst concentrations on dehydration of D-fructose*. Carbohydrate Research, 1977, **54**(2): pp. 165-176.
192. Carniti, P., Gervasini, A. and Marzo, M., *Absence of expected side-reactions in the dehydration reaction of fructose to HMF in water over niobic acid catalyst*. Catalysis Communications, 2011, **12**(12): pp. 1122-1126.
193. Busca, G., *Acid catalysts in industrial hydrocarbon chemistry*. Chemical Reviews, 2007, **107**(11): pp. 5366-5410.
194. Okuhara, T., *Water-tolerant solid acid catalysts*. Chemical Reviews, 2002, **102**(10): pp. 3641-3665.
195. Yang, F.L., Liu, Q.S., Bai, X.F. and Du, Y.G., *Conversion of biomass into 5-hydroxymethylfurfural using solid acid catalyst*. Bioresource Technology, 2011, **102**(3): pp. 3424-3429.
196. Moreau, C., Durand, R., Razigade, S., Duhamet, J., Faugeras, P., Rivalier, P., Ros, P. and Avignon, G., *Dehydration of fructose to 5-hydroxymethylfurfural over H-mordenites*. Applied Catalysis A-General, 1996, **145**(1-2): pp. 211-224.
197. Carlini, C., Patrono, P., Galletti, A.M.R. and Sbrana, G., *Heterogeneous catalysts based on vanadyl phosphate for fructose dehydration to 5-hydroxymethyl-2-furaldehyde*. Applied Catalysis A-General, 2004, **275**(1-2): pp. 111-118.
198. Takagaki, A., Ohara, M., Nishimura, S. and Ebitani, K., *A one-pot reaction for biorefinery: Combination of solid acid and base catalysts for direct production of 5-hydroxymethylfurfural from saccharides*. Chemical Communications, 2009(41): pp. 6276-6278.
199. Benvenuti, F., Carlini, C., Patrono, P., Galletti, A.M.R., Sbrana, G., Massucci, M.A. and Galli, P., *Heterogeneous zirconium and titanium catalysts for the selective synthesis of 5-hydroxymethyl-2-furaldehyde from carbohydrates*. Applied Catalysis A-General, 2000, **193**(1-2): pp. 147-153.
200. Nakamura, Y. and Morikawa, S., *The dehydration of D-fructose to 5-hydroxymethyl-2-furaldehyde*. Bulletin of the Chemical Society of Japan, 1980, **53**(12): pp. 3705-3706.
201. Rigal, L. and Gaset, A., *Optimization of the conversion of D-fructose to 5-hydroxymethyl-2-furancarboxaldehyde in a water-solvent-ion exchanger triphasic system .2. Search for a local optimum of selectivity by the simplex-method*. Biomass, 1985, **8**(4): pp. 267-276.

202. Mercadier, D., Rigal, L., Gaset, A. and Gorrichon, J.P., *Synthesis of 5-hydroxymethyl-2-furancarboxaldehyde catalyzed by cationic exchange resins .2. Analysis and discussion of the effect of the main parameters on the HMF output*. Journal of Chemical Technology and Biotechnology, 1981, **31**(8): pp. 497-502.
203. Lansalot-Matras, C. and Moreau, C., *Dehydration of fructose into 5-hydroxymethylfurfural in the presence of ionic liquids*. Catalysis Communications, 2003, **4**(10): pp. 517-520.
204. Yadav, G.D. and Nair, J.J., *Sulfated zirconia and its modified versions as promising catalysts for industrial processes*. Microporous and Mesoporous Materials, 1999, **33**(1-3): pp. 1-48.
205. Arata, K. and Hino, M., *Reaction of butane to isobutane catalyzed by the solid superacid of hfo<sub>2</sub> treated with sulfate ion*. Reaction Kinetics and Catalysis Letters, 1984, **25**(1-2): pp. 143-145.
206. Corma, A., *Inorganic solid acids and their use in acid-catalyzed hydrocarbon reactions*. Chemical Reviews, 1995, **95**(3): pp. 559-614.
207. Hino, M., Kobayashi, S. and Arata, K., *Solid catalyst treated with anion .2. Reactions of butane and isobutane catalyzed by zirconium-oxide treated with sulfate ion - solid superacid catalyst*. Journal of the American Chemical Society, 1979, **101**(21): pp. 6439-6441.
208. Yamaguchi, T., Jin, T., Ishida, T. and Tanabe, K., *Structural identification of acid sites of sulfur-promoted solid super acid and construction of its structure on silica support*. Materials Chemistry and Physics, 1987, **17**(1-2): pp. 3-19.
209. Ward, D.A. and Ko, E.I., *One-step synthesis and characterization of zirconia-sulfate aerogels as solid superacids*. Journal of Catalysis, 1994, **150**(1): pp. 18-33.
210. Bensitel, M., Saur, O., Lavalley, J.C. and Mabilon, G., *Acidity of zirconium-oxide and sulfated ZrO<sub>2</sub> samples*. Materials Chemistry and Physics, 1987, **17**(3): pp. 249-258.
211. Watanabe, M., Aizawa, Y., Iida, T., Nishimura, R. and Inomata, H., *Catalytic glucose and fructose conversions with TiO<sub>2</sub> and ZrO<sub>2</sub> in water at 473 K: Relationship between reactivity and acid-base property determined by TPD measurement*. Applied Catalysis A-General, 2005, **295**(2): pp. 150-156.
212. Qi, X.H., Watanabe, M., Aida, T.M. and Smith, R.L., *Catalytical conversion of fructose and glucose into 5-hydroxymethylfurfural in hot compressed water by microwave heating*. Catalysis Communications, 2008, **9**(13): pp. 2244-2249.
213. Qi, X.H., Watanabe, M., Aida, T.M. and Smith, R.L., *Sulfated zirconia as a solid acid catalyst for the dehydration of fructose to 5-hydroxymethylfurfural*. Catalysis Communications, 2009, **10**(13): pp. 1771-1775.
214. Seri, K., Inoue, Y. and Ishida, H., *Catalytic activity of lanthanide(iii) ions for the dehydration of hexose to 5-hydroxymethyl-2-furaldehyde in water*. Bulletin of the Chemical Society of Japan, 2001, **74**(6): pp. 1145-1150.
215. Ishida, H. and Seri, K., *Catalytic activity of lanthanoide(iii) ions for dehydration of D-glucose to 5-(hydroxymethyl)furfural*. Journal of Molecular Catalysis A-Chemical, 1996, **112**(2): pp. L163-L165.
216. Zhao, H.B., Holladay, J.E., Brown, H. and Zhang, Z.C., *Metal chlorides in ionic liquid solvents convert sugars to 5-hydroxymethylfurfural*. Science, 2007, **316**(5831): pp. 1597-1600.

217. Hsu, W.H., Lee, Y.Y., Peng, W.H. and Wu, K.C.W., *Cellulosic conversion in ionic liquids (ils): Effects of H<sub>2</sub>O/cellulose molar ratios, temperatures, times, and different ils on the production of monosaccharides and 5-hydroxymethylfurfural (HMF)*. *Catalysis Today*, 2011, **174**(1): pp. 65-69.
218. Yu, S., Brown, H.M., Huang, X.W., Zhou, X.D., Amonette, J.E. and Zhang, Z.C., *Single-step conversion of cellulose to 5-hydroxymethylfurfural (HMF), A versatile platform chemical*. *Applied Catalysis A-General*, 2009, **361**(1-2): pp. 117-122.
219. Zhang, Y.T., Du, H.B., Qian, X.H. and Chen, E.Y.X., *Ionic liquid-water mixtures: Enhanced  $k_w$  for efficient cellulosic biomass conversion*. *Energy & Fuels*, 2010, **24**: pp. 2410-2417.
220. Sheldon, R., *Catalytic reactions in ionic liquids*. *Chemical Communications*, 2001(23): pp. 2399-2407.
221. Yang, X., Fei, Z.F., Geldbach, T.J., Phillips, A.D., Hartinger, C.G., Li, Y.D. and Dyson, P.J., *Suzuki coupling reactions in ether-functionalized ionic liquids: The importance of weakly interacting cations*. *Organometallics*, 2008, **27**(15): pp. 3971-3977.
222. Moreau, C., Finiels, A. and Vanoye, L., *Dehydration of fructose and sucrose into 5-hydroxymethylfurfural in the presence of 1-H-3-methyl imidazolium chloride acting both as solvent and catalyst*. *Journal of Molecular Catalysis A-Chemical*, 2006, **253**(1-2): pp. 165-169.
223. Tong, X.L., Ma, Y. and Li, Y.D., *An efficient catalytic dehydration of fructose and sucrose to 5-hydroxymethylfurfural with protic ionic liquids*. *Carbohydrate Research*, 2010, **345**(12): pp. 1698-1701.
224. Hu, S.Q., Zhang, Z.F., Song, J.L., Zhou, Y.X. and Han, B.X., *Efficient conversion of glucose into 5-hydroxymethylfurfural catalyzed by a common lewis acid SnCl<sub>4</sub> in an ionic liquid*. *Green Chemistry*, 2009, **11**(11): pp. 1746-1749.
225. Musau, R.M. and Munavu, R.M., *The preparation of 5-hydroxymethyl-2-furaldehyde (HMF) from D-fructose in the presence of DMSO*. *Biomass*, 1987, **13**(1): pp. 67-74.
226. James, O.O., Maity, S., Usman, L.A., Ajanaku, K.O., Ajani, O.O., Siyambola, T.O., Sahu, S. and Chaubey, R., *Towards the conversion of carbohydrate biomass feedstocks to biofuels via hydroxymethylfurfural*. *Energy & Environmental Science*, 2010, **3**(12): pp. 1833-1850.
227. Ma, H., Zhou, B., Li, Y. and Argyropoulos, *Conversion of fructose to 5-hydroxymethyl-furfural with a functionalized ionic liquid*. *BioResources*, 2012, **7**(1): pp. 533-544.
228. Stahlberg, T., Fu, W.J., Woodley, J.M. and Riisager, A., *Synthesis of 5-(hydroxymethyl)furfural in ionic liquids: Paving the way to renewable chemicals*. *Chemsuschem*, 2011, **4**(4): pp. 451-458.
229. Hu, L., Sun, Y. and Lin, L., *Efficient conversion of glucose into 5-hydroxymethylfurfural by chromium(iii) chloride in inexpensive ionic liquid*. *Industrial & Engineering Chemistry Research*, 2012, **51**(3): pp. 1099-1104.
230. Qi, X., Guo, H. and Li, L., *Efficient conversion of fructose to 5-hydroxymethylfurfural catalyzed by sulfated zirconia in ionic liquids*. *Industrial & Engineering Chemistry Research*, 2011, **50**(13): pp. 7985-7989.
231. Qi, X., Watanabe, M., Aida, T.M. and Smith, J.R.L., *Efficient process for conversion of fructose to 5-hydroxymethylfurfural with ionic liquids*. *Green Chemistry*, 2009, **11**(9).

232. Cao, Q., Guo, X.C., Yao, S.X., Guan, J., Wang, X.Y., Mu, X.D. and Zhang, D.K., *Conversion of hexose into 5-hydroxymethylfurfural in imidazolium ionic liquids with and without a catalyst*. Carbohydrate Research, 2011, **346**(7): pp. 956-959.
233. Gandini, A. and Belgacem, M.N., *Furans in polymer chemistry*. Progress in Polymer Science, 1997, **22**(6): pp. 1203-1379.
234. Laita, H., Boufi, S. and Gandini, A., *The application of the diels-alder reaction to polymers bearing furan moieties .1. Reactions with maleimides*. European Polymer Journal, 1997, **33**(8): pp. 1203-1211.
235. Gousse, C., Gandini, A. and Hodge, P., *Application of the Diels-Alder reaction to polymers bearing furan moieties. 2. Diels-Alder and retro-Diels-Alder reactions involving furan rings in some styrene copolymers*. Macromolecules, 1998, **31**(2): pp. 314-321.
236. Moreau, C., Belgacem, M.N. and Gandini, A., *Recent catalytic advances in the chemistry of substituted furans from carbohydrates and in the ensuing polymers*. Topics in Catalysis, 2004, **27**(1-4): pp. 11-30.
237. Gandini, A., Silvestre, A.J.D., Neto, C.P., Sousa, A.F. and Gomes, M., *The furan counterpart of poly(ethylene terephthalate): An alternative material based on renewable resources*. Journal of Polymer Science Part A-Polymer Chemistry, 2009, **47**(1): pp. 295-298.
238. Gandini, A., *Furans as offspring of sugars and polysaccharides and progenitors of a family of remarkable polymers: A review of recent progress*. Polymer Chemistry, 2010, **1**: pp. 245-251.
239. Davis, S.E., Houk, L.R., Tamargo, E.C., Datye, A.K. and Davis, R.J., *Oxidation of 5-hydroxymethylfurfural over supported Pt, Pd and Au catalysts*. Catalysis Today, 2011, **160**(1): pp. 55-60.
240. Bokanga, M., *Biotechnology and cassava processing in africa*. IITA Research, 1996, **12**: pp. 14-18.
241. Holladay, J.E., Werpy, T.A. and Muzatko, D.S., *Catalytic hydrogenation of glutamic acid*. Applied Biochemistry and Biotechnology, 2004, **113**: pp. 857-869.
242. Verdeguer, P., Merat, N. and Gaset, A., *Catalytic-oxidation of HMF to 2,5-furandicarboxylic acid*. Journal of Molecular Catalysis, 1993, **85**(3): pp. 327-344.
243. Vinke, P., Vanderpoel, W. and Vanbekkum, H., *On the oxygen tolerance of noble-metal catalysts in liquid-phase alcohol oxidations - the influence of the support on catalyst deactivation*. In: *Heterogeneous catalysis and fine chemicals ii*. pp. 385-394.
244. Casanova, O., Iborra, S. and Corma, A., *Biomass into chemicals: Aerobic oxidation of 5-hydroxymethyl-2-furfural into 2,5-furandicarboxylic acid with gold nanoparticle catalysts*. Chemsuschem, 2009, **2**(12): pp. 1138-1144.
245. Hopkins, K.T., Wilson, W.D., Bender, B.C., Mccurdy, D.R., Hall, J.E., Tidwell, R.R., Kumar, A., Bajic, M. and Boykin, D.W., *Extended aromatic furan amidino derivatives as anti-pneumocystis carinii agents*. Journal of Medicinal Chemistry, 1998, **41**(20): pp. 3872-3878.
246. Del Poeta, M., Schell, W.A., Dykstra, C.C., Jones, S., Tidwell, R.R., Czarny, A., Bajic, M., Kumar, A., Boykin, D. and Perfect, J.R., *Structure in vitro activity relationships of pentamidine analogues and dication-substituted bis-benzimidazoles as new antifungal agents*. Antimicrobial Agents and Chemotherapy, 1998, **42**(10): pp. 2495-2502.

247. Amarasekara, A.S., Green, D. and Williams, L.D., *Renewable resources based polymers: Synthesis and characterization of 2,5-diformylfuran-urea resin*. European Polymer Journal, 2009, **45**(2): pp. 595-598.
248. Gandini, A. and Belgacem, N.M., *Recent advances in the elaboration of polymeric materials derived from biomass components*. Polymer International, 1998, **47**(3): pp. 267-276.
249. Partenheimer, W. and Grushin, V.V., *Synthesis of 2,5-diformylfuran and furan-2,5-dicarboxylic acid by catalytic air-oxidation of 5-hydroxymethylfurfural. Unexpectedly selective aerobic oxidation of benzyl alcohol to benzaldehyde with metal/bromide catalysts*. Advanced Synthesis & Catalysis, 2001, **343**(1): pp. 102-111.
250. Moreau, C., Durand, R., Pourcheron, C. and Tichit, D., *Selective oxidation of 5-hydroxymethylfurfural to 2,5-furan-dicarboxaldehyde in the presence of titania supported vanadia catalysts*. Studies in Surface Science and Catalysis, 1997, **108**: pp. 399-406.
251. Carlini, C., Patrono, P., Galletti, A.M.R., Sbrana, G. and Zima, V., *Selective oxidation of 5-hydroxymethyl-2-furaldehyde to furan-2,5-dicarboxaldehyde by catalytic systems based on vanadyl phosphate*. Applied Catalysis A-General, 2005, **289**(2): pp. 197-204.
252. Navarro, O.C., Canos, A.C. and Chornet, S.I., *Chemicals from biomass: Aerobic oxidation of 5-hydroxymethyl-2-furaldehyde into diformylfuran catalyzed by immobilized vanadyl-pyridine complexes on polymeric and organofunctionalized mesoporous supports*. Topics in Catalysis, 2009, **52**(3): pp. 304-314.
253. Adeniji, A.L., Ega, M., Akoroda, A., Adeniyi, B.U. and Balogun, A., *Cassava development in nigeria. A country case study towards a global strategy for cassava development*, Agriculture, D.O., Editor. 1997, Federal Ministry of Agriculture and Natural Resources, Lagos Nigeria.
254. Lewkowski, J., *Synthesis, chemistry and applications of 5-hydroxymethylfurfural and its derivatives*. Arkivoc, 2001: pp. 17-54.
255. Kojima, Y., Usuki, A., Kawasumi, M., Okada, A., Kurauchi, T. and Kamigaito, O., *Synthesis of nylon 6-clay hybrid by montmorillonite intercalated with  $\epsilon$ -caprolactam*. Journal of Polymer Science Part A: Polymer Chemistry, 1993, **31**(4): pp. 983-986.
256. Kojima, Y., Usuki, A., Kawasumi, M., Okada, A., Fukushima, Y., Kurauchi, T. and Kamigaito, O., *Mechanical properties of nylon 6-clay hybrid*. Journal of Materials Research, 1993, **8**(05): pp. 1185-1189.
257. Ray, S.S. and Bousmina, M., *Biodegradable polymers and their layered silicate nano composites: In greening the 21st century materials world*. Progress in Materials Science, 2005, **50**(8): pp. 962-1079.
258. Ray, S.S., Okamoto, K. and Okamoto, M., *Structure-property relationship in biodegradable poly(butylene succinate)/layered silicate nanocomposites*. Macromolecules, 2003, **36**(7): pp. 2355-2367.
259. Ray, S.S. and Okamoto, M., *Polymer/layered silicate nanocomposites: A review from preparation to processing*. Progress in Polymer Science, 2003, **28**(11): pp. 1539-1641.
260. Pavlidou, S. and Papispyrides, C.D., *A review on polymer-layered silicate nanocomposites*. Progress in Polymer Science, 2008, **33**(12): pp. 1119-1198.

261. Chen, B., Evans, J.R.G., Greenwell, H.C., Boulet, P., Coveney, P.V., Bowden, A.A. and Whiting, A., *A critical appraisal of polymer-clay nanocomposites*. Chemical Society Reviews, 2008, **37**(3): pp. 568-594.
262. Tolle, T.B. and Anderson, D.P., *Morphology development in layered silicate thermoset nanocomposites*. Composites Science and Technology, 2002, **62**(7-8): pp. 1033-1041.
263. Alexandre, M. and Dubois, P., *Polymer-layered silicate nanocomposites: Preparation, properties and uses of a new class of materials*. Materials Science & Engineering R-Reports, 2000, **28**(1-2): pp. 1-63.
264. Wilson, O.C., Olorunyolemi, T., Jaworski, A., Borum, L., Young, D., Siriwat, A., Dickens, E., Oriakhi, C. and Lerner, M., *Surface and interfacial properties of polymer-intercalated layered double hydroxide nanocomposites*. Applied Clay Science, 1999, **15**(1-2): pp. 265-279.
265. Loo, L.S. and Gleason, K.K., *Fourier transform infrared investigation of the deformation behavior of montmorillonite in nylon-6/nanoclay nanocomposite*. Macromolecules, 2003, **36**(8): pp. 2587-2590.
266. Wu, H.D., Tseng, C.R. and Chang, F.C., *Chain conformation and crystallization behavior of the syndiotactic polystyrene nanocomposites studied using fourier transform infrared analysis*. Macromolecules, 2001, **34**(9): pp. 2992-2999.
267. Jeon, H.G., Jung, H.T., Lee, S.W. and Hudson, S.D., *Morphology of polymer/silicate nanocomposites - high density polyethylene and a nitrile copolymer*. Polymer Bulletin, 1998, **41**(1): pp. 107-113.
268. Krikorian, V. and Pochan, D.J., *Poly (l-lactic acid)/layered silicate nanocomposite: Fabrication, characterization, and properties*. Chemistry of Materials, 2003, **15**(22): pp. 4317-4324.
269. Yano, K., Usuki, A., Okada, A., Kurauchi, T. and Kamigaito, O., *Synthesis and properties of polyimide clay hybrid*. Journal of Polymer Science Part A - Polymer Chemistry, 1993, **31**(10): pp. 2493-2498.
270. Tyan, H.L., Liu, Y.C. and Wei, K.H., *Enhancement of imidization of poly(amic acid) through forming poly(amic acid)/organoclay nanocomposites*. Polymer, 1999, **40**(17): pp. 4877-4886.
271. Oriakhi, C.O., Zhang, X.R. and Lerner, M.M., *Synthesis and luminescence properties of a poly(p-phenylenevinylene)/montmorillonite layered nanocomposite*. Applied Clay Science, 1999, **15**(1-2): pp. 109-118.
272. Lee, D.C. and Jang, L.W., *Preparation and characterization of pmma-clay hybrid composite by emulsion polymerization*. Journal of Applied Polymer Science, 1996, **61**(7): pp. 1117-1122.
273. Yang, F., Ou, Y.C. and Yu, Z.Z., *Polyamide 6 silica nanocomposites prepared by in situ polymerization*. Journal of Applied Polymer Science, 1998, **69**(2): pp. 355-361.
274. Lebaron, P.C., Wang, Z. and Pinnavaia, T.J., *Polymer-layered silicate nanocomposites: An overview*. Applied Clay Science, 1999, **15**(1-2): pp. 11-29.
275. Manias, E., Chen, H., Krishnamoorti, R., Genzer, J., Kramer, E.J. and Giannelis, E.P., *Intercalation kinetics of long polymers in 2 nm confinements*. Macromolecules, 2000, **33**(21): pp. 7955-7966.
276. Vaia, R.A., Jandt, K.D., Kramer, E.J. and Giannelis, E.P., *Microstructural evolution of melt intercalated polymer-organically modified layered silicates nanocomposites*. Chemistry of Materials, 1996, **8**(11): pp. 2628-2635.

277. Giannelis, E.P., *Polymer layered silicate nanocomposites*. Advanced Materials, 1996, **8**(1): pp. 29-&.
278. Fornes, T.D., Yoon, P.J., Hunter, D.L., Keskkula, H. and Paul, D.R., *Effect of organoclay structure on nylon 6 nanocomposite morphology and properties*. Polymer, 2002, **43**(22): pp. 5915-5933.
279. Huang, J.C., Zhu, Z.K., Yin, J., Qian, X.F. and Sun, Y.Y., *Poly(etherimide)/montmorillonite nanocomposites prepared by melt intercalation: Morphology, solvent resistance properties and thermal properties*. Polymer, 2001, **42**(3): pp. 873-877.
280. Chan, C.M., Wu, J.S., Li, J.X. and Cheung, Y.K., *Polypropylene/calcium carbonate nanocomposites*. Polymer, 2002, **43**(10): pp. 2981-2992.
281. Gilman, J.W., Awad, W.H., Davis, R.D., Shields, J., Harris, R.H., Davis, C., Morgan, A.B., Sutto, T.E., Callahan, J., Trulove, P.C. and Delong, H.C., *Polymer/layered silicate nanocomposites from thermally stable trialkylimidazolium-treated montmorillonite*. Chemistry of Materials, 2002, **14**(9): pp. 3776-3785.
282. Xie, W., Xie, R.C., Pan, W.P., Hunter, D., Koene, B., Tan, L.S. and Vaia, R., *Thermal stability of quaternary phosphonium modified montmorillonites*. Chemistry of Materials, 2002, **14**(11): pp. 4837-4845.
283. Park, C., Park, O.O., Lim, J.G. and Kim, H.J., *The fabrication of syndiotactic polystyrene/organophilic clay nanocomposites and their properties*. Polymer, 2001, **42**(17): pp. 7465-7475.
284. Gilman, J.W., *Flammability and thermal stability studies of polymer layered-silicate (clay) nanocomposites*. Applied Clay Science, 1999, **15**(1-2): pp. 31-49.
285. Kiliaris, P. and Papaspyrides, C.D., *Polymer/layered silicate (clay) nanocomposites: An overview of flame retardancy*. Progress in Polymer Science, 2010, **35**: pp. 902-958.
286. Utracki, L.A., Sepehr, M. and Boccaleri, E., *Synthetic, layered nanoparticles for polymeric nanocomposites*. Polymers for Advanced Technologies, 2007, **18**(1): pp. 1-37.
287. Choy, J.H., Choi, S.J., Oh, J.M. and Park, T., *Clay minerals and layered double hydroxides for novel biological applications*. Applied Clay Science, 2007, **36**(1-3): pp. 122-132.
288. Usuki, A., Koiwai, A., Kojima, Y., Kawasumi, M., Okada, A., Kurauchi, T. and Kamigaito, O., *Interaction of nylon-6 clay surface and mechanical-properties of nylon-6 clay hybrid*. Journal of Applied Polymer Science, 1995, **55**(1): pp. 119-123.
289. Causin, V., Marega, C., Marigo, A. and Ferrara, G., *Assessing organo-clay dispersion in polymer layered silicate nanocomposites: A saxs approach*. Polymer, 2005, **46**(23): pp. 9533-9537.
290. Xu, M.Z., Choi, Y.S., Kim, Y.K., Wang, K.H. and Chung, I.J., *Synthesis and characterization of exfoliated poly(styrene-co-methyl methacrylate)/clay nanocomposites via emulsion polymerization with amps*. Polymer, 2003, **44**(20): pp. 6387-6395.
291. Porter, D., Metcalfe, E. and Thomas, M.J.K., *Nanocomposite fire retardants - a review*. Fire and Materials, 2000, **24**(1): pp. 45-52.
292. Haraguchi, K., Li, H.J., Matsuda, K., Takehisa, T. and Elliott, E., *Mechanism of forming organic/inorganic network structures during in-situ free-radical*

- polymerization in pnipa-clay nanocomposite hydrogels*. *Macromolecules*, 2005, **38**(8): pp. 3482-3490.
293. Kim, Y.K., Choi, Y.S., Wang, M.H. and Chung, I.J., *Synthesis of exfoliated PS/Na-MMT nanocomposites via emulsion polymerization*. *Chemistry of Materials*, 2002, **14**(12): pp. 4990-4995.
294. Morgan, A.B. and Gilman, J.W., *Characterization of polymer-layered silicate (clay) nanocomposites by transmission electron microscopy and X-ray diffraction: A comparative study*. *Journal of Applied Polymer Science*, 2003, **87**(8): pp. 1329-1338.
295. Chen, B.Q. and Evans, J.R.G., *Thermoplastic starch-clay nanocomposites and their characteristics*. *Carbohydrate Polymers*, 2005, **61**(4): pp. 455-463.
296. De Carvalho, A.J.F., Curvelo, A.a.S. and Agnelli, J.a.M., *A first insight on composites of thermoplastic starch and kaolin*. *Carbohydrate Polymers*, 2001, **45**(2): pp. 189-194.
297. Pandey, J.K. and Singh, R.P., *Green nanocomposites from renewable resources: Effect of plasticizer on the structure and material properties of clay-filled starch*. *Starch-Starke*, 2005, **57**(1): pp. 8-15.
298. Guan, J.J. and Hanna, M.A., *Selected morphological and functional properties of extruded acetylated starch-cellulose foams*. *Bioresource Technology*, 2006, **97**(14): pp. 1716-1726.
299. Kumar, A.P. and Singh, R.P., *Biocomposites of cellulose reinforced starch: Improvement of properties by photo-induced crosslinking*. *Bioresource Technology*, 2008, **99**(18): pp. 8803-8809.
300. Lu, Y.S., Weng, L.H. and Cao, X.D., *Morphological, thermal and mechanical properties of ramie crystallites - reinforced plasticized starch biocomposites*. *Carbohydrate Polymers*, 2006, **63**(2): pp. 198-204.
301. Ma, X.F., Yu, J.G. and Wang, N., *Fly ash-reinforced thermoplastic starch composites*. *Carbohydrate Polymers*, 2007, **67**(1): pp. 32-39.
302. Fama, L., Gerschenson, L. and Goyanes, S., *Starch-vegetable fibre composites to protect food products*. *Carbohydrate Polymers*, 2009, **75**(2): pp. 230-235.
303. Kaushik, A., Singh, M. and Verma, G., *Green nanocomposites based on thermoplastic starch and steam exploded cellulose nanofibrils from wheat straw*. *Carbohydrate Polymers*, 2010, **82**(2): pp. 337-345.
304. Guimaraes, J.L., Wypych, F., Saul, C.K., Ramos, L.P. and Satyanarayana, K.G., *Studies of the processing and characterization of corn starch and its composites with banana and sugarcane fibers from Brazil*. *Carbohydrate Polymers*, 2010, **80**(1): pp. 130-138.
305. Kaith, B.S., Jindal, R., Jana, A.K. and Maiti, M., *Development of corn starch based green composites reinforced with saccharum spontaneum l fiber and graft copolymers - evaluation of thermal, physico-chemical and mechanical properties*. *Bioresource Technology*, 2010, **101**(17): pp. 6843-6851.
306. Ogata, N., Jimenez, G., Kawai, H. and Ogihara, T., *Structure and thermal/mechanical properties of poly(l-lactide)-clay blend*. *Journal of Polymer Science Part B-Polymer Physics*, 1997, **35**(2): pp. 389-396.
307. Jandas, P.J., Mohanty, S. and Nayak, S.K., *Surface treated banana fiber reinforced poly (lactic acid) nanocomposites for disposable applications*. *Journal of Cleaner Production*, 2013, **52**: pp. 392-401.
308. Ray, S.S., Maiti, P., Okamoto, M., Yamada, K. and Ueda, K., *New polylactide/layered silicate nanocomposites. I. Preparation, characterization, and properties*. *Macromolecules*, 2002, **35**(8): pp. 3104-3110.

309. Ray, S.S., Okamoto, K., Yamada, K. and Okamoto, M., *Novel porous ceramic material via burning of polylactide/layered silicate nanocomposite*. Nano Letters, 2002, **2**(4): pp. 423-425.
310. Ray, S.S., Yamada, K., Okamoto, M. and Ueda, K., *Polylactide-layered silicate nanocomposite: A novel biodegradable material*. Nano Letters, 2002, **2**(10): pp. 1093-1096.
311. Paul, M.A., Alexandre, M., Degee, P., Calberg, C., Jerome, R. and Dubois, P., *Exfoliated polylactide/clay nanocomposites by in-situ coordination-insertion polymerization*. Macromolecular Rapid Communications, 2003, **24**(9): pp. 561-566.
312. Maiti, P., Yamada, K., Okamoto, M., Ueda, K. and Okamoto, K., *New polylactide/layered silicate nanocomposites: Role of organoclays*. Chemistry of Materials, 2002, **14**(11): pp. 4654-4661.
313. Chang, J.H., An, Y.U., Cho, D.H. and Giannelis, E.P., *Poly(lactic acid) nanocomposites: Comparison of their properties with montmorillonite and synthetic mica(ii)*. Polymer, 2003, **44**(13): pp. 3715-3720.
314. Lee, S.Y., Kang, I.A., Doh, G.H., Yoon, H.G., Park, B.D. and Wu, Q.L., *Thermal and mechanical properties of wood flour/talc-filled polylactic acid composites: Effect of filler content and coupling treatment*. Journal of Thermoplastic Composite Materials, 2008, **21**(3): pp. 209-223.
315. Qu, P., Gao, Y.A., Wu, G.F. and Zhang, L.P., *Nanocomposites of poly(lactic acid) reinforced with cellulose nanofibrils*. BioResources, 2010, **5**(3): pp. 1811-1823.
316. Misra, M., Park, H., Mohanty, A.K. and Drzal, L.T., *Injection molded 'green' nanocomposite materials from renewable resources*, in *Global Plastics Environmental Conference*. 2004, Detroit, MI, USA, .
317. Mahadeva, S.K., Yun, S. and Kim, J., *Flexible humidity and temperature sensor based on cellulose-polypyrrole nanocomposite*. Sensors and Actuators a-Physical, 2011, **165**(2): pp. 194-199.
318. Halim, K.a.A., Farrell, J.B. and Kennedy, J.E., *Preparation and characterisation of polyamide 11/montmorillonite (MMT) nanocomposites for use in angioplasty balloon applications*. Materials Chemistry and Physics, 2013, **143**(1): pp. 336-348.
319. Mansa, R. and Detellier, C., *Preparation and characterization of guar-montmorillonite nanocomposites*. Materials, 2013, **6**(11): pp. 5199-5216.
320. Marsh, B.K. and Day, R.L., *Pozzolanic and cementitious reactions of fly ash in blended cement pastes*. Cement and Concrete Research, 1988, **18**(2): pp. 301-310.
321. Vargaftik, N.B., Volkov, B.N. and Voljak, L.D., *International tables of the surface-tension of water*. Journal of Physical and Chemical Reference Data, 1983, **12**(3): pp. 817-820.
322. Kaye, G.W.C. and Laby, T.H., *Tables of physical and chemical constants*. 6th ed. 1995, Essex, England, Longman Group Ltd, pp. 60.
323. Ma, J.P., Pang, Y., Wang, M., Xu, J., Ma, H. and Nie, X., *The copolymerization reactivity of diols with 2,5-furandicarboxylic acid for furan-based copolyester materials*. Journal of Materials Chemistry, 2012, **22**(8): pp. 3457-3461.
324. Yuan, X., Li, X., Zhu, E., Hu, J., Cao, S. and Sheng, W., *Synthesis and properties of silicone/montmorillonite nanocomposites by in-situ intercalative polymerization*. Carbohydrate Polymers, 2010, **79**(2): pp. 373-379.

325. ASTM D570-98, A., *Standard test method for water absorption of plastics*. 2010: USA, pp. 1-4.
326. Faç Rcas Iu, D., Li, J.Q. and Cameron, S., *Preparation of sulfated zirconia catalysts with improved control of sulfur content ii. Effect of sulfur content on physical properties and catalytic activity*. Applied Catalysis A: General, 1997, **154**(1–2): pp. 173-184.
327. Tangchupong, N., Khaodee, W., Jongsomjit, B., Laosiripojana, N., Prasertthdam, P. and Assabumrungrat, S., *Effect of calcination temperature on characteristics of sulfated zirconia and its application as catalyst for isosynthesis*. Fuel Processing Technology, 2010, **91**(1): pp. 121-126.
328. Osendi, M.I., Moya, J.S., Serna, C.J. and Soria, J., *Metastability of tetragonal zirconia powders*. Journal of the American Ceramic Society, 1985, **68**(3): pp. 135-139.
329. Evans, P.A., Stephens, R. and Binner, J.G.P., *Quantitative X-ray diffraction analysis of polymorphic mixes of pure zirconia*. Transactions and Journal of the British Ceramic Society, 1984, **83**(2): pp. 39-43.
330. Schmid, H.K., *Quantitative-analysis of polymorphic mixes of zirconia by X-ray-diffraction*. Journal of the American Ceramic Society, 1987, **70**(5): pp. 367-376.
331. Zhang, Z.H., Liu, W.J., Xie, H.B. and Zhao, Z.B.K., *An unexpected reaction between 5-hydroxymethylfurfural and imidazolium-based ionic liquids at high temperatures*. Molecules, 2011, **16**(10): pp. 8463-8474.
332. Qi, X.H., Watanabe, M., Aida, T.M. and Smith, R.L., *Selective conversion of d-fructose to 5-hydroxymethylfurfural by ion-exchange resin in acetone/dimethyl sulfoxide solvent mixtures*. Industrial & Engineering Chemistry Research, 2008, **47**(23): pp. 9234-9239.
333. Wei, Z.J., Liu, Y.X., Thushara, D. and Ren, Q.L., *Entrainer-intensified vacuum reactive distillation process for the separation of 5-hydroxymethylfurfural from the dehydration of carbohydrates catalyzed by a metal salt-ionic liquid*. Green Chemistry, 2012, **14**(4): pp. 1220-1226.
334. Hasabnis, A. and Mahajani, S., *Entrainer-based reactive distillation for esterification of glycerol with acetic acid*. Industrial & Engineering Chemistry Research, 2010, **49**(19): pp. 9058-9067.
335. Noeres, C., Kenig, E.Y. and Gorak, A., *Modelling of reactive separation processes: Reactive absorption and reactive distillation*. Chemical Engineering and Processing, 2003, **42**(3): pp. 157-178.
336. Taylor, R. and Krishna, R., *Modelling reactive distillation*. Chemical Engineering Science, 2000, **55**(22): pp. 5183-5229.
337. Guo, F., Fang, Z. and Zhou, T.J., *Conversion of fructose and glucose into 5-hydroxymethylfurfural with lignin-derived carbonaceous catalyst under microwave irradiation in dimethyl sulfoxide-ionic liquid mixtures*. Bioresource Technology, 2012, **112**: pp. 313-318.
338. Qi, X.H., Watanabe, M., Aida, T.M. and Smith, R.L., *Efficient process for conversion of fructose to 5-hydroxymethylfurfural with ionic liquids*. Green Chemistry, 2009, **11**(9): pp. 1327-1331.
339. Verevkin, S.P., Emel'yanenko, V.N., Stepurko, E.N., Ralys, R.V., Zaitsau, D.H. and Stark, A., *Biomass-derived platform chemicals: Thermodynamic studies on the conversion of 5-hydroxymethylfurfural into bulk intermediates*. Industrial & Engineering Chemistry Research, 2009, **48**(22): pp. 10087-10093.

340. Zhang, Y.M., Pidko, E.A. and Hensen, E.J.M., *Molecular aspects of glucose dehydration by chromium chlorides in ionic liquids*. Chemistry-A European Journal, 2011, **17**(19): pp. 5281-5288.
341. Tong, X.L. and Li, Y.D., *Efficient and selective dehydration of fructose to 5-hydroxymethylfurfural catalyzed by bronsted-acidic ionic liquids*. Chemsuschem, 2010, **3**(3): pp. 350-355.
342. Jadhav, H., Taarning, E., Pedersen, C.M. and Bols, M., *Conversion of d-glucose into 5-hydroxymethylfurfural (HMF) using zeolite in bmim cl or tetrabutylammonium chloride (TBAC)/CrCl<sub>2</sub>*. Tetrahedron Letters, 2012, **53**(8): pp. 983-985.
343. El Seoud, O.A., Koschella, A., Fidale, L.C., Dorn, S. and Heinze, T., *Applications of ionic liquids in carbohydrate chemistry: A window of opportunities*. Biomacromolecules, 2007, **8**(9): pp. 2629-2647.
344. Zhang, Z.C., *Catalysis in ionic liquids*. In: *Advances in catalysis, vol 49*. Gates, B.C. and Knozinger, H., Editors. Elsevier Academic Press Inc, San Diego, pp. 153-237.
345. Ebner, G., Schiehser, S., Potthast, A. and Rosenau, T., *Side reaction of cellulose with common 1-alkyl-3-methylimidazolium-based ionic liquids*. Tetrahedron Letters, 2008, **49**(51): pp. 7322-7324.
346. Anastas, P.T. and Zimmerman, J.B., *Design through the 12 principles green engineering*. Environmental Science & Technology, 2003, **37**(5): pp. 95A-101A.
347. Silverstein, R., Webster, F. and Kiemle, D., *Spectrometric identification of organic compounds*. John Wiley & Sons Inc., Hoboken, NJ. USA, pp. 72-126.
348. Mohrig, J.R., Hammond, C.N. and Schatz, P.F., *Techniques in organic chemistry*. W.H. Freeman and Company, New York, pp. 251.
349. Mitiakoudis, A. and Gandini, A., *Synthesis and characterization of furanic polyamides*. Macromolecules, 1991, **24**(4): pp. 830-835.
350. Chen, X., Gao, H. and Ploehn, H.J., *Montmorillonite-levan nanocomposites with improved thermal and mechanical properties*. Carbohydrate Polymers, 2014, **101**(0): pp. 565-573.
351. Albayrak, O., Sen, S., Cayli, G. and Ortac, B., *Bio-based polymer nanocomposites based on layered silicates having a reactive and renewable intercalant*. Journal of Applied Polymer Science, 2013, **130**(3): pp. 2031-2041.
352. Boonprasith, P., Wootthikanokkhan, J. and Nimitsiriwat, N., *Mechanical, thermal, and barrier properties of nanocomposites based on poly(butylene succinate)/thermoplastic starch blends containing different types of clay*. Journal of Applied Polymer Science, 2013, **130**(2): pp. 1114-1123.
353. Zhu, S., Peng, H., Chen, J., Li, H., Cao, Y., Yang, Y. and Feng, Z., *Intercalation behavior of poly(ethylene glycol) in organically modified montmorillonite*. Applied Surface Science, 2013, **276**(0): pp. 502-511.
354. Geist, M.F., Boussois, K., Smith, A., Peyratout, C.S. and Kurth, D.G., *Nanocomposites derived from montmorillonite and metallosupramolecular polyelectrolytes: Modular compounds for electrorheological fluids*. Langmuir, 2013, **29**(6): pp. 1743-1747.
355. Yuan, X.H., Li, X.H., Zhu, E.B., Hu, J., Cao, S.S. and Sheng, W.C., *Synthesis and properties of silicone/montmorillonite nanocomposites by in-situ*

- intercalative polymerization*. Carbohydrate Polymers, 2010, **79**(2): pp. 373-379.
356. Mashaël, A., Amal, A. and Waffa, M., *Polystyrene/montmorillonite nanocomposites: Study of the morphology and effects of sonication time on thermal stability*. Journal of Nanomaterials, 2013: pp. 1-12.
357. Tzavalas, S. and Gregoriou, V.G., *Infrared spectroscopy as a tool to monitor the extent of intercalation and exfoliation in polymer clay nanocomposites*. Vibrational Spectroscopy, 2009, **51**(1): pp. 39-43.
358. Ma, Y.H., Zhu, J.X., He, H.P., Yuan, P., Shen, W. and Liu, D., *Infrared investigation of organo-montmorillonites prepared from different surfactants*. Spectrochimica Acta Part a-Molecular and Biomolecular Spectroscopy, 2010, **76**(2): pp. 122-129.
359. Onal, M. and Sarikaya, Y., *Some physicochemical properties of methylammonium and ethylenediammonium smectites*. Colloids and Surfaces a-Physicochemical and Engineering Aspects, 2008, **312**(1): pp. 56-61.
360. Akyuz, S. and Akyuz, T., *Ft-ir spectroscopic investigations of adsorption of 2-, 3- and 4-pyridinecarboxamide on montmorillonite and saponite from anatolia*. Vibrational Spectroscopy, 2006, **42**(2): pp. 387-391.
361. Li, Z.H., Jiang, W.T. and Hong, H.L., *An FTIR investigation of hexadecyltrimethylammonium intercalation into rectorite*. Spectrochimica Acta Part a-Molecular and Biomolecular Spectroscopy, 2008, **71**(4): pp. 1525-1534.
362. Ma, J., Pang, Y., Wang, M., Xu, J., Ma, H. and Nie, X., *The copolymerization reactivity of diols with 2,5-furandicarboxylic acid for furan-based copolyester materials*. Journal of Materials Chemistry, 2012, **22**(8): pp. 3457-3461.
363. Moore, J.A. and Kelly, J.E., *Polyhydroxymethylfuroate poly(2,5-furandiylcarbonyloxymethylene)*. Journal of Polymer Science Part A-Polymer Chemistry, 1984, **22**(3): pp. 863-864.
364. Jiang, M., Liu, Q., Zhang, Q., Ye, C. and Zhou, G.Y., *A series of furan-aromatic polyesters synthesized via direct esterification method based on renewable resources*. Journal of Polymer Science Part a-Polymer Chemistry, 2012, **50**(5): pp. 1026-1036.
365. Gomes, M., Gandini, A., Silvestre, A.J.D. and Reis, B., *Synthesis and characterization of poly(2,5-furan dicarboxylate)s based on a variety of diols*. Journal of Polymer Science Part A-Polymer Chemistry, 2011, **49**(17): pp. 3759-3768.
366. *Young modulus (tensile modulus) - elastic properties - for some common materials - steel, glass, wood and more*. Retrieved from: [http://www.engineeringtoolbox.com/young-modulus-d\\_417.html](http://www.engineeringtoolbox.com/young-modulus-d_417.html) [Accessed 18th March, 2014].
367. Stuart, B.H., *Polymer analysis*. Analytical techniques in the sciences, ed. Ando, D.J. 2002, West Sussex, England, John Wiley & Sons, LTD, pp. 211.
368. Zhang, L., Zhao, N. and Xu, J., *Fabrication and application of superhydrophilic surfaces: A review*. Journal of Adhesion Science and Technology, 2014, **28**(8-9): pp. 769-790.
369. Yuan, Y. and Lee, T.R., *Contact angle and wetting properties*. In: *Surface science techniques*. Bracco, G. and Holts, B., Editors. Springer-Verlag, Berlin Heidelberg.
370. Vogler, E.A., *Structure and reactivity of water at biomaterial surfaces*. Advances in Colloid and Interface Science, 1998, **74**: pp. 69-117.

371. Guo, C.W., Wang, S.T., Liu, H., Feng, L., Song, Y.L. and Jiang, L., *Wettability alteration of polymer surfaces produced by scraping*. Journal of Adhesion Science and Technology, 2008, **22**(3-4): pp. 395-402.
372. *Chemistry matters* (2003). Retrieved from: <http://danthechemist.wordpress.com/2013/02/24/superdry-try-ultra-dry/> [Accessed on 20th March, 2014].
373. Taylor, M., Urquhart, A.J., Zelzer, M., Davies, M.C. and Alexander, M.R., *Picoliter water contact angle measurement on polymers*. Langmuir, 2007, **23**(13): pp. 6875-6878.
374. Ruiz-Cabello, F.J.M., Rodriguez-Valverde, M.A. and Cabrerizo-Vilchez, M.A., *Comparison of the relaxation of sessile drops driven by harmonic and stochastic mechanical excitations*. Langmuir, 2011, **27**(14): pp. 8748-8752.
375. Bicerano, J., *Prediction of polymer properties*. Marcel Dekker, New York, pp. 324 - 355.
376. Schweitzer, R.C. and Morris, J.B., *Improved quantitative structure property relationships for the prediction of dielectric constants for a set of diverse compounds by subsetting of the data set*. Journal of Chemical Information and Computer Sciences, 2000, **40**(5): pp. 1253-1261.
377. Hougham, G., Tesoro, G. and Viehbeck, A., *Influence of free volume change on the relative permittivity and refractive index in fluoropolyimides*. Macromolecules, 1996, **29**(10): pp. 3453-3456.
378. Xu, J., Wang, L., Liang, G.J., Wang, L.X. and Shen, X.L., *A general quantitative structure-property relationship treatment for dielectric constants of polymers*. Polymer Engineering and Science, 2011, **51**(12): pp. 2408-2416.
379. Aguilar, S.M., Shea, J.D., Al-Joumayly, M.A., Van Veen, B.D., Behdad, N. and Hagness, S.C., *Dielectric characterization of PCL-based thermoplastic materials for microwave diagnostic and therapeutic applications*. IEEE Transactions on Biomedical Engineering, 2012, **59**(3): pp. 627-633.
380. De La Fuente, J.L., Ruiz-Bermejo, M., Menor-Salván, C. and Osuna-Esteban, S., *Thermal characterization of HCN polymers by TG-MS, TG, DTA and DSC methods*. Polymer Degradation and Stability, 2011, **96**(5): pp. 943-948.
381. Chouli, F., Benyoucef, A., Yahiaoui, A., Quijada, C. and Morallon, E., *A conducting nanocomposite via intercalative polymerisation of 2-methylaniline with aniline in montmorillonite cation-exchanged*. Journal of Polymer Research, 2012, **19**(11).
382. Suryanarayana, C. and M.G, N., *X-ray diffraction. A practical approach*. 2010, Plenum Publishing Corporation, USA, pp. 1-94.
383. Scott, R.P.W.(2014) *A modern high resolution nmr machine fitted with a superconducting magnet*. Retrieved from: <http://www.analyticalspectroscopy.net/ap7-3.htm> [Accessed: 28th January, 2014].
384. William, A., *Handbook of analytical techniques*. Vol. 1. 2001, Wiley-VCH, USA, pp. 1-100.